



LUND UNIVERSITY

Multiphysics modelling of PEM fuel cells - with reacting transport phenomena at micro and macroscales

Khan, Munir

2011

[Link to publication](#)

Citation for published version (APA):

Khan, M. (2011). *Multiphysics modelling of PEM fuel cells - with reacting transport phenomena at micro and macroscales*. [Doctoral Thesis (compilation), Heat Transfer].

Total number of authors:

1

General rights

Unless other specific re-use rights are stated the following general rights apply:

Copyright and moral rights for the publications made accessible in the public portal are retained by the authors and/or other copyright owners and it is a condition of accessing publications that users recognise and abide by the legal requirements associated with these rights.

- Users may download and print one copy of any publication from the public portal for the purpose of private study or research.
- You may not further distribute the material or use it for any profit-making activity or commercial gain
- You may freely distribute the URL identifying the publication in the public portal

Read more about Creative commons licenses: <https://creativecommons.org/licenses/>

Take down policy

If you believe that this document breaches copyright please contact us providing details, and we will remove access to the work immediately and investigate your claim.

LUND UNIVERSITY

PO Box 117
221 00 Lund
+46 46-222 00 00

Multiphysics Modelling of PEM Fuel Cells

*-With Reacting Transport Phenomena at
Micro and Macroscales*

Munir Ahmed Khan

Akademisk avhandling som för avläggande av teknologie doktorsexamen vid tekniska fakulteten vid Lunds universitet kommer att offentligas försvaras måndagen den 19:e december, 2011, kl. 10:15 i hörsal M:B, på Institutionen för Energivetenskaper, M-huset, Ole Römers väg 1, Lund. Fakultetsopponent: Professor T.S. Zhao, Hong Kong University of Science and Technology, Hong Kong.

Academic thesis which, by due permission of the Faculty of Engineering at Lund University, will be publicly defended on Monday the 19th December, 2011, at 10:00 a.m. in lecture hall M:B, at the Department of Energy Sciences, M-Building, Ole Römers Väg 1, Lund, for the degree of Doctor of Philosophy in Engineering. Faculty opponent: Professor T.S. Zhao, Hong Kong University of Science and Technology, Hong Kong.



LUNDS UNIVERSITET
Lunds Tekniska Högskola

Department of Energy Sciences
Faculty of Engineering

Organization LUND UNIVERSITY Division of Heat Transfer Department of Energy Sciences Faculty of Engineering	Document name DOCTORAL DISSERTATION	
	Date of issue December 19, 2011	
	Sponsoring organization Higher Education Commission (HEC) of Pakistan European Research Council (ERC)	
Author(s) Munir Ahmed Khan		
Title and subtitle Multiphysics Modelling of PEM Fuel cells - With Reacting Transport Phenomena at Micro and Macroscales		
Abstract This thesis presents numerical simulations of reacting transport phenomena in polymer electrolyte membrane (PEM) fuel cells. Broadly, the presented work is subdivided into macro and microscale simulations. In macroscale simulations, a unit PEM fuel cell with interdigitated flow field configurations is simulated keeping in mind all the essential transport mechanisms, i.e., transport of species, ions, electrons, heat and liquid water. Additionally, the impact of different material properties is also incorporated in the work such as anisotropy of species, electrons, temperature and liquid water diffusion in the gas diffusion layers. Furthermore, to increase the accuracy of predicted results, more stringent correlations have been applied for the correction of material phases in the catalyst layer for calculating the ion transport. For simulating the electrochemical reactions in the catalyst layers, an advanced agglomerate model has also been used that takes into account the morphological details of the materials present in the catalyst layers. Since, the liquid water transport in the gas diffusion layer represents one of the most critical phenomenons, a validated approach has been utilized instead of the conventional Leverett approach which has been the most common technique used so far in numerical simulations. The simulations with all the stated mechanism have revealed that the current densities predicted by earlier models were always overestimated and the limiting current density is found to be approximately 1.0 A/cm ² , while in present work, the limiting current density is about 0.68 A/cm ² . The second part of the thesis is dedicated to the generation and simulations of a section of the catalyst layer at microscale. The catalyst layer in PEM fuel cells consists of four different types of material each with a special function to serve. The main theme of work at this section is to segregate each material so that the behavior of each component can be explicitly studied and its response to various physical processes can be noted when subjected to operation. It is observed in simulations at such scale that the selected part of the catalyst layer is much descriptive than the macroscale simulations where it is much difficult to specify each material phase separately. Additionally, at microscale, the correction factors do not need to be defined explicitly because all the processes are confined to their respective phases. The work presented here is limited to single phase flow only and the solid phase is neglected, i.e., the electric current follows the same path as the ionic current due to the limitations in the computational resources.		
Key words: PEM fuel cells, CFD, macroscale, microscale, multiphysics, multiphase, anisotropy.		
Classification system and/or index terms (if any):		
Supplementary bibliographical information:	Language English	
ISSN and key title: 0282-1990	ISBN 978-91-7473-184-2	
Recipient's notes	Number of pages 276	Price
	Security classification	

Distribution by (name and address)

I, the undersigned, being the copyright owner of the abstract of the above-mentioned dissertation, hereby grant to all reference sources permission to publish and disseminate the abstract of the above-mentioned dissertation.

Signature:



Date: November 15, 2011

Multiphysics Modelling of PEM Fuel Cells

*-With Reacting Transport Phenomena at
Micro and Macroscales*

Munir Ahmed Khan



LUNDS UNIVERSITET
Lunds Tekniska Högskola

Department of Energy Sciences
Faculty of Engineering

Division of Heat Transfer
Department of Energy Sciences
Faculty of Engineering
Lund University
Box 118
SE-221 00 Lund
Sweden
www.energy.lth.se

Doctoral Thesis in Heat Transfer

ISRN LUTMDN/TMHP-11/1085-SE
ISSN 0282-1990
ISBN 978-91-7473-184-2

© Munir Ahmed Khan
Lund 2011

"I may not be there yet, but I'm closer than I was yesterday."

To my parents:

Ihsan Ilahi
&
Mumtaz Begum

Acknowledgements

“A journey of a thousand miles ...begins with a single step”

and this is my first step. I feel lucky that I have the guidance, support and company of some amazing people who have helped me in preparing myself for the thousand mile journey. To their kindness, *Tack så mycket*.

First and foremost I offer my sincerest gratitude to my supervisors, Professor Jinliang Yuan and Professor Bengt Sundén, who have supported me throughout my thesis with their patience and knowledge whilst allowing me the room to work in my own way. I attribute the level of my thesis to their encouragement and effort and without them this thesis, too, would not have been completed or written. One simply could not wish for better or friendlier supervisors.

In my daily work I have been blessed with a friendly and cheerful group of fellow colleagues. Martin Andersson has always been a good critic and has always helped me to improve the level of work. I'm also thankful to Helgi Fridriksson for helping me to get on the road with LaTeX and all the political know-how he shared with me. Among many, I can't miss Hedvig Paradis for all her efforts to teach me Swedish and English and sharing her wits. Here I must mention that she has always been kind and helpful in making me realize all the smaller details of life. Henrik Hofgren, I really enjoy his short cuts to everything from world peace to heating system of M-building and making me to jump in ice for the first time. Thanks to Maria Navasa too for her professional advices for body fitness, which apparently don't seem to be working in my case. I'm also grateful to Erik Johansson as being a co-worker in PEM technology for his sincere and immense efforts and thanks for being my cinema pal. I would also take the opportunity to acknowledge Wamei Lin for bearing me as her office mate and I hope it was not much problematic. I am thankful to all of these nice people for such a nice time that we have spent together and also for the academic and non academic discussions from fuel cells to anything that none of us knew nothing about but always ending with some sound conclusion, more

often a hot one.

Thanks to Sweden too, for its great hospitality and some other things that I can't mention here. Thanks for making my short stay the most memorable part of my life. I would also like to thank all my friends that I have met here in Sweden from nationalities from all around the world. It will be hard for me to mention each one but, to all of you: I will remember you always. Special thanks to the Pakistani community here in Lund who have always provided a home like atmosphere here and all the food that we had together, especially with Nadeem Zafar, Asghar Akaash, Sami Khan, Taimoor Abbass, Naveed Butt, Tahir Irshad, Muhammad Atif and Malik Badshah. My sincerest gratitude to the Pathans of Lund Taimoor Kakakhel, Rashid Mansoor, Nadir Khan and Irfan Khan for providing a beautiful company all the times. I must also thank my corridor mates for the nice and good time together.

I'm grateful to the Higher Education Commission (HEC) of Pakistan for providing my living expenses in Sweden and the Swedish Institute (SI) for managing the scholarship. I am also thankful to the European Research Council (ERC) for financially supporting the research work.

My parents: Ihsan Ilahi and Mumtaz Begum. I pride myself in having the most lovable parents and all this is their part of hard work. I am grateful to my father especially who constantly encouraged me to continue my education, sometimes using his kung-fu techniques, but, at the end I feel proud to be his son. Thanks to my brothers Naseer Khan and Tauqir Khan and my sisters Ayesha Khan, Fatima Khan and Amna Khan for being such a nice members of our squad. I still miss fights with them.

My very special thanks to my better half, Tania Khattak. First I'm sorry that I haven't been able to give you enough time and secondly, thanks a lot for bearing me as your husband and giving me the most beautiful, handsome and lovely gift: Adam Khan, my son.

Finally, I would thank Allah Almighty for all the blessings He has bestowed upon me. And I pray to him to grant me the courage and will to fulfil the duties with honesty and sincerity that He has chosen for me. A'meen.

Thank you all.

“The happiness of a drop is to die in river”

Populärvetenskaplig sammanfattning

Polymermembranbränsleceller (PEM) anses vara en mycket lovande teknik inom fordonindustrin på grund av dess kompakthet i storlek, höga verkningsgrader samt låga arbetstryck och temperaturer. De senaste åren har tekniken varit fokus för en anseelig mängd forskning. PEM-bränsleceller har den stora fördelen att energiomvandlingseffektiviteten har potential för att vara betydligt högre än för till exempel en bensin- eller en dieselmotor. En ökad effektivitet leder till en minskad förbrukning av fossila bränslen. Bränslet som används i en PEM-bränslecell är vätgas, som i sin tur kan framställas både från fossila och förnyelsebara bränslen.

PEM-bränsleceller arbetar efter en mycket enkel princip. Vätgasen reagerar vid cellens anod och bildar elektroner och protoner. Protonerna färdas via ett membran till katoden, medan elektronerna färdas till katoden via en extern last. Syrgas reagerar med elektronerna och protonerna vid katoden och vatten bildas som restprodukt. På detta sätt kan elektricitet bildas utan att bränslet genomgår ett förbränningssteg.

Att kombinera vätgas och syrgas, två av de enklaste grundämnena som finns, kan på pappret låta enkelt men vid en närmare undersökning ser man PEM-teknologi inte är lika raktfram som en första anblick kan ge sken av. Problem består bland annat av vattenhantering. Till dags dato har mycket resurser lagts på forskning inom de olika fenomen som är viktiga för bränsleceller. Allt från design av storskaliga stack-system till grundläggande forskning med syfte att förstå hur de elektrokemiska reaktionerna i cellen fungerar har undersökts. Väldigt många framsteg har gjorts, men det finns fortfarande mycket som behöver lösas innan tekniken kan kommersialiseras till fullo.

Ett av de största problemen är bränslecellens katod. Långsam reaktionskinetik och komplicerad vattenhantering vid katoden tillhör de största problemen för förbättrad prestanda i cellen. PEM-bränsleceller arbetar vid låga temperaturer, ofta omkring 80 °C, och det vatten som bildas vid katoden kan därför vid vissa lokala förhållanden kondensera, vilket gör att hänsyn måste tas till fluidflöde i två faser – något som inte förekommer i

andra typer av bränsleceller.

I denna avhandling har datorbaserade strömningsberäkningar (CFD) använts för att utföra detaljrika simuleringar av PEM-bränsleceller med syfte att förstå de inre fenomen som sker i cellen så som transport av joner, elektroner, gaser och vätskor, elektrokemiska reaktioner och hur de materiella egenskaperna hos de enskilda materialen som bränslecellen byggs av påverkar dess prestanda. Arbetet är uppdelat i två huvudsakliga delar, mikroskalig och makroskalig simulering. I den makroskaliga simuleringen har alla grundläggande fenomen som sker i cellen kvantiserats med avseende på transportmekanismer och strukturella parametrar för varje enskild process. För att simulera transport av flytande vatten i cellen har ett nytt tillvägagångssätt som är exklusivt framtaget för flöde i de porösa materialen i bränslecellens elektroder använts.

Även om makroskaliga simuleringar resulterar i noggranna resultat gällande cellens övergripande prestanda så är de begränsade såtillvida att det är snudd på omöjligt att skilja på de olika material som cellen består av. Speciellt inne i katalysatorlagret där de elektrokemiska reaktionerna sker kan detta vara ett problem. Katalysatorlagret i en PEM-bränslecell består av kol, platina och Nafion (ett protonledande membranmaterial) samt tomrum. Dessa tre olika material samt tomrummet fyller alla väldigt specifika syften. I den mikroskaliga modelleringen har varje fas i katalysatorlagret genererats och behandlats enskilt så att de processer som sker kan undersökas utifrån de olika fasernas inverkan. På grund av den beräkningskraft som krävs för att göra denna typ av simuleringar har förenklingar gjorts i form av att flödet som simulerats har antagits endast innehålla vatten i gasform. Dessutom har den inre delen av den solida fasen bestående av kol- och platinapartiklar uteslutits ur simuleringarna. Utan dessa förenklingar skulle simuleringarna inte gå att utföra på en enskild dator utan datakluster skulle behöva användas.

Abstract

This thesis presents numerical simulations of reacting transport phenomena in polymer electrolyte membrane (PEM) fuel cells. Broadly, the presented work is subdivided into macro and microscale simulations. In macroscale simulations, a unit PEM fuel cell with interdigitated flow field configurations is simulated keeping in mind all the essential transport mechanisms, i.e., transport of species, ions, electrons, heat and liquid water. Additionally, the impact of different material properties is also incorporated in the work such as anisotropy of species, electrons, temperature and liquid water diffusion in the gas diffusion layers. Furthermore, to increase the accuracy of predicted results, more stringent correlations have been applied for the correction of material phases in the catalyst layer for calculating the ion transport. For simulating the electrochemical reactions in the catalyst layers, an advanced agglomerate model has also been used that takes into account the morphological details of the materials present in the catalyst layers. Since, the liquid water transport in the gas diffusion layer represents one of the most critical phenomenons, a validated approach has been utilized instead of the conventional Leverett approach which has been the most common technique used so far in numerical simulations. The simulations with all the stated mechanism have revealed that the current densities predicted by earlier models were always overestimated and the limiting current density is found to be approximately 1.0 A/cm^2 , while in present work, the limiting current density is about 0.68 A/cm^2 .

The second part of the thesis is dedicated to the generation and simulations of a section of the catalyst layer at microscale. The catalyst layer in PEM fuel cells consists of four different types of material each with a special function to serve. The main theme of work at this section is to segregate each material so that the behavior of each component can be explicitly studied and its response to various physical processes can be noted when subjected to operation. It is observed in simulations at such scale that the selected part of the catalyst layer is much descriptive than the macroscale simulations where it is much difficult to specify each material phase separately. Additionally, at microscales, the correction factors do not need to be defined explicitly because all the processes are

confined to their respective phases. The work presented here is limited to single phase flow only and the solid phase is neglected, i.e., the electric current follows the same path as the ionic current due to the limitations in the computational resources.

List of Papers

The main body of this thesis is based on the following papers:

- A. Khan, M.A., Sundén, B., and Yuan, J., 2011. “Analysis of multi-phase transport phenomena with catalyst reactions in polymer electrolyte membrane fuel cells - A review”, *Journal of Power Sources*, vol. 196, pp. 7899-7916.
- B. Khan, M.A., Sundén, B., and Yuan, J., 2011. “Water saturation modeling in polymer electrolyte membrane (PEM) fuel cells using a validated approach”, In *International Green Energy Conference*, 2-9 June, Eskişehir, Turkey (*Invited and recommended to International Journal of Energy Research*).
- C. Khan, M.A., Xiao, Y., Sundén, B., Yuan, J., 2011. “Analysis of multiphase transport phenomena in PEMFCs by incorporating microscopic model for catalyst layer structures”, In *ASME 2011 International Mechanical Engineering Congress*, (IMECE2011-65142), 11-17 November, Colorado, USA.
- D. Khan, M.A., Sundén, B., Yuan, J., 2011. “Numerical quantification of water saturation, back diffusion, electro-osmotic drag and water generation in polymer electrolyte membrane fuel cells”, (*submitted to Journal of Power Sources*).
- E. Khan, M.A., Johansson, E., Sundén, B., Yuan, J., 2011. “Analysis of anisotropic transport in the polymer electrolyte membrane fuel cells and its effect on performance”, (*submitted to Journal of Power Sources*).

For Papers A, B and D, the majority of the work has been performed by the first author. For Paper C, Dr. Xiao equally contributed in generating the geometry and preliminary mesh for the microscale simulations. In Paper E, Johansson, E. helped in collecting data, verifying empirical relationships and provided discussion for some of the parameters.

Work Presented by the author during his Ph.D. studies, but not included in the thesis, either because they have been covered by in latest work or lie outside the scope of the thesis:

- a. Khan, M.A., Sundén, B., Yuan, J., 2008. “Species and temperature distribution in cathode of PEMFC”, In *7th International Symposium on Heat Transfer*, 26-29 October, Beijing, China.
- b. Khan, M.A., Sundén, B., Yuan, J., 2009. “LTNE approach to simulate temperature of cathode in a PEMFC”, In *6th International Symposium on Multiphase Flow, Heat Mass Transfer and Energy Conversion*, 11-15 July, Xi’an, China.
- c. Khan, M.A., 2009. “Numerical simulation of multi-scale transport processes and reactions in PEM fuel cells using two-phase models”, Licentiate Thesis, ISRN LUTMDN/TMHP-09/ 7066-SE. Lund University, Lund, Sweden.
- d. Khan, M.A., Sundén, B., Yuan, J., 2010. “Simulation of multiphase transport phenomena in PEMFC involving water phase change”, In *18th World Hydrogen Energy Conference*, 16-21 May, Essen, Germany.

Contents

Acknowledgements	i
Populärvetenskaplig sammanfattning	iii
Abstract	v
List of Papers	vii
Symbols	xiii
1 Introduction	1
1.1 Why Fuel Cells?	1
1.2 Applications of Fuel Cells	2
1.3 Types of Fuel Cells	2
1.4 PEM Fuel Cell Basics	3
1.4.1 Electrolyte (Membrane)	5
1.4.2 Gas Diffusion Layer (GDL)	5
1.4.3 Catalyst Layer (CL)	6
1.4.4 Bipolar Plates	6
1.5 Fuel Cell Irreversibility	7
1.5.1 Activation Losses	7
1.5.2 Ohmic (Resistive) Losses	8
1.5.3 Concentration Losses	8
1.5.4 Fuel Crossover and Internal Currents	8
1.6 Motivation for this Work	9
2 Modelling Approaches	11
2.1 Revision of PEM fuel cell Models	11
2.2 Modelling Discrepancies	13
2.2.1 Anisotropy of Species Diffusion in GDL	13

2.2.2	Effective Charge Conductivity	16
2.2.3	Anisotropic Permeability	19
2.2.4	Anisotropy of Thermal Conductivity	20
2.3	Multiphase Flow Models and Water Phase Change	21
2.3.1	Multi-Fluid Flow Model	22
2.3.2	Mixture Model	23
2.3.3	Moisture Diffusion Model	24
2.3.4	Porosity Correction Model	24
2.4	Water Management	25
2.4.1	Conventional Capillary Pressure Approach	27
3	Numerical Modelling	31
3.1	Porous Media	31
3.2	Conservation of Mass	32
3.3	Conservation of Momentum	32
3.4	Conservation of Energy	34
3.5	Conservation of Species	36
3.5.1	Fick's Law	36
3.5.2	Stefan-Maxwell Equation	37
3.5.3	Knudsen Correction to Species Flux	38
3.6	Liquid Water Transport	39
3.7	Physico- Electrochemical Model	40
3.8	Charge Transport (Ions and Electrons)	43
3.9	Water Transport in Electrolyte (membrane)	44
3.10	Source Terms for Conservation Equations	44
3.11	Microscale Modelling Review	45
3.12	Microstructure Reconstruction	47
3.12.1	Regularly Distributed Sphere Method	47
3.12.2	Catalyst Layer Microstructure Reconstruction	48
3.13	CFD Implementation	51
3.13.1	Macroscale Modelling	51
3.13.2	Microscale Models and Governing Equations	56
3.13.3	Model Development for Microscopic Transport and Reactions	57
4	Results & Discussion	63
4.1	Macro Model	63
4.1.1	Pressure Distribution	64
4.1.2	Species Distribution	65
4.1.3	Charge Distribution	66
4.1.4	Temperature Distribution	72
4.1.5	Water Management	75
4.1.6	CFD Model Verification and Comparison	80
4.2	Micromodel Simulation Results	82
4.2.1	Oxygen Distribution	82
4.2.2	Proton Conductivity and Water Distribution	82
4.2.3	Temperature Distribution	84

5	Summary	87
5.1	Macroscale Analysis	88
5.2	Microscale Analysis	90
6	Bibliography	93
7	Paper A	A1
8	Paper B	B1
9	Paper C	C1
10	Paper D	D1
11	Paper E	E1

Symbols

Roman Symbols

a	specific agglomerate surface area, m^2/m^3 or water activity
C	evaporation ($1/\text{atm s}$) or condensation ($1/\text{s}$) rate constant
c_p	specific heat capacity, J/kg K
C_w	water content
d	diameter, m
d	void length scale, m
E	energy, W/m^3
E_r	effectiveness of spherical agglomerate
\vec{F}	force, N
F	Faraday's constant, C/mol
f	volume fraction
g	gravitational acceleration, m/s^2
h_v	interstitial heat transfer coefficient, $\text{W/m}^3 \text{K}$
i	current density, A/cm^2
\mathbf{J}	heat flux, W/m^2
k	reaction rate, $1/\text{s}$
k	thermal conductivity, W/m K
K	permeability, m^2
K_n	Knudsen number
\mathbf{K}	permeability tensor, m^2
l	system length scale, m
\dot{m}	mass transfer rate, $\text{kg/m}^3 \text{s}$
M	molar mass, kg/mol
m_{Pt}	platinum loading, mg/cm^2
N	Nafion TM
p	pressure, Pa
\dot{q}	interstitial heat transfer, W/m^3

R	gas constant, J/mol K
r	radius, m
s	saturation or volume fraction of liquid
S	source, kg/m ³ s or W/m ³
T	temperature, K
\mathbf{V}	velocity, m/s
V	volume, m ³
X	species mass fraction
Y	mole fraction
z	number of electrons

Greek Symbols

α	phase volume fraction
α_a	anodic transfer coefficient
α_c	cathodic transfer coefficient
δ	thickness of ionomer coverig agglomerate, m
ε	porosity
η	activation overpotential, V
γ	surface tension, N/m
γ_k	kinetic evaporation constant
λ	mean free path of molecules, water index
μ	viscosity, Pa s
\dot{w}	mass transfer rate between water vapour and liquid water, kg/m ³ s
ϕ	charge potential, V
Φ_L	Thiele's modulus
π	geometric constant
Π_h	Peltier coefficient, W/m ³
ρ	density, kg/m ³
σ	proton conductivity, S/m or 1/ Ω m
$\bar{\tau}$	stress tensor, Pa
τ	tortousity
Θ	molar concentration of species, mol/m ³
θ	contact angle in degrees
ξ	diffusion volume, m ³

Subscripts & Superscripts

a	anode
agg	agglomerate
c	cathode
CL	catalyst layer
con	condensation
eff	effective
evp	evaporation
f	fluid phase

<i>g</i>	gas
<i>I</i>	ionomer
<i>i</i>	species identification
<i>l</i>	liquid, local
<i>m</i>	mixture, ionomer or membrane phase
<i>nw</i>	non-wetting
<i>por</i>	pore
<i>p, q</i>	phase identifier
<i>r</i>	relative
<i>s</i>	agglomerate surface
<i>sat</i>	saturation
<i>s</i>	solid
<i>v</i>	vapour, void
<i>wv</i>	water vapour
<i>w</i>	wetting

Abbreviations

AFC	alkaline fuel cells
APU	auxillary power unit
CFD	computational fluid dynamics
CHHP	combined heat, hydrogen and power
CHP	combined heat and power
CL	catalyst layer
DMFC	direct methanol fuel cells
FC	fuel cells
FIB	focused ion beam
GDL	gas diffusion layer
GT	gas turbine
HO	hydrogen oxidation
LTE	local thermal equilibrium
LTNE	local thermal non-equilibrium
MCFC	molten carbonate fuel cells
OR	oxygen reduction
PAFC	phosphoric acid fuel cells
PEFC	polmer electrolyte fuel cells (<i>synonym of PEMFC</i>)
PEMFC	proton exchange membrane fuel cells or, polymer electrolyte membrane fuel cells
PTL	porous transport layer
SEM	scanning electron microscope
QUICK	quadratic upwind differencing scheme
SIMPLE	semi implicit method for pressure linked equations
SOFC	solid oxide fuel cells
TEM	transmission electron microscopy
TPB	triple phase boundary

1 Introduction

“The defining feature of global energy markets remains high and volatile prices, reflecting a tight balance of supply and demand. This has put issues such as energy security and alternative energies at the forefront of the political agenda worldwide”

Tony Hayward, BP, Feb 2011

With depletion of fossil fuels and ever increasing consumption, an alternate energy source is imminent for the survival of the present industrial and fast paced world. Many alternatives have been proposed but only few can have the opportunity to take over the conventional and very efficient combustion engines. This opportunity for other energy sources is directly linked to present day research society as they stand responsible for making them efficient, stable and cost effective. Among many, the fuel cells have emerged as one of the competitors with some biasing because of their compactness, fuel flexibility and environment friendly operation.

1.1 Why Fuel Cells?

In 1960s, the use of fuel cells was limited to niche applications only like space missions, etc., majorly due to their high costs. But, with the progress in science and technology in the past 50 years, the cost barrier has been reduced almost by 50% and it is speculated that the fuel cells will become a dominant source of energy in future. The fuel cells have shown a dramatic performance in terms of efficiency of 40 to 50% and when they are used with CHP they can reach efficiencies of almost 80% while the efficiency of the current internal combustion engines is limited to about 30% [1]. In addition, having no moving parts also makes them suitable for longer operating periods. The emissions of the fuel cell, while in operation, are also quite low because the output of an ideal fuel cell is pure water depending on the type of fuel cell and the fuel used [2]. Furthermore, due

to the absence of moving parts and conversion of energy via electrochemical reactions, as opposed to burning, they have a silent operation, i.e., low noise pollution too. All these major and favourable features make fuel cells an excellent choice for future power generation.

1.2 Applications of Fuel Cells

Fuel cells are applicable in the whole of the energy demand spectrum. Depending on the type of fuel cell, they are capable of producing energy in the range of 1 W to 10 MW so they can be used for any energy requirements. One of the major applications for fuel cells is the domestic and public transportation system both as a vehicle traction system and for APU applications. The adaptability of the fuel cells to present day vehicular applications is graced due to its replacement of complex mechanical and thermal systems. Although, batteries can perform the same function but are limited in range and need recharging before they can run again. Additionally, the fuel cells provide much higher current densities than the most of the current commercialized batteries.

1.3 Types of Fuel Cells

Different types of the fuel cells are mainly distinguished by the type of electrolyte for ion conduction. The classification based on the electrolyte also determines the type of chemical reactions taking place in the cell, the catalyst type, operating temperature and the fuel used. All these factors, in turn, determine the application for each fuel cell type. Hence, all types of fuel cells are not an alternate to each other but may serve as a complement. The advantages and limitations for specific applications are given in Table 1.1. The main types of fuel cells are;

- alkaline fuel cell (AFC),
- polymer electrolyte membrane fuel cell (PEMFC),
- phosphoric acid fuel cell (PAFC),
- molten carbonate fuel cell (MCFC),
- solid oxide fuel cell (SOFC).

Fig. 1.1 compares different types of fuel cells and their operational strategy, i.e., type of fuel, the direction and the type of ion exchange between the anode and the cathode of the cell. Among all, the PEM fuel cells have potential for generating high power densities, hence, making the technology attractive for portable and mobile applications [3]. Especially many automobile manufacturers have imagined the PEM fuel cell as a choice of future prime mover component. In PEM fuel cells, a solid polymer membrane is used as a separator or the electrolyte and this distinguishes it from other types of the fuel cells. Due to the polymer membrane, PEM fuel cell typically operates at low temperatures (60 to 80 °C) having excellent start-up characteristics compared to high temperature fuel cells. PEM fuel cells are considered the main candidate for light-duty transportation applications. One of the limitations of the PEM fuel cell is that it only operates on pure

Table 1.1: *Typical stack size, applications, advantages and disadvantages of different types of fuel cells^a.*

Type of FC	Power	Advantages	Disadvantages
AFC	10-100 kW	High performance, low cost components	Sensitive to CO ₂ , electrolyte management
PEMFC	1-100 kW	solid Electrolyte reduces corrosion & Electrolyte management problems, low temperature, quick start-ups	Expensive catalysts, sensitive to fuel impurities, low temperature waste heat
PAFC	100-400 kW	High CHP efficiency, increased tolerance to fuel impurities	Expensive catalyst, long start-up times, low current and power
MCFC	300 kW - 3 MW	High efficiency, fuel flexibility, variety of catalysts, solid electrolyte, suitable of CHP	High temperature corrosion and bread down, long start-ups, low power density
SOFC	1 kW - 2 MW	High efficiency, fuel flexibility, variety of catalysts, solid electrolyte, suitable for CHP and CHHP, hybrid/GT cycle	High temperature corrosion, long start-ups

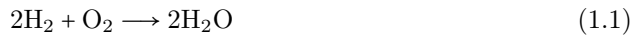
^a data sheet by US Department of Energy, <http://www.hydrogenandfuelcells.energy.gov>, February 2011.

hydrogen, but, fuel processors have been developed that will allow conventional fuel such as natural gas or petrol to be used in the cell. Furthermore, a unique implementation of PEM fuel cells has also been developed that uses methanol without the fuel processor. This is called the direct methanol fuel cells (DMFC). It is prime candidate for use in cameras, notebook computers and other portable electronics [1].

Keeping in mind the advantages offered by the PEM fuel cell technology as a candidate for future power generation for small to medium power applications, a bright prospect is being offered unless the confidence and reliability in this technology are enhanced. Still an extensive and in-depth research is required to make PEM fuel cells commercially feasible.

1.4 PEM Fuel Cell Basics

A fuel cell is a device that produces the flow of current (electrical energy) via electro-chemical reaction of the fuel. For PEM fuel cells, the global reaction is given as;



In order to necessitate Eq. (1.1), the fuel cell is electrically divided into an anode (negative

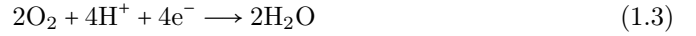
	AFC 80°C	PEM 80°C	PAFC 200°C	MCFC 650°C	SOFC 1000°C	
Oxidant →	O ₂	O ₂ + H ₂ O	O ₂ + H ₂ O	CO ₂ + O ₂	O ₂	
						Cathode
	↓ OH ⁻	↑ H ⁺	↑ H ⁺	↓ CO ₃ ⁻	↓ O ₂ ⁻	Electrolyte
						Anode
Fuel →	H ₂ + H ₂ O	H ₂ + H ₂ O	H ₂	H ₂ + H ₂ O + CO + CO ₂	H ₂ + H ₂ O + CO + CO ₂	

Fig. 1.1: *Types of fuel cells, operating temperatures, fuel utilized and the type of ion exchange.*

terminal) and a cathode (positive terminal) insulated from each other. The hydrogen is split into electrons and protons (or H⁺ ions) at the anode. The electrons are harnessed to produce the electrical energy while the protons are transferred to the cathode of the cell where they re-combine with electrons in presence of oxygen to produce water, or in other words, the electrolysis is being reversed. Thus, splitting Eq. (1.1) yields;



and



where Eqs (1.2) and (1.3) are the hydrogen oxidation (HO) and oxygen reduction (OR) reactions, respectively. For the operation of PEM fuel cells, some basic components are required that facilitate the following operations;

- feed the hydrogen and oxygen at the anode and cathode, respectively,
- prevent the direct mixing of the fuel and the oxidant,
- carry the electrical charge (electrons) through an external circuit via the load,
- dissipate the heat released during the operation,
- remove water from the cell to maintain efficient performance.

In order to carry out the above stated operations, the basic components, as utilized in PEM technology, are;

- the ion exchange membrane,
- electrically conductive porous backing called the gas diffusion layer,
- an electro-catalyst layer,
- the bipolar plates.

Each component is briefly discussed below. However, for complete understanding, references like [2, 3] are recommended.

1.4.1 Electrolyte (Membrane)

The electrolyte constitutes one of the essential components of all types of fuel cells. Mostly, the name given to fuel cells is based on the type of electrolyte used. For PEM fuel cells a polymer membrane is used in between anode and cathode. The membrane is made by substituting fluorine for hydrogen in long chain polymers in the process called perfluorination. After this, a side chain is added, ending with sulphonic acid. The perfluorination of the polymer gives it the chemical resistance and mechanical strength while the addition of sulphonic acid gives it the property to carry the positive ions, hydrogen ions in this case and, as a result, ion conduction takes place via ionic groups within the polymer structure. Therefore, the membrane in PEM fuel cells is sometimes also called proton exchange membrane. In short all the electrolytes should essentially have the following properties;

- they should be chemically resistant,
- they should be strong so that they can be casted in very small thicknesses,
- they should be acidic,
- they should absorb large quantities of water and,
- when they are hydrated, hydrogen ion should move freely (higher protonic conductivity).

One of the main limitations of using such membrane materials is that the ion transport at such sites is highly dependent on the bound and free water associated with those sites.

1.4.2 Gas Diffusion Layer (GDL)

The gas diffusion layer (also sometimes referred to as the porous transport layer, PTL) essentially serves some of the very important functions inside PEM fuel cells, namely;

- to distribute fuel and oxidant evenly to the catalyst layer,
- help in effective water removal to avoid water flooding,
- effectively remove heat generated by electrochemical reactions,
- effectively conduct electronic current.

In order to achieve the above results, usually carbon paper or cloth are selected as the material for the gas diffusion layer and is also sulphonated to achieve the hydrophobic properties for effective removal of water.

The sandwiched structure of the anode and the cathode gas diffusion and catalyst layers and the membrane is also sometimes referred to as the Membrane Electrode Assembly (MEA), the heart of a single cell. This MEA is placed between the bipolar plates to complete a single unit of PEM fuel cells.

1.4.3 Catalyst Layer (CL)

The electrochemical reactions occur in the catalyst layer with the help of platinum catalyst. Platinum (Pt) is one of the best catalysts available for the electrochemical reactions in PEM fuel cells. During the construction of the catalyst layer for PEM fuel cells, small Pt particles are formed on somewhat larger carbon particles. Most often, a carbon based powder (Cobot[®]) is used as carbon particle because of its excellent electrical properties. The catalyst layer also needs the property to conduct ions coming from the anode side of the cell, so the membrane phase (electrolyte) is also spread out in the catalyst layer. Henceforth, there are four material phases in the catalyst layer, i.e., carbon, platinum, membrane phase and the void phase.

Initially the development of the PEM fuel cells has suffered a lot due to the high costs of the platinum catalyst used (approx. 28 mg/cm² [2]) in the catalyst layer and many potential users switched to other types of fuel cells due to the cost factor. However, the development over the recent years has helped in increasing the current densities to a higher level, while at the same time reducing the amount of platinum used over a factor of 100 and nowadays, the Pt loading of the catalyst layer has been reduced to almost 0.2 to 0.4 mg/cm² [2, 4].

1.4.4 Bipolar Plates

The voltage produced by a single cell is quite small. Thus, in order to produce usable voltage, many cells have to be connected in series, and, the combination of such cells is called a stack. The bi-polar plates serve the following functions;

- connect cells in series (stacks),
- collect current,
- provide means of fuel or oxidant distribution evenly in the cell,
- cooling of the cell.

For connection and current collection, the bipolar plates are usually made of high electrically conductive material, e.g., graphite or stainless steel. For the distribution of fuel and oxidant, these plates have channels cut in them so that gas can flow over the faces of electrodes. At the same time, they are made in such a way that they provide a good electrical contact with the surface of each electrode.

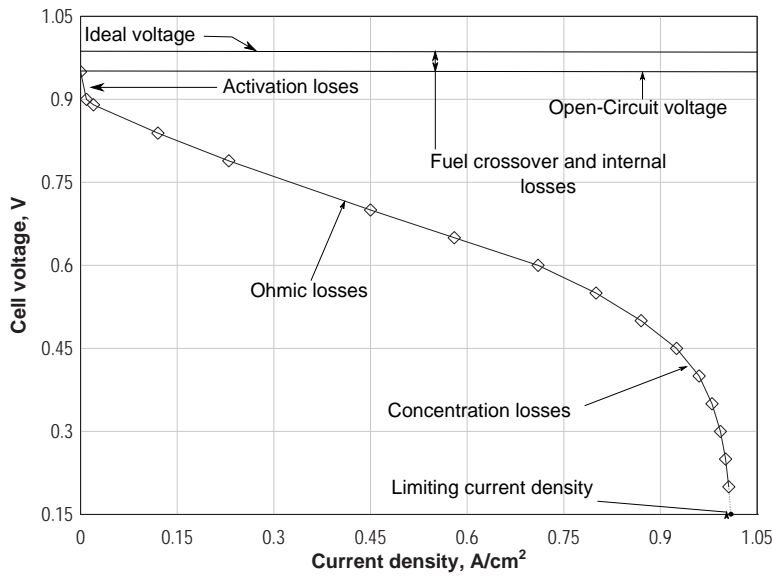


Fig. 1.2: Potential losses in a PEM fuel cell.

1.5 Fuel Cell Irreversibility

For given operating conditions (i.e., temperature and pressure etc.) and when the circuit is open, it is expected that the cell potential is approximately equal to the ideal or theoretical voltage. However, it is very common that this voltage (generally called the open circuit voltage, OCV) is always less than the theoretical or ideal voltage suggesting that there are always some losses in the fuel cell even when it is not connected to any load. In the closed circuit configuration, i.e., when the cell is connected to a load, the potential is expected to drop even further due to the reason explained below [5];

- kinetics of the electrochemical reactions,
- internal electrical and ionic resistance,
- difficulties in getting the reactants to reaction sites,
- internal (stray) currents,
- crossover of reactants.

Different types of voltage losses (or sometimes referred to as the polarization or the overpotential) are presented in Fig. 1.2 and briefly explained here;

1.5.1 Activation Losses

For every reaction, a certain amount of energy barrier has to be crossed to proceed. In fuel cells, electrochemical reactions are occurring at the electrodes. Some of the voltage

generated is lost in driving these electrochemical reactions. This type of loss is highly nonlinear and results in a sharp decrease at higher voltages. These losses occur both at the anode and the cathode of the cell. However, the oxygen reduction reaction requires higher overpotential and is almost four to six times slower than the hydrogen reduction reaction [6].

1.5.2 Ohmic (Resistive) Losses

These losses represent the wastage of energy as heat when electrons and protons flow through the respective materials. The ohmic losses are proportional to the voltage and current density, therefore, depicting linear behaviour. They are also sometimes called the resistive losses. These losses are expressed by the Ohm's law;

$$\Delta V_{\text{ohm}} = I \cdot R \quad (1.4)$$

where I is the current density and R represents the total cell resistance (including ionic and electronic). However, the electronic resistance in the PEM fuel cell is quite small when compared to the protonic resistance of the material.

1.5.3 Concentration Losses

The performance reduction due to low concentration of fuel or oxidant at higher currents are referred to the mass transport losses or concentration losses. These losses are considerable at higher currents when the consumption rate of the reactants is much higher and there is lack of transport of reactants to the reaction site. These type of losses are also highly nonlinear and can be observed as a sudden drop in voltage at higher current densities.

The reactant concentration at the catalyst surface is dependent on the current density [5]. The consumption rate of reactants increases by increasing the current density and an imbalance is created when the diffusion rate to the catalyst surface is exceeded by the consumption rate and the current density does not increase any more. The current density at a such scenario is called the limiting current density and determines the maximum that can be achieved by a PEM fuel cell at given conditions.

1.5.4 Fuel Crossover and Internal Currents

As can be seen in Fig. 1.2, the open circuit voltage in the cell is always less than the ideal or theoretical voltage. This is because the membrane material or electrolyte is not a perfect insulator for the electronic current and there is always some amount of short circuiting. Additionally, one of the other purposes of the electrolyte is to act as the wall between the two terminals of the cell and protect against the crossover of the reactants from both sides, but, in reality, such cross-over exists and some degree of idealism is lost.

Combining all the losses and representing the cell voltage in terms of the open circuit voltage, Fig. 1.2, the equation reads as;

$$V_{\text{cell}} = V_{\text{open circuit}} - V_{\text{activation}} - V_{\text{ohmic}} - V_{\text{concentration}} \quad (1.5)$$

where,

$$V_{\text{open circuit}} = V_{\text{ideal}} - V_{\text{cross-over}} \quad (1.6)$$

1.6 Motivation for this Work

PEM fuel cells have been envisioned as the next generation of environment friendly energy alternatives, especially in automotive industry that has been much dependant on fossil fuels in present times. Fuel cells on the other hand, offer promising application because of their low operating conditions with low to zero emissions, a modular structure, quick start-up time, corrosion resistance and high power density [7].

In recent years, the efforts targeted in achieving an in-depth understanding of the multiphysics within PEM fuel cells have gained a lot of attention in the research community to make them commercially viable and get the desired output levels. An outlook of PEM fuel cells has a deceptive presentation as being very simple and straightforward piece of equipment in both manufacturing and service. However, turning around the coin indicates that they are not more simple than any other energy production devices, and quantifying and measuring all the processes and phenomena inside PEM fuel cells is not only impossible [8] but the highly reactive environment also makes it quite difficult to measure even simple parameters like temperature, pressure, electric potential and species gradients, etc. [9]. In recent years, much critical work has been performed in various disciplines of PEM fuel cells from basic electrochemistry to design of stacks, but, many issues are still pending and need to be resolved for commercial viability and many improvements are deemed necessary to lower some of the raised eye brows about the future of PEM fuel cells as an alternative energy production unit.

It is well established that cathode performance is one of the key issues still under intensive investigation without any proper remedy yet proposed [10]. The important factors affecting the cathode performance are [11];

- slow reaction kinetics,
- formation of liquid water and water management,
- thermal management.

In PEM fuel cells, the OR reaction is the rate determining step for the overall electrochemical reactions. Despite the active research in improving the physio-chemical behaviour of the cathode catalyst it has been determined that the OR reactions are about four to six times slower than the hydrogen oxidation reactions occurring at the anode [11, 12]. Formation of liquid water at the cathode of PEM fuel cells is another major contributor to the under-grade performance of the cathode, especially at high loads by blanketing

the reaction sites by making them unavailable for three-phase contact and blocking of the gaseous passage through the porous media.

The numerical computation of fuel cell models have proven to be a valuable tool for the researchers helping them in undertaking reliable and accurate simulations for studying the performance. However, previously there have been no complete and generic computational models for PEM fuel cells which can account for all the complexities and multiphysics processes in a single mathematical framework [6, 7, 13].

In this thesis, an attempt has been made to collect all the phenomena at one platform and study the behaviour and the response of the fuel cell. The work is divided in two parts, i.e., macroscale and the microscale simulations. The macro simulations are performed on a single cell with considering all the transport mechanism such as species, heat, charge and liquid water. The salient features of this numerical work consist of;

- agglomerate model for electrochemical reactions,
- quantification of water movement across the membrane,
- introduction of validated approach for modelling transport of liquid water in porous media,
- effect of material anisotropy on the transport characteristics.

The numerical model used in this work is a three dimensional model of a PEM fuel cell with interdigitated flow field designs. The reasons for choosing such a flow field configuration are that this type of flow field helps in establishing a convective flow through the domain. Thus increases the performance of the fuel cell in terms of the reaction rate. Additionally, the shear force of the convective flow helps in removing the liquid water condensed in the gas diffusion layer, thereby reducing the cathode flooding problem [14]. Nevertheless, such scale study provides a good analysis but it is limited in scope because each parameter and property is volume-averaged and it is not possible to distinguish the response of each material phase separately.

In microscale simulations, only a section of the catalyst layer has been selected and each material phase has been developed distinctively in order to categorize each physical process according to the material representation of the catalyst layers. However, due to high computational power demands at this scale, the model is limited to single phase flow only.

*“James is driving the future of cars ...
... and it’s powered by hydrogen”*

2 Modelling Approaches

The PEM fuel cell modelling has received special attention in the last decade and a variety of models have been proposed ranging from purely models of fluid flow to the models for the entire stack and systems. However, in this chapter, the focus is limited to numerical models of unit cells keeping in mind the multiphase flow coupled with reactions and water phase change. The main theme of this chapter is to highlight the shortcomings and various discrepancies still present in the modelling approaches.

2.1 Revision of PEM fuel cell Models

In the last decades, a lot of effort has been spent on the PEM fuel cell modelling. There have been various models produced based on various analytical, and multidimensional PEM fuel cell approaches. Among all, the pioneering work related to PEM fuel cell modelling based on semi-empirical formulations derived from membrane experimental data was presented by Bernardi and Verbrugge [15], Springer et al. [16] and Nguyen and White [17]. Later on, Wang et al. [18], developed an advanced two dimensional model for two phase flow and species transport in PEM fuel cell using a multiphase mixing model. Despite the comprehensiveness of this modelling approach, it was limited to the cathode side only.

Further on, an improved version of a multicomponent mixture model by Wang and Cheng [19] was produced in two dimensions describing the two phase flow in the channels, and further the gas diffusion layer by You and Liu [20]. Although, the two dimensional models are well enough to predict the overall cell performance in the rate limited regimes, however, when mass limitation effects come into consideration, the accuracy of such models is highly dubious as they do not consider the geometric constraints of the mass transport [7].

Dutta et al. [21] developed a three dimensional model for PEM fuel cells configured to match the model predictions by Yi and Nyugen [22, 23] and Fuller and Newman [24].

To incorporate the water transport effects in three dimensions, Mazumder and Cole [25] developed an extensive model with multiphase transport effects on the performance. One of the key findings of their work was to accurately capture the localised water saturation levels and predict the actual performance of the cell, not only a three dimensional model but also the multiphase flow modelling is necessary.

He et al. [26] also performed multiphase simulations of PEM fuel cell. In their model, the droplet size of water was taken as the prime parameter to study the multiphase flow. A multiphase mixture model was applied to a 3D geometry. The interaction effect between the phases was studied by considering droplet size, drag coefficient, Reynolds number, velocity and droplet relaxation time. The equation for calculating the droplet size was adopted from Zhang et al. [27]. The advantage associated with this model is that it includes the effect of liquid water removal from the channels of the PEM fuel cell. In this work, all the simulations were performed on a commercial CFD software. Yuan and Sundén [28] also developed a 3D model to understand the effect of liquid water on cell performance. The model presented is a half-cell model considering cathode only because of its slower kinetics. The electro-chemical reactions were modelled to occur in a thin layer while simulating the flow in GDL and the channels. The salient features of this work were the use of combined thermal boundary conditions and mass transfer along with the effect of saturation on current density profile. The calculation domain was discretized by the finite volume method and a combination of uniform and non-uniform grid spaces. The simulations were performed using an in-house CFD code. The saturation was evaluated based on the saturation pressure and the local temperature of the flow.

Meng [29] presented a multidimensional two-phase model including a microporous layer sandwiched between the catalyst layer and the GDL. A microporous layer has been found to reduce the water saturation levels thus enhancing the oxygen transport to the reaction sites and the efficiency [30]. This model has enhanced techniques employed to properly incorporate the interfacial liquid water transport phenomena between the different porous media. Furthermore, the effects of the current collector and the gas flow channel on the saturation of the porous media have also been explicitly studied. The results of this model were verified with high resolution neutron imaging data [31] and other numerical data. Zhou et al. [32] have also presented a multiphase and multicomponent two dimensional model of a PEM fuel cell with pressure and phase change effects to further understand the influence of the inlet humidification and pressure. One of the major assumptions in this model was that liquid water was assumed to exist in form of small droplets with no volume. Berning and Djilali [33–35] also carried out series of three dimensional work to study the effects of temperature and water management on the performance of fuel cells. In their work, a single fuel cell was divided into one main and three sub-domains. All the domains were coupled through adjustment of appropriate boundary conditions for the interfaces between the subdomains. Similarly, Hu et al. [36, 37] also developed and analysed a two phase PEM model considering species transport in both anode and cathode sides. A special consideration was given to the impact of ribs on the species transport and SIMPLE algorithm with fourth order Runge-Kutta method was used in their model.

2.2 Modelling Discrepancies

With advances in computer technologies and enhanced speeds, CFD modelling approach has provided scientists and engineers with internal anatomy of fundamental processes of a PEM fuel cell [38]. To date many models for PEM fuel cells have been proposed with varying complexity and texture, however, there is no single complete model that would effectively and efficiently explain the phenomena altogether. Nevertheless, for a descriptive model of PEM fuel cell, Biyikoğlu [13] has outlined basic conditions or processes, inclusion of which can result in a descriptive model, given as;

- balanced charge distribution and flow,
- control of water flow,
- efficient removal of liquid water,
- removal of excessive heat.

Although, basic outline, as explained above, is very useful in developing a CFD model of PEM fuel cells, as ultimate and complete PEM fuel cell model is quite difficult to be developed due to inherent limitations of the analysis and outputs desired. The main limitations still blocking the researchers from attaining the ultimate goal of completeness, as given by Mench [39], are the inclusion of the physico-chemical phenomena, knowledge of the transport phenomena, computational power and proper validation of the models.

Apart from the inherent limitations of CFD modelling, there are still some basic issues that must be accounted for to increasing the accuracy of the numerical predictions. These have been stated in segregated work by many researchers [6, 39] and are briefly discussed in the forthcoming sections.

2.2.1 Anisotropy of Species Diffusion in GDL

Mostly, for the fabrication of the gas diffusion media, two types of materials are commonly used;

- carbon cloth,
- carbon paper.

The common fabrication component in both the material types is the carbon fibre. In fabrication of carbon cloth, woven tows of carbon fibre are used, whereas, randomly laced fibres are used for the carbon paper. The pore diameter for both the materials is approximately 10 μm and the porosity fluctuates between 40 to 60%. One of the salient features of such fabrication from carbon fibres is that the material properties vary in spatial uniformity and show high degrees of anisotropy.

In PEM fuel cells, prehumidified air with multicomponents is supplied at the cathode side, while fuel, i.e., H_2 , is supplied at the anode side which is also humidified before entering the inlet channel. In order to carry out the electrochemical reactions at the catalyst layer,

both the air and fuel have to diffuse through the gas diffusion layer. Mathematically this is given as;

$$\vec{J}_i = \rho D^{\text{eff}} \nabla X_i \quad (2.1)$$

where \vec{J} , D^{eff} and X are the diffusion flux, the effective diffusivity and the mass fraction of the species in consideration, respectively and i identifies the species under consideration. In order to correct the diffusivity for the geometric constraints of the porous media, a mathematical factor is usually employed, so called the Bruggeman correction or approximation [33].

$$D^{\text{eff}} = \varepsilon^\tau D \quad (2.2)$$

where τ is the tortuosity, representing the increase in the path length due to porous media, and given as [40];

$$\tau = \left(\frac{\text{actual path length}}{\text{point to point path length}} \right)^2 \quad (2.3)$$

A typical value of τ generally applied in PEM fuel cells is 1.5 [33]. The Bruggeman correlation has been a popular tool in CFD modelling of fuel cells due to its simplicity. However, it assumes that the GDL is isotropic, which is not always a fair assumption. Flückinger et al. [41] did a comparative study of common GDL materials, measuring the anisotropy, and found that in general, the in-plane diffusivity is on average about twice as large as the through-plane diffusivity. They also found that the amount of Teflon used in the gas diffusion layer has a strong effect on diffusivities, where addition of Teflon even in smaller quantities will sharply increase the diffusivity. To account for this anisotropy in modelling, there have been several attempts by different research groups.

The diffusion models can be correlated to structural parameters as well as liquid water saturation according to the following general model [42];

$$D^{\text{eff}} = D f(\varepsilon) g(s) \quad (2.4)$$

where $f(\varepsilon)$ is a function of the structural parameters only, corresponding to the transport of gaseous species in a dry GDL, and the function $g(s)$ takes into account the impact of liquid water saturation. Tomadakis and Sotirchos [43] suggested a percolation type correlation which was later expanded by Nam and Kaviani [30]. Das et al. [44] developed an expression for relative diffusivity using an effective bulk modulus formulation originally developed to investigate the effective conductivity of a coated sphere assemblage. Wu et al. [42] developed an expression using pore network modelling approach, also accounting for the impact of different degrees of Teflon layer coating, and Wu et al. [45] developed a

Table 2.1: *Different models for capturing anisotropic effects on the gas diffusion in the GDL.*

Contributor	$f(\varepsilon)$
Tomadakis and Soitchos [43]	$\varepsilon \left(\frac{\varepsilon - \varepsilon_p}{1 - \varepsilon_p} \right)^\alpha$
Das et. al [44]	$1 - \left(\frac{3(1 - \varepsilon)}{3 - \varepsilon} \right)$
Wu et. al [42]	$\exp \left(\varepsilon - \frac{1}{0.222} - 0.161 C_p \right)$
Wu et al. [45]	$\frac{\varepsilon(2 - d_f)(\lambda_{\max}^{1+d_t-d_f} - \lambda_{\min}^{1+d_t-d_f})}{L_0^{d_t-1}(1+d_t-d_f)(\lambda_{\max}^{2-d_f} - \lambda_{\min}^{2-d_f})}$

fractal model for determining the effective diffusivity, stressing the importance of impact by Knudsen diffusion. Table 2.1 summarizes some of the models presented for anisotropic diffusion. In the model by Tomadakis and Sotirchos, ε_p is a percolation threshold and α is an empirical constant; in the model by Wu et al., C_p is the teflon content, and λ_{\max} , λ_{\min} , L_0 , d_t , and d_f are maximum and minimum capillary diameter, GDL thickness, tortuosity fractal dimension and area fractal dimension as used by Wu et al [45], respectively. The function $g(s)$ in Eq. (2.4) is most oftenly given in the form;

$$g(s) = (1 - s)^m \quad (2.5)$$

where s is the liquid water saturation, and m is an empirical constant. The constant m varies a lot depending on the model being used: Nam and Kaviani [30] suggested a value of 2.0, and Wu et al. [42] suggested that m should vary between 2.6 and 3.6 depending on of the GDL structure. For the case presented in Eq. (2.5) the value of m is usually 1.5. In this work, the expression developed by Nam and Kaviani [30] has been applied, and with the numerical values inserted for percolation threshold and the empirical constant m , it reads:

$$D^{\text{eff}} = D f(\varepsilon) g(s) = D \varepsilon \left(\frac{\varepsilon - \varepsilon_p}{1 - \varepsilon_p} \right)^\alpha (1 - s)^{2.0} \quad (2.6)$$

$$\alpha = \begin{cases} 0.521 & \text{in-plane} \\ 0.785 & \text{through-plane} \end{cases}$$

where the percolation critical value, ε_p is taken as 0.11 [46]. Fig. 2.1 compares the correction factors for the Bruggeman correction and the model presented by Nam and Kaviani [30]. As can be seen in the figure, the Bruggeman correction always over predicts the correction factor compared to both of the in-plane and through-plane correction factors. Thus, the diffusion of species predicted by the Bruggeman model will always be overestimated, which may result in inaccurate high current densities.

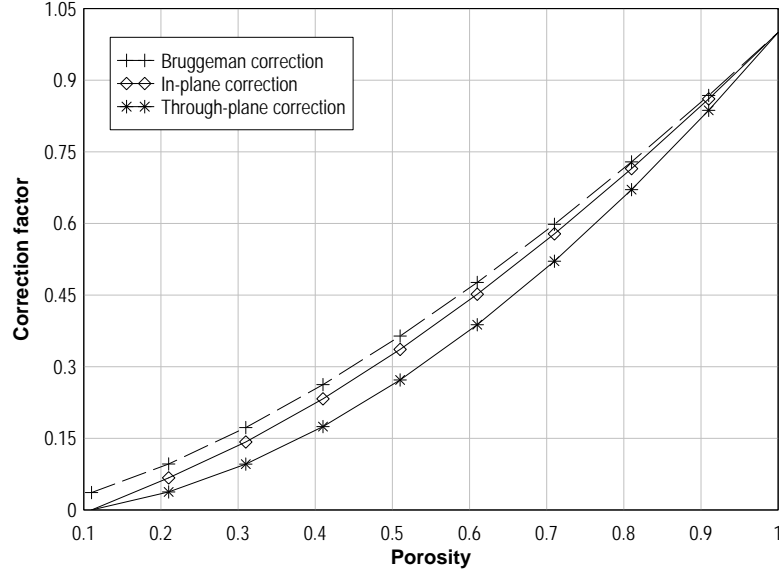


Fig. 2.1: Comparison of correction factors by Bruggeman correction [33] and anisotropic correction [30].

2.2.2 Effective Charge Conductivity

The catalyst layer in the PEM fuel cell consists of four types of material phases, named as;

- platinum particles,
- carbon particles,
- ionomer (membrane phase),
- voids (pores or open space).

The Pt phase in form of fine particles is dispersed on the larger carbon particles (Cobot™) called the Pt|C assemblage. The Pt|C forms the agglomerate which is dispersed in the ionomer (membrane) phase surrounded by the open space. The schematic representation of the three phase composite (carbon and Pt particles are assumed to be in one phase i.e., the solid phase) is given in Fig. 2.2. The effective proton conductivity of the three phase composite is given as [44];

$$(\sigma^{\text{eff}})_{\text{CL}} = \sigma_m + \frac{3(1 - f_s - f_m)\sigma_m}{(f_s + f_m) - \frac{3\sigma_m}{\sigma_m - \sigma_v}} \quad (2.7)$$

where σ_m is the protonic conductivity of the ionomer or the membrane phase in the catalyst layer and σ_v represents the void conductivity of protons. f_m and f_s are the

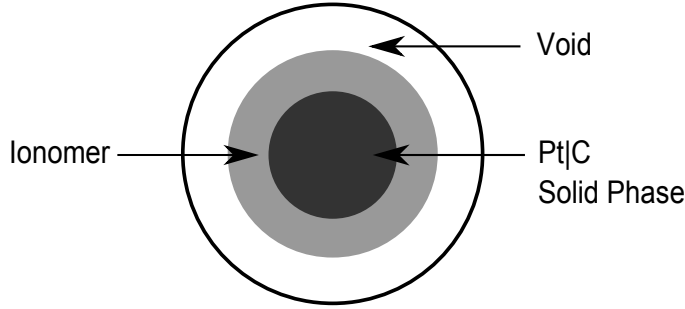


Fig. 2.2: Schematic of a simple material phase construction in the catalyst layer of PEM fuel cells.

respective volume fractions of the ionomer and the solid phases in the catalyst layer, such that;

$$f_m + f_s + f_v = 1 \quad (2.8)$$

In the catalyst layer of a PEM fuel cell, the void space is filled with the reactant gaseous species, hence, the protonic conductivity of the void space is zero, i.e., $\sigma_v = 0$. In case when the void space is filled with liquid water due to the saturation effects, there can be some protonic conduction but it is negligible as compared to the conduction in the ionomer due to the absence of the free acidic groups [44]. The effective protonic conductivity of the ionomer in the catalyst layer is then given as;

$$(\sigma^{\text{eff}})_{\text{CL}} = \sigma_m - \frac{3\lambda_m(1-f_m)\sigma_m}{3-f_m} - \frac{3\lambda_m f_v \left(\sigma_m - \frac{3(1-f_m)}{3-f_m} \right)}{2+f_v} \quad (2.9)$$

where λ_m is the multiplication factor which is assumed to be unity [44]. The volume fraction of the ionomer phase in the catalyst layer can be calculated as [47];

$$f_m = \frac{\%N}{(1-\%N)\rho_m} \frac{m_{\text{Pt}}}{(\%Pt)\delta_{\text{CL}}} \quad (2.10)$$

where ρ_m is the density of the ionomer phase and $\%N$ is weight percentage of the ionomer in the total sum of the ionomer and the solid particles. Similarly, m_{Pt} and $\%Pt$ represent the Pt loading and mass percentage of the platinum in the combined total mass of the Pt and carbon, respectively.

Among various techniques available to evaluate the effective properties of the composite system in accurate form [44, 48, 49], Bruggeman approximation has been used widely especially by CFD analysts because of its broad range and application diversity. The

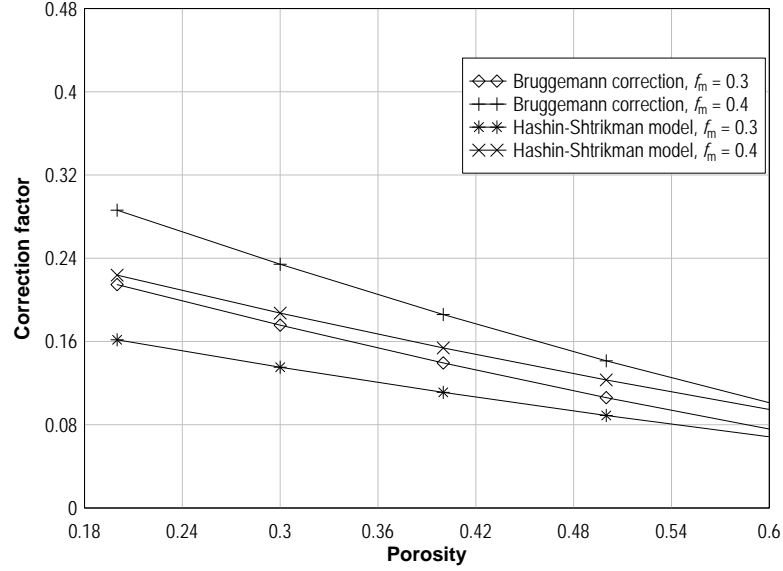


Fig. 2.3: Comparison of the models to calculate the effective protonic conductivity of the catalyst layer in PEM fuel cell. For simplification, it has been assumed that $\sigma_m = 1$.

bruggeman correlation adopted for protonic conductivity of ionomer in PEM fuel cells is given as;

$$(\sigma^{\text{eff}})_{\text{CL}} = \sigma_m (f_m (1 - f_v)) \quad (2.11)$$

However, Das et al. [44], recently compared the bruggeman model to the Hashin-Shtrikman model [50] and calculated the applicable conditions and found that the applicability of the correlations depends on the porosity or the volume fraction of void, i.e., Bruggeman approximation shows a better agreement for $0 < \varepsilon < 0.2$. But for porosity range of $0.2 < \varepsilon < 0.6$, the Hashin-Shtrikman model has better agreement for the effective protonic conductivity. Fig. 2.3 compares the Bruggeman model to the one outlined here for two different ionomer phase volume fraction ($f_m = 0.3$ and $f_m = 0.4$). It can be seen that for both the cases, the correction factor predicted by the Bruggeman approximation over-predicts the effectiveness to its respective counterpart.

Similarly, for the electronic conduction, both the void and ionomer phases act as electrical insulators and only the solid phases conduct electrons. However, because the electronic conduction in the catalyst layer is much higher than the protonic conduction, it is safe to assume that the effective electronic conduction is close to its maximum value and also the electronic conduction is less sensitive in causing any performance loss in the PEM fuel cells.

2.2.3 Anisotropic Permeability

The permeability of GDL materials is important to consider for a serpentine or an interdigitated fuel cell design where convective flow is of importance. Pharoah [51] showed that the onset of convective flow in GDL occurs at permeabilities of 10^{-13} m^2 , and because, virtually all experimental measurements of the gas diffusion layer materials are larger than this value, convective flow can safely be assumed to occur. Pharoah [51] also explored GDL as orthotropic media, and found that the in-plane parameter is the most significant parameter. There is also a pressure drop in the GDL in the in-plane direction due to a pressure difference from channel to channel making convective flow between channels possible and in the through-plane direction due to the consumption of reactants in the fuel cell [52]. Gostick et al. [53] investigated the difference between the in-plane and the through-plane permeability of several common GDL materials, and found that the permeability can vary by a factor of two between the different directions, and thus the anisotropic permeability is an important parameter to take into consideration when modeling fuel flow through gas diffusion layers. It is common to evaluate the permeability of the GDL as orthotropic, as seen in the models by Pasaogullari et al. [54] and Yang et al. [55]. Both of the aforementioned models use an in-plane permeability of $3.00 \times 10^{-12} \text{ m}^2/\text{s}$ [56] and a through-plane permeability of $8.69 \times 10^{-12} \text{ m}^2/\text{s}$ [57]. It is interesting to note that other experimental sources cite the in-plane permeability to be higher than the through-plane permeability. Becker et al. [58] also showed both experimentally and numerically that the permeability is dependant on the porosity of the material, and the same conclusion was reached by van Doormaal and Pharoah [52]. In the work by Van Doormaal and Pharoah to determine the porosity, permeability, flow direction and fiber directions to have a deeper insight of GDL, the geometry was generated using the modified Monte Carlo technique by Hamilton [59]. The alignment of fibers was varied from 0 to 90°, i.e., from parallel to perpendicular directions and numbers of cases were simulated for all directions with porosity ranging from 0.6 to 0.81. The proposed relation between porosity and the permeability of the GDL by the authors [59] is given as;

$$\mathbf{K} = \begin{cases} 0.26 \frac{\varepsilon^{3.6}}{1-\varepsilon} r^2 & \text{in-plane} \\ 0.28 \frac{\varepsilon^{4.3}}{1-\varepsilon} r^2 & \text{through-plane} \end{cases} \quad (2.12)$$

where r is the fibre radius and predictions were found to be within 95% of the prediction by Carmen-Kozeny equation [60]. In CFD codes, to accommodate the effect of the anisotropy of the permeability of the gas diffusion layer, a tensor is utilized and given as;

$$\mathbf{K} = \begin{bmatrix} K_x & 0 & 0 \\ 0 & K_y & 0 \\ 0 & 0 & K_z \end{bmatrix} \quad (2.13)$$

where K_x , K_y and K_z represent the different permeabilities in x, y and z directions of the analysis domain in the gas diffusion media of the PEM fuel cells.

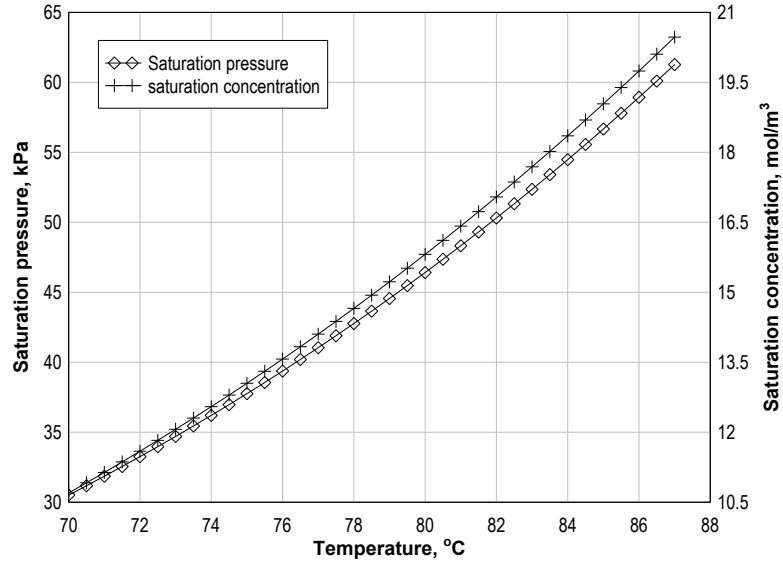


Fig. 2.4: *Dependence of saturation pressure and concentration on the temperature.*

2.2.4 Anisotropy of Thermal Conductivity

The thermal management in PEM fuel cells is one of the key factors affecting the performance and dictates the life span of cell. The energy conversion efficiency of PEM fuel cells is roughly 50% and almost the same amount of heat is generated. Additionally, the temperature variation tolerance of PEM fuel cells is only about 5 °C [61] which is because of the high dependency of the ionomer on hydration levels for the protonic conduction which in turn is a strong function of the temperature that also controls the water activity. Fig. 2.4 compares the saturation concentration and pressure to the temperature. As can be seen, almost 1 °C change in temperature brings about approximately 5% change in the saturation pressure and 4% change in the saturation concentration of the water vapours.

Thus, the information of accurate temperature distribution inside PEM fuel cells is very important not only to have higher efficiencies but also for the longevity [54]. In regard to the temperature distribution in PEM fuel cells, a lot of work has been done [26, 28, 61–65] but the thermal management of the GDL needs further attention due to large amount of heat produced in the cathode catalyst layer that must travel through the GDL in order to reach the cooling plate. The thermal conductivity of the GDL materials are anisotropic, due to the alignment of their fibres. Thermal conductivity in the GDL is often treated as isotropic. However, the thermal conductivity is stated as ~12 times higher for the in-plane as compared to the through-plane direction by the manufacturer [54], which can lead to large anisotropic effects in the heat conduction. Bapat and Thynell [66] investigated the effects of anisotropic conductance explicitly and found that an in-plane conductivity that is higher than the through-plane conductivity leads to a more uniform heat distribution,

while a lower in-plane conductivity can lead to undesirable local hot spots, and that the in-plane conductivity is of the highest importance in order to keep the thermal gradient to a minimum. Pasaogullari et al. [54] compared the case when the heat conduction is taken to be isotropic with the anisotropic case and reached similar conclusions that the anisotropic case displayed a more uniform temperature distribution. The conduction of heat in the PEM fuel cells can be quantified as;

$$\mathbf{J}_{\text{cond}} = -k^{\text{eff}} \cdot \nabla T \quad (2.14)$$

where k^{eff} is the effective thermal conductivity of the medium (different methods to calculate the effective diffusivity for the porous media are explained in Sec. 3.4 but the thermal conductivity of the solid phase is anisotropic in nature that must be managed for calculating the overall thermal conductivity of the porous medium.

$$k_{\text{eff}}^{\text{solid}} = \begin{bmatrix} k_x^{\text{solid}} & 0 & 0 \\ 0 & k_y^{\text{solid}} & 0 \\ 0 & 0 & k_z^{\text{solid}} \end{bmatrix} \quad (2.15)$$

The conduction heat flux for the porous media is given as [54];

$$\mathbf{J}_{\text{cond}} = j_x \mathbf{i} + j_y \mathbf{j} + j_z \mathbf{k} \quad (2.16)$$

where j_x , j_y and j_z are the heat fluxes in respective x , y and z directions.

2.3 Multiphase Flow Models and Water Phase Change

One of the main advantages of PEM fuel cell, as compared to other types of cells, is that they operate at low temperature conditions (<100 °C). Since the chemical product of the PEM fuel cells is pure water, the advantage of having low operating temperature turns into a complex problem for the PEM technologists. The condensation of water vapours into the liquid state is one of the most common phenomena in PEM fuel cells and represents a multiphase flow regime. For PEM fuel cells, many multiphase models have been proposed and used with varying complexity.

Broadly, the multiphase models can be subdivided into two main classes, as shown in Fig. 2.5. The basis of the division into two classes is done on the inter-effect of each phase on one another. In the liquid independent class, it is assumed that the only driving force is the surface tension for the liquid phase, whereas, in the convection class, the pressure of gas phase is equally contributing on the liquid phase transport. Another distinguishing feature of the two main classes is that for low saturation cases, the convection class is not applicable [67]. One of the simplification for all multiphase models applicable to porous media, as encountered in fuel cells, is that the flow is considered non inertial. The advantage of such an assumption is that it provides a well behaved laminar flow.

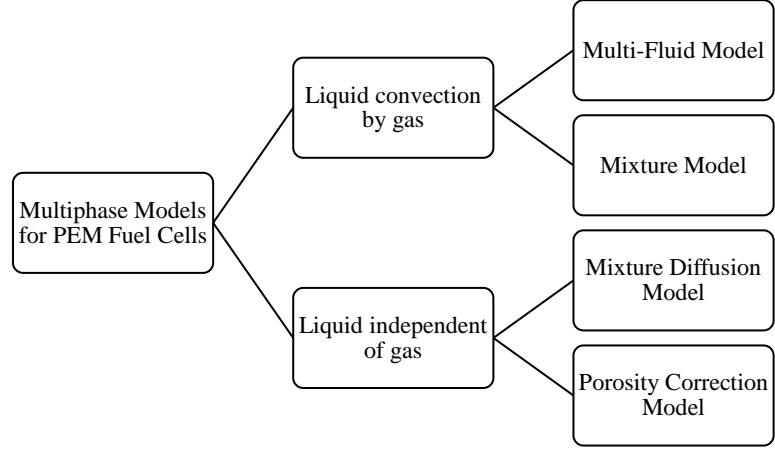


Fig. 2.5: *Classification of multiphase models.*

2.3.1 Multi-Fluid Flow Model

The tracking of the interface(s) between the phases is accomplished by solving the continuity equation for the volume fraction of each phase. For the q^{th} phase, this equation has the following form;

$$\frac{1}{\rho_q} \left[\frac{\partial}{\partial t} (\alpha_q \rho_q) + \nabla \cdot (\alpha_q \rho_q \mathbf{V}_q) \right] = S_{\alpha_q} + \sum_{p=1}^n (\dot{m}_{pq} - \dot{m}_{qp}) \quad (2.17)$$

where \dot{m}_{pq} is the mass transfer from phase q to phase p and \dot{m}_{qp} is the mass transfer from phase p to phase q , respectively, and α_q is the volume fraction of phase q . Similarly, the momentum equation for multi-fluid model for the q^{th} phase is given as;

$$\begin{aligned} \frac{\partial}{\partial t} (\alpha_q \rho_q \mathbf{V}_q) + \nabla \cdot (\alpha_q \rho_q \mathbf{V}_q \mathbf{V}_q) = & -\alpha_q \nabla p_q + \nabla \cdot (\alpha_q \mu_q \nabla \mathbf{V}_q) \\ & + \sum_{p=1}^n (\dot{m}_{pq} \mathbf{V}_{pq} - \dot{m}_{qp} \mathbf{V}_{qp}) + \vec{F} \end{aligned} \quad (2.18)$$

where $\sum_{p=1}^n (\dot{m}_{pq} \mathbf{V}_{pq} - \dot{m}_{qp} \mathbf{V}_{qp})$ balances the change in momentum due to the transfer of mass from one phase to the other. Because in PEM fuel cells, the two phases are air containing water vapour and the liquid water, Eames et al. [68] have provided an empirical relationship for the mass transfer between the water vapour and the liquid water at the interface of the two phases;

$$\dot{m} = \gamma_k \left(\frac{M_{\text{H}_2\text{O}}}{2\pi R} \right)^{1/2} (P_{\text{sat}} - P_{\text{wv}}) \quad (2.19)$$

where p_{sat} and p_v are the saturation and partial pressure of the water vapours, respectively. γ_k is the kinetic evaporation constant under the thermal equilibrium conditions between the two phases and ranges from 0.001 to 1 [69].

When utilizing the multifluid approach for PEM fuel cells, where phase p is assumed to be in the liquid state in the porous media, the pressure correction for the capillary effect is done by adding the term [70];

$$-\nabla p_p = - \left(\frac{\partial p_c}{\partial \alpha_p} \nabla \alpha_p + \nabla p_q \right) \quad (2.20)$$

where p_c is the capillary pressure. In order to correct the mechanism to account for the effect of porous media, the volume fraction α of each phase (p and q) is multiplied with the porosity ε (explained in Sec. 3.1) of the medium.

2.3.2 Mixture Model

In contrast to multi-fluid model where both the continuity and momentum equations are solved separately for each phase, in a mixture model the equations are solved for the mixture of all phases. The continuity equation for the mixture model is given as;

$$\frac{\partial \rho_m}{\partial t} + \nabla \cdot (\rho_m \mathbf{V}_m) = 0 \quad (2.21)$$

where ρ_m is the density of the mixture of the two phases and \mathbf{V}_m is the volume average mixture velocity, calculated as;

$$\mathbf{V}_m = \frac{\sum_{p=1}^n \alpha_p \rho_p \mathbf{V}_p}{\rho_m} \quad (2.22)$$

The momentum equation for the mixture can be obtained by summing the individual momentum equations for all phases. It can be expressed as;

$$\frac{\partial}{\partial t} (\rho_m \mathbf{V}_m) + \nabla \cdot (\rho_m \mathbf{V}_m \mathbf{V}_m) = K \left[\frac{K_{rp}}{\mu_p} \nabla p_p + \frac{K_{rq}}{\mu_q} \nabla p_q \right] \quad (2.23)$$

where μ_p and μ_q are the respective phase viscosity. K is the absolute permeability of the porous medium where K_{rp} and K_{rq} are the relative permeabilities of each phase because of the reduction in volume occupied by each phase and are calculated as;

$$K_{rp} = \frac{K_p}{K} = \alpha_p \quad \text{and} \quad K_{rq} = \frac{K_q}{K} = \alpha_q \quad (2.24)$$

Since in mixture model, the continuity and the momentum equations are solved over the mixture, the individual velocities of each phase are extracted in the post processing stage [67].

2.3.3 Moisture Diffusion Model

Moisture diffusion model is based on the unsaturated flow theory [19] and it is assumed in this model that capillary pressure is the only driving force for the liquid. One of the general limitation of this model is that it is applicable only when there is capillarity such as in porous media. In this approach, the continuity and the momentum equations are solved only for gas phase while for the liquid phase, a separate conservation equation for the volume fraction of liquid phase is solved, given as [19];

$$\frac{\partial}{\partial t}(\rho_l s) + \nabla \cdot (\rho_l \mathbf{V}_l s) = \dot{m} \quad (2.25)$$

here the subscript l represents the liquid phase while s is the volume fraction of the liquid phase. In highly resistive porous media, the convective term is replaced by the diffusive term, as;

$$\nabla \cdot (\rho_l \mathbf{V}_l s) = \nabla \cdot \left[\rho_l \frac{K_l}{\mu_l} \frac{dp_c}{ds} \nabla s \right] \quad (2.26)$$

and \dot{m} in Eq. (2.25) is the mass source due to the phase change and needs to be calculate in form of rate as in multifluid model. In order to correct the volume phase of the gases, the porosity is multiplied by $(1 - s)$.

2.3.4 Porosity Correction Model

The porosity correction model represents one of the simplest multiphase models by neglecting the transport of the liquid phase by assuming it be in stationary state. The temperature and the level of saturation is calculated iteratively by the internal energy and the density of the water in the system [71]. The volume fraction open for the gas phase is given as;

$$\varepsilon_g = \varepsilon(1 - s) \quad (2.27)$$

One of the advantages of this model is that it is highly efficient when the saturation levels are quite low.

All the multiphase models are compared against the limitations of each model and the applicability in Table 2.2.

Table 2.2: *Limitations and applicability of multiphase models.*

Multiphase Model	Limitations	Applicability
multifluid model	- number of variables is highest	- suitable for high saturation levels
	- highest requirement of computational resources	- when gas has the same influence as that of the surface tension
mixture model	- may be unstable due to coupling of the phases	
	- because gas and liquid have different velocity, convergence can be a problem at higher saturations	- gas pressure is dominant on the capillary pressure
	- no inter-phase transfer	- large pores and high permeability
	- same velocity for the liquid and gases	
moisture diffusion model	- large number of mixture quantities	
	- the influence of gas pressure is not accounted for	- When surface tension is dominant
porosity correction		- small pores and low permeability
	- no liquid transport	- very low humidity and pore size

2.4 Water Management

Formation of liquid water at the cathode of PEM fuel cells is a major contributor to the under-grade performance of the cathode especially at high loads by blanketing the reaction sites by making them unavailable for three-phase contact [11].

Different processes contributing to water formation or removal during the operation of PEM fuel cells at the cathode are; [38] (the negative mechanisms in the water source represent removal of water content while increase in water quantity inside the fuel cell is represented by the positive sources);

- oxygen reduction reaction (positive)
- electro-osmotic diffusion (positive)
- condensation of water vapour (positive)
- back diffusion (negative)
- evaporation (negative)

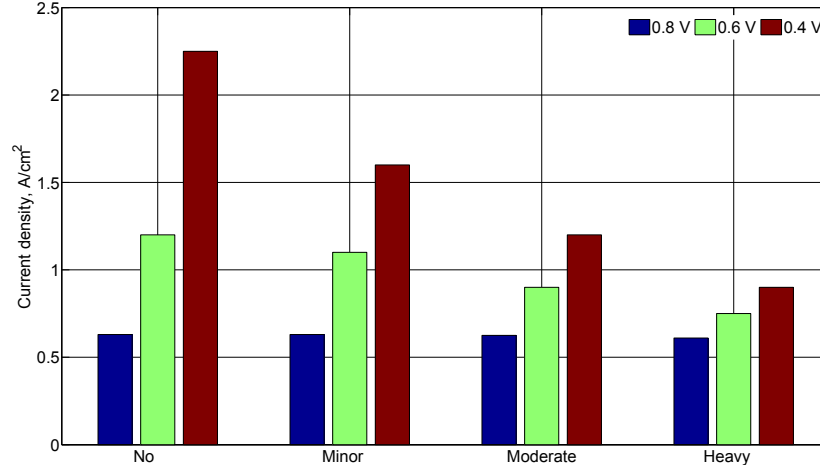


Fig. 2.6: Comparison of current density at different voltages with various levels of water flooding in the porous media.

The ion transport in form of H_3O^+ uses water molecules as a carrier from anode to cathode of a PEM fuel cell. It is estimated that one to five molecules of water are dragged per proton migration from anode to cathode side [72, 73]. Similarly, along the production of water due to OR reactions, condensation of water vapours also proves to be handy in formation of liquid water if the vapour quantity exceeds its local saturation limit in the PEM fuel cell. The anti-measures for the formation of water are back diffusion resulting due to the concentration difference in water quantity across the anode and the cathode, and the evaporation of liquid water due to high temperatures. If the formation rate of water is not balanced by the removal rate, accumulation of liquid water occurs at the cathode resulting in water flooding. This non-equilibrium of production and removal is known to cause a major performance hold-up to PEM fuel cells in terms of efficiency, stability and reliability [74, 75].

Although, water formation has been labeled as one of the performance defectors in PEM technology, many processes inside the PEM fuel cells are itself highly water dependent. As already stated, the proton migration from anode to cathode i.e., the protonic conductivity of the membrane material incorporated in low temperature ($<100^\circ\text{C}$) PEM fuel cells, is highly water dependent. The dryness of the membrane will render it from low to zero conductivity causing major suffering in performance by considerably increasing the ohmic losses [73]. To ensure proper hydration of the membrane, a balance between inlet humidification and evaporation rate has to be maintained. Thus, in overall, the formation and removal rate of water has to be closely monitored and balanced not only to avoid flooding of the cathode but also for proper wetting of the membrane.

As discussed above, the water management problem is one of the major issues related to the optimum performance and stable operation in PEM fuel cells. A comparison of different water flooding levels is given in Fig. 2.6 for the current density produced for

each operating voltage. As can be seen, when the water flooding increases, the maximum current density for a specific voltage decreases considerably. At high voltages, the current density is almost the same for all levels because at such low operating conditions the reaction rate is quite low and water formation due to both ORR and electro-osmotic drag is not significant but at the highest levels of water flooding there is decrease of almost 80% in the current density produced at 0.4 V.

In order to render PEM fuel cells viable for full scale commercialization, the water management issue has to be addressed and a proper remedy is yet to be found for this problem [10]. The minimum hydration level maintenance is comparatively easy to achieve and can be accomplished by the external humidification of air and fuel supply to the PEM fuel cells and many authors have shown that external humidification of inlet gaseous species improves the cell performance [2, 76]. However, the transport mechanism of the liquid water in the diffusion media is still under rigorous work, and knowing the fact that it is the major set back for PEM fuel cells, this field has not been fully overcome in terms of understanding the process and the effect of materials on the transport mechanism of liquid water [77].

With the advances in computing technology, computational fluid dynamics (CFD) modelling has become one of the most effective tools to study the internal anatomy of PEM fuel cells [8]. To date, number of models with varying complexity have been formulated and implemented by various researchers for the water management issue in PEM fuel cells with main focus on water saturation and the transport mechanism in the diffusion media especially at the cathode side [33, 38, 78]. However, recent analytical techniques used to capture the liquid water distribution inside the diffusion media have revealed that many of the theories and assumptions used for liquid water transport mechanism are inappropriate under normal operating conditions [79, 80]. One of the reasons for this experimental and modelling deviation is that most of the models utilize the traditional Leverett J-function [30, 81–83] for the liquid water saturation and its transport in the porous media. However, material used for manufacturing of the catalyst and porous transport layers are heterogeneous in nature with mixed wettability characteristics [77] and the Leverett J-function is not sufficient to model the transport mechanism in the porous media of PEM fuel cells. Furthermore, the effects of material hydrophobicity, compression and the temperature are also not encapsulated by the traditional relation [77, 84, 85].

2.4.1 Conventional Capillary Pressure Approach

The capillary pressure or the capillarity is the result of the pressure difference caused across the interface between the immiscible fluids which in turn is caused by the imbalance of the molecular forces at the interface [67, 77]. Mathematically, the capillarity is proportional to the ratio of the surface tension (γ) between the two fluids and the pore radius (r);

$$p_c \propto \frac{\gamma}{r} \quad (2.28)$$

Eq. (2.28) represents the microscopic capillary pressure [67]. When there is a bulk motion of the two fluids, the capillary pressure for cylindrical pores is given as [77];

$$p_c = p_{nw} - p_w \quad (2.29)$$

where p_{nw} and p_w are the pressure exerted by non-wetting and the wetting phases of fluids. However, in porous media like the one in PEM fuel cells, the surface tension between the fluid phases and the solid phase also needs to be accounted. The surface tension depends on the wettability, or the hydrophobicity characteristics of the fluid-solid interface. So, the collective representation of the capillary pressure in the porous medium can be given as;

$$p_c = p_{nw} - p_w = \frac{2\gamma \cos \theta}{r} \quad (2.30)$$

where θ is the contact angle and depicts the effects of the hydrophobicity, such that, if $\theta > 90^\circ$, the material represent hydrophobic characteristics and the gas phase is the wetting phase [67].

On the basis of the above theory, Leverett [82], in 1941, postulated a non-dimensional relationship for the capillary pressure and the saturation effects, given as;

$$J(s) = \frac{p_c}{\gamma} \left(\frac{K}{\varepsilon} \right)^{1/2} \quad (2.31)$$

This function is generally referred as the Leverett J-function. Later, Udell [83], performed series of experiments on one dimensional packed sand with porosity ranging from 0.33 to 0.39 and permeabilities from 1.39 - $10.3 \times 10^{-12} \text{ m}^2$, in order to determine the J-function in Eq. (2.31). To account for the effect of the hydrophobicity in PEM fuel cells, Pasaogullari and Wang [81] and Nam and Kaviani [30], later on, modified the Leverett J-function, such that;

$$p_c = \gamma \cos \theta \left(\frac{\varepsilon}{K} \right)^{1/2} J(s) \quad (2.32)$$

where,

$$J(s) = \begin{cases} 1.417s_w - 2.120s_w^2 + 1.263s_w^3 & \text{if } \theta < 90^\circ \\ 1.417s_{nw} - 2.120s_{nw}^2 + 1.263s_{nw}^3 & \text{if } \theta > 90^\circ \end{cases} \quad (2.33)$$

Similarly, many other authors have also presented the other types of J-functions [86], e.g., the Scheidegger's formulation [87] and the van Genuchten [88] function. However,

in PEM fuel cell modelling, the modified Leverett function, Eqs (2.32) and (2.33), have been extensively used and most of the two phase models are based on the capillary flow determined through these formulations. Nevertheless, they are still limited by some of its inherent drawback, such as;

- as for Leverett and Udell's representation, the formulations are for packed sands and there is a lack of material evaluating capillary pressure in fibrous porous media [54, 67, 70, 77],
- the calculation of the contact angle θ is also not accurate and precise [67, 77],
- the modified Leverett J-function is not capable of incorporating the heterogeneity of the material used in PEM fuel cells [77].

Thus, keeping in mind the importance of the liquid water transport and phase change in the porous media of PEM fuel cells, accurate and verified approach needs to be developed and implemented in CFD analysis.

3 Numerical Modelling

This chapter defines the governing equations used for simulation of the PEM fuel cells and is divided in two parts. The first part deals with the macroscale modelling which is a volume average technique based on the finite volume method (FVM) [89]. Whereas, the second part is dedicated to the methodology developed to reconstruct and simulate the micromodels.

3.1 Porous Media

Previously, transport in porous media had been limited to selected fields, e.g., mechanical, chemical and petroleum engineering. However, the roots to porous media studies grew in the field of geology where porous media is naturally found in sand beds and rocks, etc. Lately, the interest in porous media has been built-up due to the appearance in advanced technologies, especially fuel cells which rely on porous components for their operation.

A porous media is a network of continuously connected open spaces, called voids, in a solid matrix. The voids are filled with fluid (gas and liquid) that transports through them due to interconnectivity. In order to quantify the volume occupied by the voids in the solid matrix, the term porosity is usually referred, and it is given by;

$$\varepsilon = \frac{V_f}{V_f + V_s} = \frac{V_f}{V_{\text{tot}}} \quad (3.1)$$

where ε is the porosity or the volume fraction of the voids. And V_f and V_s are the volume of voids and the solid matrix, respectively, in Eq. (3.1). Conversely, $(1 - \varepsilon)$ is the volume fraction of the solid matrix. Alternatively, the void fraction and solid fraction can be symbolized by assuming a geometric function $g(x, y, z, t)$, which is unity (1) in void and null (0) in solid matrix, the porosity is defined as [70];

$$\varepsilon = \frac{1}{\Delta V} \int_{\Delta V} g dV \quad (3.2)$$

where ΔV is the element volume of the porous zone. However, inside the porous media, the length scales are quite different. There are two types of length scales in the porous media, i.e., the void length scale d and the system or porous zone length l . Considering PEM fuel cells, since, the void length scale is usually very small compared to the system or porous zone scale, i.e., $d \ll l$, usually a mean velocity of the fluid is computed instead of direct simulation of the transport characteristics [70]. As shown in Fig. 3.1, the actual velocity in the void is simulated using the volume-averaged velocity. For analysis of transport in the porous media, two types of velocities are often used;

- intrinsic average velocity,
- extrinsic average velocity.

The intrinsic averaged velocity (\mathbf{V}) is the volume-averaged velocity over the volume excluding the solid phase, while, the extrinsic averaged velocity (\mathbf{V}') encapsulates the entire volume including the solid phase. Both the intrinsic and extrinsic average velocities are related using the Dupuit-Forchheimer relationship, as [70];

$$\mathbf{V}' = \varepsilon \mathbf{V} \quad (3.3)$$

Having established the relationship between the different types of velocities in the porous media, the governing equations for the fluid phase can be developed assuming that the porous medium is saturated with the fluid phase.

3.2 Conservation of Mass

In terms of material phases, the porous media can be assumed to be composed of two phases, i.e., the solid and the fluid phase. The continuity equation for the fluid phase in the porous media is given as;

$$\frac{\partial}{\partial t} (\varepsilon \rho_f) + \nabla \cdot (\varepsilon \rho_f \mathbf{V}) = S \quad (3.4)$$

where \mathbf{V} is the intrinsic phase-averaged velocity and ρ_f is the average density of the fluid phase.

3.3 Conservation of Momentum

In 1856, Henry Darcy for the first time formulated the resistance to a steady, one dimensional, gravitationally driven flow in a solid matrix having uniform and isotropic properties. A relationship between the dynamic viscosity and the pressure gradient or

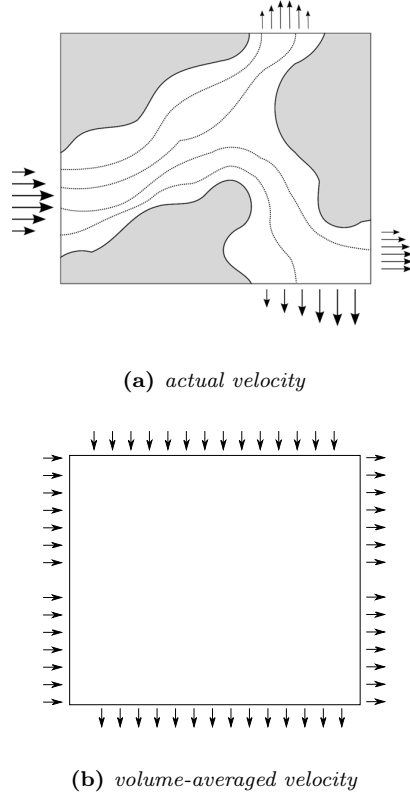


Fig. 3.1: *Velocity distribution comparison in elementary volume.*

resistance was developed based on the extrinsic velocity and the permeability of the solid matrix, given as;

$$\rho g - \frac{1}{\varepsilon} \nabla (\varepsilon p) = \frac{\mu_f}{K} \mathbf{V}' \quad (3.5)$$

If the solid matrix, instead of having isotropic properties, exhibits anisotropy than the Darcy's extension for such a matrix is given as;

$$\rho g - \frac{1}{\varepsilon} \nabla (\varepsilon p) = \frac{\mu_f}{\mathbf{K}} \mathbf{V}' \quad (3.6)$$

where \mathbf{K} is a second order symmetric tensor. Combining Darcy's law with inertial drag yields [70];

$$\rho g - \frac{1}{\varepsilon} \nabla (\varepsilon p) = \frac{\mu_f}{\mathbf{K}} \mathbf{V}' + \frac{C_f}{\mathbf{K}^{1/2}} \rho_f |\mathbf{V}'| \mathbf{V}' \quad (3.7)$$

Incorporating the pressure drop, as given in Eq. (3.7), the volume average momentum equation for the fluid phase in terms of extrinsic average velocity, can be written as;

$$\frac{\partial}{\partial t} (\varepsilon \rho_f \mathbf{V}) + \nabla \cdot (\varepsilon \rho_f \mathbf{V} \mathbf{V}) = \nabla \cdot (\varepsilon \bar{\tau}) + \varepsilon \rho_f g + \varepsilon \frac{\mu_f}{K} \mathbf{V} + \varepsilon \frac{C_f}{K^{1/2}} \rho_f |\mathbf{V}| \mathbf{V} + S \quad (3.8)$$

where $\bar{\tau}$ is the stress tensor and is usually given as;

$$\bar{\tau} = p + \mu_f [\nabla \mathbf{V}] \quad (3.9)$$

where μ_f is the fluid viscosity. The Eq. (3.8) is valid for the porous media only. However, for the gas channels, the last two terms are neglected and the momentum equation reduces to;

$$\frac{\partial}{\partial t} (\varepsilon \rho_f \mathbf{V}) + \nabla \cdot (\varepsilon \rho_f \mathbf{V} \mathbf{V}) = \nabla \cdot (\varepsilon \bar{\tau}) + \varepsilon \rho_f g \quad (3.10)$$

3.4 Conservation of Energy

The energy equation in the porous media is derived on the same principles as the continuity and the momentum equations. The volume-averaged energy equations is applied to both the fluid and the solid phase of the porous media. Assuming the fluid to be incompressible and neglecting the viscous dissipation effects, the energy equation for the fluid phase is given as;

$$\frac{\partial}{\partial t} (\varepsilon \rho_f E_f) + \nabla \cdot (\varepsilon \rho_f \mathbf{V} E_f) = \nabla \cdot (\varepsilon k_f \nabla E_f) \quad (3.11)$$

Assuming the energy E_f to be a function of temperature (T) only, Eq. (3.11) for the fluid phase reduces to;

$$\frac{\partial}{\partial t} (\varepsilon c_{p,f} \rho_f T_f) + \nabla \cdot (\varepsilon c_{p,f} \rho_f \mathbf{V} T_f) = \nabla \cdot (\varepsilon c_{p,f} k_f \nabla T_f) \quad (3.12)$$

where $c_{p,f}$ and k_f are the specific heat and the thermal conductivity of the fluid phase, respectively. For the solid matrix, the volume averaged energy equation consists only of the diffusive term, i.e.;

$$\frac{\partial}{\partial t} ((1 - \varepsilon) c_{p,s} \rho_s T_s) = \nabla \cdot ((1 - \varepsilon) k_s \nabla T_s) \quad (3.13)$$

The term $(1 - \varepsilon)$ represents the volume fraction of the solid matrix and $c_{p,s}$ and k_s are the specific heat and the thermal conductivity of the solid material, respectively.

Eqs (3.12) and (3.13) are the general energy equations for the fluid and solid phases without any thermal equilibrium between the two energy equations. If it is assumed that both the phases are in thermal equilibrium ($T_f = T_s$), the energy equation reduces to the following general form;

$$\frac{\partial}{\partial t} ((c_p \rho)_{\text{eff}} T) + \nabla \cdot (\varepsilon c_{p,f} \rho_f \mathbf{V} T) = \nabla \cdot ((c_p k)_{\text{eff}} \nabla T) + S \quad (3.14)$$

The effective density and specific heat are calculated as;

$$(\rho c_p)_{\text{eff}} = \varepsilon \rho_f c_{p,f} + (1 - \varepsilon) \rho_s c_{p,s} \quad (3.15)$$

The effective thermal conductivity of the fluid and the solid phase in the porous media depends on the porosity, pore structure and the thermal conductivities of each phase [70]. When the thermal conductivities of the two phases are close to each other, i.e., ($k_f \sim k_s$), the effective thermal conductivity is calculated using the classical mixing law [90].

$$k_{\text{eff}} = \varepsilon k_f + (1 - \varepsilon) k_s \quad (3.16)$$

However, when there is a significant difference in the thermal conductivities of the fluid and the solid phase of the porous media, Hadley [91] proposed an alternate relation that should be implemented, i.e.;

$$\begin{aligned} \frac{k_{\text{eff}}}{k_f} = (1 - \alpha_0) & \frac{\varepsilon f_0 + (1 - \varepsilon f_0) k_s / k_f}{1 - \varepsilon(1 - f_0) + \varepsilon(1 - f_0)} \\ & + \alpha_0 \frac{2(1 - \varepsilon)(k_s / k_f)^2 + (1 + 2\varepsilon) k_s / k_f}{(2 + \varepsilon) k_s / k_f + 1 - \varepsilon} \end{aligned} \quad (3.17)$$

where,

$$\begin{aligned} f_0 &= 0.8 + 0.1\varepsilon \\ \log \alpha_0 &= \begin{cases} -4.898\varepsilon & 0 \leq \varepsilon \leq 0.0827 \\ -0.405 - 3.154(\varepsilon - 0.0827) & 0.0827 \leq \varepsilon \leq 0.298 \\ -1.084 - 6.778(\varepsilon - 0.298) & 0.298 \leq \varepsilon \leq 0.580 \end{cases} \end{aligned} \quad (3.18)$$

Local thermal equilibrium (LTE) is usually a hypothesis used in calculating the temperature in the porous media [70]. When there is a wide difference in the thermal properties of the system, the fluid and solid energy equations need to be separated, as given in Eqs (3.12) and (3.13) and such an approach is called the local thermal non-equilibrium (LTNE). In order to link the two equations to cope with the inter-transfer of energy between the phases (\dot{q}), an interstitial heat transfer (h_v) coefficient is utilized. This is commonly given as;

$$\dot{q} = h_v(T_s - T_f) \quad (3.19)$$

The term \dot{q} is added as a source term in Eqs (3.12) and (3.13). Although the LTNE approach represents more accurate temperature distribution in the porous media, its use is limited due to the empirical relationship for the interstitial heat transfer coefficient which has not been quantified for all materials yet [70, 92].

3.5 Conservation of Species

In PEM fuel cell, there are four different gaseous species altogether, namely: hydrogen and water vapour at the anode side, and, oxygen, water vapour and nitrogen at the cathode side. In order to predict the local mass fraction of each species in the cell, a general conservation equation is used, given as;

$$\frac{\partial}{\partial t} (\varepsilon \rho X_i) + \nabla \cdot (\varepsilon \rho \mathbf{V} X_i) = -\nabla \cdot \vec{J}_i + S \quad (3.20)$$

where \vec{J}_i is the diffusion flux of species i in the mixture and has already been defined in Eq. (2.1). In order to precisely solve the conservation equation for species, diffusive mass flux has to be determined accurately [93]. In the literature three different models are available for determining the diffusive mass flux.

3.5.1 Fick's Law

Fick's law represents the simplest of the diffusive models for gaseous species transport, given as;

$$\vec{J}_i = D_{i,j} \nabla X_i \quad (3.21)$$

where $D_{i,j}$ is the binary diffusion coefficient of species i in j , such that;

$$D_{i,j} = \frac{T^{1.75}}{p} \sqrt{\frac{1}{M_i} + \frac{1}{M_j}} (\xi^{1/3} + \xi^{1/3})^{-1} \quad (3.22)$$

where ξ is the diffusion volume and M is the molar mass of species i and j . One of the main limitations of Fickian mass flux is that it is well suited for applications involving two gas species. If three or more gas species are present, as in case of PEM fuel cells, a multicomponent diffusion model is more suitable such as Stefan-Maxwell model.

3.5.2 Stefan-Maxwell Equation

In Stefan-Maxwell approach for the multicomponent diffusion of species involving more than one component, the flux equation is replaced by the difference in species velocities. In terms of mole fraction (Y_i) of species, it is given as [90, 93, 94].

$$\sum_{\substack{j=1 \\ j \neq i}}^N \frac{Y_i Y_j}{D_{i,j}} (\mathbf{V}_j - \mathbf{V}_i) = \vec{d}_i - \frac{\nabla T}{T} \sum_{\substack{j=1 \\ j \neq i}}^N \frac{Y_i Y_j}{D_{i,j}} \left(\frac{D_{T,j}}{\rho_j} - \frac{D_{T,i}}{\rho_i} \right) \quad (3.23)$$

where $D_{i,j}$ is the binary mass diffusion coefficient, \mathbf{V} is the diffusion velocity and D_T is the thermal diffusion coefficient. In case of an ideal gas assumption, the Maxwell diffusion coefficients are equal to the binary diffusion coefficients [90]. If the diffusion of species due to thermal gradients is assumed to be negligible, Eq. (3.23) reduces to the following general form [90];

$$\sum_{\substack{j=1 \\ j \neq i}}^N \frac{Y_i Y_j}{D_{i,j}} (\mathbf{V}_j - \mathbf{V}_i) = \vec{d}_i \quad (3.24)$$

Neglecting pressure diffusion and assuming equal force on all the species, then $\vec{d}_i = \nabla Y_i$ and $\vec{J}_i = \rho_i \mathbf{V}$, Eq. (3.24) can be written in terms of the diffusive mass flux \vec{J}_i and mass fractions of species X_j ;

$$\vec{J}_i = \sum_{j=1}^{N-1} \rho_i D_{i,j} \nabla X_j \quad (3.25)$$

and the binary diffusion coefficient $D_{i,j}$ is calculated as [90];

$$D_{ij} = [D] = [A]^{-1} [B] \quad (3.26)$$

where,

$$A_{i,i} = - \left(\frac{X_i}{D_{i,N}} \frac{M_w}{M_{w,N}} + \sum_{\substack{j=1 \\ j \neq i}}^N \frac{X_j}{D_{i,j}} \frac{M_w}{M_{w,i}} \right) \quad (3.27a)$$

$$A_{i,j} = X_i \left(\frac{1}{D_{i,j}} \frac{M_w}{M_{w,j}} - \frac{1}{D_{i,N}} \frac{M_w}{M_{w,N}} \right) \quad (3.27b)$$

$$B_{i,i} = - \left(X_i \frac{M_w}{M_{w,N}} + (1 - X_i) \frac{M_w}{M_{w,i}} \right) \quad (3.27c)$$

$$B_{i,j} = X_i \left(\frac{M_w}{M_{w,j}} - \frac{M_w}{M_{w,N}} \right) \quad (3.27d)$$

whereas, $[D]$ in Eq. (3.26) is the generalized Fick's law diffusion coefficients [95]. In porous media, the diffusion coefficient also needs correction for including the spatial dependence of the material used. In PEM fuel cells, the gas diffusion layer is fabricated using either the carbon paper or the carbon cloth, the effective diffusivity of species varies in through-plane and in-plane directions as explained in Sec. 2.2.1.

3.5.3 Knudsen Correction to Species Flux

Inside porous media, the diffusion of species varies with the length scale of the pores. At certain size of pores, the diffusion of species not only occurs due to inter-collision of molecules (Brownian motion) but the wall effect also starts influencing the diffusion mechanism due to the collision of molecules with the walls of the pores [6]. In order to characterize the wall effects, a non-dimensional number parameter called the Knudsen number is used which is the ratio of the mean free path of the molecules to the dimensions of the pore, given as;

$$K_n = \frac{\lambda}{d_{\text{por}}} \quad (3.28)$$

where λ is the mean free path and d_{por} is the pore diameter. When the Knudsen number is greater than 0.01 ($K_n > 0.01$), the Knudsen effects are considerable and must be included while calculating the species diffusion in the porous media, particularly in PEM fuel cells [6, 38, 67, 96–98], calculated as;

$$D_{K_n,i} = \frac{1}{3} d_{\text{por}} \left(\frac{8RT}{\pi M_i} \right)^{1/2} \quad (3.29)$$

So, the species diffusion flux in Eq. (3.20) based on both the the multicomponent and Knudsen diffusion is given as [67];

$$\bar{J}_i = \frac{1}{M_i} \sum_{\substack{j=1 \\ j \neq i}}^N \left(\frac{Y_j}{M_i} - \frac{Y_i}{M_j} \right) \left(\frac{1}{D_{i,j}^{\text{eff}}} \right) \quad (3.30)$$

where $D_{i,j}^{\text{eff}}$ is the effective diffusion of species i in the porous media. The Eq. (3.30) is the Stefan-Maxwell equation corrected for the Knudsen effects, and is sometimes called the dusty gas model [93]. The effective diffusion coefficient, in this case, is given as;

$$\frac{1}{D_{i,j}^{\text{eff}}} = \frac{1}{D_{i,j}} + \frac{1}{D_{K_n,i}} \quad (3.31)$$

The diffusion coefficient, $D_{i,j}$, is calculated using Eq. (3.26).

3.6 Liquid Water Transport

A common approach currently used in modelling studies for predicting the liquid water distribution profiles in porous media is the direct implementation of an empirical correlation describing the capillary pressure as a function of liquid saturation. Several empirical and semi-empirical expressions are available that attempt to describe the behaviour of capillary pressure in terms of porous media and fluid properties, as given in Sec. 2.4.1. The traditional Leverett J-function approach has been widely adopted by the PEM fuel cell community. Although the modified Leverett J-function approach represents a useful starting point towards achieving an accurate two-phase transport model in fuel cell studies, the origin of this approach does not precisely represent the complex heterogeneous structure of fuel cell diffusion media.

Gostick et al. [99] performed porosimetry for different GDLs to generate the relation between capillary pressure and the saturation and found that the acquired data can only be approximated with either van Genuchten [88] or the Leverett approach. Kumbur et al. [77, 84, 85], later on, presented three distinct levels of water saturation capturing the heterogeneous and mixed wettability characteristics of the GDLs using an extended form of the Leverett function. It was noted that in this approach, the calculated capillary function provided a superior fit to the experimental data obtained via porosimetric studies of the selected GDLs.

In this work, an experimentally validated approach [77, 84, 85] has been used to study the behaviour of water saturation in fuel cell porous media. The key feature of this correlation is that the connection between the liquid saturation and the mixed wettability characteristics of the diffusion media is precisely linked to the capillary pressure and further incorporating the temperature and compressional effects of the media.

$$p_c = \left(\frac{293}{T} \right)^6 \gamma(T) 2^{0.4C} \left(\frac{\varepsilon}{K} \right)^{1/2} K(s_{\text{nw}}) \quad (3.32)$$

where T is the local temperature, while, $\gamma(T)$ is the temperature corrected surface tension, and $K(s_{nw})$ represents the latest developed water saturation function, evaluated as;

$$K(s_{nw}) = \begin{cases} \text{wt}\%[0.0469 - 0.00152(\text{wt}\%) - 0.0406s_{nw}^2 \\ \quad + 0.143s_{nw}^3] + 0.0561 \ln s_{nw} & 0 < s_{nw} < 0.50 \\ \text{wt}\%[1.534 - 0.00152(\text{wt}\%) - 12.68s_{nw}^2 \\ \quad + 18.824s_{nw}^3] + 3.416 \ln s_{nw} & 0.50 < s_{nw} < 0.65 \\ \text{wt}\%[1.7 - 0.0324(\text{wt}\%) - 14.1s_{nw}^2 \\ \quad - 14.1s_{nw}^3] + 3.79 \ln s_{nw} & 0.65 < s_{nw} < 1.00 \end{cases} \quad (3.33)$$

where wt% and s_{nw} represent the weight percentage of PTFE content in the diffusion media and non-wetting phase saturation. The experimental details and information about derivation of Eqs (3.32) and (3.33) and can be found in [77, 84, 85]. For implementation of the capillary pressure in CFD model of the PEM fuel cells, the moisture diffusion model is implemented, as given in Sec. 2.3.3 [100]. In order to model the mass transfer rate between the vapour and the liquid phases, the relationship provided by Hwang [63] is utilized;

$$\dot{\omega} = \begin{cases} C_{\text{con}} (1 - s) X_{\text{H}_2\text{O}} \frac{p_{\text{wv}} - p_{\text{sat}}}{RT_f} & p_{\text{wv}} - p_{\text{sat}} \geq 0 \\ C_{\text{evp}}(s) \frac{\rho_l}{M_{\text{H}_2\text{O}}} (p_{\text{wv}} - p_{\text{sat}}) & p_{\text{wv}} - p_{\text{sat}} < 0 \end{cases} \quad (3.34)$$

where $\dot{\omega}$ is rate of the phase change based on the saturation pressure of water vapours in air [62]. Additionally, to transfer the effects of water saturation in the porous media, Eqs (3.4), (3.8) and (3.20) is corrected for the reduced porosity by multiplying $(1 - s)$.

3.7 Physico- Electrochemical Model

The main driving mechanism in PEM fuel cells is the electrochemical reactions occurring in the catalyst layer of both the anode and the cathode. Thus, electrochemical modelling of the catalyst layer is one of the most crucial aspect of the CFD modelling for the accuracy of the results. In open literature many mathematical models for the catalyst layer have been proposed from zero to three dimensional models. Among all, the flooded agglomerate model is the most descriptive and predicting model [101]. In this model, the carbon supported Pt particles in form of agglomerate are immersed in a thin film of membrane (ionomer). The catalyst layer consists of a network of interconnected micro and macro sized pores through which the gaseous species reach the surface of the agglomerates. There upon, the reactant species diffuse through a thin layer of the ionomer to reach the reaction site [102]. The agglomerate model has been able to give deeper insight into the physico- electrochemical phenomena in simulations and modelling of the catalyst layer. However, the consideration of the catalyst layer to be composed of carbon supported Pt with flooded membrane (ionomer) film as a continuum medium has made

it difficult to analyse the discrete distribution of the catalyst phase in the agglomerate [103].

Yan and Wu [102], Antonio et al. [104] and Bultel et al. [105] have developed various micro models for the catalyst layers in which mass and ion transfer have been addressed separately by treating the agglomerate and the electrolyte material (NafionTM) as discrete and segregated components. The proposed micro models have been able to provide deeper insight into the detailed mass and ion transfer mechanisms at pore levels, and particle size relation and dependence in the overall performance for the electrochemical reactions.

In order for electrochemical reactions to proceed in the catalyst layer, four (4) processes need to be accomplish. These are summarized as [106];

- diffusion of chemical species to the catalyst layer,
- diffusion of chemical species in the catalyst layer,
- reactant species dissolution at the ionomer and pore interface,
- diffusion of the reactant species in the ionomer,
- diffusion of the dissolved reactants in the agglomerate.

However, for the simplification of the model, it is assumed that the agglomerates are of spherical shape and evenly distributed in the entire catalyst layer [106]. The transport of the species to the surface of the ionomer covering the agglomerate is accomplished using the process defined in Sec. 3.5. The reactant species flux at the surface of the Pt, where electrochemical reactions take place, can be written as;

$$N'_i = D \frac{r_{\text{agg}}}{(r_{\text{agg}} + \delta)} \frac{(\Theta_{i,g|I} - \Theta_{i,I|s})}{\delta} \quad (3.35)$$

where Θ is the molar concentration of the species i at the gas/ionomer interface ($g|I$) and the outer surface of the agglomerate ($I|s$), as shown in Fig. 3.2. The total amount that actually reacts at the reaction site depends on $\Theta_{i,I|s}$, so the reaction rate is calculated as;

$$R_i = E_r k_i \Theta_{i,I|s} \quad (3.36)$$

where E_r is the effectiveness of the spherical agglomerates and is given as [93];

$$E_r = \frac{1}{\Phi_L} \left(\frac{1}{\tanh(3\Phi_L)} - \frac{1}{3\Phi_L} \right) \quad (3.37)$$

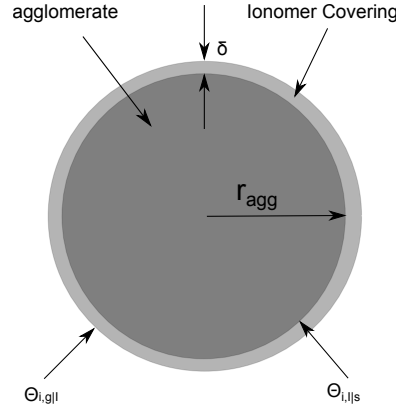


Fig. 3.2: Schematic of the ionomer covering the agglomerate.

The parameter Φ_L is commonly known as the Thiele's modulus and has been calculated by various authors for the spherical agglomerates [93, 106, 107]. The current density produced as a result of the electrochemical reactions based on the concentration of the species i at the surface of the agglomerate can be expressed as;

$$\nabla \cdot i_i = zFE_{\text{r}}k_i\Theta_{i,I|s} \quad (3.38)$$

In the above equation, F represents the Faraday constant and $\nabla \cdot i$ is the transfer current or the electrochemical reaction rate. In order to correct the reaction rate for the porosity of the catalyst layer, the Eq. (3.38) is multiplied by $(1 - \varepsilon)$. Writing $\Theta_{i,I|s}$ in terms of $\Theta_{i,g|I}$ and using the Henry's equilibrium relationship for species dissolution and species mass balance, the transfer current or the reaction rate equation can be represented in the following general form [106, 107];

$$\nabla \cdot i_i = zF \frac{p_i}{H_i} \left(\frac{1}{E_{\text{r}}k_i(1 - \varepsilon)} + \frac{(r_{\text{agg}} + \delta)\delta}{a_{\text{agg}}r_{\text{agg}}D_{i-I}} \right)^{-1} \quad (3.39)$$

and the expression for the reaction rate, k_i is given as [106, 107];

$$k_i = \frac{a_{\text{Pt}}^{\text{eff}}}{zF(1 - \varepsilon)} \left(\frac{i_{\text{o}}^{\text{ref}}}{\Theta_i^{\text{ref}}} \right) \left[-\exp\left(\frac{\alpha_{\text{a}}F}{RT}\eta\right) + \exp\left(\frac{-\alpha_{\text{c}}F}{RT}\eta\right) \right] \quad (3.40)$$

where $a_{\text{Pt}}^{\text{eff}}$ is the effective Pt surface area, α_{a} and α_{c} are the anodic and cathodic transfer coefficients and η is the activation overpotential or the energy consumed to carry out the electrochemical reactions, respectively.

3.8 Charge Transport (Ions and Electrons)

PEM fuel cells are labelled as clean energy production devices compared to conventional power generators where combustion of fuel is the main source of energy. The primary driving mechanism in PEM fuel cells is the electrochemical reactions where hydrogen is split into electrons and protons at the anode side which combine exothermically in presence of oxygen at the cathode to produce water. The electrons generated at the anode follow an external circuit through the load while protons are directly transferred via the electrolyte (*membrane*) towards the cathode. Therefore, for complete electrochemical reaction description, two equations have been used in present model. One of the equations deals with the electron (e^-) transport, while the other quantifies the protonic (H^+) conduction.

$$\nabla \cdot (\sigma_s \nabla \phi_s) + R_s = 0 \quad (3.41)$$

and,

$$\nabla \cdot (\sigma_m \nabla \phi_m) + R_m = 0 \quad (3.42)$$

where the subscripts ‘s’ and ‘m’ refer to the electronic (solid) and ionic (membrane) phase conductivity (σ) or potential (ϕ). R in Eqs (3.41) and (3.42) is the transfer current or electrochemical source term at the anode and the cathode catalyst layer with conventions as given in Table 3.1 based on the Eq. (3.39).

The solid phase potential equation, Eq. (3.41) is solved in the current collector, the gas diffusion and the catalyst layer on both sides. So far, many CFD models have been proposed to accurately predict the electronic conductivity of different material in the PEM fuel cells [107–110]. The ionic conductivity of the membrane phase is given as [16];

$$\sigma_m = (0.514\lambda - 0.326) \exp\left(1268\left(\frac{1}{303} - \frac{1}{T}\right)\right) \quad (3.43)$$

where λ is the water index and is related to the water activity in the membrane phase [16];

Table 3.1: *Transfer currents in the anode and cathode of PEM fuel cells.*

	Anode	Cathode
R_s	$-\nabla \cdot i_{H_2}$	$\nabla \cdot i_{O_2}$
R_m	$\nabla \cdot i_{H_2}$	$-\nabla \cdot i_{O_2}$

$$\lambda = \begin{cases} 0.043 + 17.18a - 39.85a^2 + 36a^3 & (a < 1) \\ 14 + 1.4(a - 1) & (a > 1) \end{cases} \quad (3.44)$$

The water activity a in Eq. (3.44) is the sum of the ratio of the partial pressure of water vapour to the saturation pressure and the liquid saturation. The protonic conductivity of the ionomer is corrected for the porosity and the volume fraction of the conducting material by implementing Eq. (2.9)

3.9 Water Transport in Electrolyte (membrane)

The water transport in the electrolyte (membrane) is governed by a diffusive equation, given as [65];

$$\nabla \cdot \left(-D_1 \nabla C_w + \frac{n_d \sigma_m}{F} \nabla \phi_m \right) = 0 \quad (3.45)$$

where C_w represents the water content of the electrolyte and D_1 is the water diffusivity through the electrolyte and is a function of temperature and the water index [65].

$$D_1 = 10^{-10} \exp \left[2416 \left(\frac{1}{303} - \frac{1}{T} \right) \right] \times f(\lambda) \quad (3.46)$$

such that,

$$f(\lambda) = \begin{cases} 2.563 - 0.33\lambda + 0.0264\lambda^2 - 0.000671\lambda^3 & (4 < \lambda) \\ -1.25\lambda + 6.65 & (3 < \lambda \leq 4) \\ 2.05\lambda - 3.25 & (2 < \lambda \leq 3) \\ 1 & (2 \geq \lambda) \end{cases} \quad (3.47)$$

The first term in Eq. (3.45) is the diffusion of water to the anode side because of the concentration difference called the back diffusion, while, the second part accommodates the water drag due to the proton migration to the cathode side, where n_d is the electro-osmotic drag coefficient.

3.10 Source Terms for Conservation Equations

During the operation of a PEM fuel cell, there is always consumption and production of species due to electrochemical reactions. Additionally, the heat generated as a result of reactions, the resistance of the material to conduct charge and phase change of water, not only increase the temperature of the cell but also needs to be included in the model for more accurate prediction of the cell behaviour. The different types of source terms and their applicable equation and domains are tabulated in Table 3.2.

Table 3.2: *Source terms ‘S’ for the governing equations.*

Equation			Term	Domain
Continuity	Eq. (3.4)	a	$-\frac{M_{H_2}}{2F} \nabla \cdot i$	CL
	Eq. (3.4)	c	$-\frac{M_{O_2}}{4F} \nabla \cdot i$	CL
	Eq. (3.4)		$\frac{M_{H_2O}}{2F} \nabla \cdot i$	CL
Momentum	Eq. (3.8)	a	$\varepsilon \frac{\mu_f}{K} \mathbf{V} + \varepsilon \frac{C_f}{K^{1/2}} \rho_f \mathbf{V} \mathbf{V}$	CL, GDL
	Eq. (3.8)		$\mathbf{V} \left(-\frac{M_{H_2}}{2F} \nabla \cdot i \right)$	CL
	Eq. (3.8)	c	$\varepsilon \frac{\mu_f}{K} \mathbf{V} + \varepsilon \frac{C_f}{K^{1/2}} \rho_f \mathbf{V} \mathbf{V}$	CL, GDL
	Eq. (3.8)		$\mathbf{V} \left(\frac{M_{O_2}}{4F} \nabla \cdot i \right)$	CL, GDL
	Eq. (3.8)		$\mathbf{V} \left(\frac{M_{H_2O}}{2F} \nabla \cdot i \right)$	CL
Species	Eq. (3.20)	a	$-\frac{M_{H_2}}{2F} \nabla \cdot i$	CL
	Eq. (3.20)	c	$-\frac{M_{O_2}}{4F} \nabla \cdot i$	CL
	Eq. (3.20)		$\frac{M_{H_2O}}{2F} \nabla \cdot i$	CL
Phase Change	Eq. (2.25)	c	Eq. (3.34)	CL, GDL
Energy	Eq. (3.14)	a	$(\nabla \cdot i) \eta$	CL
	Eq. (3.14)		$\frac{\nabla \phi_m^2}{\sigma_m}$	CL
	Eq. (3.14)		$\frac{\nabla \phi_s^2}{\sigma_s}$	CL, GDL, CC
	Eq. (3.14)	c	$(\nabla \cdot i) \eta$	CL
	Eq. (3.14)		$\frac{\nabla \phi_m^2}{\sigma_m}$	CL
	Eq. (3.14)		$\frac{\nabla \phi_s^2}{\sigma_s}$	CL, GDL, CC
	Eq. (3.14)	m	$\frac{\nabla \phi_m^2}{\sigma_m}$	-

3.11 Microscale Modelling Review

The catalyst layers are at the heart of PEM fuel cells. The incorporation of nanosized catalysts has been proven highly successful in increasing the active areas and the catalyst

activity, thus leading to significant improvements in the performance and utilization. There are various phases inside the catalyst layer, namely: carbon, Pt particles, ionomer and voids. Platinum is used as the catalyst to carry out the oxidation and reduction reactions of hydrogen and oxygen at respective catalyst layers while the carbon particles serve as support to Pt and electron conduction. The ionomer establishes the essential skeleton to distribute the so formed carbon/platinum (C|Pt) and conduct the ions while the voids help in transport of the reactants and the products to and from the reaction sites. They also provide pathways for the transport of reactants, protons, electrons and products while facilitating oxygen reduction at the cathode and hydrogen oxidation at the anode [111]. In addition to multiphase transport processes, water generation/transfer processes occurring in nanostructured catalyst layers are critical and very complicated, particularly when water phase change is involved at nano/micro pore levels when the pore sizes approach extreme values. The catalyst layers play a crucial role in the PEM fuel cell water management aimed at maintaining a delicate balance between reactant transport from the gas channels and water removal from the electrochemically active sites. There are several multiphysics and electrochemical phenomena, taking place in catalyst layers during fuel cell operation. The reactions and the transport phenomena occurring in fuel cell catalyst layers are considered localized rather than uniform (contrary to volume averaged properties as discussed in previous sections). For example, the TPB between catalysts/ionomers/gas pores determines the important parameters, such as electrochemically active area (ECA) and exchange current density. It is also true that the percolation within the catalyst layers provides transport pathways for reactants, as well as water and heat [112].

Detailed description of a porous micro structure is an essential prerequisite to pore-scale modelling. The three dimensional volume data of a porous sample can be obtained either by experimental imaging or by a computer simulation method. Several experimental techniques can be deployed to image the pore structure even in three dimensions. Non-invasive techniques such as X-ray micro tomography, magnetic resonance imaging and confocal microscopy are the preferred choices [113–116]. The computer reconstruction of catalyst layer can be either stochastic [117–119], semi-deterministic [112, 120] or regular [121]. There have been increasing efforts to reconstruct the catalyst layer and simulate reactions at the microscale level. In the following sections, the evaluation of the PEM fuel cell catalyst layer microstructures and the effects on the reactive transport phenomena is outlined and highlighted.

The first published work on catalyst layer reconstruction was done in two dimensions [76]. This model was later extended to three dimensions and applied to a regular micro structure and a random one. In this work, the catalyst layer was first represented by idealized regular micro structures [121], followed by computer generated random microstructures [122] and further by stochastically reconstructed microstructures based on statistical information from a two dimensional TEM images [117]. The latter method was further extended for the generation of bi-layer catalyst layer structures with varied pore and electrolyte volume fractions [123]. Their reconstruction involves only two phases, i.e., void and solid, and the electrolyte and C|Pt are treated as a single phase during the reconstruction. A different approach was presented by Kim and Pitsch to computa-

tionally reconstruct a PEM fuel cell catalyst layer [124]. They represented the catalyst layer as consisting of carbon spheres surrounded by an ionomer film. The reconstructed three dimensional catalyst layer includes a thin layer of ionomer phase evenly distributed around the C|Pt spherical agglomerates. It involves three phases (ionomer, C|Pt, void). Knudsen diffusion was accounted for by computing an average pore radius which was used to compute a Knudsen diffusion coefficient for all pores in the solution domain. In another effort, Lange and co-workers used a stochastic approach to reconstruct a section of a PEM fuel cell catalyst layer and modelled transport and electrochemical reactions for a wide range of random micro structures [111, 118, 125]. Hundreds of different micro structures were used, resulting in a large number of effective transport parameters at different pore, ionomer and carbon volume fractions. In those work, the reconstruction also involves three phases: C|Pt, ionomer, and pores. In addition, most of the previous catalyst layer modelling efforts have used a mean pore radius to compute the Knudsen diffusion coefficient that was further applied to all sized pores in the computational domain. Recently, Siddique and Liu reconstructed and modelled a small section of PEM fuel cell catalyst layer with a high resolution [112]. A random reconstruction algorithm, reflecting the experimental fabrication process, attempts to account for agglomeration in the model. Their reconstruction involved four phases, i.e., the Pt, carbon, ionomer and pore space, and the isolated area for each phase was distinguished in detail. In addition, the electrochemically active area determined by the interface between transport Pt and ionomer regions has been quantified, as a good indicator of phase connection and interaction.

Recent efforts also include three dimensional experimental imaging of the PEM fuel cell catalyst layer microstructure using x-ray computed tomography. The first published work on three dimensionally reconstructed catalyst layer was presented by Ziegler and co-workers [126]. Their reconstruction of the catalyst layer was based on highly sensitive focused ion beam/scanning electron microscope (FIB/SEM) analysis. The carbon and pore distribution was shown and quantitatively analysed and the pore size distribution was evaluated. By the experimental methods, the reconstruction involves only solid and pore phases. Whereas, by numerical methods, the reconstruction can only involve three phases and the TPB for the electrochemical reaction and water generation has not been identified, neither. In this study, we use a regular numerical method to reconstruct four phase micro structure and TPB by using three-dimensional commercial software directly, for the objective to develop a microscopic model for water generation and species transport via Knudsen diffusion through the voids, i.e., smaller pores in the domain will have lower Knudsen diffusivity than larger pores. The proton transport in the ionomer has been included here to aim for the rigorousness of the work. In addition, local electrochemical reactions have been simulated at the interfaces satisfying the TBP conditions.

3.12 Microstructure Reconstruction

3.12.1 Regularly Distributed Sphere Method

The catalyst layer structure is complex, generally composed of four phases: carbon (C), which allows for conduction of electrons (e^-) and support of the platinum nano particles;

ionomer, the ionic phase which is typically NafionTM and provides a path for proton (H^+) conduction; platinum (Pt) particles, which provide sites for electrochemical reactions; and pores, which allow reactants and product gases to diffuse through the catalyst layers. In addition to multiphase transport processes, water generation/transfer processes occurring in nanostructured catalyst layers are critical and very complicated, where the electrochemical reactions occur at the TPBs. In order to simulate the coupled electrochemical reactions and transport phenomena at microscale, a regular sphere based method is adopted to reconstruct the catalyst layer with four phases and TPBs by using three dimensional commercial software.

3.12.2 Catalyst Layer Microstructure Reconstruction

The overall morphology of agglomerate structures in the thin film catalyst layers can be characterized by the spatial distribution of C|Pt particles [118, 127]. Because the pore scale phenomena on the order of $100\text{ nm} \sim 1\text{ }\mu\text{m}$ are of primary interest, e.g., the reactions occurring at the TPBs, the detailed structure of carbon and platinum particles cannot be neglected. Thus, assuming the carbon support and platinum particles to be of spherical geometry.

The catalyst layer is assumed to consist of connected C|Pt spheres which are covered by a uniform thin ionomer layer. The assumptions of methodology are listed below:

- Each big carbon sphere is combined with a pre-specified number of small Pt spheres, and half of individual Pt particles stick out, which represents the primary carbon/platinum (C|Pt) particle interaction.
- There are two types of TPBs, namely: TPB length and TPB area, in this reconstruction method:
 - all C|Pt are covered by an ionomer layer of specified thickness, except at Pt faces and where carbon spheres overlap. Each Pt particle sticks out from the thin ionomer films, hence, the place of TPBs, where the electronic, ions and void phases meet, can be identified, as illustrated in Fig. 3.3a. The TPB length is defined by the circle length between a Pt particle and ionomer film, as shown by the dashed line in Fig. 3.3a.
 - all C|Pt are covered by an ionomer layer of specified thickness, except at where carbon spheres overlap. Each Pt particle is covered by the same thickness of thin ionomer films. In this case, the area of TPBs is the surface of sticking out Pt, as illustrated in Fig. 3.3b

The reconstruction is performed by arranging the C|Pt spheres regularly in three directions, in such a way that the spatial distribution of the spheres follows that of C|Pt volume fraction in the catalyst layer. The ionomer layers are periodic in the same way. According to above assumptions, the proposed reconstruction procedure is performed by using a three dimensional commercial software directly.

Firstly, only the solid and pore phases is considered to investigate the basic parameters, like porosity and specific surface area (SSA) in microscale. The porosity is the ratio of the

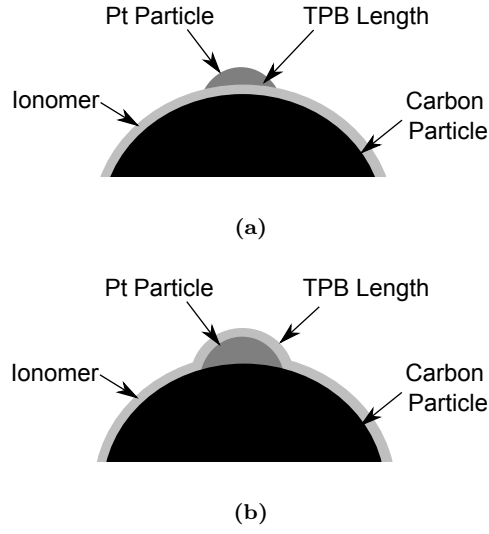


Fig. 3.3: A schematic drawing of the TPB.

Table 3.3: Porosity and specific surface area changed with the radii.

	Unit	$l = L/2r = 0.9$				
r	μm	0.2	0.4	0.6	0.8	1
$\frac{V_p}{V_t}$	%	31.16	30.38	31.65	29.90	29.03
$\frac{A_s}{V_t}$	10^6m^{-1}	7.64	3.77	2.51	1.84	1.47

void volume to the total volume; the specific surface area is the ratio of the solid surface area to the total volume. The simulation can supply the void volume and solid surface area directly. It is assumed that all solid spheres radii r and the distance L between each spheres are keep constant, and the arrangement of spheres at x , y and z direction are the same as shown in Fig. 3.4. The ratio between distance and diameter $l (= L/2r)$ is constant (0.9), while the sphere radii was varied from 0.2 to 1 μm , the predicted porosity and specific surface area are listed in Table 3.3. It shows that the porosity is around 30%, while the specific surface area decreased with the radii increasing. To keep the radii constant (1 μm) and change the distance ratio from 0.8 to 0.98, the porosity and specific surface area values are evaluated in Table 3.4. It shows that the porosity increases from 15.9% to 42.6% with increasing of distance ratio, and the specific surface area increased slightly.

Normally, for the PEM fuel cell catalyst layer, the porosity is about 20%~60%, the specific surface area is around $1 \sim 3 \times 10^6 \text{ m}^{-1}$, the thickness of ionomer is about 10 ~ 80 nm, and the Pt loading is about 0.4 (mg cm^{-2}), the C|Pt agglomerates spherical is about 1 μm . According to the experimental results of pore size distribution, the pore space radius is

Table 3.4: Porosity and specific surface area changed with distance ratio.

	Unit	$r = 1 \text{ } \mu\text{m}$				
l^a	–	0.8	0.85	0.9	0.95	0.98
$\frac{V_p}{V_t}$	%	15.90	23.98	29.03	36.45	42.61
$\frac{A_s}{V_t}$	10^6m^{-1}	1.29	1.44	1.47	1.51	1.55

$$^a l = \frac{L}{2r}$$

Table 3.5: The micro structure parameters of PEM fuel cell CL predicted by four phase reconstruction method.

Parameter	Symbol	Value	Unit
cell size		4.1	μm
carbon radius	r_c	0.99	μm
ionomer thickness	δ	0.01	μm
Pt radius	r_{pt}	0.1	μm
porosity	$\frac{V_p}{V_t}$	29.95	%
SSA ^a	$\frac{A_s}{V_t}$	1.57	10^6 m^{-1}
TPB LD ^b	$\frac{L_{\text{TPB}}}{V_t}$	0.67	μm^{-2}
Pt loading	m_{Pt}	0.10	mg cm^{-2}

^a SSA = Specific surface area

^b LD = length density

around 20 nm to 200 nm [126].

Secondly, the three dimensional catalyst layer with four phases and TPB is reconstructed using the above given parametric values. If the particles are arranged regularly in x, y and z direction, the size of pore space radius will be very large. In order to decrease the pore radius, the particles can be offset by a certain distance m, as shown in Fig. 3.4.

According to the first above, the distance ratio of 0.9 and the ionomer thickness of 10 nm are used along with the carbon sphere radii of 0.99 μm and the Pt sphere radii of 100 nm. Each big carbon sphere is combined with 6 Pt spheres, and half of each Pt particles stick out inside the thin ionomer film. The combined C|Pt and ionomer spheres are regularly arranged in the computational domain. Fig. 3.5 shows the reconstructed CL for a domain size $4.1 \times 4.1 \times 4.1 \text{ } \mu\text{m}^3$ and some of the parameters of reconstructed CL are given in Table 3.5.

The mean porosity of CL cell is calculated using a value counting method [122]. Fig. 3.6 shows the relationship between the calculated porosity and the size of the domain at the

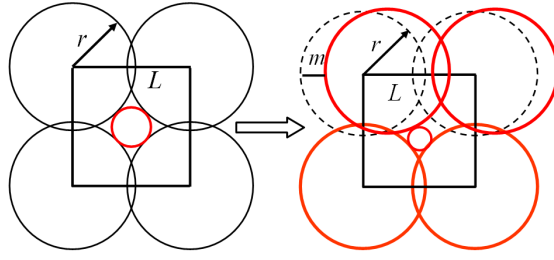


Fig. 3.4: *Offset arrangement of particles*

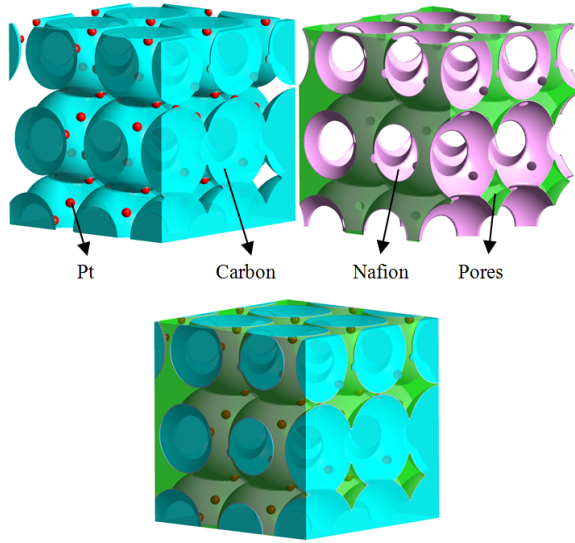


Fig. 3.5: *Four phase CL reconstruction ($4.1\mu\text{m} \times 4.1\mu\text{m} \times 4.1\mu\text{m}$). Carbon spheres are in sky blue, Pt particles red, ionomer is pink and pores are green or transparent.*

distance ratio of 0.9. Below a certain sample size the porosity of the sample fluctuates due to the local structure effects and is not representative of the entire PEM fuel cell CL. The porosity is required to be independent of the domain size, for the objective to have a structure that is representative of the bulk CL. In order to determine this parameter, a study is performed by increasing the sample size and it is found that the porosity keeps almost constant when the domain size is 6 times of carbon radius, resulting in a domain representing of the entire CL structure.

3.13 CFD Implementation

3.13.1 Macroscale Modelling

With in-house self-developed and open-source CFD models, many commercial software products are available in the market that have proved to be very efficient and robust. Re-

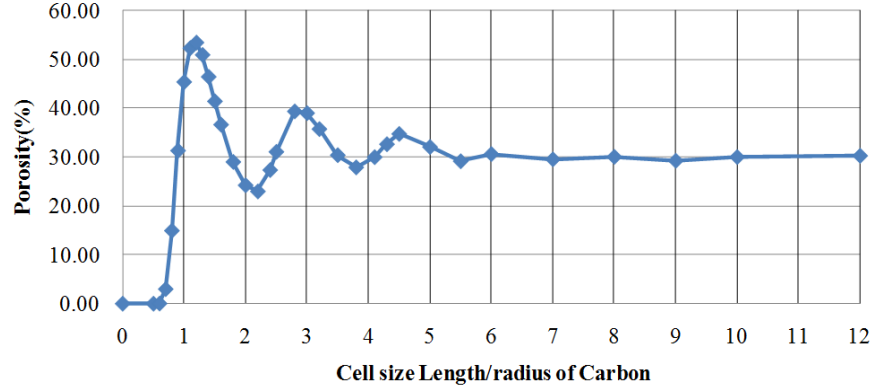


Fig. 3.6: *Fluctuations in the porosity of the representative volume calculated by increasing the size of the volume.*

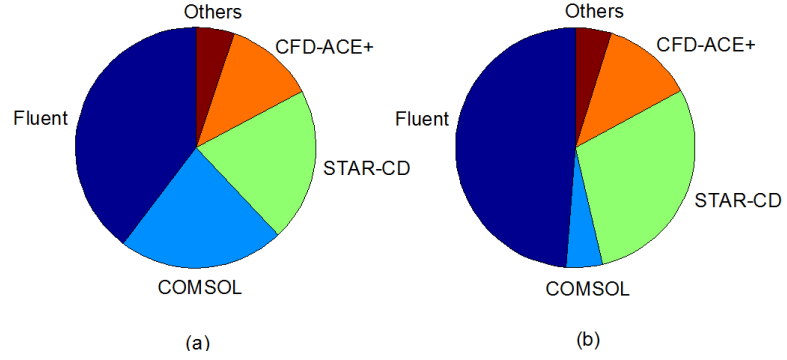


Fig. 3.7: *Comparison of various software used for PEM fuel cell modelling. (a) 2D geometry (b) 3D geometry.*

regardless of inherited disadvantage of limited freedom in equation manipulation and controls, many researchers have opted for commercial software products as prime CFD tool. Among many, the most commonly used are FLUENTTM, COMSOLTM, STAR-CDTM and CFD-ACE⁺TM, and the contribution of each in CFD modeling is shown pictorially in Fig. 3.7 [8].

ANSYSTM FluentTM [128] is one of the most preferable commercial CFD product in the market offering sophisticated numerics and robust formulations including a pressure-based segregated and coupled solvers, and a density based solver technique to ensure optimum and reliable results. It is well suited for a number of complex physical models utilizing unstructured meshes both for two dimensional and three dimensional cases based on finite volume method (FVM). Meshes can be created using ANSYSTM meshing products or other robust products like ICEMTM and GAMBITTM. To further enhance the flexibility of model variant situations, FluentTM provides the use of user-defined-functions (UDFs)

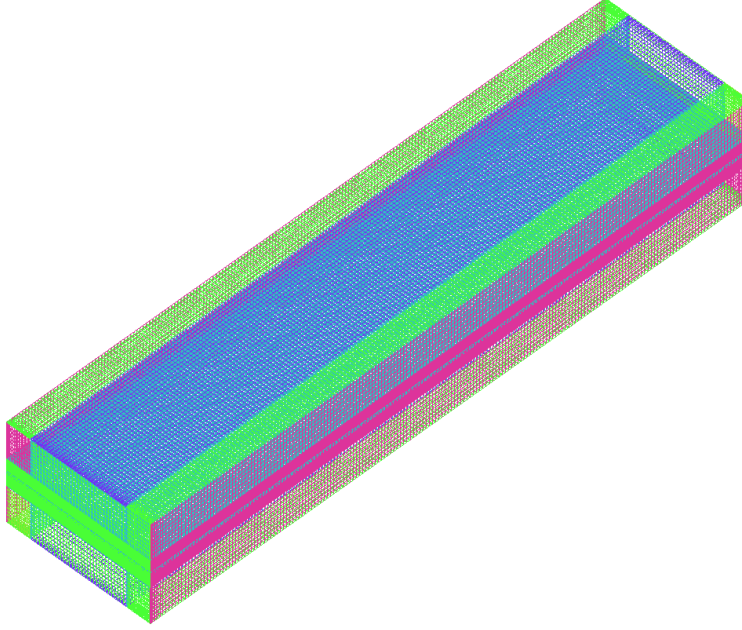


Fig. 3.8: Mesh generation for a single PEM fuel cell using ICEM™.

that helps to tailor the model to specific needs or requirements. For all the present modelling work, Fluent™ has been used as the primary modelling tool.

The mesh for the present modelling consists of the a single section of PEM fuel cell with interdigitated flow field configuration created with ICEM™ as shown in Fig. 3.8. The mesh is divided in 0.6 million hexahedral cells with varying mesh densities in different zones. The membrane, catalyst layer and the gas diffusion layer on both sides comprise of 75% of the total cells. Keeping in mind the strong pressure velocity coupling due to the interdigitated flow field, the SIMPLEC scheme has been employed because it helps in achieving quicker convergence for laminar flows, as encountered in PEM fuel cell modelling [90]. Additionally, due to the implementation of hexahedral cells, unique upstream and downstream faces exist, so, QUICK scheme has been used for spatial discretization [90].

For the present work, it is assumed that the domain is cooled ideally at the outer surface of both anode and cathode current collector at 343 K, as shown in Fig. 3.9. Additionally, the inlet temperature for both hydrogen and air is also maintained at 343 K. For simulating the electronic current flow in the domain, a constant voltage is applied at the cathode current collector outer surface, which is also the operating voltage of the cell. In order to quantify the water saturation, the air and hydrogen inlet faces are specified with a constant value (zero in this case). Table 3.6 gives the value of different parameters as used in present modelling approach.

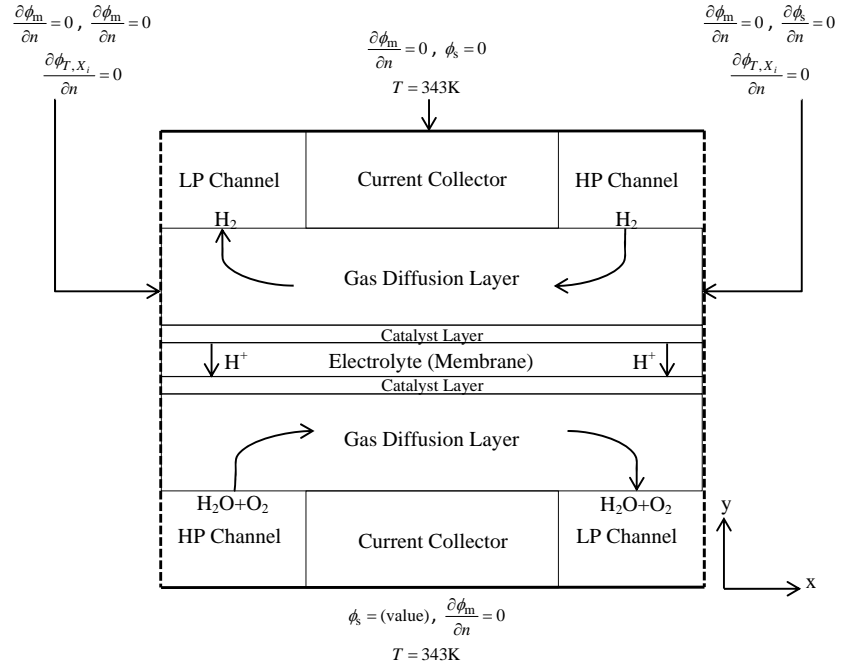


Fig. 3.9: A two dimensional front end schematic of the model with boundary conditions.

Fig. 3.10 highlights different components and boundaries of the working domain. The air enters the domain through the inlet and is diverted to the cathode side gas diffusion layer because the far end of the channel is blocked. Similar procedure is followed by the hydrogen at the anode side. Both the air and hydrogen exit through the outlet at adjacent channel at their respective sides. One of the advantages offered by the such configuration is that the flow of reactant species is convected through the gas diffusion layer by maintaining a pressure difference between the inlet and the outlet faces.

Table 3.6: Physical parameters and properties.

Parameters	Value	Units	
Faraday constant, F	96487.0	C/mol	
Gas Constant, R	8.3142	J/mol K	
Thickness of GDL	0.21	mm	
Porosity of GDL	0.7	-	[67]
Thickness of CL	0.012	mm	
Porosity of CL	0.2	-	[44]
Compression pressure, C	0.6	MPa	[85]
Continued on next page			

Table 3.6 – continued ...

Parameters	Value	Units	
Pt loading, m_{Pt}	0.4	mg/cm ²	[106]
Pt particle diameter, r_{Pt}	2.5	nm	[106]
Agglomerate Radius, r_{agg}	1	μm	[106]
Agglomerate surface area, a_{agg}	3.6×10^5	m ² /m ³	[106]
Anodic transfer coefficient, a_{an}	1	-	[129]
Cathodic transfer coefficient, a_{cat}			
low slope $\geq 0.8\text{V}$	1	-	[130]
high slope $< 0.8\text{V}$	0.61	-	[130]
Ref. exchange current density, i_0^{ref}			
low slope $\geq 0.8\text{V}$	3.85×10^{-8}	A/cm ²	[130]
high slope $< 0.8\text{V}$	1.5×10^{-6}	A/cm ²	[130]
Henry's constant for H ₂ , H_{H_2}	3.9×10^4	Pa m ³ /mol	[131]
Henry's constant for O ₂ , H_{O_2}	3.2×10^4	Pa m ³ /mol	[131]
Inlet O ₂ mass fraction	0.2	-	
Inlet H ₂ mass fractions	0.5	-	
Agglomerate covering thickness, δ	8.0×10^{-9}	m	[101]
Volume fraction of ionomer in CL, f_v	0.3	-	[44]
Effective Pt surface ratio, ϵ_{eff}	0.75	-	[106]
PTFE wieght percentage, wt%	10	-	[77]
Fuel and air inlet temperature, T	343	K	
Thermal conductivity of electrolyte, k_{mem}	0.29	W/m K	[132]
Thermal conductivity of CL, k_{CL}	0.27	W/m K	[132]
Thermal conductivity of GDL, k_{GDL}			
In-plane	1.7	W/m K	[54]
Through-plane	21	W/m K	[54]
Evaporation rate constant, C_{evp}	100	1/s	
Condensation rate constant, C_{con}	100	1/atm s	
Permeability of CL, K_{CL}	1.2×10^{-13}	m ²	[133]
Permeability of GDL, K_{GDL}			
in-plane	3×10^{-12}	m ²	[54]
through-plane	8.69×10^{-12}	m ²	[54]
in-plane	0.6×10^{-11}	m ²	[58]
though-plane	0.2×10^{-11}	m ²	[58]
Specific heat capacity, c_p			
Electrolyte	800	J/kg K	[65]
CL	1000	J/kg K	[65]
GDL	1000	J/kg K	[65]
Air	1006.43	J/kg K	[65]
H ₂	1428.3	J/kg K	[65]

Continued on next page

Table 3.6 – continued ...

Parameters	Value	Units	
CC	800	J/kg K	[65]
Membrane density, ρ_m	1980	kg/m ³	[129]
Membrane equivalent weight, M_1	1100	kg/kmol	[134]

3.13.2 Microscale Models and Governing Equations

Since the sample of cathode catalyst layer represents the arbitrarily chosen portion, the boundary conditions applied are also symmetry/periodic except at the inlet and the outlet. For species transport, the inlet boundary conditions is applied at face 1x as given in Fig. 3.11 of the void region. For portions of ionomer and carbon spheres intersected by face 1x are set to be symmetry and wall, respectively. Similarly, the portion of void intersected by face 1x' is set to be outflow while the conditions for ionomer and the carbon particle remain same as the inlet. All other sides of the domain (2z, 2z', 3y and 3y') are selected as symmetric for the species, i.e., assuming similar operating conditions on all sides. The boundary condition for membrane phase potential is specified at the face 3y of the domain with continuity of ionic current on all sides except the left (face 1x) and right sides (face 1x') (sides coinciding with species inlet and outlet) where symmetric conditions are applied. For the present work the inlet concentration of species is specified as 0.21 and 0.1 for oxygen and water vapour, respectively, while the potential at the top side for membrane is a constant value of 1 V. The mesh used in the present work is shown in Fig. 3.12.

All the calculations in this work have been performed using ANSYSTM FluentTM. Since only diffusive flow has been assumed in this work, all the governing equations have been solved using the User-Defined-Scalar (UDS) equations with appropriate under relaxation factors for each scalar quantity. The generalized diffusion equation is written as;

$$-\frac{\partial}{\partial x_i} \left(\Gamma_k \frac{\partial \phi_k}{\partial x_i} \right) = S_{\phi_k} \quad k = 1, \dots, N \quad (3.48)$$

where Γ_k and S_{ϕ_k} are the diffusion coefficient and source term for each scalar variable being solved. In present case the variables being solved are species mass fraction, temperature, solid phase and membrane phase potential. The diffusion and source terms for the variables are calculated and linked through the UDFs (User Defined Functions).

The calculation domain is discretized into 0.991 million hybrid cells with varying mesh density for each material region. In order to verify the grid independency of the calculated results, all the calculations have been performed for various mesh densities ranging from 0.51 to 1.2 million cells. It was observed that by further increasing the mesh density above 0.991 million cells, there was no change in the calculated values of the scalar quantities. For spatial discretization of conservation equations, a 2nd order scheme has

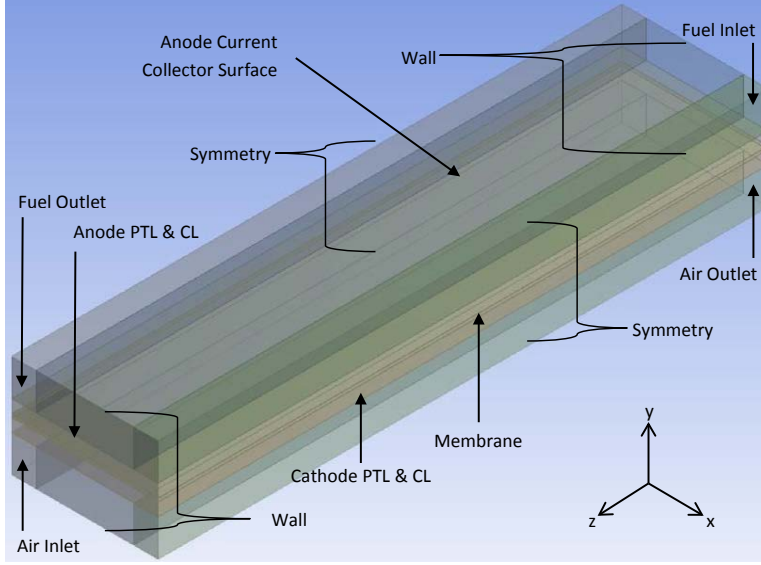


Fig. 3.10: *Different components of PEM fuel cell with interdigitated flow field configuration.*

been utilized with convergence criteria limited to a difference of 1×10^{-6} between consecutive iterations. All the calculations were performed on i7 core with 8 GB of memory consuming approximately 20 hours for the converged results.

3.13.3 Model Development for Microscopic Transport and Reactions

This work has been carried out by simulating the governing equations for air, energy, protonic current and the electronic current densities. The inlet humidity of the air has been so selected that the condensation of water vapours into liquid state is avoided i.e., 50%. Additionally, the convective force for species transport has also been neglected i.e., only the diffusive flux governs the species movement inside the domain. The electrochemical reactions occur at the surface of the Pt particles and quantified by using the Tafel approximation [135]. The continuity equations for the oxygen transport is given as;

$$0 = \nabla \cdot \left[D_{O_2} \nabla Y_{O_2} - \frac{1}{4F} i_o \frac{Y_{O_2}}{Y_{O_2,ref}} \exp \left(\frac{\alpha_c F}{RT} \eta \right) \right] \quad (3.49)$$

where Y_{O_2} represents the local concentration of oxygen in the air. The Eq. (3.49) consists of two parts on the right hand side: the first part represents the diffusion of species through the domain while the second part gives the electrochemical reaction related oxygen consumption. Since in this work there are total of two media through which the oxygen species has to diffuse, i.e., the void and the ionomer, so each species has different diffusion coefficients for the two media while the Pt particles are immune to any sort

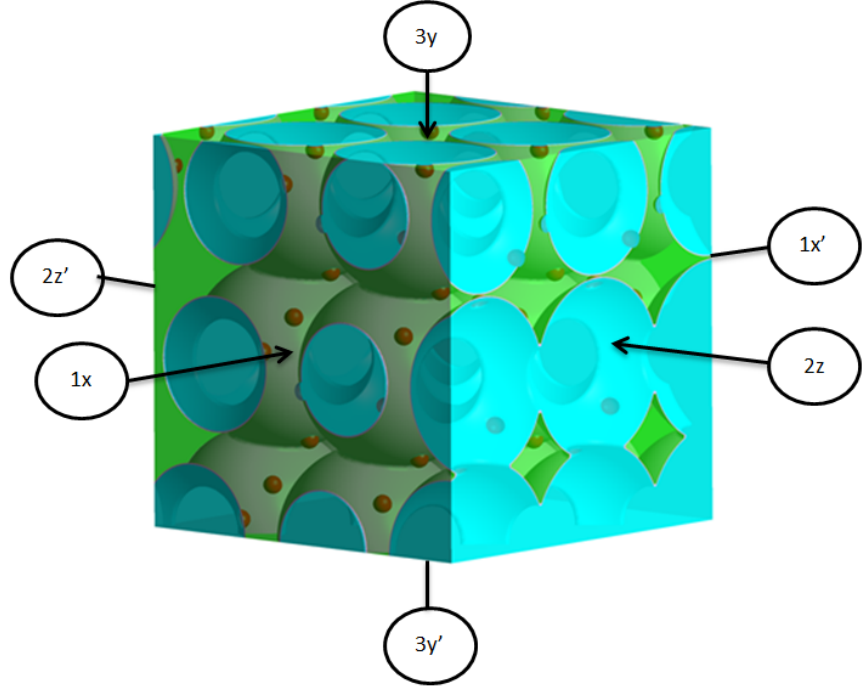


Fig. 3.11: Boundary faces for the computational domain.

of diffusion. For diffusion of species in voids, the diffusion coefficient is based on both the bulk diffusion and the Knudsen diffusion because of the small pore diameter. The Knudsen diffusion coefficient reads,

$$D_{O_2, kn} = 0.485d_p \sqrt{\frac{T}{32}} \quad (3.50)$$

where d_p is the local pore diameter and is based on the average of maximum and minimum values. The bulk diffusivity is evaluated according to the binary diffusion of oxygen [136], given as;

$$D_{O_2, b} = 2.2 \times 10^{-5} \left(\frac{T}{T_o} \right)^{1.5} \left(\frac{p_o}{p} \right) \quad (3.51)$$

The total oxygen diffusivity is calculated in the void region as [137];

$$\frac{1}{D_{O_2}} = \frac{1}{D_{O_2, kn}} + \frac{1}{D_{O_2, b}} \quad (3.52)$$

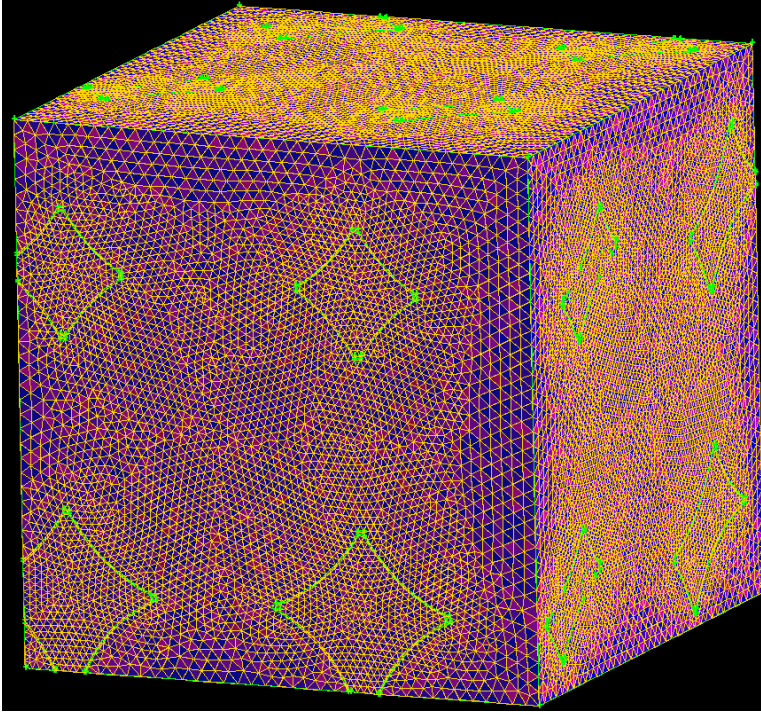


Fig. 3.12: *Mesh for the micromodel.*

To reach the reaction site i.e., the Pt surface, the oxygen has to diffuse through the ionomer (membrane). The diffusivity of oxygen in the ionomer (membrane) is related to local temperature, as [138];

$$D_{O_2} = 10^{-10} \times (0.1543 (T - T_o) - 1.65) \quad (3.53)$$

Similarly, the governing equation for water vapour diffusion and production takes the following form [135];

$$0 = \nabla \cdot \left[D_{H_2O} \nabla Y_{H_2O} + \frac{n_d \sigma_m}{F} \nabla \phi_m \right] + \nabla \cdot \left[\frac{1}{2F} i_o \frac{Y_{H_2O}}{Y_{H_2O,ref}} \exp \left(\frac{\alpha_c F}{RT} \eta \right) \right] \quad (3.54)$$

The Eq. (3.54) contains an extra source term for the addition of water in the domain due to the electro-osmotic drag. The bulk diffusion and the Knudsen diffusion coefficients for water vapours in the void region are calculated as [135, 136];

Table 3.7: *Curve-fitted Parameters for protonic conductivity of membrane (adopted from Lange et al. [135])*

Coefficient	Value
c_1	2.8133×10^{-2}
c_2	1.328355
c_3	-1.1642×10^{-2}
c_4	3.442175×10^{-5}
c_5	-3.33815×10^{-8}
c_6	-7.2939×10^{-2}

$$D_{\text{H}_2\text{O},b} = 2.93 \times 10^{-5} \left(\frac{T}{T_o} \right)^{1.5} \left(\frac{p_o}{p} \right) \quad (3.55)$$

and,

$$D_{\text{H}_2\text{O},kn} = 0.485 d_p \sqrt{\frac{T}{18}} \quad (3.56)$$

For the ionomer region, the diffusion of water vapour has been assumed to have a constant value of $6 \times 10^{-10} \text{ m}^2/\text{s}$. The term α_c in Eqs (3.49) and (3.54) is the cathodic transfer coefficient and is given as [130]

$$\alpha_c = (2.25 \times 10^{-3}) T - 0.178 \quad (3.57)$$

Also, i_o , the exchange current density, is based on the local temperature as [130];

$$i_o = 0.029825 \times 10^{-1521.93/T} \quad (3.58)$$

Since there are two types of current flowing in the domain i.e, protonic current and the electronic current, two conservation equations have been employed for simulating the current flow, given as;

$$\nabla \cdot (\sigma_m \nabla \phi_m - S) = 0 \quad (3.59)$$

where σ_m accounts for the protonic conductivity of the membrane and is given as [135];

$$\sigma_m = (c_1 \exp[(c_2 T - c_3 T^2 + c_4 T^3 - c_5 T^4) \omega] + c_6) \quad (3.60)$$

where ω is the relative humidity and constants c_1 to c_6 are the curve fitted values [135], as given in Table 3.7. Similarly, the conservation equation for the electronic current is given as;

$$\nabla \cdot (\sigma_s \nabla \phi_s - S) = 0 \quad (3.61)$$

The source term S in both Eqs (3.59) and (3.61) models the consumption of protons and electrons at the Pt surface, respectively, and is evaluated as;

$$S = i_o \frac{Y_{O_2}}{Y_{O_2, \text{ref}}} \exp\left(\frac{\alpha_c F}{RT} \eta\right) \quad (3.62)$$

The activation overpotential, η , used in Eqs (3.49), (3.54) and (3.62) is estimated as [106, 107];

$$\eta = \phi_{m,l} - \phi_{s,l} - \phi_{\text{ref}} \quad (3.63)$$

where $\phi_{m,l}$ and $\phi_{s,l}$ are the local membrane phase (protonic) and solid phase (electronic) potentials, respectively, and ϕ_{ref} is the reference potential that depends on the type of electrode. Since in this work, only the cathode catalyst layer has been focused, so the reference potential is set to 0 [101].

In order to simulate the temperature distribution inside the calculation domain, the energy conservation equation has been applied and consists of heat conduction through various media of the domain, ohmic heating due to flow of protons and electrons and the reaction heating [135].

$$0 = \nabla \cdot (k \nabla T) + \frac{(\nabla \phi_s)^2}{\sigma_s} + \frac{(\nabla \phi_m)^2}{\sigma_m} + \nabla \cdot \left[i_o \frac{Y_{O_2}}{Y_{O_2, \text{ref}}} \exp\left(\frac{\alpha_c F}{RT} \eta\right) \right] (\eta + \Pi) \quad (3.64)$$

where Π is the Peltier coefficient for the oxygen reduction reaction approximated as [135, 139];

$$\Pi_h \approx T \frac{\Delta S_h}{4F} \quad (3.65)$$

ΔS_h is the entropy change for the half cell reaction and has been assumed a constant in this work (326.6 J/mol K [140]).

4 Results & Discussion

This chapter highlights the results obtained by the simulation of both macro and micro models as presented in earlier chapters. The first part of the chapter represents the modelling assumptions and the results of macro level, while, the second part is dedicated for the results obtained by the microscale simulations.

4.1 Macro Model

All numerical simulations are performed by solving a set of mathematical equations simultaneously, number of assumptions are always made for two reasons;

- not all physical parameters are well understood and documented,
- to keep the simulations in workable limits in terms of computational power requirements and time consumption.

The modelling simplifications used in present work are listed below:

- all processes are time independent, so the term $\frac{\partial}{\partial t}$ in all equations defined in Ch. 3 are ignored,
- the gas behaves as an ideal gas,
- the gas flow is laminar,
- liquid water is in form of fine mist in the channels and moves with the same velocity as the gases, however, inside porous media the capillary pressure dictates the liquid diffusion independent of gases,
- there is no current loss at the interfaces of components, i.e., perfect connections are assumed,
- to simulate the electrochemical reactions, the catalyst agglomerate model is applied, and the local overpotential within an agglomerate is assumed to be constant.

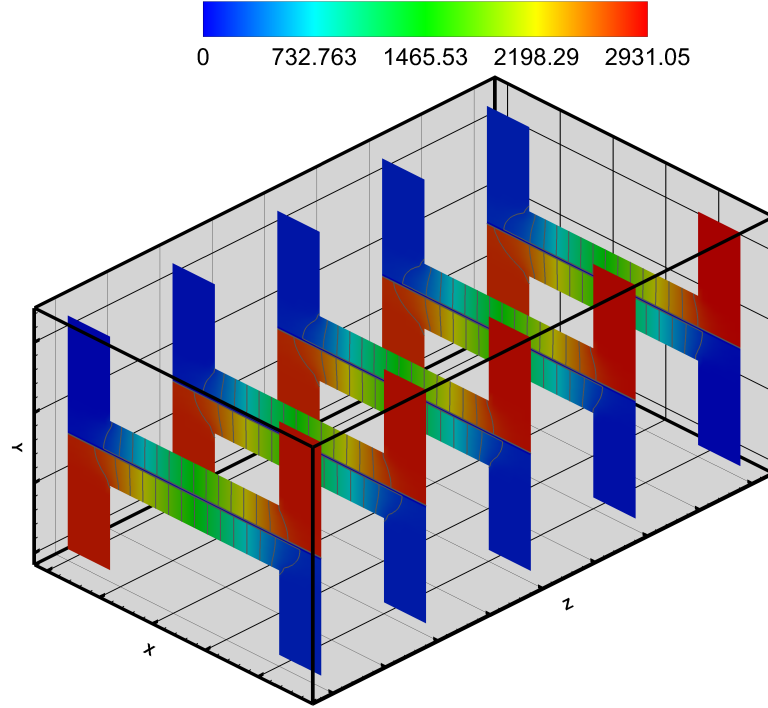


Fig. 4.1: *Pressure distribution in PEM fuel cell with interdigitated flow field, Pa.*

4.1.1 Pressure Distribution

Fig. 4.1 shows the pressure distribution in the PEM fuel cell along the length of the cell at various cross sections as shown in Fig. 4.2. The main advantages associated with interdigitated flow fields are that they help in establishing a convective flow through the domain and remove the liquid water due to the shear force. The interdigitated flow field is designed such that each channel is dedicated either to inflow or the outflow of both the air and fuel sides, i.e., the cathode and the anode, respectively. By maintaining the pressure difference between the inlet and outlet on the respective sides, the flow is diverted to the gas diffusion layer contrary to the conventional flow fields where the flow slides on the interface between the channels and the gas diffusion layers, and only diffusive flow occurs in the gas diffusion layer. One of the distinctive features as seen here is that in such flow field configurations, the pressure drop occurs in the gas diffusion layers only and there is almost no pressure drop in the channels along the length of the cell. This helps in providing almost the same amount of both fuel and air throughout the length of the cell, whereas, in other types of flow field, the distribution is uneven, i.e., more at the start and less towards the end. Additionally, it can also be seen in Fig. 4.1 that there is a pressure drop in the catalyst layer and the gas diffusion layer due to high resistance offered by the porous media as defined by Eq. (3.7).

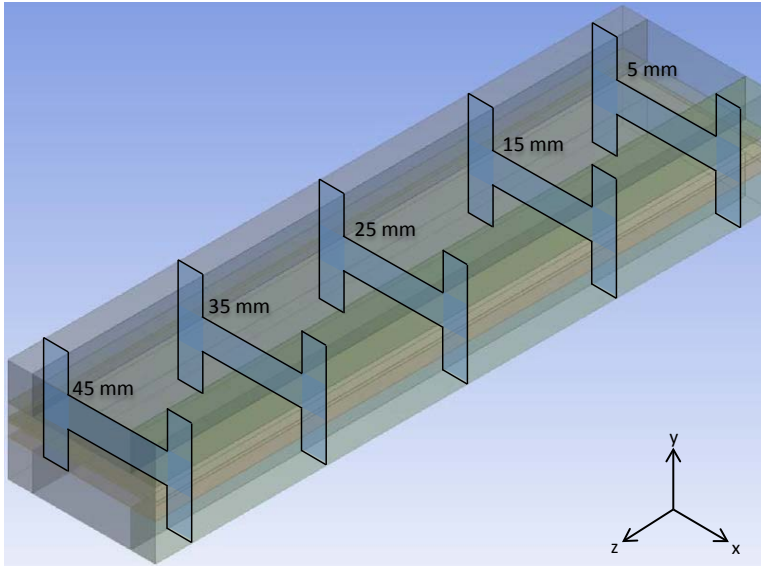


Fig. 4.2: Location of cross-sections in PEM fuel cell for pressure, velocity and species distribution.

4.1.2 Species Distribution

It has been established in Sec. 2.2.1 that the gas diffusion layer is fabricated from various layers of carbon fibres, so the transport of species via diffusion flux is highly dependant on the orientation of such carbon fibres. One of the most common techniques, used mostly in numerical quantification of species in the work domain is to use the Bruggeman approximation that only corrects for the porosity of the material and does not reflect the impact of the material. Fig. 4.3 represents the oxygen distribution at the cathode side of PEM fuel cell using the simple approach, i.e., the Bruggeman approach at the cross sections given in Fig. 4.2 but only for the cathode side. In such approach, the diffusivity of the species is equal in both the in-plane and through-plane directions as depicted here. One of the down sides of such approximation is that due to equal diffusive flux in all directions, the concentration of reacting species in the catalyst layer is always over-predicted which results in higher current densities than the actual case.

However, in actual scenarios, the diffusive flux of species is different in in-plane and through-plane directions, such that, the in-plane diffusivity is always higher than the through-plane diffusivity. Such a variation of diffusivity results in less diffusion flux to the catalyst layer thereby limiting the current density to a lower values as compared to the isotropic effects. Fig. 4.4 represents the mass fraction of oxygen by simulating the diffusive flux using the anisotropic formulation as given by Eq. (2.6). By comparing the two cases, i.e., Figs 4.3 and 4.4, it can be seen that in situations with anisotropic effects, the oxygen mass fraction even above the air inlet channel is less than the one predicted by the isotropic case. However, the difference in both the predictions is quite small at the

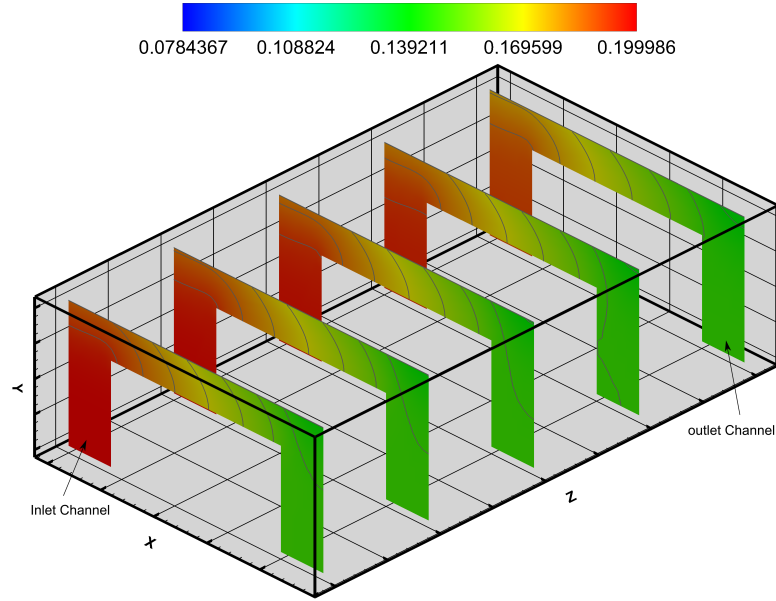


Fig. 4.3: *Oxygen (O_2) distribution in isotropic gas diffusion layer of PEM fuel cell.*

membrane/catalyst layer interface at the location above the inlet channel, but a major deficit is shown by moving in the x direction where the oxygen mass fraction is at the lowest over the outlet channel. So, it can be concluded from this result that in order to predict the performance of the cell in accurate manner, the Bruggeman approximation should be replaced by the anisotropic diffusion flux or otherwise the predicted mass distribution and in turn the current density is an ideal one but not real, and the same is true for hydrogen at the anode side. Fig. 4.5 compares the oxygen mass fraction at the interface of the gas diffusion layer and the catalyst layer further promoting the use of anisotropic species diffusivity because the isotropic case is responsible for overestimating the supply of oxygen to the catalyst layer.

4.1.3 Charge Distribution

When the hydrogen reacts electrochemically at the anode of the cell, it splits into the hydrogen ion and the electron. The electrons are harnessed for driving the external loads and must travel externally to reach the cathode side. So the path followed by the electrons is that they are generated at the anode catalyst layer and via the anode gas diffusion layer, are collected at the anode current collector which feeds the electrical flow to the external load. After passing through the load they arrive at the cathode catalyst layer via the cathode current collector and the gas diffusion layer. However, the protons, on the other hand, arrive at the cathode catalyst layer via the electrolyte (membrane). So, in order to simulate the two types of charge flow, two conservation equations are required for each type of flow and the driving force for such flow is the electronic and protonic potentials between the anode and cathode current collectors and the anode and

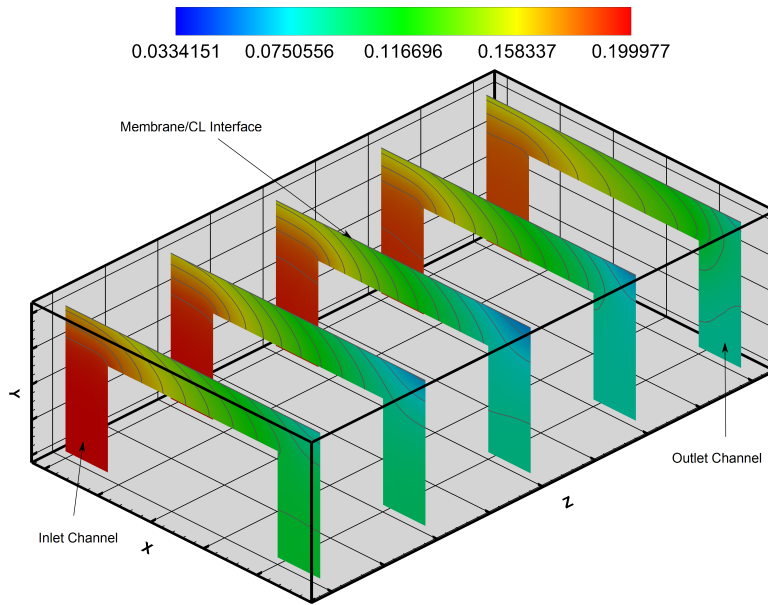


Fig. 4.4: *Oxygen (O_2) distribution using the anisotropy of the gas diffusion layer.*

cathode catalyst layers, respectively.

Fig. 4.6 represents the distribution of the electrical potential at the anode side of the PEM fuel cell at different cross sections when the operating voltage is 0.4 volts, while, Fig. 4.7 shows the electric potential for the cathode side at the same operating voltage. The sign convention in the anode side is because of the fact that the electrons travel out of the domain (the electrolyte or the membrane is perfect insulator for electrons) and in the cathode side, they travel into the domain. In order to simulate such scenario, the operating voltage is fixed at the cathode current collector outer surface while the surface of the anode current collector is set at 0 volts. As it can be seen in both the figures that the maximum electric potential exists at the area above the inlet channel at the cathode side, referring to maximum activity in terms of electron transfer, or, in other words, most of the electrons are being generated in the catalyst layer of anode at the location just above the inlet gas channel or below the outlet fuel channel and similarly, most of the consumption is in the same region in the cathode side.

Fig. 4.8 shows the distribution of the protonic potential in the anode catalyst layer, the membrane and the cathode catalyst layer at various cross sections in the length of the cell. Since the protonic potential dictates the flow of hydrogen ions, which is dependent on the ionomer or the presence of membrane phase so that the range of protonic migration is limited in between the anode catalyst/gas diffusion layer interface and the cathode catalyst/gas diffusion layer interface only. Furthermore, it can be seen that the protonic potential is higher in the anode catalyst layer than the cathode catalyst layer, showing the migration direction of protons from the anode side to the cathode side via the membrane.

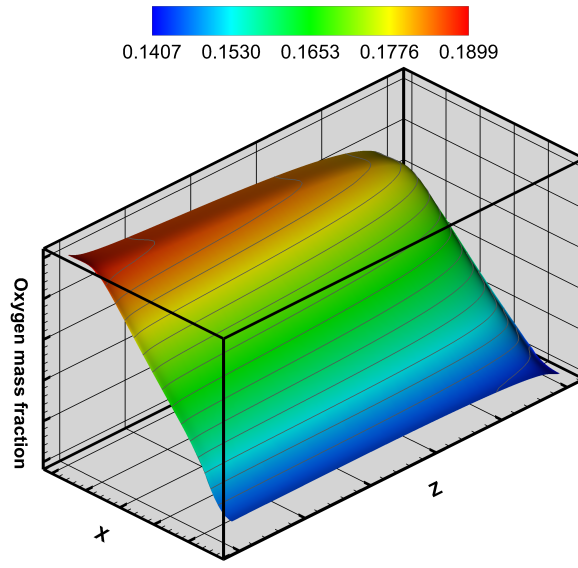
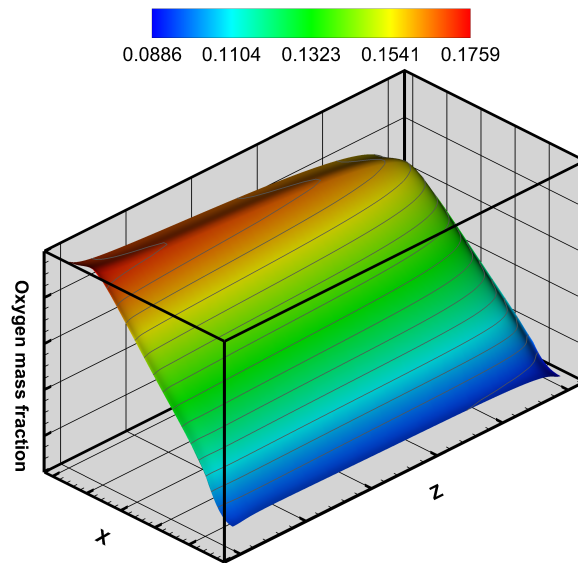
(a) *Isotropic diffusion*(b) *Anisotropic diffusion*

Fig. 4.5: *Oxygen mass fraction at the interface between the gas diffusion layer and the catalyst layer.*

Furthermore, the potential drop is almost constant in the proximal membrane region

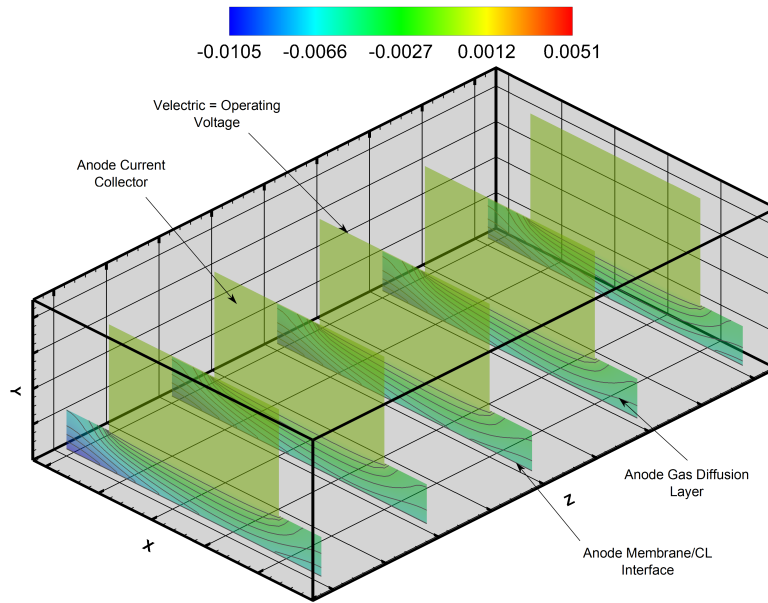


Fig. 4.6: *Electric potential distribution at the anode of the PEM fuel cell, V.*

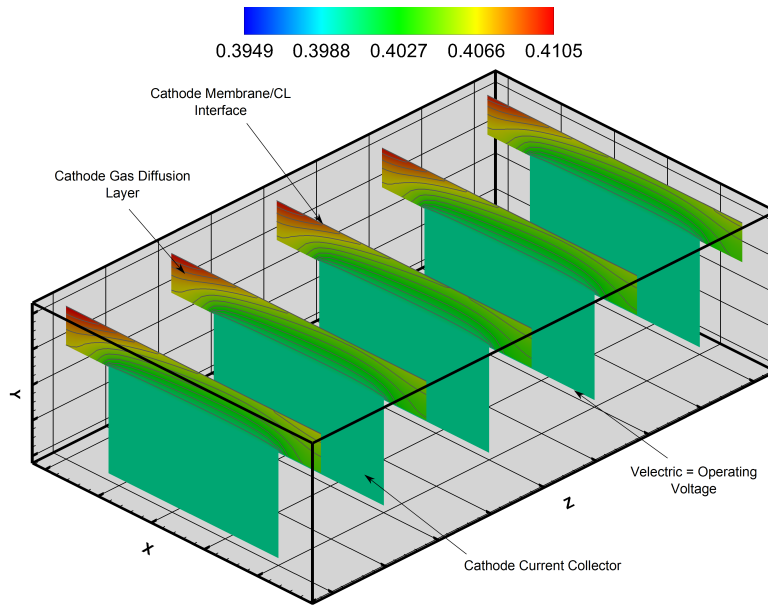


Fig. 4.7: *Electric potential distribution at the cathode of the PEM fuel cell, V.*

showing no consumption or production of the protonic current. Additionally, another important factor for the migration of protons is the hydration levels because the protonic

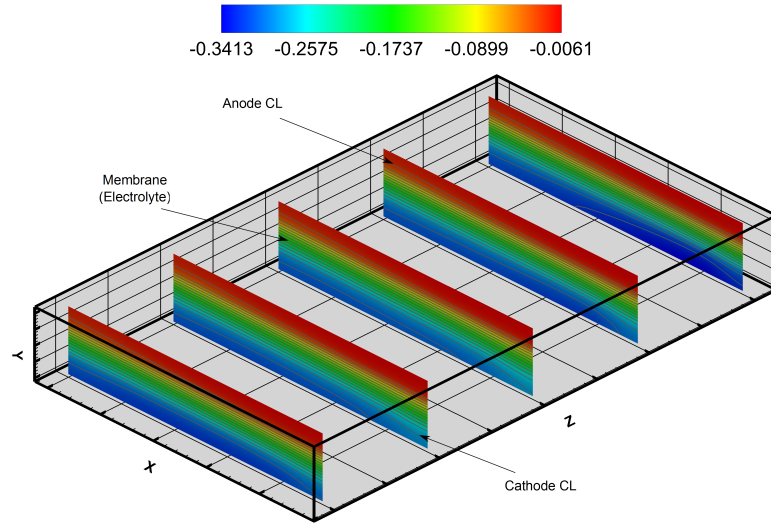


Fig. 4.8: Protonic potential distribution in the anode and cathode catalyst layer and the membrane along the length of the cell, V.

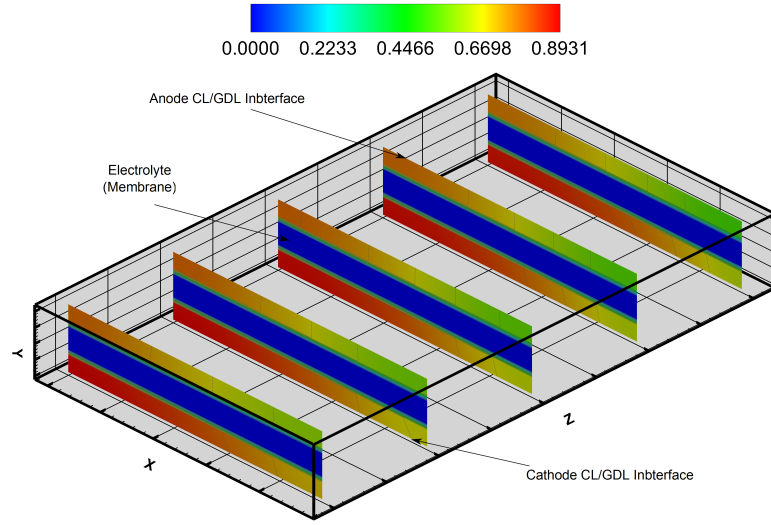


Fig. 4.9: Water activity in the catalyst layer and the membrane of a PEM fuel cell.

conductivity of the membrane phase is highly water dependant. Fig. 4.9 shows the water activity in the catalyst layers and the membrane of the PEM fuel cell. As it can be observed that the water activity is highest in the cathode catalyst layer due to the fact that there are three different process that increase the water quantity, i.e., the electrochemical reactions, electro-osmotic drag and the pre-humidification of the inlet air. However, on the anode side of the cell, it can be observed that the highest activity

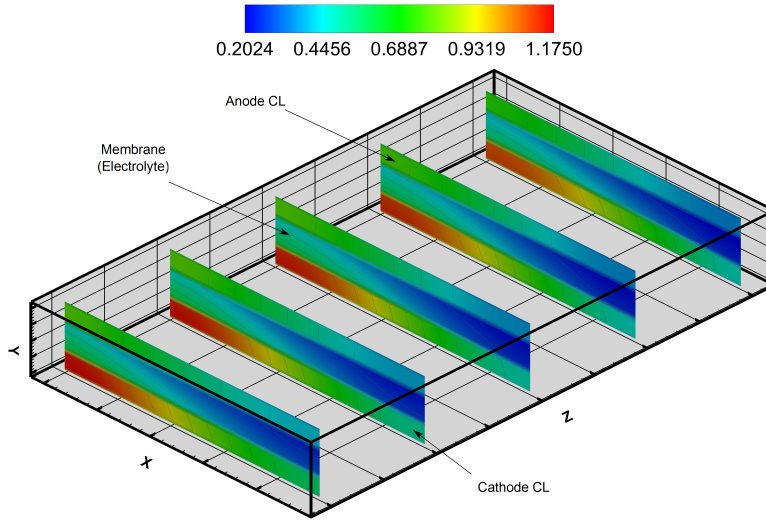


Fig. 4.10: Protonic conductivity of the membrane and the anode and cathode catalyst layer calculate using Eq. (2.9), S/m.

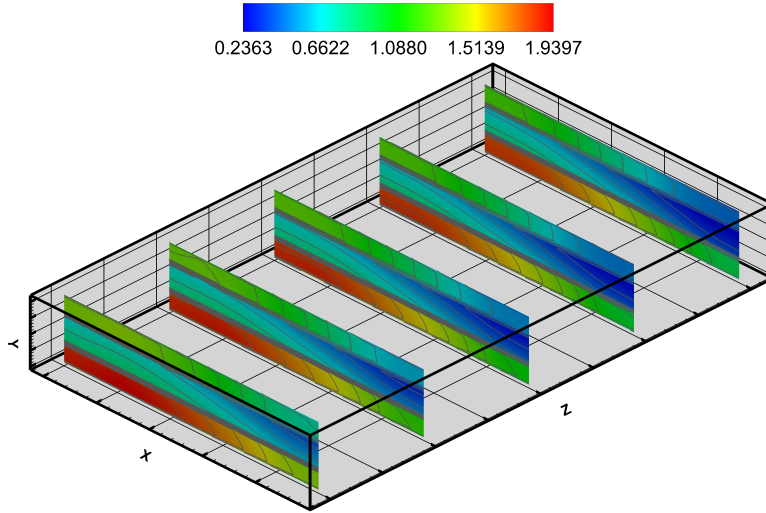


Fig. 4.11: Protonic conductivity calculation using the Bruggeman approximation in Eq. (2.11), S/m.

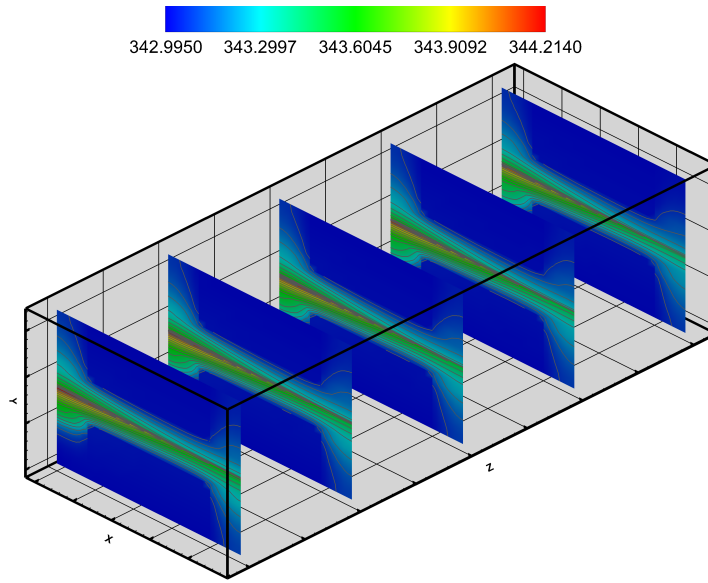
is located below the anode outlet channel because the hydrogen fed into the cell is pre-humidified to a certain value and as the hydrogen is being consumed, the relative humidity of water increases helping in hydration of the cell, and additionally the back diffusion also helps in maintaining the high hydration levels thus increasing the water activity.

Since the diffusion coefficient for the protonic migration or the protonic conductivity is

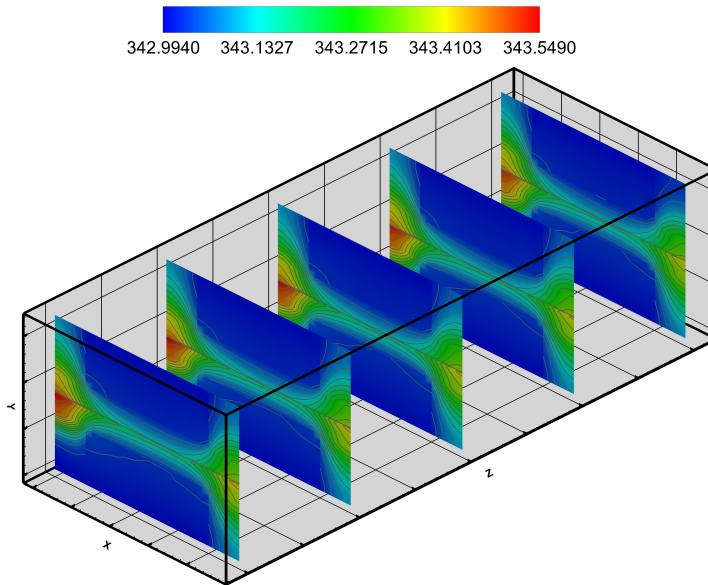
highly dependent on the hydration levels of the membrane material, so other than the driving potential, the water activity in the cell is also one of the determining factor for the magnitude of the migration of protons from anode to the cathode side. The protonic conductivity at an operating level of 0.4 V is shown in Fig. 4.10. It can be observed that the region to the left side of the cathode catalyst layer above the inlet channel shows the highest conduction due to the reasons explained above. However, the right side of both the membrane and anode catalyst layers show the minimum also because of the lower water activity in that region. However, comparing the Fig. 4.10 to Fig. 4.11, where latter has been calculated using the Bruggeman approximation reveals a significant difference in the magnitude of the two. Additionally, With Bruggeman approximation, it can also be observed that comparatively, a large region of the cathode catalyst layer shows high conductivity, whereas, in other case, the maximum region is limited to region associated with the cathode inlet channels.

4.1.4 Temperature Distribution

The in-plane thermal conductivity of the gas diffusion layer is higher than the through-plane conductivity because of the configuration of the material that are typically used, i.e., the fibre orientation in the medium. The reason for such small thermal conductivity in through-plane direction is due to the void space present between the layers of carbon fibre bundles, while in the in-plane direction, the heat is transferred through the length of each fibre thus depicting more thermal conductivity. Fig. 4.12a, shows the temperature distribution for the PEM fuel cell at cross-sections as presented in Fig. 4.2. It can be observed that the maximum temperature exists at the left side of the plane corresponding to the region of the catalyst layer right above the inlet channel for the air. Since the thermal conductivity of the gas diffusion layer is 21 W/m K in the in-plane direction and only 1.7 W/m K in through-plane direction, the high temperature zone is restricted to the the cathode catalyst layer opposite to the air inlet channel, but, in the horizontal direction, the maximum temperature region stretches almost to the middle of the plane or section. The region near to the current collector is noted to be at a minimum because it is being cooled by the current collector that also serves as the heat sink, maintained at 343 K. Additionally, the air in the channel also helps in reducing the temperature through convection. On the contrary, Fig. 4.12b, shows the temperature profile while simulating the cell using isotropic heat conduction of the diffusion media at operating voltage of 0.5 volts. The maximum temperature region, for this scenario, is also located in the region directly above the inlet channel. Comparing the Figs 4.12a and 4.12b, a considerable difference is observed. In the case with isotropic thermal conductivity, the maximum temperature region is confined to the upper left corner and equally extends into the gas diffusion layer while in anisotropic case it is limited to the region near to the upper boundary but extends in the horizontal direction. This can be explained by the equal conduction of heat in all directions in the isotropic case while in anisotropic case it is restricted in the through-plane direction. The other difference is the maximum value of the temperature in the domain. As observed, the maximum temperature for isotropic conductivity increases by just a fraction of the inlet temperature, i.e., 343.508 K, but, for anisotropic conductivity, there is a difference of almost 1 K. The difference becomes even more noticeable when considering that the current densities for the two cases. Although



(a) *Anisotropic thermal conductivity*



(b) *Isotropic thermal conductivity*

Fig. 4.12: Comparison of temperature profile with isotropic and anisotropic thermal conductivities at 0.5 V.

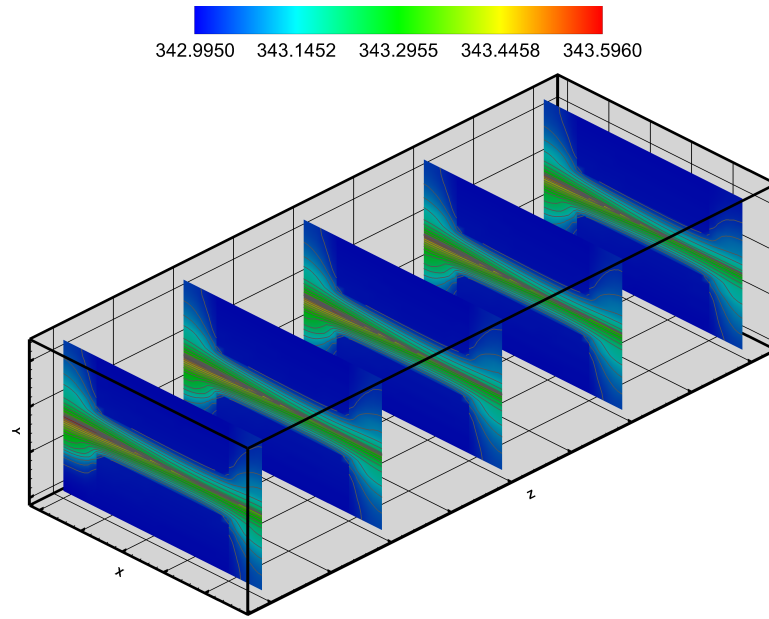


Fig. 4.13: *Temperature distribution in PEM fuel cell unit at 0.6 V, K.*

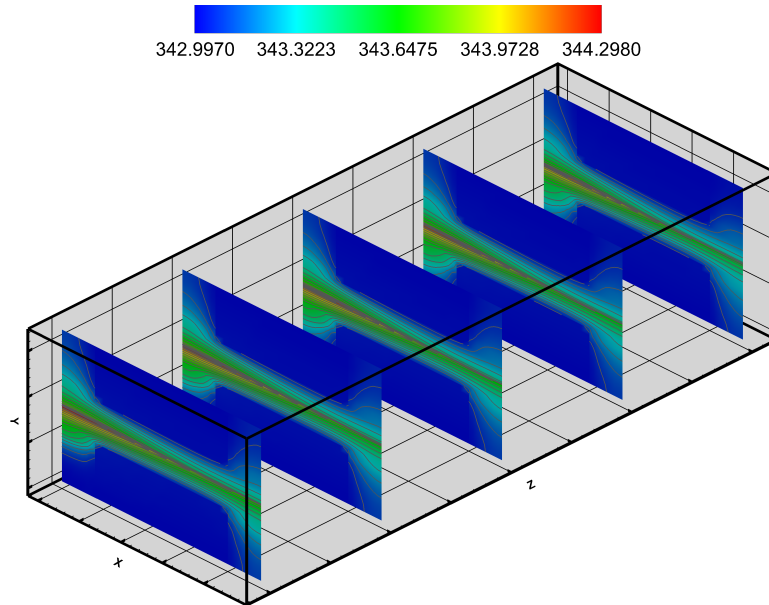


Fig. 4.14: *Temperature ditribution at 0.4 V in a unit PEM fuel cell, K.*

both the simulations present the result for 0.5 V operating level but the current densities are quite different i.e., approximately 0.62 A/cm^2 for the anisotropic and 0.78 A/cm^2 for

the isotropic case, as can be seen in Fig. 4.20. Since higher current densities have higher electrochemical reaction rates, thus, higher reaction heat, but, as seen in the figures, the anisotropic case is not capable of showing the accurate temperature profile inside the cell.

Figs 4.13 and 4.14 compares the temperature distribution in the PEM fuel cell for the operating voltages of 0.6 and 0.4 volts. One of the main difference in the temperature distributions at these two operating levels is the range of maximum temperatures. Since, as expected, the electrochemical reaction rate is higher at lower voltage levels, so, the temperature profile also depicts higher temperature. For both the operating levels, it can also be observed that the high temperature zone thins down along the length of the cell, while the rate of shrinkage is higher for 0.6 V operating level. The reduction in the maximum temperature zone along the length of the fuel cell can be explained by considering the electrochemical reactions rate that reduces as the oxygen is being consumed along the length. One of the most important fact to be noted in the Figs 4.13 and 4.14 is that the maximum temperature zone exist in the cathode side of the fuel cell. The catalyst and the gas diffusion layers on the anode side do not achieve the same temperature levels due to the fact that the heat generated at the anode catalyst layer due to electrochemical reactions is lower as compared to the heat generated at the cathode side. The second reasoning to the lower temperature profile on the anode side is that the membrane which is parting the two electrodes has a very low thermal conductivity, i.e., 0.21 W/m K, the transfer of major portion of heat - generated in the cathode catalyst layer - is directed through the gas diffusion layer to the current collector at the cathode side. Furthermore, since the membrane is also considered impermeable to all species (diffusion and convection), there is no convective heat removal in the membrane.

4.1.5 Water Management

In Fig. 4.15 the water generation rate due to the electrochemical reactions has been compared to those by the back diffusion and electro-osmotic drag sources. There are two significant unique trends in terms of the electrochemical water generation rate. Firstly, by comparison it can be observed that the water generation rate in the cathode of the PEM fuel cell is less than the water addition due to the electro-osmotic drag and difference becomes exaggerated at lower voltages as compared to the high voltage level. This difference in the generation of water due to osmotic drag and electrochemical reaction is due to the fact that the volume averaged value of the electro-osmotic drag coefficient is higher than unity in all cases. Secondly, by observing Fig. 4.15, it can be seen that the water production rate increases by reducing the operating voltage, as expected, because of the enhanced rate of electrochemical reactions, but, from reducing the voltage level from 0.7 to 0.5 V, the increase in the water generation due to the electrochemical reactions is approximately 60%. Whereas, by decreasing the voltage from 0.5 to 0.3 V, the increase in the average electrochemical water generation is only ~11%. Thus, the small increase in the water generation rate at low operating voltage (0.3 V) due to electrochemical reactions indicate the concentration losses have increased considerably and fuel cell is operating in the mass limitation range.

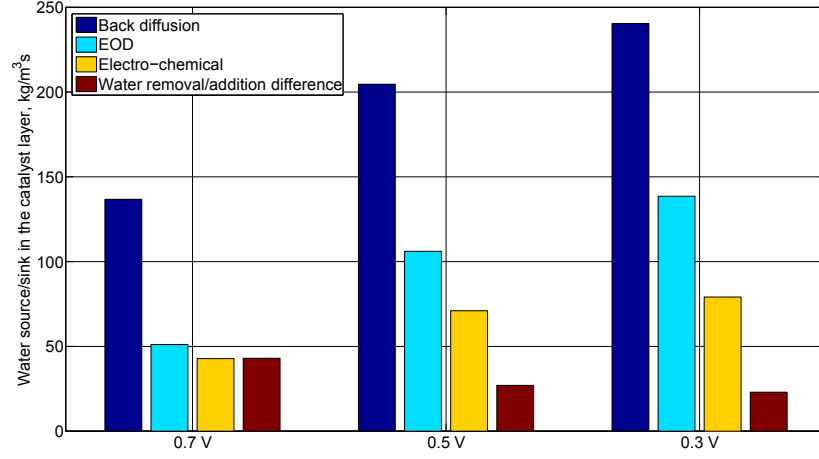


Fig. 4.15: Back diffusion, electro-osmotic drag and the electrochemical generation of water for different operating voltages at the cathode side of PEM fuel cell (averaged over the cathode catalyst layer volume).

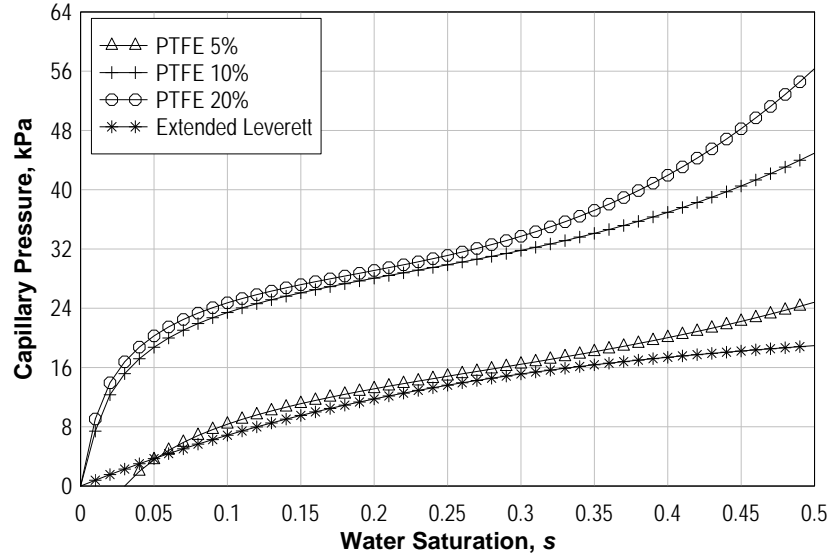
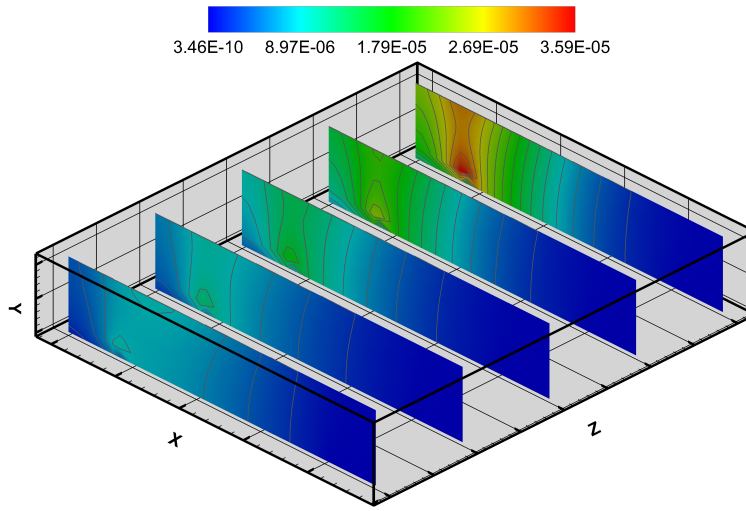
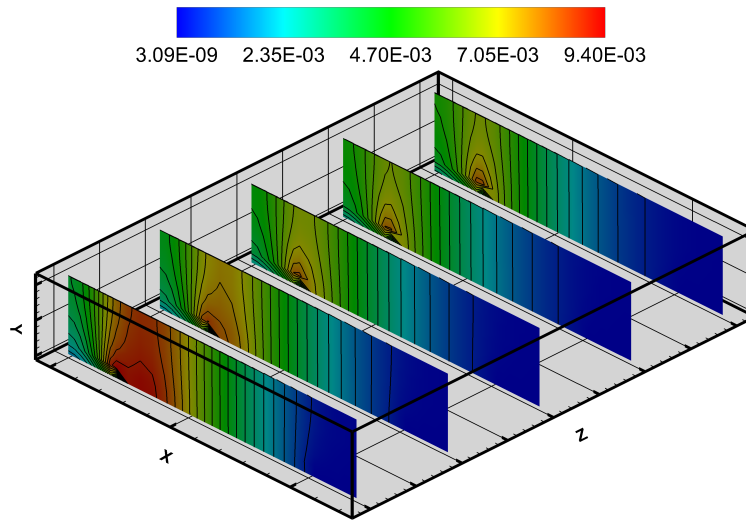


Fig. 4.16: Comparison of capillary pressure based on conventional Leverett and validated approach.

The materials used in manufacturing of PEM fuel cell porous electrodes is highly heterogeneous in nature representing mixed wettability properties and the standard formulation for modelling the water saturation is considered ineffective for such calculations due to such material property. Also, the effects of hydrophobic (PTFE) loading, assembly compression and the operating temperature on the capillary transport mechanism are not



(a) Operating voltage = 0.7 V



(b) Operating voltage = 0.3 V

Fig. 4.17: Comparison of water saturation in the cathode catalyst layer and the gas diffusion layer using isotropic permeability of the gas diffusion layer.

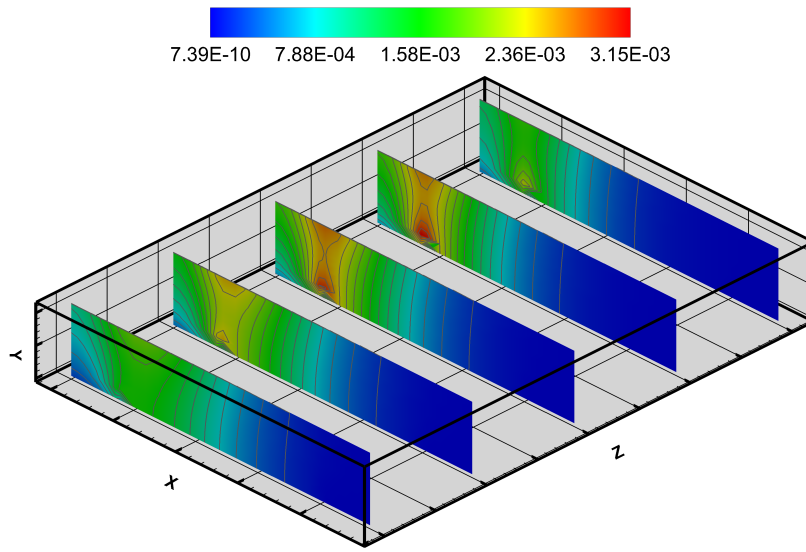
incorporated in the standard approach. The validated approach for modelling the water saturation is compared to the conventional Leverett approach in Fig. 4.16. As it can be seen that the capillary pressure calculated with PTFE content of 5% is almost compar-

able with the conventional Leverett model. But by increasing the hydrophobicity of the material i.e., more PTFE loading, the difference is significant to be neglected. Additionally, comparing the 10% and 20% PTFE loadings, both profiles follow a similar pattern until the saturation level is approximately 0.25, but beyond this range, the increase in the capillary pressure for 20% PTFE loading is higher than that for the 10% loading. In this work, the PTFE content of 10% has been used as the standard loading. The advantage associated with such approach is that the validated formulation eliminates the need for selecting a representative contact angle. Furthermore, it correlates the water saturation to material properties thus accounting for the structural heterogeneity.

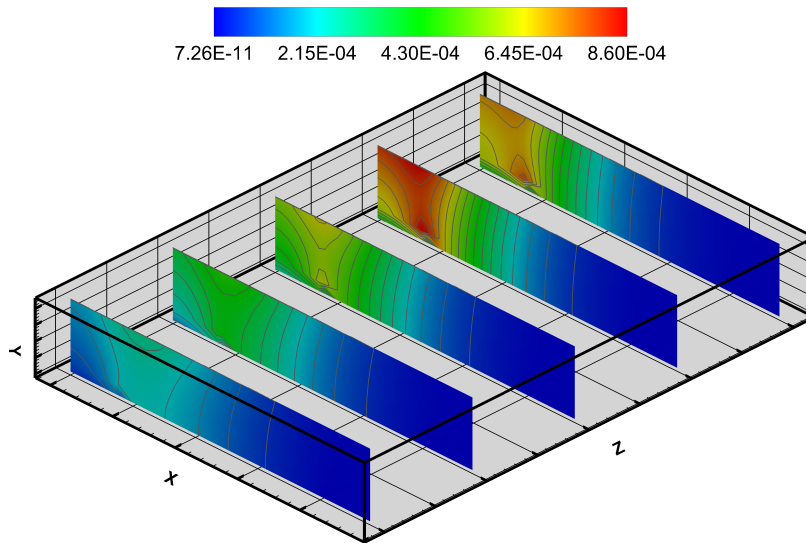
Fig. 4.17 shows the different water saturation patterns at the cathode side of PEM fuel cell for various operating voltages (0.7 and 0.3 V) while considering isotropic permeability of the gas diffusion layer. As it can be seen that at 0.7 V operating level, Fig. 4.17a, the water saturation is minimum near the inlet region. But as the air flows through the domain, the relative humidity becomes higher because of water production due to electrochemical reactions and the capacity to hold more water decreases as it transverses through the domain. At the far region of inlet, the water saturation increases because, as explained, the capacity of air to hold water has considerably reduced to an extent where the condensation of water vapours to liquid water is quite high. The water saturation profile at 0.3 V, Fig. 4.17b, shows increased levels near the air inlet region as compared to other cases due to the fact that the rate of electrochemical reactions is quite high at such voltages and the capacity of air to digest more water vapours has reduced considerably.

The permeability of the gas diffusion layer has been known to have significant effects on the water saturation in the PEM fuel cells. The quantity and distribution of the liquid phase is dependent on the temperature, oxygen and charge distributions that in turn determine the current density. In the present study, two cases have been simulated for the same operating levels, i.e., 0.4 V, with different permeabilities as given in the literature. Pasaogullari and co-workers [54] previously published results based on permeabilities being higher in the through-plane direction as compared to the in-plane direction. However, the opposite has been proposed in the literature by different sources [58]. Therefore, both cases have been simulated and the results are shown in Fig. 4.18.

Fig. 4.18a presents the case for the higher through-plane permeability as given in [54], while, Fig. 4.18b shows the results for higher in-plane permeability as given in [58]. As can be observed in the two figures, both the cases present unique results. The general trend in both the figures is that the saturation level increases along the length of the cell which is due to the decrease in the ability of air to accommodate water as the partial pressure of water vapour increases and approaches the saturation pressure. Another common trend in both the cases is that the liquid water tends to accommodate in the gas diffusion layer near the interface of the current collector due to higher porosity of the gas diffusion layer. However, it can also be noted by comparing the two cases that when the in-plane permeability is higher than the through-plane permeability (Fig. 4.18b), the catalyst layer is equally affected with the saturation effects which leads to decrease in the current densities by blocking the pathways for species transport and insulating the active sites for the electrochemical reactions. Another notable difference in the two cases is the



(a) Anisotropic permeability [54]



(b) Anisotropic permeability [58]

Fig. 4.18: Water saturation profile at 0.4 V for different material behaviours.

total saturation level where the case with higher through-plane permeability has higher saturation levels (Fig. 4.18a) than the case with higher in-plane permeability (Fig. 4.18b).

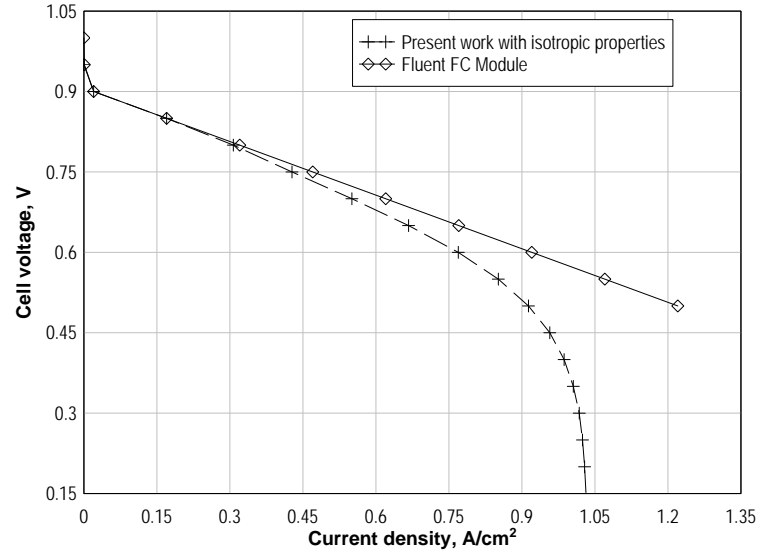


Fig. 4.19: Verification of modelling with *Fluent™* PEM fuel cell module.

This difference in the total saturation levels can be explained by considering the fact that the electrochemical reaction rate is higher when only the gas diffusion layer is the most affected part, i.e., less blockage of pathways and the reaction sites in the catalyst layer which leads to higher reaction rates.

4.1.6 CFD Model Verification and Comparison

The CFD analysis involves a solution of a set of mathematical equations and parameters simultaneously. In order to keep the solution in manageable limits both in terms of time and computations, there are always some simplifications applied to the governing equations. Furthermore, usually the parameters in PEM fuel cells simulations are borrowed from the open literature and not all of them have been validated due to the practical limitations in the experimental work and the large diversity of the processes occurring inside the fuel cell [39]. Furthermore, the characteristics presented by each component of the fuel cell are quite different and the same physical process may vary in different components. So, the validation of the results for CFD modelling have prime importance as it determines the applicability of a certain set of assumptions, simplifications and the parameter values.

Usually, for CFD modeling of PEM fuel cells, the V-I curve has become a standard to compare the results of modelling and experimental work. However, the applicability of such a comparison is questionable because the V-I curve only presents the overall effects. As stated by Mench [39], there can be a good agreement between the models based on a simple V-I curve but internal parameters can be quite different, e.g., the under-prediction

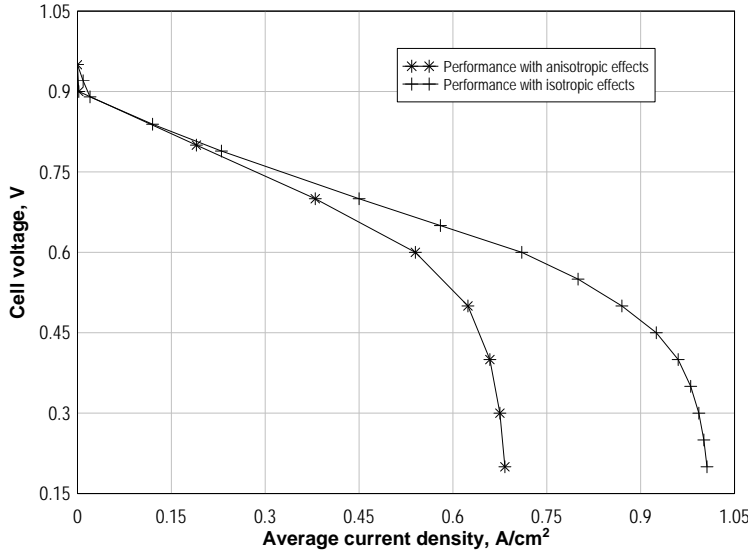


Fig. 4.20: *Comparison of the modelling approaches.*

of one parameter may be balanced by the over-prediction of the other. Furthermore, the comparison of different models to each other based on the V-I curve can also be ambiguous because the operating conditions set in one model may not be applicable to others or not all operating conditions are stated in the literature.

Despite of urgent need to address the validation limitations stated above, this work has been compared to the add-on PEM fuel cell module by Fluent™ for isotropic case with similar operating conditions. As can be seen in Fig. 4.19, there is an overall difference in the magnitude of the current density profile for a specific cell voltage arising due to the fact that the add-on module utilizes Butler-Volmer kinetics for simulating the electrochemical reactions while in this work an improved agglomerate model presented by Sun et al. [106] has been employed. This is more conservative by considering the structural limitations of the catalyst layer. The other difference between the two cases is the sudden dip of the V-I curve at higher current densities in present model due to the fact that Butler-Volmer kinetics cannot account for the concentration losses at higher current densities and always over-predicts to a large amount.

The overall performance of the model with anisotropic effects is compared to the case with isotropic effects in Fig. 4.20 where typical V-I curves for PEM fuel cell are shown. As can be observed, there is an initial sharp decline in the voltage with only minor increase in the current density. Such losses are caused by the slowness of the electrochemical reactions because a part of the energy is wasted in driving the reactions and energy production at such high voltages is quite low. Therefore most of it is consumed within the cell. The linear portion of the graph represents a linear increase in the average ohmic

loss which is linearly proportional to the amount of current flowing through the material. At low voltage levels, mass transport or the concentration losses make the curve to bend sharply which results from the change in the concentration of reactants, i.e., oxygen and hydrogen, as the fuel is consumed. However, the performance of the present model compared to one simulating without accounting for the effective transport mechanism is better in terms of the current density. However, in the actual scenarios, because there are limitations in transport of species, charge and heat due to porosity, tortuosity, volume fraction of ionomer in the catalyst layer and the anisotropy of the gas diffusion layer, the present study reveals more realistic results.

4.2 Micromodel Simulation Results

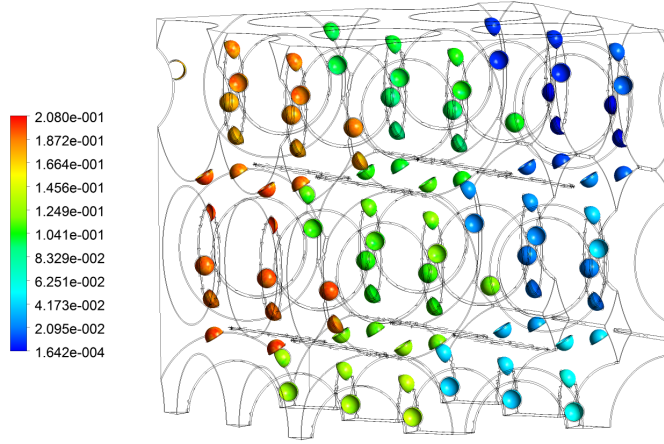
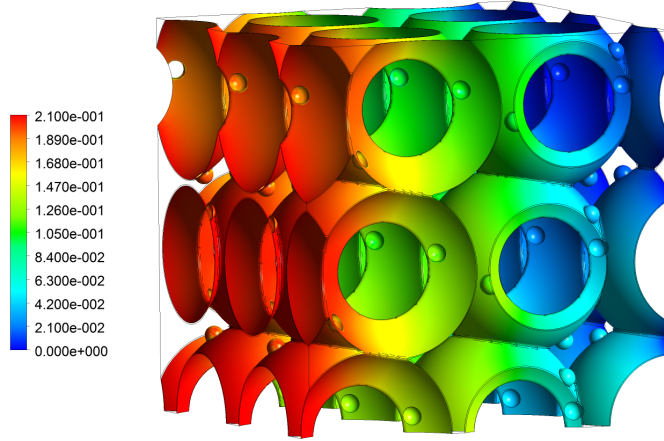
4.2.1 Oxygen Distribution

In this work, three dimensional microscale simulations have been performed for an arbitrary chosen segment of the PEM fuel cell cathode side catalyst layer. The electrochemical reactions are assumed to occur at the interface of Pt particles and the ionomer, i.e., the TPB exists at the surface of the Pt particles satisfying the contact conditions to carry out the electrochemical reactions. The TPB acts as a sink for the oxygen concentration due to reactions by converting to water. Moving away from the inlet boundary (face 1x) shows a decrease in the oxygen concentration is found. As already stated, the outlet boundary (face 1x') for the species is treated as continuity, and there is no convective flow, an overall decrease in the concentration is also observed with reducing reaction rates at the TPBs in low concentration zones. Such a boundary condition, i.e., without specifying any outlet mass fraction, has been selected so that parametric effects can be observed for different concentrations of oxygen.

The diffusion coefficient of oxygen in this work is observed to be in the range of 1×10^{-7} m²/s in the void area, while the values typically used in macromodels are in the range of 1×10^{-5} to 1×10^{-6} m²/s [106, 107] showing a considerable mismatch. Additionally, it is also observed that at this scale, approximately 70% of the total diffusion effect is contributed by the Knudsen effect where pore dimensions are based on the average of maximum and minimum size through-out the domain. As far as the diffusivity of oxygen in ionomer is concerned, the volume averaged value is calculated to 6.2×10^{-11} m²/s. The oxygen has to diffuse through ionomer to reach the reaction surfaces, hence, the diffusivity of oxygen in ionomer can be considered as the limiting factor for the reaction rates. Although, the agglomerate catalyst model for macroscale simulations accounts for the thickness of ionomer covering the agglomerate but practically neglects the local effects. The oxygen distribution for the present work is shown in Figs 4.21a and 4.21b, at TPB and ionomer interface, respectively.

4.2.2 Proton Conductivity and Water Distribution

Apart from oxygen concentration, the protonic conductivity also plays a major role in calibrating the reaction rate, which in turn is highly dependant on the water content of the ionomer. Because the reaction rate is higher near the inlet region, which means a higher water production. Figs 4.22 and 4.23 show that both the profiles for water distribution

(a) *TPB*(b) *Ionomer***Fig. 4.21:** *Oxygen mass fraction distribution profile.*

and protonic conductivity almost overlap. Similarly, at the exit region, because the water content is quite low due to low reaction rates and water diffusivity, the conductivity is reduced to almost 10~15% of the maximum. This represents another difference in micro and macroscale predictions, and in the latter case the protonic conductivity has a maximum value of approximately 2.1 S/m and higher [38], depending on the local conditions. Thus, keeping in mind the current analysis and given thickness of the ionomer surrounding the carbon particles, a much lower proton conductivity has been predicted which may significantly alter the macroscale results depending on the local concentration

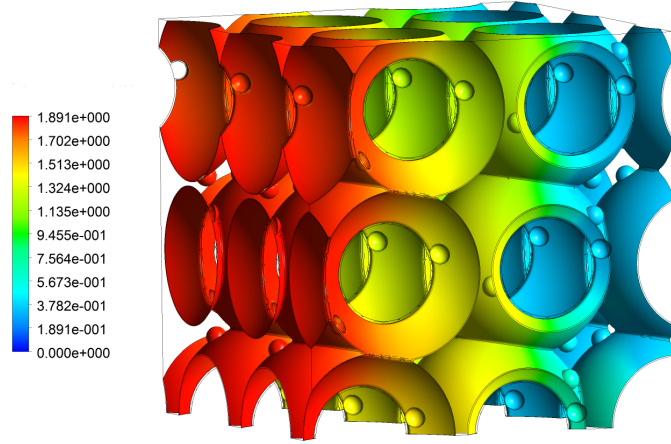


Fig. 4.22: *Protonic conductivity of ionomer as calculated in this work, S/m.*

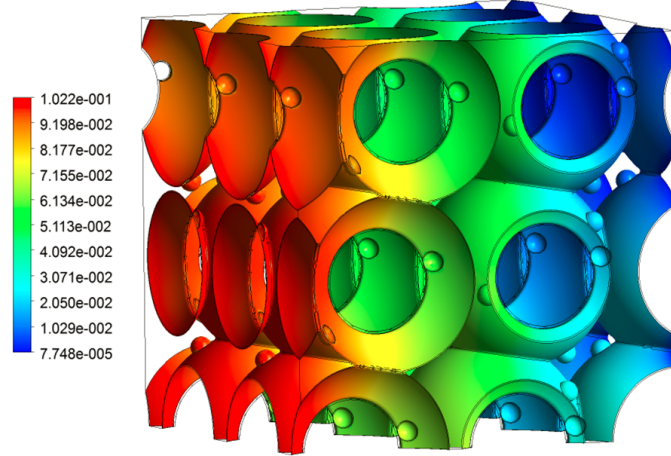


Fig. 4.23: *Water distribution profile in the ionomer portion of the catalyst layer.*

of oxygen and the water saturation.

4.2.3 Temperature Distribution

In the catalyst layer, most the parameters are also highly temperature dependant and in order to perform in-depth analysis, prediction of temperature distribution has to be incorporated with thermal conductivity values adopted from Lange et al. [135]. In this work, the sources for temperature rise are heat released during electrochemical reactions and the ohmic losses due to proton immigration. For the specific case implemented in this work, it has been observed that the heat released due to electrochemical reactions

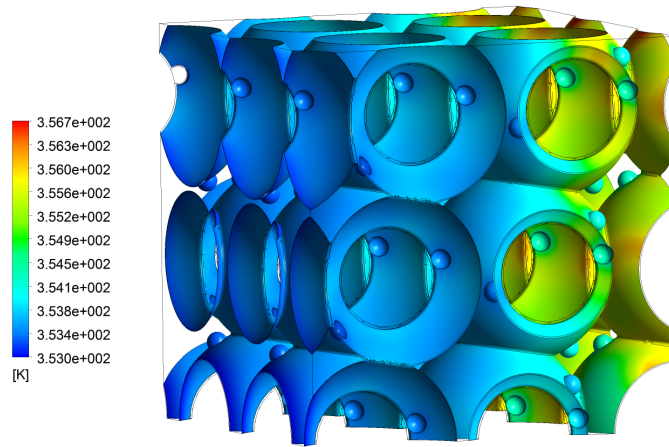


Fig. 4.24: *Temperature distribution profile in the catalyst layer, K.*

only makes up 5~10% of the temperature rise while the major part is contributed via ohmic losses especially in low conductivity region, as can be seen in Fig. 4.24. Near the inlet region the temperature rise is quite small (about 0.2~0.5 K) due to the reaction heat. However, the change in temperature becomes significant near the outlet region of the calculation domain (~3 K).

5 Summary

Fuel cells are electrochemical devices that directly convert chemical energy to electrical energy and have high efficiency and low environmental impact. Because mechanical work and combustion in the fuel cells are avoided, they are not limited by thermodynamic limitations of the heat engines such as Carnot cycle efficiency. Additionally, because combustion is avoided, fuel cells produce power with minimal pollutants.

The discovery of the basic principle of fuel cell dates back to 1838, credited to Welsh lawyer turned scientist, **William Robert Grove** (1811-1896). The ‘Grove cell’, as it was known then, used a platinum electrode immersed in nitric acid and a zinc electrode in zinc sulphate to generate 12 A of current at 1.8 V. Although, decomposition of water to oxygen and hydrogen using the electricity had been described earlier, but combining the gases to produce electricity and water was, according to Grove, “a step further than any hitherto recorded.” Later on, by combining several sets of these electrodes in a series circuit he soon accomplished “gas battery”— the first fuel cell. At times of the first fuel cell, scientists were puzzled with the working principle of the gas battery and the scientific community was struggling to understand the basic principles of chemistry and electricity and what causes the flow of current between two materials and not others. The two renowned theories at that time were the ‘contact theory’ and the ‘chemical theory’ and Grove’s gas battery became a football in the sometimes heated argument between backers of the two competing theories. **Friedrich Wilhelm Ostwald** (1853 -1932), a founder of the field of physical chemistry, finally provided much of the theoretical understanding of fuel cells operation. In 1893, he experimentally determined the interconnected roles of the various components of the fuel cell: electrodes, electrolyte, oxidizing and reducing agents, anions, and cations.

The first ever PEM fuel cell was developed by General Electric to be used in two person Gemini Space Vehicle in early 1960s. Instead of proving to be the mile stone in history of PEM fuel cells, this trip to space caused a back lash to the further development of PEM fuel cells. One of the main reasons being the water management inside the cell,

so, for further space missions alkaline fuel cells were the preferred choice. In mid 1960s, Dupont developed NafionTM membrane that showed improved performance and increased lifetime and, once more, PEM fuel cells were taken to space but this time in biosatellite mission in 1968. But as before, the water management problem proved to be too difficult to handle. Again, the management and developers of the space program were forced to choose Alkaline fuel cells as an alternate for later missions. In 1970s and early 80s, further development in PEM fuel cells was set aside, mainly due to;

- PEM fuel cells were more expensive to their counterparts like phosphoric acid (PAFCs) and alkaline fuel cells (AFCs),
- the membrane and the catalyst (platinum) were very expensive,
- PEM fuel cells are very prone to carbon-monoxide (CO) poisoning
- Water management was too difficult to handle efficiently

But in late 1980s and early 1990s, the credited efforts of Ballard Power Systems and the Los Alamos National Laboratory, revival of PEM fuel cells occurred by the development of new catalyst loading techniques and membrane properties. And since then, PEM fuel cells have secured a high respect in research industry and many companies are focusing on PEM fuel cells to be used in future products that range from a cell-phone to submarines.

As of today, the PEM technology is approaching a commercial era where it needs to stand in competition with its long time rivals, i.e., the long tested batteries and powerful conventional combustion engines. The activity in PEM community has taken pace in the last decade to make them more efficient and responsive to needs of the consumers. To date, much efforts have been spared in various disciplines from basic electrochemistry to the design of stacks, but, number of issues are still pending and need to be resolved before fuel cell can convince the users and investors alike as being highly dependable and efficient energy converters. It has already been established that the cathode performance is one of the major defector. The reason for this inefficiency is mainly the slower reaction kinetics at the cathode side and the water and thermal management issues. Since the product of electrochemical combination of hydrogen and oxygen results in water, lower operating temperature and pressure condenses the vapour phase to liquid state and hence the only type of fuel cells having multiphase regime are the PEM fuel cell and placed with an extra qualification of multiphase flows.

In this thesis, computational fluid dynamics (CFD) has been utilized to formulate and measure the internal phenomena with increased details. The work is divided into two major classes based on macro and microscale dimensions.

5.1 Macroscale Analysis

In macroscale scale, all the significant phenomena have been quantized keeping in mind all the transport mechanisms with structural material response for each process. The salient features of this modelling approach can be summerized as;

- multiphysics model describing transport of gaseous species, charged quantities, heat and liquid water,
- agglomerate catalyst model for simulating the electrochemical reactions in the catalyst layers,
- Multicomponent diffusion of species with Knudsen correction,
- inclusion of effects caused by the anisotropic response of materials, i.e., anisotropic diffusion of species, heat and electrical conductivity.
- effects of anisotropic permeability on water saturation,
- correction of material phases for protonic conduction in the catalyst layer using more advanced approximation,
- simulating diffusion of liquid water in the porous media using a validated approach and water phase change.

It was observed that the anisotropy of material has a profound effect on the performance of the fuel cells. The isotropic cases always exhibit higher current densities for a given voltage. The oxygen concentration was noted to be quite less in the catalyst layer when the fuel cell was simulated using the anisotropic diffusion. Considering the anisotropy of the heat conduction through the gas diffusion layer, it was observed that heat was trapped in the catalyst layer because of the low thermal conductivity in the through-plane direction. Additionally, because of the lower heat conduction of the membrane between the two electrodes, the highest temperature within the cell was noted in the cathode catalyst layer. Previously it has been shown that the catalyst layer of the PEM fuel cell is more problematic than the anode side because of two reasons. The first reason is that the oxidation reduction reactions are much slower than the hydrogen oxidation reactions, and, secondly, due to the water generation at the cathode side makes it more prone to flooding effects. However, considering the anisotropic heat conduction of the gas diffusion layer, the third problem can be listed as high temperature rise at the cathode side of the PEM fuel cell. All these three scenarios make the cathode of PEM fuel cell the centre hub of inefficiencies of the cell.

The present study also utilizes a more conservative approach to calculate the protonic conductivity of the membrane phase in the catalyst layer. It was previously established that the Bruggeman approximation over-predicts the effective material properties for the porous media when the porosity is higher than 0.2. It was further shown that the protonic conductivity varied in the cell for the cathode catalyst layer both in width and the length of the cell. However, a unique trend was observed where an increase was noted in the protonic conduction when the water saturation effects were maximum.

The anisotropic permeability of the gas diffusion layer also affects the water saturation in the PEM fuel cell. In the present work a comparative study was also carried out at different in-plane and through-plane permeabilities. It was noted that with higher permeability in through-plane direction, the maximum saturation was located near the

current collector and the inlet gas channel. However, in other case when the through-plane permeability was lower as compared to the in-plane permeability, the location of maximum saturation is shifted to the opposite side, i.e., in the catalyst layer. Furthermore, all the transport limitations, as incorporated in this work, were compared to the one having isotropic heat and species transport and isotropic permeability of the gas diffusion layer and it was observed that the present model under-performed at the same operating levels and mass limitation effects or the concentration losses were seen to come into effect at quite low current densities, i.e., approximately less than 0.6 A/cm^2 .

Although, the macroscale simulations provide an accurate and precise knowledge of the overall efficiency and performance behaviour, they are limited in sense that it is virtually impossible to distinguish the response of each material and process explicitly inside the cell, especially the catalyst layer where the electrochemical reactions occur.

5.2 Microscale Analysis

The catalyst layer of PEM fuel cell is fabricated by combination of four different materials each serving a very specialized purpose. In the micro model development, each phase has been independently generated and distinguished so that all the processes can be studied in segregated manner and calculate the response as governed by each material. However, due to the high computational resources demand at such scale, the micro model has been limited to single phase flow only and the solid phase comprising of carbon and platinum particles have also been omitted because it is virtually impossible to simulate on a single computer even having state of art technology with multiple cores.

The general features of the microscale analysis are;

- four phase reconstruction of the catalyst layer,
- identification of each material phase,
- identification of the triple phase boundary (TPB),
- calculation of flow parameters (tortuosity and permeability),
- segregated diffusion of species in ionomer and voids,
- model development for simulation of microscopic transport phenomena and reactions.

The main advantage of simulating the micromodel of the catalyst layer is that the need for correction factors as incorporated in macromodels is nullified and exact scenarios can be simulated. Furthermore, such models also help in determining the material properties and limits the use of values borrowed from other sources. It was noted during the simulations that the basic analysis of the species, charge conduction and heat as compared to complex and most comprehensive macroscale models, the micromodels aptly capture all the physics of the processes and are classifiable according to the material, i.e., the response of each material phase was segregated. Such an approach is useful for

understanding of the internal anatomy of the catalyst layer and can help in revealing the coupling of the processes. However, the present model as in this work is limited in the sense that the solid phase was ejected and the electronic current density was assumed to flow through the membrane phase. This assumption is not the limitation of the micromodel but needs higher computation resources.

6 Bibliography

- [1] EG&C Technical Services, 2004, *Fuel Cell Handbook*, Morgantown, West Virginia.
- [2] Larminie, J., and Dicks, A., 2003. *Fuel Cell Systems Explained*, 2nd ed. John Wiley & Sons Ltd., West Sussex.
- [3] Sundén, B., and Faghri, M., 2005. *Transport Phenomena in Fuel Cells*. WIT Press, Southampton.
- [4] Basu, S., 2007. *Recent Trends in Fuel Cell Science and Technology*. Asamaya Publishers, New Delhi.
- [5] Frano, B., 2005. *PEM Fuel Cells*. Theory and Practice. Academic Press, Burlington.
- [6] Khan, M., Sundén, B., and Yuan, J., 2011. “Analysis of multi-phase transport phenomena with catalyst reactions in polymer electrolyte membrane fuel cells: A review”. *J. Power Sources*, **196**(19), pp. 7899–7916.
- [7] Dawes, J. E., Hanspal, N. S., Family, O. A., and Turan, A., 2009. “Three-dimensional CFD modelling of PEM fuel cells: An investigation into the effects of water flooding”. *Chem. Eng. Sci.*, **64**(12), pp. 2781–2794.
- [8] Siegel, C., 2008. “Review of computational heat and mass transfer modeling on polymer-electrolyte-membrane (PEM) fuel cells”. *J. Energy*, **33**, pp. 1331–52.
- [9] Cheddie, D., and Munroe, N., 2005. “Review and comparison of approaches to proton exchange membrane fuel cell modeling”. *J. Power Sources*, **147**, pp. 72–84.
- [10] Natarajan, D., and van Nguyen, T., 2003. “Three-dimensional effects of liquid water flooding in the cathode of a PEM fuel cell”. *J. Power Sources*, **115**(1), pp. 66–80.

- [11] Li, H., Tang, Y., Wang, Z., Shi, Z., Wu, S., Song, D., Zhang, J., Fatih, K., Wang, H., Liu, Z., Abouatallah, R., and Mazza, A., 2008. "A review of water flooding issues in the proton exchange membrane fuel cell". *J. Power Sources*, **178**(1), pp. 103–117.
- [12] Song, C., Tang, Y., Zhang, J. L., Zhang, J., Wang, H., Shen, J., McDermid, S., Li, J., and Kozak, P., 2007. "PEM fuel cell reaction kinetics in the temperature range of 23–120 °C". *Electrochimica Acta*, **52**(7), pp. 2552–2561.
- [13] Biyikoğlu, A., 2005. "Review of proton exchange membrane fuel cell models". *Intl. J. Hydrogen Energy*, **30**(11), pp. 1181–1212.
- [14] Yu, L.-J., Ren, G. P., Qin, M. J., and Jiang, X. M., 2009. "Transport mechanisms and performance simulations of a PEM fuel cell with interdigitated flow field". *Renewable Energy*, **34**(3), pp. 530–543.
- [15] Bernardi, D. M., and Verbrugge, M. W., 1991. "Mathematical model of a gas diffusion electrode bonded to a polymer electrolyte". *AIChE Journal*, **37**(8), pp. 1151–1163.
- [16] Springer, T., Zawodzinski, T., and Gottesfeld, S., 1991. "Polymer electrolyte fuel cell model". *J. Electrochem. Soc.*, **138**, pp. 2334–2342.
- [17] Nguyen, T. V., and White, R., 1993. "A water and heat management model for proton-exchange membrane fuel cells". *J. Electrochem Soc.*, **140**, pp. 2178–87.
- [18] Wang, Z., Wang, C., and Chen, K., 2001. "Two-phase flow and transport in the air cathode of proton exchange membrane fuel cells". *J. Power Sources*, **94**, pp. 40–50.
- [19] Wang, C. Y., and Cheng, P., 1997. "Multiphase flow and heat transfer in porous media". *Adv. Heat Transfer*, **30**, pp. 30–196.
- [20] You, L., and Liu, H., 2006. "A two-phase flow and transport model for PEM fuel cells". *J. Power Sources*, **155**(2), pp. 219–230.
- [21] Dutta, S., Shimpalee, S., and Van Zee, J., 2001. "Numerical prediction of mass-exchange between cathode and anode channels in a PEM fuel cell". *Intl. J. Heat Mass Transfer*, **44**, pp. 2029–2042.
- [22] Yi, J. S., and Nguyen, T., 1998. "An along the channel model for proton exchange membrane fuel cells". *J. Electrochem. Soc.*, **145**(4), pp. 1149–1159.
- [23] Yi, J., and Nguyen, T. V., 1999. "Multicomponent transport in porous electrodes of proton exchange membrane fuel cells using interdigitated gas distributors". *J. Electrochem. Soc.*, **146**, pp. 38–45.
- [24] Fuller, T., and Newman, J., 1993. "Water and thermal management in solid-polymer-electrolyte fuel cells". *J. Power Sources*, **140**, pp. 1218–1225.
- [25] Mazumder, S., and Cole, J., 2003. "Rigorous 3-D mathematical modeling of PEM fuel cells: II. Model predictions with liquid water transport". *J. Electrochem. Soc.*, **150**(11), pp. A1510–A1517.

- [26] He, G., Yamazaki, Y., and Abudula, A., 2009. "A droplet size dependent multiphase mixture model for two phase flow in PEMFCs". *J. Power Sources*, **194**(1), pp. 190–198.
- [27] Zhang, F. Y., Yang, X. G., and Wang, C. Y., 2006. "Liquid water removal from a polymer electrolyte fuel cell". *J. Electrochem. Soc.*, **153**(2), pp. A225–A232.
- [28] Yuan, J., and Sundén, B., 2004. "Two-phase flow analysis in a cathode duct of PEFCs". *Electrochimica Acta*, **50**, pp. 677–683.
- [29] Meng, H., 2009. "Multi-component liquid water transport in the cathode of a PEM fuel cell with consideration of the micro-porous layer (mpl)". *Intl. J. Hydrogen Energy*, **34**, pp. 5488–5497.
- [30] , 2003. "Effective diffusivity and water-saturation distribution in single- and two-layer PEMFC diffusion medium". *Intl. J. Heat Mass Transfer*, **46**(24), pp. 4595 – 4611.
- [31] Hickner, M., Siegel, N., Chen, K., Hussey, D., Jacobson, D., and Arif, M., 2008. "In situ high-resolution neutron radiography of cross-sectional liquid water profiles in proton exchange membrane fuel cells". *J. Electrochem Soc.*, **155**(B427-434).
- [32] Zhou, B., Huang, W., Zong, Y., and Sobiesiak, A., 2006. "Water and pressure effects on a single PEM fuel cell". *J. Power Sources*, **155**(2), pp. 190–202.
- [33] Berning, T., and Djilali, N., 2003. "A 3d, multiphase, multicomponent model of the cathode and anode of a PEM fuel cell". *J. Electrochem Soc.*, **150**(12), pp. A1589–A1598.
- [34] Berning, T., and Djilali, N., 2003. "Three-dimensional computational analysis of transport phenomena in a PEM fuel cell - a parametric study". *J. Power Sources*, **124**, pp. 440–452.
- [35] Berning, T., Lu, D., and Djilali, N., 2002. "Three-dimensional computational analysis of transport phenomena in PEM fuel cells". *J. Power Sources*, **106**, pp. 284–294.
- [36] Hu, M., Gu, A., Wang, M., Zhu, X., and Yu, L., 2003. "Three dimensional, two phase flow mathematical model for PEM fuel cell: Part I. Model development". *Energy Conv. & Mang*, **45**, pp. 1861–1882.
- [37] Hu, M., Zhu, X., Wang, M., Gu, A., and Yu, L., 2004. "Three dimensional, two phase flow mathematical model for PEM fuel cell: Part II. analysis and discussion of the internal transport mechanisms". *Energy Conv. & Mang*, **45**(11-12), pp. 1883–1916.
- [38] Khan, M., 2009. *Numerical Simulation of Multi-Scale Transport Processes and Reactions in PEM Fuel Cells using Two-Phase Models*. Licentiate Thesis, ISRN LUTMDN/TMHP-09/7066-SE, Lund University, Lund.

- [39] Mench, M., 2010. *Advanced modeling in fuel cell systems: a review of modeling approaches*. Wiley-VCH Verlag GmbH & Co. KGaA, Weinheim, pp. 89–118.
- [40] Cussler, E., 2003. *Diffusion-Mass Transfer in Fluid Systems*. Cambridge University Press, New York.
- [41] Flückiger, R., Freunberger, S., Kramer, D., Wokaun, A., Scherer, G., and Büchi, F., 2008. “Anisotropic, effective diffusivity of porous gas diffusion layer materials for PEFC”. *Electrochimica Acta*, **54**(2), pp. 551 – 559.
- [42] Wu, R., Zhu, X., Liao, Q., Wang, H., d. Ding, Y., Li, J., and d. Ye, D., 2010. “Determination of oxygen effective diffusivity in porous gas diffusion layer using a three-dimensional pore network model”. *Electrochimica Acta*, **55**(24), pp. 7394 – 7403.
- [43] Tomadakis, M., and Sotirchos, S., 1993. “Ordinary and transition regime diffusion in random fiber structures”. *AIChE Journal*, **39**(3), pp. 397–412.
- [44] Das, P., Li, X., and Liu, Z.-S., 2010. “Effective transport coefficients in PEM fuel cell catalyst and gas diffusion layers: Beyond Bruggeman approximation”. *Applied Energy*, **87**(9), pp. 2785 – 2796.
- [45] Wu, R., Liao, Q., Zhu, X., and Wang, H., 2011. “A fractal model for determining oxygen effective diffusivity of gas diffusion layer under the dry and wet conditions”. *Intl. J. Heat Mass Transfer*, **54**(19-20), pp. 4341 – 4348.
- [46] Pharoah, J., Karan, K., and Sun, W., 2006. “On effective transport coefficients in PEM fuel cell electrodes: Anisotropy of the porous transport layers”. *J. Power Sources*, **161**(1), pp. 214–224.
- [47] Song, D., Wang, Q., Liu, Z., Eikerling, M., Xie, Z., Navessin, T., and Holdcroft, S., 2005. “A method for optimizing distributions of nafion and pt in cathode catalyst layers of PEM fuel cells”. *Electrochimica Acta*, **50**(16-17), pp. 3347–3358.
- [48] Uvarov, N., 2000. “Estimation of composites conductivity using a general mixing rule”. *Solid State Ionics*, **136**, pp. 1267–1272.
- [49] Belova, I., and Murch, G., 2005. “Calculation of the effective conductivity and diffusivity in composite solid electrolytes”. *J. Phys. Chem. Solids*, **66**, pp. 772–778.
- [50] Hashin, Z., and Shtrikman, S., 1962. “A variational approach to the theory of the effective magnetic permeability of multiphase materials”. *J. Applied Physics*, **33**(10), pp. 3125–3131.
- [51] Pharoah, J. G., 2005. “On the permeability of the gas diffusion media used in PEM fuel cells”. *J. Power Sources*, **144**(1), pp. 77–82.
- [52] van Doormaal, M., and Pharoah, J., 2009. “Determination of permeability in fibrous porous media using the lattice boltzmann method with application to PEM fuel cells”. *Intl. J. Numerical Methods in Fluids*, **59**(1), pp. 75–89.

- [53] Gostick, J., Fowler, M., Pritzker, M., Ioannidis, M., and Behra, L., 2006. “In-plane and through-plane gas permeability of carbon fiber electrode backing layer”. *J. Power Sources*, **162**(1), pp. 228–238.
- [54] Pasaogullari, U., Mukherjee, P., Wang, C., and Chen, K., 2007. “Anisotropic heat and water transport in PEFC cathode gas diffusion layer”. *J. Electrochem. Soc.*, **154**(8), pp. B823–B834.
- [55] Yang, W., Zhao, T., and He, Y., 2008. “Modelling of coupled electron and mass transport in anisotropic proton-exchange membrane fuel cell electrodes”. *J. Power Sources*, **185**(2), pp. 765–775.
- [56] Bluemle, M., Gurau, V., Mann, J., Zawodzinski, T., Castro, E. D., and Tsou, Y., 2004. “Characterization of transport properties in gas diffusion layers for PEMFCs”. In 206th Meeting of The Electrochemical Society, Inc.
- [57] Williams, M., Begg, E., Bonville, L., Kunz, H., and Fenton, J., 2004. “Characterization of gas diffusion layers for PEMFC”. *J. Electrochem. Soc.*, **151**(8), pp. A1173–A1180.
- [58] Becker, J., Flückiger, R., Reum, M., Buchi, F., Marone, F., and Stampanoni, M., 2009. “Determination of material properties of gas diffusion layers: Experiments and simulations using phase contrast tomographic microscopy”. *J. Electrochem. Soc.*, **156**(10), pp. B1175–B1181.
- [59] Hamilton, D., 2005. “A numerical method to determine effective transport coefficients in porous media with application to PEM fuel cells”. PhD thesis.
- [60] Valdes-Parada, F. J., Ochoa-Tapia, J. A., and Alvarez-Ramirez, J., 2009. “Validity of the permeability Carman-Kozeny equation: A volume averaging approach”. *Physica A: Statistical Mechanics and its Applications*, **388**(6), pp. 789–798.
- [61] Ju, H., Meng, H., and Wang, C.-Y., 2005. “A single phase, non-isothermal model for PEM fuel cells”. *Intl. J. Heat Mass Transfer*, **48**, pp. 1303–15.
- [62] Hwang, J., 2007. “A complete two-phase model of a porous cathode of a PEM fuel cell”. *J. Power Sources*, **164**(1), pp. 174–181.
- [63] Hwang, J. J., 2007. “A complete two-phase model of a porous cathode of a PEM fuel cell”. *J. Power Sources*, **164**(1), pp. 174–181.
- [64] Hwang, J., and P.Y., C., 2006. “Heat/mass transfer in porous electrodes of fuel cells”. *Intl. J. Heat Mass Transfer*, **49**, pp. 2315–27.
- [65] He, G., Yamazaki, Y., and Abudula, A., 2010. “A three-dimensional analysis of the effect of anisotropic gas diffusion layer(GDL) thermal conductivity on the heat transfer and two-phase behavior in a proton exchange membrane fuel cell(PEMFC)”. *J. Power Sources*, **195**(6), pp. 1551–1560.
- [66] Bapat, C., and Thynell, S., 2007. “Anisotropic heat conduction effects in proton-exchange membrane fuel cells”. *J. Heat Transfer*, **129**(9), pp. 1109–1118.

- [67] Litster, S., and Djilali, N., 2005. *Two-phase Transport in Porous Gas Diffusion Electrodes*. WIT Press, Southampton, pp. 175–213.
- [68] Eames, I., Marr, N., and Sabir, H., 1997. “The evaporation coefficient of water: A review”. *Intl. J. Heat Mass Transfer*, **40**(1), pp. 2963–2973.
- [69] Marek, R., and Straub, J., 2001. “Analysis of evaporation coefficient and the condensation coefficient of water”. *Intl. J. Heat Mass Transfer*, **44**, pp. 39–53.
- [70] Faghri, A., and Zhang, Y., 2006. *Transport Phenomena in Multiphase Systems*. Elsevier Academic Press.
- [71] Kermani, M., Stockie, J., and Gerber, A., 2004. “Condensation in the cathode of a PEM fuel cell”. In 11th Annual Conference of CFD Society, Canada.
- [72] Ren, X., and Gottesfeld, S., 2001. “Electro-osmotic drag of water in poly(perfluorosulfonic acid) membranes”. *J. Electrochem. Soc.*, **148**(1), pp. A87–A93.
- [73] Thomas A. Zawodzinski, J., Derouin, C., Radzinski, S., Sherman, R. J., Smith, V. T., Springer, T. E., and Gottesfeld, S., 1993. “Water uptake by and transport through nafion™ 117 membranes”. *J. Electrochem. Soc.*, **140**(4), pp. 1041–1047.
- [74] Wilkinson, D. P., Voss, H. H., and Prater, K., 1994. “Water management and stack design for solid polymer fuel cells”. *J. Power Sources*, **49**(1-3), pp. 117–127.
- [75] Yi, J. S., Yang, J. D., and King, C., 2004. “Water management along the flow channels of PEM fuel cells”. *AIChE J.*, **50**(10), pp. 2594–2603.
- [76] Wang, G., 2003. Tech. rep., Ph.D. thesis, the Pennsylvania State University, USA.
- [77] Kumbur, E., Sharp, K., and Mench, M., 2007. “A validated Leverett approach to multiphase flow in polymer electrolyte fuel cell diffusion media. Part I. Hydrophobicity effect”. *J. Electrochem. Soc.*, **154**(12), pp. B1295–B1304.
- [78] Yuan, J., Sundén, B., Hou, M., and Huamin, Z., 2004. *Three-dimensional Analysis of Two-Phase Flow and its Effects on the Cell Performance of PEMFC*. Taylor & Francis.
- [79] Hartnig, C., Manke, I., Kuhn, R., Kardjilov, N., Banhart, J., and Lehnert, W., 2008. “Cross-sectional insight in the water evolution and transport in polymer electrolyte fuel cells”. *Appl. Phys. Letters*, **92**(13), p. 134106.
- [80] Turhan, A., Kim, S., Hatzell, M., and Mench, M., 2010. “Impact of channel wall hydrophobicity on through-plane water distribution and flooding behavior in a polymer electrolyte fuel cell”. *Electrochimica Acta*, **55**(8), pp. 2734–2745.
- [81] Pasaogullari, U., and Wang, C. Y., 2004. “Liquid water transport in gas diffusion layer of polymer electrolyte fuel cells”. *J. Electrochem. Soc.*, **151**(3), pp. A399–A406.

-
- [82] Leverett, M., 1941. “Capillary behaviour in porous solids”. *Pet. Trans., AIME(Am. Inst. Min. Metall. Eng.)*, **142**, pp. 152–169.
- [83] Udell, K., 1985. “Heat transfer in porous media considering phase change and capillarity—the heat pipe effect”. *Intl. J. Heat Mass Transfer*, **28**(2), pp. 485–495.
- [84] Kumbur, E., Sharp, K., and Mench, M., 2007. “A validated Leverett approach to multiphase flow in polymer electrolyte fuel cell diffusion media. Part II. Compression effect and capillary”. *J. Electrochem. Soc.*, **154**(12), pp. B1305–B1314.
- [85] Kumbur, E., Sharp, K., and Mench, M. M., 2007. “A validated Leverett approach to multiphase flow in polymer electrolyte fuel cell diffusion media. Part III. Temperature effect and unified approach”. *J. Electrochem. Soc.*, **154**(12), pp. B1315–B1324.
- [86] Kaviany, M., 1991. *Principles of Heat Transfer in Porous Media*. Springer-Verlag, New York.
- [87] Scheidegger, A., 1974. *The Physics of Flow Through Porous Media*. University of Toronto Press, Toronto.
- [88] van Genuchten, M., 1980. “A closed-form equation for predicting the hydraulic conductivity of unsaturated soils”. *Soil Sci. Soc. America J.*, **44**(5), pp. 892–898.
- [89] Versteeg, H., and Malalasekera, W., 1995. *An Introduction to Computational Fluid Dynamics: The Finite Volume Method*. Longmann Scientific & Technical, Burnt Hill, Harlow, England.
- [90] “ANSYS™ FLUENT™ v12.0, theory guide, www.fluent.com, 2009”.
- [91] Hadley, G., 1986. “Thermal conductivity of packed metal powders”. *Intl. J. Heat Mass Transfer*, **29**(6), pp. 909–920.
- [92] Wamei, L., 2011. *Modeling and Performance Analysis of Alternative Heat Exchangers for Heavy Vehicles*. Licentiate Thesis, ISRN LUTMDN/TMHP-11/7076-SE, Lund University, Lund.
- [93] Spiegel, C., 2008. *PEM Fuel Cell Modeling and Simulation Using Matlab*. Academic Press.
- [94] Merk, H., 1958. “The macroscopic equations for simultaneous heat and mass transfer in isotropic, continuous and closed systems”. *Appl. Sci. Res.*, **8**, pp. 73–99.
- [95] Taylor, R., and Krishna, R., 1993. *Multicomponent Mass Transfer*. John Wiley & Sons Ltd., New York.
- [96] Yuan, J., Lv, X., Sundén, B., and Yue, D., 2007. “Analysis of parameter effects on the transport phenomena in conjunction with chemical reactions in ducts relevant for methane reformers”. *Intl. J. Hydrogen Energy*, **32**, pp. 3887–98.

-
- [97] Mu, D., Liu, Z.-S., Huang, C., and Djilali, N., 2008. "Determination of the effective diffusion coefficient in porous media including Knudsen effects". *Microfluidics and Nanofluidics*, **4**(3), pp. 257–260.
- [98] Reid, C. R., Prausnitz, J. M., and E., P. B., 1986. *The Properties of Gases & Liquids*, 4th ed. McGraw-Hill Book Company, New York.
- [99] Gostick, J., Fowler, M., Ioannidis, M., Pritzker, M., Volfkovich, Y. M., and Sakars, A., 2006. "Capillary pressure and hydrophilic porosity in gas diffusion layers for polymer electrolyte fuel cells". *J. Power Sources*, **156**(2), pp. 375–387.
- [100] He, G., Zhao, Z., Ming, P., Abuliti, A., and Yin, C., 2007. "A fractal model for predicting permeability and liquid water relative permeability in the gas diffusion layer (GDL) of PEMFCs". *J. Power Sources*, **163**(2), pp. 846–852.
- [101] Harvey, D., Pharoah, J. G., and Karan, K., 2008. "A comparison of different approaches to modelling the PEMFC catalyst layer". *J. Power Sources*, **179**(1), pp. 209–219.
- [102] Yan, Q., and Wu, J., 2008. "Modeling of single catalyst particle in cathode of PEM fuel cells". *Energy Conv. & Mang.*, **49**(8), pp. 2425–2433.
- [103] Um, S., and Wang, C. Y., 2004. "Three-dimensional analysis of transport and electrochemical reactions in polymer electrolyte fuel cells". *J. Power Sources*, **125**(1), pp. 40–51.
- [104] Antonio, O., Bultel, Y., Durand, R., and Ozil, P., 1998. "Catalyst gradient for cathode active layer of proton exchange membrane fuel cell". *Electrochim. Acta*, **43**(24), p. 3681.
- [105] Bultel, Y., Ozil, P., and Durand, R., 1998. "Modelling of mass transfer within the PEM fuel cell active layer: Limitations at the particle level". *J. Appl. Electrochem.*, **28**, p. 269.
- [106] Sun, W., Peppley, B., and Karan, K., 2005. "An improved two-dimensional agglomerate cathode model to study the influence of catalyst layer structural parameters". *Electrochim. Acta*, **50**, pp. 3359–3374.
- [107] Sun, W., Peppley, B., and Karan, K., 2005. "Modeling the influence of gdl and flow-field plate parameters on the reaction distribution in the PEMFC cathode catalyst layer". *J. Power Sources*, **144**, pp. 42–53.
- [108] Senn, S., and Poulikakos, D., 2005. "Multiphase transport phenomena in the diffusion zone of a PEM fuel cell". *J. Heat Transfer*, **127**, pp. 1245–59.
- [109] Meng, H., and Wang, C.-Y., 2004. "Electron transport in PEFCs". *J. Electrochem. Soc.*, **151**(3), pp. A358–A367.
- [110] Bapat, C. J., and Thynell, S. T., 2008. "Effect of anisotropic electrical resistivity of gas diffusion layers (gdl) on current density and temperature distribution in a polymer electrolyte membrane (PEM) fuel cell". *J. Power Sources*, **185**(1), pp. 428–432.

-
- [111] Lange, K. J., Chinmay, M., Sui, P. C., and Djilal, N., 2011. "A numerical study on preconditioning and partitioning schemes for reactive transport in a PEMFC catalyst layer". *Comput. Methods Appl. Mech. Eng.*, **200**, pp. 905–916.
- [112] Siddique, N., and Liu, F., 2010. "Process based reconstruction and simulation of a three-dimensional fuel cell catalyst layer". *Electrochimica Acta*, **55**, pp. 5357–5366.
- [113] More, K. L., and Reeves, K. S., 2005. "Microstructural characterization of PEM fuel cell MEAs". In DOE Hydrogen Program Annual Merit Review, 23-26 May, Arlington, USA.
- [114] Xie, Z., Navessin, T., Shi, K., Chow, R., Wang, Q., Song, D., Andreaus, B., Eikering, M., Liu, Z., and Holdcroft, S., 2010. "Process based reconstruction and simulation of a three-dimensional fuel cell catalyst layer". *Electrochimica Acta*, **55**, pp. 5357–5366.
- [115] Liu, F., and Wang, C., 2006. "Optimization of cathode catalyst layer for direct methanol fuel cells. Part I. experimental investigation". *Electrochimica Acta*, **52**, pp. 1417–1425.
- [116] Lei, C., Bessarabov, D., Ye, S., Xie, Z., Holdcroft, S., and Navessin, T., 2011. "Low equivalent weight short-side-chain perfluorosulfonic acid ionomers in fuel cell cathode catalyst layers". *J. Power Sources*, **142**, p. 82.
- [117] Mukherjee, P., and Wang, C., 2006. "Stochastic microstructure reconstruction and direct numerical simulation of the PEFC catalyst layer". *J. Electrochem. Soc.*, **153**, pp. A840–A849.
- [118] Lange, K., Sui, P., and Djilali, N., 2010. "Pore scale simulation of transport and electrochemical reactions in reconstructed PEMFC catalyst layers". *J. Electrochem. Soc.*, **157**, pp. B1434–B1442.
- [119] Barbosa, R., Andaverde, J., Escobar, B., and Cano, U., 2011. "Stochastic reconstruction and a scaling method to determine effective transport coefficients of a proton exchange membrane fuel cell catalyst layer". *J. Power Sources*, **196**, pp. 1248–1257.
- [120] Hu, J., Sui, P., and Djilali, N., 2008. "Numerical investigation on the transport in a PEMFC using a microstructure reconstruction technique". In Proceedings of the proton exchange membrane fuel cells, 12-17 Oct. Honolulu, USA.
- [121] Wang, G., Mukherjee, P., and Wang, C., 2006. "Direct numerical simulation (DNS) modeling of PEFC electrodes, Part I. regular microstructure". *Electrochimica Acta*, **51**, pp. 3139–3150.
- [122] Wang, G., Mukherjee, P., and Wang, C., 2006. "Direct numerical simulation (DNS) modeling of PEFC electrodes, Part II. random microstructure". *Electrochimica Acta*, **51**, pp. 3150–3160.

- [123] Mukherjee, P., and Wang, C., 2007. "Direct numerical simulation modeling of bilayer cathode catalyst layers in polymer electrolyte fuel cells". *J. Electrochem. Soc.*, **154**, pp. B1121–B1130.
- [124] Kim, S. H., and Pitsch, H., 2009. "Reconstruction and effective transport properties of the catalyst layer in PEM fuel cells". *J. Electrochem. Soc.*, **156**, pp. B673–B681.
- [125] Lange, K., Sui, P., and Djilali, N., 2011. "Pore scale modeling of a proton exchange membrane fuel cell catalyst layer: Effects of water vapor and temperature". *J. Power Sources*, **196**, pp. 3195–3203.
- [126] Ziegler, C., Thiele, S., and Zengerle, R., 2011. "Direct three-dimensional reconstruction of a nanoporous catalyst layer for a polymer electrolyte fuel cell". *J. Power Sources*, **196**, pp. 2094–2097.
- [127] Wilson, M., and Gottesfeld, S., 1992. "High performance catalyzed membranes of ultra-low Pt loadings for polymer electrolyte fuel cells". *J. Electrochem. Soc.*, **139**, pp. L28–L30.
- [128] ANSYSTM FLUENTTM software, <http://www.fluent.com>.
- [129] Iranzo, A., Muñoz, M., Rosa, F., and Pino, J., 2010. "Numerical model for the performance prediction of a PEM fuel cell. Model results and experimental validation". *Intl. J. Hydrogen Energy*, **35**, pp. 11533–11550.
- [130] Parthasarathy, A., Srinivasan, S., Appleby, A. J., and Martin, C. R., 1992. "Temperature dependence of the electrode kinetics of oxygen reduction at the platinum/nafictionTM interface - a microelectrode investigation". *J. Electrochem. Soc.*, **139**(9), pp. 2530–2537.
- [131] Mann, R., Amphlett, J., Peppley, B., and Thurgood, C., 2006. "Henry's law and the solubilities of reactant gases in the modeling of pem fuel cells". *J. Power Sources*, **161**, pp. 768–774.
- [132] Khandelwal, M., and Mench, M., 2006. "Direct measurement of through-plane thermal conductivity and contact resistance in fuel cell materials". *J. Power Sources*, **161**(2), pp. 1106 – 1115.
- [133] "ANSYSTM FLUENTTM v12.0, fuel cell module manual, 2009, www.fluent.com".
- [134] Slade, S., Campbell, S., Ralph, T., and Walsh, F., 2002. "Ionic conductivity of an extruded Nafion 1100 EW series membranes". *J. Electrochem. Soc.*, **149**(12), pp. A1556–A1164.
- [135] Lange, K. J., Sui, P.-C., and Djilali, N., 2011. "Pore scale modeling of a proton exchange membrane fuel cell catalyst layer: Effects of water vapor and temperature". *J. Power Sources*, **196**(6), pp. 3195–3203.
- [136] Cussler, E., 2001. *Mass Transfer in Fluid Systems*. Cambridge University Press.
- [137] Pollard, W. G., and Present, R. D., 1948. "On gaseous self-diffusion in long capillary tubes". *Phys. Rev.*, **73**(7), pp. 762–774.

-
- [138] Lee, K., Ishihara, A., Mitsushima, S., Kamiya, N., and ichiro Ota, K., 2004. “Effect of recast temperature on diffusion and dissolution of oxygen and morphological properties in recast nafion”. *J. Electrochem. Soc.*, **151**(4), pp. A639–A645.
- [139] Weber, A. Z., and Newman, J., 2006. “Coupled thermal and water management in polymer electrolyte fuel cells”. *J. Electrochem. Soc.*, **153**(12), pp. A2205–A2214.
- [140] Hottinen, T., and Himanen, O., 2007. “PEMFC temperature distribution caused by inhomogeneous compression of GDL”. *Electrochem. Comm.*, **9**, pp. 1047–1052.

Paper A

Khan, M.A., Sundén, B., and Yuan, J., 2011. “Analysis of multi-phase transport phenomena with catalyst reactions in polymer electrolyte membrane fuel cells - A review”, *Journal of Power Sources*, vol. 196, pp. 7899-7916.

© 2011 Elsevier B.V.
The layout has been revised

Analysis of multi-phase transport phenomena with catalyst reactions in polymer electrolyte membrane fuel cells - A review

Munir Ahmed Khan, Bengt Sundén, Jinliang Yuan

Abstract

A review is presented for two-phase modeling approaches to study various transport processes and reactions in polymer electrolyte membrane (PEM) fuel cells along with some experimental work. It has been noted that water management is still one of the least accurate modeled phenomena. The lackness in complete descriptive models for water management inside PEM fuel cells can be attributed to the complexity of the phenomena, lack of empirical or measured data and non-availability of apt governing equations.

Another discrepancy found in present models is the proper validation of the numerical work as it has been observed that mere comparison with V-I curve can sometimes lead to misguided conclusions. Additionally, keeping in mind the multi-scale nature of a PEM fuel cell, application of the Lattice Boltzmann (LB) method has also been reviewed in this work and it was noticed that LB methods offer bright perspective at meso-scale by incorporating details of local structure. Furthermore, a brief description of the catalyst layer models is also presented with some technological developments at nano-scale to improve the physio- and electro-chemical properties. A test case for a 2D PEM cathode is also simulated for different operating voltages to predict the water saturation effects.

Key words: PEMFC, multi-phase, macroscopic models, modelling discrepancies, meso-scale modeling, validation.

1 Introduction

Fuel cells have become a pivot of energy research activities in the present decade. With increasing energy demands and depleting organic fuels, a need for sustainable and efficient energy production had never been felt so urged as of today. With many different alternative proposals provided by the scientific and engineering communities, fuel cells stand a biased position because of their high efficiency with a byproduct of low to zero greenhouse gas emissions and abundance of fuel availability. Among many different types of fuel cells, polymer electrolyte membrane (PEM) fuel cells have taken the lead because of their low operating parameters, cost effectiveness, high current density and compactness for mobile applications [1–3].

An outlook of PEM fuel cells has a deceptive presentation as being very simple and straightforward piece of equipment in both making and service. However, turning around the coin indicates that they are not more simpler than any other energy production devices, and quantifying and measuring all the processes and phenomena inside PEM

fuel cells is not only impossible [1] but the highly reactive environment also makes it quite difficult to measure even simple parameters like temperature, pressure, electric potential and species gradients, etc. [4]. In recent years, much critical work has been performed in various disciplines of PEM fuel cells from basic electro-chemistry to design of stacks, but, numbers of issues are still pending and need to be resolved for commercial viability and many improvements are deemed necessary to remove the big question mark about the future of PEM fuel cells as an alternative energy production unit.

It has been well established that cathode performance is one of the key issue still under intensive investigation without any proper remedy yet proposed [5]. The important factors affecting the cathode performance are [6];

- slow reaction kinetics,
- formation of liquid water and water management,
- thermal management.

In PEM fuel cells, the oxygen reduction reaction (ORR) is the rate determining step for the overall electro-chemical reaction. Despite the active research in improving the physio-chemical behavior of the cathode catalyst it has been determined that the ORR is about four to six times slower to the hydrogen oxidation reactions (HOR) occurring at the anode [6, 7]. Formation of liquid water at the cathode of PEM fuel cell is an another major contributor to the under-grade performance of the cathode especially at high loads by blanketing the reaction sites by making them unavailable for three-phase contact.

Different processes contributing to water formation or removal during the operation of PEM fuel cells at the cathode are; [8] (the negative mechanisms in water source represent removal of water content while increase in water quantity inside the fuel cell is represented by the positive sources);

- oxygen reduction reaction (positive)
- electro-osmotic diffusion (positive)
- condensation of water vapors (positive)
- back diffusion (negative).
- evaporation (negative).

The ion transport in form of H_3O^+ uses water molecules as a carrier from anode to cathode of a PEM fuel cell. It is estimated that one to five molecules of water are dragged per proton migration from anode to cathode side [9, 10]. Similarly, along the production of water due to ORR, condensation of water vapors also proves to be handy in formation of liquid water if the vapor quantity exceeds its saturation limit in the inlet air supply to PEM fuel cell. The antimeasures for the formation of water are back diffusion resulting due to the concentration difference in water across the anode and the cathode, and the evaporation of liquid water due to high inlet temperature or saturation pressure. If the

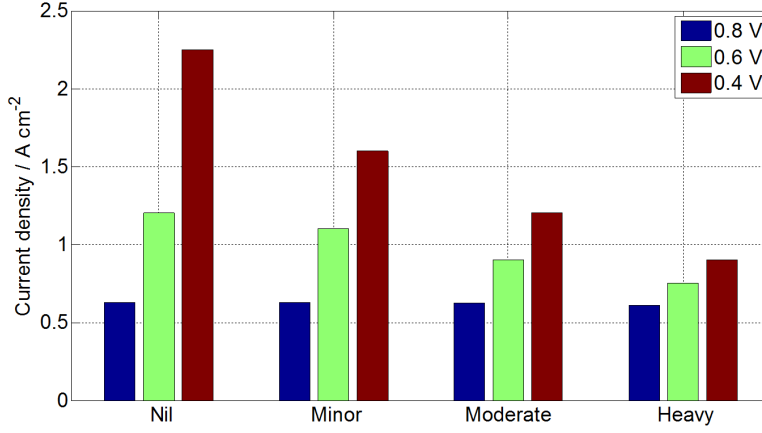


Fig. 1: Comparison of current density at different voltages with various levels of water flooding in the porous media.

formation rate of water is not balanced by the removal rate, accumulation of liquid water occurs at the cathode resulting in water flooding. This non-equilibrium of production and removal is known to cause major performance hold ups to PEM fuel cells in terms of efficiency, stability and reliability [11, 12].

Although, water formation has been labeled as one of the performance defectors in PEM technology, many processes inside the PEM fuel cells are itself highly water dependent. As already stated, the proton migration from anode to cathode i.e., the protonic conductivity of the membrane material incorporated in low temperature ($<100\text{ }^{\circ}\text{C}$) PEM fuel cells, is highly water dependent. The dryness of the membrane will render it from low to zero conductivity causing major suffering in performance by considerably increasing the ohmic losses [10]. To ensure proper hydration of the membrane, a balance between inlet humidification and evaporation rate has to be maintained. So, overall, the formation and removal rate of water has to be closely monitored and balanced not only to avoid flooding of the cathode but also for proper wetting of the membrane. As discussed above, the water management problem is one of the major issues related to the optimum performance and stable operation in PEM fuel cells. A comparison of different water flooding levels is given in Fig. 1 for the current produced for each operating voltage. As it can be seen that, when the water flooding increases, the maximum current density for a specific voltage decreases considerably. At low current densities, the current density is almost the same for all levels because at such low operating conditions the reaction rate is quite low and water formation due to both ORR and electro-osmotic drag is not significant but at higher levels of water flooding there is decrease of almost 80% in the current density produced at 0.4 V.

Many reviews of PEM fuel cell modeling have been published by, e.g., Biyikoglu [13], Cheddie and Munroe [4], Wang [14], Haraldsson and Wipke [15], Siegel [3] and Mench [16] etc. Most of the reviews were conducted for general models related to conservation

equations, spatial dimensions and level of model complexity. The present work is limited to two-phase flow models as the water management still remains one of the key issues for PEM fuel cells. Also, a brief insight will be provided for micro-scale model developments in PEM fuel cell both in terms of Computational Fluid Dynamics (CFD) analysis and catalyst layer modeling.

2 Classification of models

Because of vast diversity of technologies incorporated in a single PEM fuel cell, it is quite difficult to classify and fix a certain model to a particular subclass, e.g., even in CFD modeling, equations of voltages need to be solved for electro-chemical reaction rates besides verification of modeling. Similarly, electrical, heat and species transport losses need to be accounted for the simplest of the models. Apart from this, anisotropy of material properties extend the models floating in various domains.

Many authors have already attempted to classify PEM fuel cell models according to their own dominions, e.g. Khan [8] has classified PEM models based on thermal analysis (isothermal and non-isothermal), flow (single- or two-phase) and the electrochemical model used to simulate the reactions in the catalyst layer. Similarly, Cheddie and Munroe [4] have categorized PEM fuel cell models based on modeling approach used, i.e., analytical models, semi-empirical models and mechanistic models. Analytical models represent the simplest of all as many simplifying assumptions are employed that results in approximate analytical voltages versus the current density relationships [17–19]. In semi-empirical models, empirically determined properties are used with theoretical differential and algebraic equations [20], while, mechanistic models have been more popular in modeling in which the differential equations are derived from physics and electro-chemistry of the internal phenomena in PEM fuel cells [21–23].

Siegel [3] has categorized PEM fuel cell models in his review article based on geometric constraints of the models from one to three dimensions. Classification based on the length scales of the computational domains has also been proposed by Mench [16] and Djilali and Sui [24]. The length scale varies from the molecular level to full system size with different purposes and outcomes. The molecular models deal more with an attempt to model transport of charge, mass and heat to interpret the limitations that significantly affect the overall performance of fuel cells [16, 25–28] whereas, system or stack models deal more with efficiencies, losses and geometric limitations of the complete energy system [19, 29–38].

3 Macroscopic models and challenging issues

Basically, a fuel cell is an electro-chemical device that converts the chemical energy into the electrical energy without any intermediating assistance or device. Main components of a single PEM fuel cell can be listed as;

- membrane

- catalyst layer
- gas diffusion layer (GDL, also known as porous transport layer, PTL)
- current collectors
- flow channels.

Membrane is the parting component between anode and cathode sides of the fuel cell while catalyst layer, GDL and current collectors on either side of the membrane constitute the electric poles of the cell. Fuel (hydrogen) is fed to the anode side of the fuel cells, and is distributed on the catalyst layer by the GDL to produce electrons and protons according to Eq. (1);



Electrons are forced to flow through the external path, while, protons migrate internally through membrane by selecting such a material that poses high electron resistivity and proton conductivity (the detailed structure of membrane materials can be found in [39]). Oxygen and charged entities (e^- and H^+) transported from anode combine at the cathode to produce water as a product.



Eqs (1) and (2) represent the half-cell reactions of anode and cathode sides respectively and are catalyzed with platinum present in the catalyst layer on either sides.

With advances in computer technologies and enhanced speeds, CFD modeling approach has provided scientists and engineers with internal anatomy of fundamental processes of a PEM fuel cell [8]. To date many models for PEM fuel cells have been proposed with varying complexity and texture, however, there is no single complete model that would effectively and efficiently explain and chalk out the phenomena altogether. Nevertheless, for a descriptive model of PEM fuel cell, Biyikoglu [13] has outlined basic conditions or processes, inclusion of which can result in a much descriptive model, given as;

- balanced current distribution
- control of water flow
- efficient removal of liquid water
- removal of excessive heat.

Table 1: *Governing equations for PEM fuel cell models and applicable component of the PEM fuel cell.*

Equation		Region of application	Remarks
1.	Continuity	CL, GDL, flow channels	X
2.	Momentum	CL, GDL, flow channels	X
3.	Species transport	CL, GDL, flow channels	X
4.	Energy equation	All regions	One equation or LTNE approach
5.	Electric potential	All regions except flow channels	Solid phase and membrane phase potential
6.	Secondary phase	All regions except current collectors	Multi-phase models in gas channels, water saturation equation in CL and GDL, water flux in membrane

Table 2: *Source terms for the governing equations.*

Equations	Source term	Gas diffusion layer (GDL)	Catalyst layer (CL)
Momentum	$\dot{m}_{\text{ORR}, \text{O}_2}$	0	$-\frac{M_{\text{O}_2}}{4F} \nabla \cdot \mathbf{i}$
	$\dot{m}_{\text{ORR}, \text{H}_2\text{O}}$	0	$-\frac{M_{\text{H}_2\text{O}}}{2F} \nabla \cdot \mathbf{i}$
	\dot{m}_{phase}	Eq. (12)	Eq. (12)
Energy	\dot{q}_{Ω}	$\frac{i_s^2}{\sigma_{s,\text{eff}}}$	$\frac{i_s^2}{\sigma_{s,\text{eff}}} + \frac{i_m^2}{\sigma_{m,\text{eff}}}$
	\dot{q}_{phase}	$\dot{m}_{\text{phase}} \times h_{fg}$	$\dot{m}_{\text{phase}} \times h_{fg}$
	\dot{q}_{it}	$h_v(T_s - T_f)$	0
	\dot{q}_{ORR}	0	$(\phi_m - \phi_s) \times \nabla \cdot \mathbf{i}$
Charge	S_{ϕ_s}	0	$\nabla \cdot \mathbf{i}$
	S_{ϕ_m}	0	$-\nabla \cdot \mathbf{i}$

Although, basic outline, as explained above, is very useful in developing a CFD model of PEM fuel cells, still ultimate and complete PEM fuel cell model is quite difficult to achieve due to inherent limitations of the analysis and outputs desired. The main limitations still blocking the researchers from attaining the ultimate goal of completeness, as given by Mench [16], are the inclusion of the physico-chemical phenomena, knowledge of the transport phenomena, computational power and proper validation of the models.

The governing equations used in PEM fuel cell models are given in Table 1 with applicable component regime and the source terms for each governing equations are given in Table 2 for a typical PEM fuel cell CFD model. The detailed description of the governing equations along with nomenclature and source term evaluation for all the fundamental processes can be found in [8], here some of the important and usually ignored factors are outlined.

3.1 Anisotropy of physical properties

Regarding the porous media of PEM fuel cells, it is revealed that it comprises of fibrous media that has significant anisotropy due to its orientation of the fibers. Due to this, the in-plane and throughplane properties vary significantly [40, 41]. The major properties influenced by anisotropy are;

- species transport
- heat conduction
- electrical conduction
- water saturation

For species transport in the porous media, most of the authors use Bruggeman's correction factor. However, accounting for anisotropy, the effective diffusion coefficient is a tensor rather than scalar quantity. As presented by Nam and Kaviani [42], the effective diffusion coefficient in the porous media in PEM fuel cells is better depicted by using percolation theory, given as;

$$D_g^{\text{eff}} = f(\varepsilon) \times D_g^i \quad (3)$$

$$f(\varepsilon) = \varepsilon \left(\frac{\varepsilon - \varepsilon_p}{1 - \varepsilon_p} \right)^\alpha \quad \alpha = \begin{cases} 0.521 & \text{in-plane} \\ 0.785 & \text{through-plane} \end{cases}$$

where ε_p is the percolation critical value and has been reported to be 0.11 and 0.13 by Pharoah et al. [43] and Liu and Wang [44], respectively. The results produced by the anisotropic diffusion coefficient reveal that the gas flow is much higher in in-plane direction than through-plane directions suffocating the reaction sites in the catalyst layer. Similarly, the thermal conductivity of the porous media is almost 14 times more in in-plane direction and temperature differential of more than 5 °C in through-plane was observed in work by Pasaogullari et al. [41]. Meng [40] has also suggested anisotropic electrical conductivity of the porous media and a difference of more than 2000 (S m⁻¹) was reported to exist in in-plane and through-plane directions. Similarly, apart from anisotropic effects, the experimental and CFD modeling results also vary as the temperature gradients observed are much lower while simulated numerically using the parallel resistance approach, given as [43];

$$k_{\text{eff}} = \varepsilon k_v + (1 - \varepsilon) k_s \quad (4)$$

where k_s and k_v are solid and void thermal conductivities, respectively. The conduction of heat, as predicted by Eq. (5) is assumed to travel either through void or solid regions contrary to combined path. Pharoah et al. [43] suggested a novel approach by stacking the solid and void regions so that all of the heat is passed through combined solid and void regions termed as the network resistance approach.

$$k_{\text{eff}} = \frac{k_s k_v}{\varepsilon k_s + (1 + \varepsilon) k_v} \quad (5)$$

The heat transport predicted by utilizing the thermal coefficient as given by Eq. (5) is approximately the same as encountered in reality [43].

Similarly, most of the two-phase models use Leverett function to simulate the water flow in PEM fuel cells [8, 41, 45]. This function is highly dependent on the permeability of the porous media which in turn is actually anisotropic in nature, as given by [41];

$$j_x = C_1 k_{xx} \quad \text{and} \quad C_2 k_{yy} \quad (6)$$

where j_x and j_y are the mass flux of liquid water in respective directions, k_{xx} and k_{yy} represent the anisotropic permeability in the principle directions of the porous media. It is found that water saturation levels are always higher in this case, thus reducing the overall performance of the PEM fuel cells [41].

3.2 Local thermal equilibrium (LTNE) approach

The condition to use one equation model for heat transport or local thermal equilibrium (LTE) is only valid when the temperature difference between the fluid and the solid phases of the porous electrode is much lower than the overall system temperature difference. Since, PEM fuel cells are low operating temperature devices, the magnitude of both the temperature differences between phases and the overall temperature difference is almost same, given mathematically as [46];

$$O \left| \frac{\Delta T_{\text{loc}}}{\Delta T_{\text{sys}}} \right| \quad (7)$$

where ΔT_{loc} is local temperature difference between the phases while ΔT_{sys} represents the overall system temperature difference. In LTNE approach both the phases i.e., void and solid portions of the porous media are represented by separate equations and interlinked through a volumetric heat transfer coefficient h_v ($\text{W m}^3 \text{ K}^{-1}$). The exact value of h_v has not been measured yet but experimental results obtained for the aluminum foam ranging from 3×10^4 to 1.5×10^5 ($\text{W m}^3 \text{ K}^{-1}$) [46] has been used by some authors. To date many researchers have implemented LTNE approach in both single phase and two-phase flow regimes but limiting the geometry to 2D only [8, 23, 46–49]. Since many parameters in PEM fuel cell are temperature dependent, LTNE approach to 3D models need to be evaluated and compared with the local thermal equilibrium or the so-called one equation models.

3.3 Knudsen diffusion

Usually effective diffusion coefficient modified by Bruggeman's correction is employed in species transport of oxidants and fuels in the porous media of the PEM fuel cells. However, the texture of porous media is very complex and the relative influence of ordinary diffusion or Knudsen diffusion on species transport is governed by the pore geometry [50]. According to Malek and Coppens [51], for the media with pore dimensions of 2–50 nm, Knudsen diffusion is the predominant transport mechanism which results from the collision of gas molecules with the pore walls instead of intra-molecular collision (Brownian motion). The Knudsen diffusion coefficient for CFD calculations can be used in the form of [52];

$$D_k = \frac{2}{3} r_e \sqrt{\left(\frac{8RT}{\pi M_i} \right)} \quad (8)$$

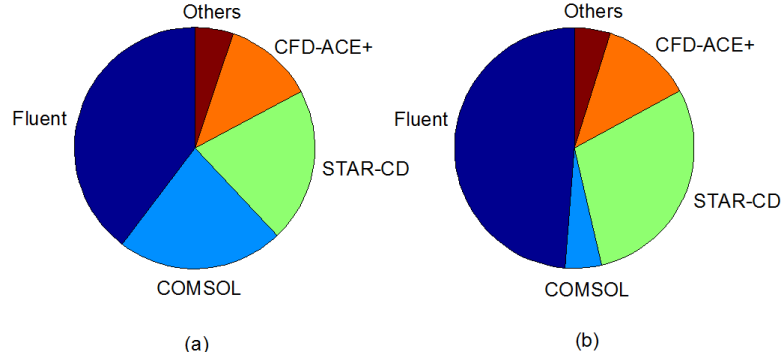


Fig. 2: Comparison of commercial and non-commercial software used for PEM fuel cell CFD. (a) Trend of software used for CFD modeling in overall; (b) trend of software used for 3D modeling. For commercial software, data is adopted from Siegel [3].

The effective diffusion coefficient based on both bulk diffusion and knudsen diffusion can be calculated as [53];

$$\frac{1}{D_{\text{eff}}} = \left(\frac{1}{D_b} + \frac{1}{D_k} \right) \times f(\varepsilon) \quad (9)$$

where $f(\varepsilon)$ is the correction factor for the porous medium and can be evaluated according to Eq. (3).

3.4 Modeling software and solutions

With in-house self-developed and open-source CFD models, many commercial software products are available in the market that have proved to be very efficient and robust. Regardless of inherited disadvantage of limited freedom in equation manipulation and controls, many researchers have opted for commercial software products as prime CFD tool. Among many, the most commonly used are FLUENT[®], COMSOL[®], STAR-CD[®] and CFD-ACE+[®], and the contribution of each in CFD modeling is shown pictorially in Fig. 2 [3].

ANSYS[®] Fluent[®] [54] is a powerful commercial software available in the market offering sophisticated numerics and robust formulations including a pressure-based segregated and coupled solvers, and a density based solver technique to ensure optimum and reliable results. It is well suited for a number of complex physical models utilizing unstructured meshes both for 2D and 3D cases based on finite volume method (FVM). Meshes can be created using ANSYS[®] meshing products or other robust products like ICEM[®] and GAMBIT[®]. To further enhance the flexibility of model variant situations, Fluent[®] provides the use of user-defined-functions (UDFs) that help to tailor the model to specific needs or requirements. With the increase in demands for fuel cells CFD analysis, an add-on is provided to simulate typical PEM fuel cells. In this module, the twophase

flow in the porous media is solved using the Leverett function while in gas channels it is assumed that both gases and water flow with the same velocity in form of fine mist. The potential equations for both solid and membrane phases are also solved to get the inside distribution of electric and ionic currents, respectively. The additional capability of Fluent[®] software to solve user-defined-scalars provides a handy tool to simulate most of the internal phenomena occurring inside PEM fuel cells. Fluent also offers extended post-processing tool and provides provision to export the data to other post-processing software solutions. In order to simulate the electro-chemical reactions, a choice is also provided to select either Tafel formulation or the advanced Butler-Volmer kinetics. Furthermore, to enhance the flexibility of the PEM fuel cell module, it is also made possible to specify requirement based specific functions and models through a modifiable source code.

COMSOL Multiphysics[®] [55] is another commercial software product available widely for simulating fluid flow incorporating finite element method (FEM) with stiff chemistry solvers. This software also offers flexible equation based modeling with various degrees of mesh complexity. The user can also include partial differential equations (PDEs) using various formulations and the software can automatically detect the best possible solver and settings for a particular problem along with manual tuning. Since fuel cells have become a beacon of future power, an add-on module has been released in the latest version V4. Compared to Fluent[®] in which add-on module is only available for PEM and solid oxide fuel cells (SOFCs), COMSOL[®], on the other hand, also supports alkaline, molten carbonate and direct methanol fuel cells. As far the mesh generation for COMSOL applications is concerned, a built-in geometry and mesh generator is available in standard package with sound post-processing facility.

STAR-CD[®] [56] and CFD-ACE+[®] [57] are other finite volume based CFD software products also commercially available. Both products have strong parallel computing capabilities with aptitude to handle complex geometries including multiphysics modules for PEM fuel cells that can be handled quite easily. CFD-ACE+[®] also offers the facility to carryout stress and strain analysis within the PEM fuel cells. Alongside licensed commercial software, Open-FOAM is open code software with pre-developed modules for simulating complex multiphysics problems with good pre- and post-processing utilities also based on finite volume technique. Additionally, meshes from other software can also be imported and manipulated. The advantages offered by OpenFOAM are that users can extend or create own libraries and manipulate the solver to suit the demands. Although no fuel cell modules are provided built-in but with good coding knowledge, efficient and robust models can be developed that can handle a variety of problems [3].

4 Two-phase models

Water management inside PEM fuel cell is of paramount importance because operation of a PEM fuel cell is highly dependent on the water content as protonic conductivity of the membrane material, typically used for low operating temperature fuel cells, is highly dependent on the amount of water present [39, 58]. Decrease in water content

can cause dry out of membrane and reduce protonic migration, thus, it is very essential that the membrane remains fully hydrated all the times. However, excessive water inside PEM fuel cell can lead to clogging of channels [59, 60], and, flooding of the catalyst layer [59, 61, 62] and long term liquid water accumulation inside PEM fuel cell is also one of the major contributor to the degradation of the catalyst and its carbon support material, ionomer poisoning and hydrophobicity loss [63]. In this section, an insight into selected two-phase models is presented with a summarized outline in Table 3. The list presented here is not an exhausted one but it has been made to include different variety of two-phase CFD models used in the research society in last 10 years.

4.1 CFD modeling review

He et al. [64] performed multi-phase simulations of PEM fuel cell. In their model, the droplet size of water was taken as the prime parameter to study the multi-phase flow. A multi-phase mixture model was applied to a 3D geometry. The interaction effect between the phases was studied by considering droplet size, drag coefficient, Reynolds number, velocity and droplet relaxation time. The equation for calculating the droplet size was adapted from Zhang et al. [60]. The advantage associated with this model is that it includes the effect of liquid water removal from the channels of PEM fuel cell. In this work all the simulations were performed on a commercial CFD software.

Yuan and Sundén [65] also developed a 3D model to understand the effect of liquid water on cell performance. The model presented is a half-cell model considering cathode only because of its slower kinetics. The electro-chemical reactions were modeled to occur in a thin layer while simulating the flow in GDL and the channels. The salient features of this work were the use of combined thermal boundary conditions and mass transfer along with the effect of saturation on current density profile. The calculation domain was discretized by finite volume method and a combination of uniform and non-uniform grid spaces. The simulations were performed using an in-house CFD code. The saturation was evaluated based on the saturation pressure and the local temperature of the flow. Wang et al. [66] also proposed a two-phase model of PEM fuel channels to simulate the flow of liquid water and gaseous reactants. Darcy's law and multi-phase mixture model was employed for estimation of the key parameters such as overall pressure drop and liquid saturation profile along the channel and flow analogy to random porous media. The physical model used in this work consisted of a single straight channel for the cathode side. Fully or partially humidified air feed was used at the inlet and the water produced as a result of electro-chemical reactions was injected into the channel along its length.

He et al. [21] performed a 2D analysis of a PEM fuel cell with interdigitated flow field by solving two-phase, multi-component transport equations. Darcy law was used to simulate the gas phase transport, while for liquid water, both the capillary pressure and the shear force between the two-phase was considered as the prime transport mechanisms. The modeled region consisted of a GDL and the current collector. The electro-chemical reactions were assumed to occur at the boundary of GDL, i.e., a thin layer model was

used.

Le and Zhou [67] presented a general model of PEM fuel cell which accounted for fluid flow, heat transfer, species transport, electro-chemical reactions and water saturation. Detailed thermo-electro-chemistry studies were carried out on a 3D geometry where saturation effects were evaluated with explicit gas-liquid interface tracking using VOF multi-phase model. Commercial software Fluent[®] was employed for simulations and calculations. In this model, all the components of a complete single fuel cell unit were included to broaden the results scope and the effect of liquid saturation along with porous media was also studied. The flow field design employed in this model was the serpentine flow field. Initially, water droplets of 0.4 mm were assumed suspended in the flow field and their behavior was studied at different time steps at an operating voltage of 0.5 V.

Hwang [23] has also developed a 2D model of PEM fuel cell in which two separate momentum equations were applied for gaseous and liquid flow. Heat distribution was simulated using the LTNE approach that considered separate energy equations for fluid and solid components in the GDL. Also, irreversible heat generation due to the electro-chemical reactions, the ohmic losses and the heat of evaporation and/or condensation were explicitly considered in this model. The calculation domain consisted of two porous layers of the cathode of PEM fuel cell. The geometry considered in this model was interdigitated flow field with two regions of the porous media distinguished according to the position, i.e., the area under the inlet or the area under the current collector. Finite element technique was employed to the solution domain considering the liquid flow force due to the imbalance of the liquid water pressure and the gaseous pressure. The correlation provided by Leverett [68] was employed to quantify the water saturation effects in the porous media.

Senn and Poulikakos [45] have also presented a 2D model of PEM fuel cell that accounted for multi-component species diffusion, formation of liquid water, heat transfer and electronic current. All the governing equations in this model were non-dimensional and FVM was employed to solve the equations. The main focus of the work was to study the effects of varying the channel, current collector and GDL dimensions. The catalyst layer was assumed to be very thin and treated as a boundary condition for the electro-chemical reactions and the heat source. The distinguished feature of this work was the introduction of a performance variable based on the average current density to measure the effects of mass transfer, water saturation and heat transfer.

A two-phase flow model has also been presented by You and Liu [69, 70] for the cathode of PEM fuel cell. The concept of multi-phase mixture model coupled for the porous media and the gas channel was implemented to study the saturation effects. The model presented by Wang and Chen [71] was extended to incorporate detailed effects of levels of multi-phase mixtures instead of separate phases (i.e., two fluid model) including non-zero interfacial areas. The multi-phase model used in this work is derived as given by Wang and Chen [71] and Abriola and Pinder [72]. This model was limited to 2D and the cathode of a PEM fuel cell and explicit results were obtained for the current density

affected by different saturation levels along with inlet air humidification.

Siegel et al. [73] also carried out comprehensive modeling of a 2D PEM fuel cell including water transport within the porous media by the capillary pressure. The rate equation for electro-chemical reactions was adapted to the agglomerate structure of the catalyst layer. Major focus of this article was to study the effects of different factors affecting the PEM performance, e.g., geometry, porosity, and polymer properties, etc. The physical properties used in this model were derived by direct measurement from a base case fuel cell experimental model. The results obtained from these simulations were used to study the effect of liquid water on reaction rate and local decrease in the porosity of the catalyst layer and GDL.

Yu et al. [74] presented a 3D model with interdigitated flow field for a PEM fuel cell. In this work two-phase flow and transport mechanism was developed to study the performance of a cell under different operational parameters. A detailed physical insight was provided for the velocity, the species concentration, the water content and concentration, and the current density distribution. All the model equations were discretized using finite volume technique and simulated using commercial CFD software. Coppo et al. [75] also developed a CFD model that incorporates all the major phenomena in PEM fuel cell, i.e., three-phase flow (the third phase refers to the dissolved phase), proton and species transport etc. and agglomerate model was employed to determine the reaction kinetics. The pivot of this work was to evaluate the temperature dependence of all the physical properties used in general PEM models. Moreover, a novel model was also incorporated to describe the liquid water from the porous media surface by advection of water droplets due to the gas streams in the gas channel. All the simulations were performed at different temperature levels and experimentally verified for the accuracy of this approach.

Another complete 2D PEM fuel cell model with two-phase flow was presented by You and Liu [70]. This model was a continuation of earlier models presented by same authors [69, 76]. A coupled flow, species, electrical potential and current density was solved in the flow channels, GDLs, catalyst layer and the membrane. The coupling of governing equations on both the cathode and the anode sides including the membrane provided a much deeper insight of the various parameters and water content. To obtain a converged solution, the authors first assumed the overpotential at the catalyst/ membrane interface and calculated the local current density which in turn was used to simulate the net water flux across the boundary and the protonic current. Finally the oxygen and the calculated water flux were used as the boundary condition for the working domain. All the coupled equations were solved iteratively and the average current density was measured by averaging the local current densities along the flow path. Acosta et al. [77] also presented a 2D, non-isothermal, two-phase model for PEM fuel cells with both conventional and interdigitated flow field designs. A continuum approach was utilized to simulate gas and liquid water with extended Darcy's law. The physical properties used in the model, e.g., wettability, permeability and porosity etc., were determined experimentally. For the measurements of the saturation content in the porous media, a method based on mercury intrusion porosimetry was used to quantify the capillary pressure. This model was also limited to the cathode side only and the continuum

approach was used to solve the coupled governing equations. All the governing equations were solved iteratively using an in-house code called MUFTE UG which is based on the concepts and algorithms presented by Helmig [78] or Class [79]. For simulation of water saturation, the Eulerian approach was used where discontinuities in pressure between the two fluid interface was balanced by employing the capillary pressure effects that exist in the porous media.

Meng [80] presented a multi-dimensional two-phase model including a micro-porous layer sandwiched between the catalyst layer and the GDL. A micro-porous layer has been found to reduce the water saturation levels thus enhancing the oxygen transport to the reaction sites and the efficiency [81]. This model has enhanced techniques employed to properly incorporate the interfacial liquid water transport phenomena between the different porous media. Furthermore, the effects of the current collector and the gas flow channel on the saturation of the porous media have also been explicitly studied. The results of this model were verified with high-resolution neutron imaging data [82] and other numerical data. Zhou et al. [83] has also presented a multi-phase and -component 2D model of a PEM fuel cell with pressure and phase change effects to further understand the influence of the inlet humidification and pressure. One of the major assumptions in this model was that liquid water was assumed to exist in form of small droplets with no volume. Berning and Djilali [84–86] also carried out series of 3D work to study the effects of temperature and water management on the performance of fuel cells. In their work, a single fuel cell was divided into one main and three sub-domains. All the domains were coupled through adjustment of appropriate boundary conditions. Similarly, Hu et al. [22, 87] also developed and analyzed a two-phase PEM model considering species transport in both anode and cathode sides. A special consideration was given to the impact of ribs on the species transport and SIMPLE algorithm with fourth order Runge-Kutta method was used in their model.

4.2 Experimental analysis of water transport

Additionally, many authors have experimentally studied water transport for specific components of PEM fuel cells, i.e., the catalyst layer, the membrane and the GDL that are of paramount importance because individual component has different behavior under different saturation and water content levels. A brief description of such methods is presented here with briefly stating the findings of the studies.

There are two types of water transport in the membrane of a PEM fuel cells, the electro-osmotic drag and the back diffusion [88]. For complete understanding and accurate modeling of membrane materials it is very essential to accurately estimate the electro-osmotic and back diffusion coefficient of the membrane material. Yan et al. [89] reported a value of 1.5-2.6 for drag coefficient for Nafion[™] 117 for different inlet humidification conditions. Similarly Ge et al. [90] determined that varying the thickness of the membrane of the PEM fuel cell has significant effect on the water transport through the membrane and hydrophobicity of the membrane material also alters the absorption and desorption of water at the membrane/catalyst interface thus impacting the overall water transport

through the membrane material.

The flooding of the GDL is one of the most investigated phenomena in numerical work but Yamada et al. [91] performed experimental analysis for the extent of water flooding of the cathode GDL with switching interdigitated and conventional flow field designs to measure pressure drop and concluded that water flooding is a direct function of the wetting properties of the catalyst layer and the GDL. Additionally Benziger et al. [92] measured the resistance to the flow of water through the GDL by applying hydrostatic pressure across the GDL and the effects of pressure on the water transport through the voids were analyzed in detail. It was concluded that water flowed through only 1% of the void volume in the GDL. Lin and Nguyen [93] also employed pressure drop calculations to measure the effect of GDL thickness and hydrophobicity on flooding levels. An optimum condition was suggested for both water flooding levels and the species transport through the porous GDL because the hydrophobic pores support the gaseous transport while the hydrophilicity aided the liquid water transport. It was also noticed that employing micro-porous layer (MPL) in-between the catalyst layer and GDL reduced the water flooding which makes it possible to use thinner GDLs for same operation performance level of PEM fuel cell. Litster et al. [94] developed a novel approach to visually study the water flooding levels in the porous GDL by using fluorescence microscopy technique. The movement of water was monitored by following the light emitting dye with a microscope fitted with CCD camera. It was shown that liquid water is transported by fingering and channeling similar to the blotting paper effect.

In many CFD analysis of PEM fuel cells, the flooding of the gas channels is usually ignored keeping in view the fact that liquid portion makes up only minute fraction of the total volume of the gas channel. However, it is very desirable for liquid water in gas channels to be removed because of two adverse effects that can severely degrade the effective operation of PEM fuel cells, i.e., flooding in channels cause a liquid film to cover the GDL surface and hinders in optimum transport of gaseous species inside GDL. And, removal of liquid water at shutdown may not be performed adequately [88]. Kumbur et al. [95] have experimentally investigated the droplet behavior and instability in rectangular PEM fuel cell channels because the physics of detachment size and behavior of water droplets plays an effective role in the liquid water removal from a surface. The findings of this work indicated a strong relation between contact angles (wettability) and the departure diameter on each other along with the surface roughness of the GDL and the characteristics of the fluid flow through the channel. Zhang et al. [60] have also performed similar investigations but mainly focused on the water accumulations at the geometric corners of the flow field at low flow rates.

Table 3: Summarized features of the reviewed articles.

Author	Chemical Kinetics	Saturation Equation	Model Validation	Geometry	Major Conclusions
1. He <i>et al.</i> [64]	Butler-Volmer	$\frac{\partial}{\partial t}(ap_s) + \nabla \cdot \left(\frac{Ks^3}{\mu_l} \frac{d}{ds} (\rho_c \nabla s) \right) = S$	Experimental Fluent Module	3D PEM	<ul style="list-style-type: none"> Large water droplets increase saturation. Liquid water hinders heat transfer in gas diffusion layer and catalyst layer causing hot spots.
2. Yuan and Sundén [65]	Tafel Equation	$s = \frac{\rho_{\text{H}_2} - \rho_g \phi_{\text{H}_2}}{\rho_{\text{H}_2} - \rho_g \phi_{\text{H}_2}}$	X	3D Cathode only	<ul style="list-style-type: none"> Co-flow pattern is disadvantageous for PEM fuel cells as compared to counter-flow pattern. The non-uniformity in the current distribution resulted because of uneven distribution and transport of the reacting air. Higher saturation levels resulted in low current densities. Low operating parameters (temperature and humidity) also decreases the current density.
3. Wansheng et al. [21]	Tafel Equation	$v^I = f_s s^g - D_c \nabla s$	Experimental	2D Cathode only	<ul style="list-style-type: none"> In interdigitated flow fields along with evaporation of liquid water, the liquid water transport also acts as water removal mechanism Higher oxygen flow improves the reactant transport The thickness of electrodes effects the current density For interdigitated flow fields, a shorter rib dimensions improves the performance.
4. Le and Zhou [67]	Butler-Volmer	$\frac{\partial}{\partial t} (cs_l \rho) + \nabla (s_l \rho \vec{v}) = S$	Visual	3D	<ul style="list-style-type: none"> Liquid droplets cause high pressure drop regions The tuning areas of the serpentine flow field showed increased water droplet formation causing a substantial air flow blockage. The channel structure significantly influences the water distribution inside the cell. High saturation causes excessive concentration losses. Area under the channels give higher reaction rates. However, the presence of liquid water reduced the overall temperature of the cell.
Hwang [23]	Butler-Volmer	$\frac{1}{\sigma} \nabla \cdot (\rho u_g u_g) = -e [\nabla p_c + (\rho_w - \rho_g) g] + \nabla \cdot (\mu_w \nabla u_w) - \frac{\partial \mu_w u_w}{\partial t} - \frac{\partial \mu_g u_g}{\partial t}$	Experimental	2D	<ul style="list-style-type: none"> Increasing the current collector temperature reduces water saturation by helping evaporation.

Table 3: Continued ...

Author	Chemical Kinetics	Saturation Equation	Model Validation	Geometry	Major Conclusions
6. Senn and Poulidakos [45]	Tafel Equation	$p_c = \frac{\sigma \cos \theta}{\sqrt{\gamma}} J(s)$ $J(s) = 1.417s - 2.12s^2 + 1.263s^3$	X	2D	<ul style="list-style-type: none"> Decreasing the dimensions of current collector width, channel width and GDL thickness improved the performance of the PEM fuel cell For small channel widths, a thin GDL performed better than thick GDL.
7. Seiged <i>et al.</i> [73]	Agglomerate	$\vec{u} \cdot \nabla s = \nabla \cdot \left(D_{L_2}^{eff} \nabla s \right) + S$	Experimental	2D	<ul style="list-style-type: none"> Liquid water has significant effect on fuel cell performance. Water content in catalyst layer and transport through membrane also effect the ohmic losses and reactant transport properties in the cathode catalyst. 20-40% of the liquid water is accumulated in the cathode catalyst layer.
8. Yu <i>et al.</i> [74]	Butler-Volmer	$\nabla \cdot (\phi \mu C_a) = -\nabla \cdot J_a + S$	Experimental	3D	<ul style="list-style-type: none"> Pure oxygen instead of inlet air increases fuel cell performance. A thin PEM fuel cell has better performance characteristics than a thicker one. High inlet velocity increases the current density Increasing current collector width has no prominent effect on the current density.
9. You and Liu [69, 70]	Butler-Volmer	$e \frac{\partial}{\partial t} (\rho C^a) + \nabla \cdot (\rho_a \mu C^a) = \nabla \cdot (\phi \rho D \nabla C^a) + \nabla \cdot \left[\varepsilon \sum_k \left[\rho_k s_k D_k^e (\nabla C_k^e - \nabla C^a) \right] - \nabla \cdot \left[\sum_k C_k^a J_k \right] \right]$	Experimental	2D	<ul style="list-style-type: none"> The water content increasing along the thickness of the membrane towards the cathode indicating large water migration from anode to cathode. Increasing the current increases oxygen consumption. At the cathode side, the protonic current is zero at the GDL/catalyst layer interface and increases towards the catalyst/membrane interface and is higher for high current density. Similarly, the overpotential corresponds directly to the magnitude of current density.
10. Meng [80]	Butler-Volmer	$\nabla \cdot \left[\frac{\rho_s K_s K}{\mu^l} \frac{\partial p_c}{\partial s} \nabla s \right] - \nabla \cdot \left[\frac{\rho_s K_s K}{\mu^l} \nabla p \right] = S$	Experimental and model comparison	2D	<ul style="list-style-type: none"> Water saturation level is highest in the catalyst layer. Water saturation level is minimum in micro-porous layer. Micro-porous layer serves as a barrier for liquid water and prevents coveing up of the interface between gas flow channel and the GDL, thus, increasing the species transport in the porous media.
11. Coppo <i>et al.</i> [75]	Agglomerate	$\frac{\partial s}{\partial t} + \vec{\nabla} \cdot (\vec{u} s) - \vec{\nabla} \cdot \left(D_{H_2O}^l \vec{\nabla} s \right) = S$	Experimental	3D	<ul style="list-style-type: none"> High temperature increases the reaction rate Higher temperature results in higher membrane conductivity. Higher temperature increases the species diffusivity.

Table 3: Continued ...

Author	Chemical Kinetics	Saturation Equation	Model Validation	Geometry	Major Conclusions
12. Zhou <i>et al.</i> [83]	Tafel Equation	$\frac{dN_{H_2,liquid}(x)}{dx} = \left(\frac{k_{H_2,ld}}{R_g T_H(x)} \right) \left[\sum_i N_{H_2,i}(x) \left(p_{H_2}(x) - p_{H_2,out}(x) \right) \right]$	X	2D	<ul style="list-style-type: none"> Higher water diffusivity results have been noticed by increasing the temperature in a highly hydrophobic materials. Water advection increases at the interface of GDL and gas channel at higher levels. Humidification of anode and cathode inlet is very important. Water content on the anode side dominates the membrane performance by delivery the protons to the cathode side. Liquid water injection at anode improves cell performance while injection at cathode hinders the effective water removal. Pressure loss in PEMs is one of the major parameters affecting the overall performance of cell. High inlet humidity at cathode decreases the overall system performance by increasing the pumping power.
13. Berring [86]	Tafel Equation	Schlogl equation for liquid water through membrane	Experimental	3D	<ul style="list-style-type: none"> Distribution of three dimensional flow velocities, species concentration, mass transfer rates, electric current and temperature were illustrated.
14. Hu <i>et al.</i> [22, 87]	Butler-Volmer	$s = \frac{V_w}{V_p}$	Experimental	3D	<ul style="list-style-type: none"> Interdigitated flow fields enhance the reaction rates by providing better flow through GDL as compared to other flow field distributions. Water saturation levels are low with interdigitated flow fields. The humidification of inlet species is more significant when utilizing interdigitated flow fields as compared to conventional flow fields.
15. Wang <i>et al.</i> [66]	X	$s = \frac{C^{H_2O} - C_{sat}}{\frac{\partial}{\partial y} - C_{sat}} \frac{V_w}{M_{H_2O}}$	Experimental	2D, 3D	<ul style="list-style-type: none"> Liquid water buildup is faster near inlet region under full humidification inlet conditions. Liquid saturation level upto 20% was observed near inlet. It was observed that water was trapped at geometric changes (bend etc.).

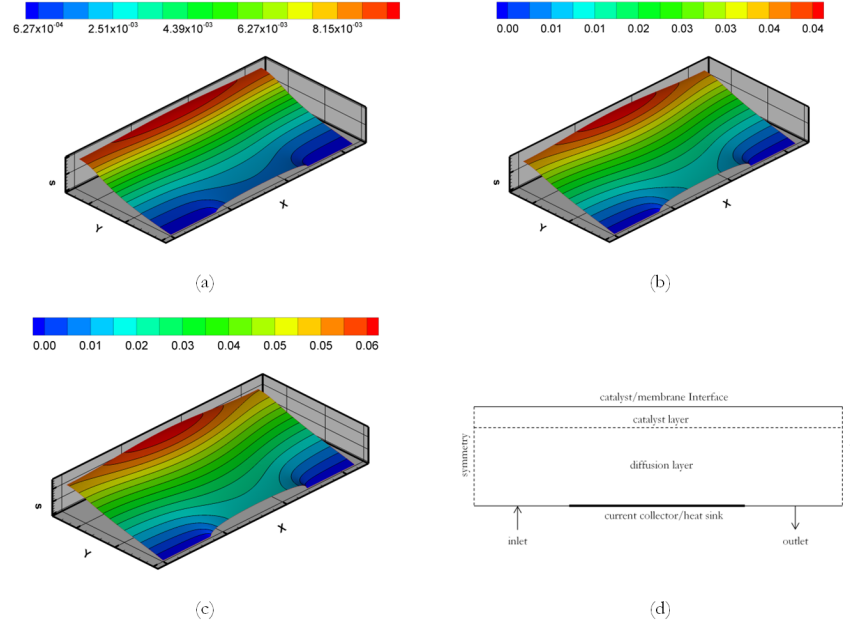


Fig. 3: *Contours of water saturation at different loads; (a) 0.2 A/cm², (b) 0.5 A/cm², (c) 0.7 A/cm², (d) the calculation domain.*

4.3 Case study of liquid water simulation in a cathode of PEM fuel cell

A two dimensional model of a cathode of PEM fuel cell has been simulated to study the effect of liquid water on the performance in terms of current density and voltage. The reason of selecting the cathode side only is based on the fact that the oxygen reduction reaction (ORR) is the rate limiting reaction in PEM fuel cell electro-chemistry [65]. The salient features of this work are that agglomerate catalyst model was used to predict the reaction rate and the effect of Knudsen diffusion was also included alongside multi-component diffusion of gaseous species as given in Eqs (8) and (9). To include the effect of temperature, LTNE approach was utilized because it has been previously established [46, 48] that fluid temperature is lower than predicted by one equation model because of higher thermal conductivity of the solid structure of the media. All the simulations were performed on Fluent[®] with 3rd order of spatial discretization of the domain. In this case, both the inlet and the out of the domain were simulated as infinite sink for liquid water, i.e., zero saturation value at the both the boundaries of the working domain (Fig. 3d).

The simulated results of the water saturation for three load levels i.e., 0.2, 0.5 and 0.8 (A cm⁻²) are presented in Fig. 3(a, b, and c). In all cases it can be seen that despite of zero water saturation values at the inlet and outlet, the catalyst layer is the most affected part having higher levels of water saturation as compared to GDL that can cause significant loss in efficiency of overall process by making reaction sites unavailable

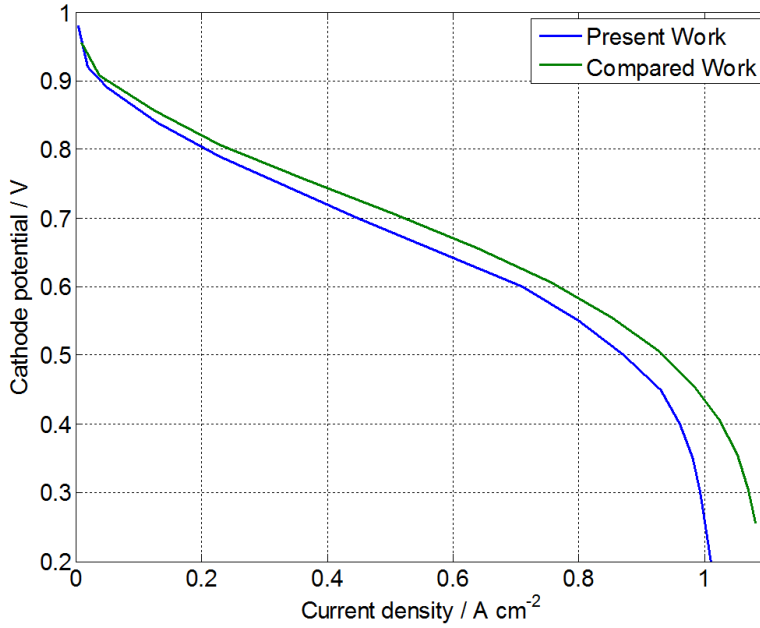


Fig. 4: Comparison of single and two-phase models for PEM fuel cells.

for the reactions. Also, it can be seen that by increasing the current density or load the saturation level also increases suggesting higher reaction rates and water production according to Eq. (2). Other sources that contribute to the overall generation of water are condensation of water vapors and the electro-osmotic drag that can move one to five water molecules from anode to cathode per ion transfer [96]. Although, operation at low loads inherently safe guards the cathode from water flooding but at such conditions a significant loss in protonic conductivity was also observed as compared to high load operation of PEM fuel cell.

To validate the model, the results of this case study were compared to those produced by Sun et al. [97] in which the agglomerate model for electro-chemical reactions was developed to study the influence of the structural parameters on the catalyst layer. As seen in Fig. 4 that both the predictions almost coincide at low current densities but as the current density is increased a gradual deviation is observed between the two cases where the model presented by Sun et al. over-predicts the current density. This deviation between the two cases can be attributed to the effects of water saturation because the model presented by Sun et al. was single phase only i.e., no liquid water was assumed to exist in the computational domain. So, it can be concluded that one of the effects of liquid water inside calculation domain is to limit the reaction kinetics by effectively covering the reaction sites and blocking the path of the reactant gaseous flow.

4.4 Two-phase model discrepancies

The list of two-phase models for PEM fuel cells can continue to an infinite number. Many authors, as reviewed before, have produced novel models and validated their results against previously established or experimental work. With increase in the computational power, the numerical modeling of the PEM fuel cells has outpaced experimental work. However, experimental work is still considered the ultimate test for all CFD models and for thorough validation it is necessary that a comparison check should be made between theoretical (CFD) and experimental findings. Keeping this in view, Mench [16] has recently compared the CFD work with high-resolution neutron and X-ray imaging results of liquid water distribution by Turhan et al. [98], Weber and Hickner [99] and Hartnig et al. [100] and found out that various assumptions and theories about liquid water distribution are actually quite misleading under normal operating conditions and development of new models was highly urged. The miss-match of experimental and theoretical findings can be attributed to the reasons discussed below (for detailed discussion the readers is referred to [16], this section only summarizes the latest findings in the same reference).

4.4.1 Large liquid water accumulation at CL/MPL interface

Two phenomena have been pointed out by Mench [16] that result in accumulation of liquid water in large quantities at the CL/MPL interface;

- i) Due to the surface roughness of mating catalyst layer and MPL, there is always a chance that large voids regions are left behind even at high commercial scale compactness.
- ii) Cracks found at the stated interface are highly probable. As reported by Mench [16], cracks of 20 μm wide may run through MPL and CL and constitute total of 8% of the surface areas.

In CFD modeling the above two anomalies are generally neglected and a perfect CL/MPL interface is assumed. Recent X-ray images [100] have shown a large quantity of water accumulation at the interface and sometimes they represent 5-20% of the total liquid water. Furthermore, the presence of large scale cracks alters the flow pattern of liquid water by providing large flows through these cracks.

4.5 Applicability of Leverett function for liquid water

Not all, but many two-phase models proposed for water management in PEM fuel cells utilize the Leverett function that gives dominance to capillary flow in the porous media, given as [101];

$$J(s) = \frac{P_c}{\sigma} \sqrt{\frac{K}{\varepsilon}} \quad (10)$$

where P_c , σ , ε and K represent the capillary pressure, interfacial tension between phases, porosity and the absolute permeability of the medium, respectively. However, the proposed Leverett function (also called J-function) was initially proposed for flow of water through soil, whereas, the porous media used for PEM fuel cell construction is highly compact and anisotropic in nature. Kumbur et al. [102] has shown that significant deviation in direct measurement of water quantity as compared to the proposed distribution by the Leverett function. So, it is very urgent that new and well descriptive governing equations are developed for water flow in PEM fuel cell porous media. Recently, Kumbur et al. has proposed new relationships for governing the capillary flow in PEM porous media [103–105], based on direct measurement by experimental techniques.

4.5.1 Bruggeman approximation

Usually the effect of saturation in the porous media is approximated by Bruggeman's relation that only restricts the flow of species in terms of reduced porosity, as;

$$D_{\text{eff}} = D_i \times [\varepsilon^\tau (1 - s)] \quad (11)$$

According to Eq. (11), the only effect by the presence of liquid water is to reduce diffusivity of the gaseous species by reducing the void volume in porous media. However, as noted by Mench [16], this relation ignores the effect of blocking of pathways for gaseous flow through porous media that can significantly affect the fuel cell performance.

4.5.2 Other discrepancies in two-phase models

Apart from the previously explained ignorance reigning the two-phase models, few more considerations need to be taken into account for vivid description and picture of saturation in PEM fuel cells, as outlined here;

- i) The inter-phase change between water humidified gaseous species and liquid water is usually modeled as [8, 23];

$$\dot{m} = \begin{cases} k_{\text{con}}(1 - s)X_{\text{H}_2\text{O}} \frac{P_{\text{H}_2\text{O}} - P_{\text{H}_2\text{O}}^{\text{sat}}}{RT_f} \\ k_{\text{evp}} \left(\frac{\rho_w}{M_{\text{H}_2\text{O}}} \right) (P_{\text{H}_2\text{O}} - P_{\text{H}_2\text{O}}^{\text{sat}}) \end{cases} \quad (12)$$

The evaporation/condensation process in PEM fuel cells is governed by the saturation pressure of the water vapor and the temperature. The validity of this process is still a question mark as it has not been experimentally verified and experimental works suggest that even fractional difference in temperature can have significant deviation from the simulated results by Eq. (12) [16].

- ii) Modeling of liquid water distribution, usually a porous jump condition is assumed at the interfaces of components because of the difference in porosity and radius of pores in two adjacent materials to account for the continuity. These assumptions

predict that GDL has more capacity to store liquid water as compared to MPL because of its higher porosity, but, experimental results show the other way, i.e., GDL represents low accumulation region for liquid water [16].

As discussed above, despite of active model developments for PEM fuel cells and understanding the water management issue, many inter-related phenomena still need to be accounted and a vigorous and robust approach is required that can encircle all the PEM fuel cell issues and produce efficient and stable results that can help in commercialization and help PEM fuel cells to compete with highly developed conventional counterparts that have taken centuries to grow and groom.

5 Meso-scale models for the cathode

The electrodes of a PEM fuel cell are volumetric and are composed of catalyst layer and GDL. One of the key components of PEM fuel cell is the catalyst layer where electro-chemical reactions take place. The catalyst layer is often made of porous mixture of carbon supported platinum particles (Pt|C), ion and electron conducting material (Nafion), and also provides the transport of reactant gaseous species to the reaction sites. Each electrode in PEM fuel cells is separated by an ion conducting electrolyte that is usually 20-100 μm thick [106]. The Pt|C particles have the typical dimensions of 100 nm and are thoroughly distributed in the catalyst layer. Furthermore, Pt|C particles are covered with the same ionic conducting material ($\sim 10^{-7}$ m thick [107]) as used in electrolyte preparation to insure three-phase contact. Additionally, for even distribution of the gaseous species and the electron conduction from/to the catalyst layer, a GDL is incorporated to a thickness of mm. On component and system scale, the dimensions are ranged between 10 and 100 cm and more [108]. In order to encompass all the length scales in PEM fuel cells, a multi-scale model needs to be developed that has much shorter range (beyond continuum approximation) than current CFD scales that are mostly based on Navier-Stokes. For categorization of the fluid flow regime, the most commonly tool used is the Knudsen number defined as;

$$k_n = \frac{\lambda}{l} \quad (13)$$

where λ is the mean free path of the molecules, and l represents the characteristic flow dimension. The selection of the characteristic dimension depends on the length scales of the gradients of pressure, density, velocity and temperature. The Knudsen number is useful for determining whether statistical mechanics or the continuum mechanics formulation of fluid dynamics should be valid: if the Knudsen number is near or greater than one, the mean free path of a molecule is comparable to or larger than the length scale of the problem, and the continuum assumption of fluid mechanics is no longer a good approximation. In recent years, for PEM fuel cell multi-scale modeling many authors have opted the Lattice Boltzmann (LB) method which is applicable over the whole range of Knudsen number, including the continuum regime. The LB method provides a better alternative to conventional CFD analysis of fluid flow for deeper insight.

5.1 Lattice Boltzmann method for fluid flows

In recent years, Lattice Boltzmann (LB) method has emerged as an alternative simulation tool for predicting fluid flows and has been found very successful for interfacial dynamics and complex boundaries. Lattice Boltzmann method is based on microscopic models and mesoscopic kinetic equations, unlike conventional numerical methods in which macroscopic equations are discretized over the spatial domain [109]. The underlying theory of the Lattice Boltzmann method is to develop simplified kinetic models capturing key features of micro- or mesoscopic physics so that the desired macroscopic equations are satisfied since macroscopic fluid flow is a collection of many microscopic particles in the system [109, 110]. Here, the LB method is briefly presented for basic knowhow, for detailed understanding one can refer to Succi [111] Chen and Doolen [109], Sukop and Throne [112], Park et al. [113], and Spaid and Phelan [114].

The Lattice Boltzmann method is a mesoscopic method that is considered in-between the continuum based technique and the molecular dynamics technique which handles individual particles in the flow field. In this method, a large group of molecules are assumed to move about a lattice and collide with each other. At each lattice point, the particles translate at discrete directions and all particles in one direction are grouped together. Generally LB method can be divided into two sequential steps as (i) streaming and (ii) collision. The streaming process describes the movement of a particles to adjacent lattice point in the direction of travel while keeping mass and momentum as conserved quantities. The intra collision of particles is defined by the collision step [115]. The general governing equation for the LB method is given as [109];

$$n_i(\mathbf{x} + \mathbf{e}_i \Delta x, t + \Delta t) = n_i(\mathbf{x}, t) + \omega_i(n(\mathbf{x}, t)) \quad i = 0, 1, \dots, M \quad (14)$$

The Eq. (14) is itself quite cumbersome to solve because of an infinite sets of particles moving along different directions and collisions occurring with respect to the scattering rule. A modification is generally enforced to limit only one particle moving in certain direction with a certain velocity. This simplification is termed as the exclusion principle and reduces tracking of particles to a finite and manageable number for a given time step [109]. For scattering step, which is non-linear in nature, Higuera and Jiménez [116] proposed to assume the distribution close to equilibrium state to avoid non-linearization. In Eq. (14), n_i is a real variable representing the mass per unit volume of the particle translating with a speed i , while, \mathbf{e}_i is the direction vector and M represents the total number of lattice points in consideration. For 2D geometries M ranges from 4 to 9, whereas, for 3D cases the total number of lattice points can be either 15, 17 or 19.

Since 1992, a considerable attention has been paid to use LB methods for different technologies. According to the data collected by Sukop and Throne [112], a variety of fields have adopted this technique with physics and mathematics being the main bearers. However, only a few papers with LB method and PEM fuel cells as title or keywords have been produced to date. Here a review of these is presented that are specifically focused

on PEM fuel cells.

Generally GDL is treated as homogeneous and isotropic porous material without considering the manufacturing details of the preparing material. Bundles of carbon fibers are used to prepare the carbon papers that are stacked together to form the GDL. Due to the structural alignment of carbon fibers there is strong dependency of physical properties to spatial directions, i.e., in-plane (parallel to surface) and through-plane (perpendicular to surface). As described in [115], GDL can be aptly assumed to consist of randomly arranged cylinders with diameter (7-12 μm) being very small as compared to their length. So, due to inherent alignment formed during making of carbon papers for PEM fuel cells there is a preferential fiber direction. Van Doormaal and Pharoah [115] have applied LB method to determine the porosity, permeability, flow direction and fiber directions to have a deeper insight of GDL. The geometry for this study was generated using the modified Monte Carlo technique by Himilton [117]. The alignment of fibers was varied from 0 to 90°, i.e., from parallel to perpendicular directions and numbers of cases were simulated for all directions with porosity ranging from 0.6 to 0.81. The proposed relation between porosity and the permeability of the GDL by the authors is given as;

$$k = \begin{cases} 0.26 \frac{\varepsilon^{3.6}}{1-\varepsilon} r^2 & \text{in-plane} \\ 0.28 \frac{\varepsilon^{4.3}}{1-\varepsilon} r^2 & \text{through-plane} \end{cases} \quad (15)$$

where r is the fiber radius and predictions were found to be within 95% of the prediction by Carmen-Kozeny equation [118].

Park and Li [113, 119] have also performed LB simulations for the inhomogeneous GDL of a PEM fuel cell with considering multi-phase flow via two different LB formulations. The simulation domain for this study was 400 μm^2 consisting of voids and solid obstacles represented by the fiber material. It was demonstrated that flow squeezed at narrow paths in-between the fibers causing pressure drop and increase in velocity. Additionally, it was noted that large flow blockages can be caused by even small obstacles due to their inherent orientation and fibers in parallel to the main flow directions had no significant effect on flow resistance implying that the permeability is not only a function of the porosity of the GDL material but it is greatly affected by the orientation of the fibers also. To include the effect of liquid water, the inter-particle interaction model was also used as LB methods are capable of providing robust predictions of the interfaces between two or more phases [119]. One of the findings by the authors was that some of the liquid water moving along the flow direction was captured in the porous media and it can be concluded that the captured water can cause either blocking of the porous path or covering of reaction sites if it is in the catalyst layer. Similarly it was also predicted that LB method is far superior to conventional CFD techniques to portray unsteady liquid water accumulation/removal process. Karimi and Li [120] carried out numerical calculations for a single pore of the membrane material to investigate the electro-osmotic flow through Poisson-Boltzmann and Navier-Stokes equations, and predicted that the pore dimensions have significant impact on the drag coefficient for water transport. Similar work was carried out on

microstructure of the membrane material by Okada et al. [121] to demonstrate the dependence of the ion mobility on the microstructure of the membrane material.

6 Microscopic models for the catalyst layers

It has been already stated in the previous sections that the physio-chemical features of the catalyst layer is one of the performance limiter in PEM fuel cells. The catalytic activity in PEM fuel cells is dependent on the catalyst particle size, shape, distribution, gaseous access to the reaction sites, ionic and electronic conductivity and thermal distribution. Catalyst material, processing and catalytic reactions are all inter-related disciplines and a good optimum design can only ensure high performance catalyst layer [122].

Liu [122] has developed top-down and bottom-up approaches in analysis of the catalyst materials. In top-down approach, a multiscale analysis approach is used to segregate the catalyst material into individual technology components signifying the interaction of each to the overall performance, while the bottom-up approach helps in developing and improving the catalyst design and stability. Although, with advances in modern science and technology, higher degree of understanding has been attained for the catalyst materials and performance, but still, it is treated as a black box in most of the modeling techniques. A need is felt here to study the catalyst layer at particle or pore-size levels.

6.1 Catalyst layer modeling at particle- and pore-size level

The catalyst layer in PEM fuel cells forms the backbone of the unit cells. Apart from the design considerations for other components, the optimization of the catalyst material and its distribution inside the layer is very essential for high performance and utilization. Recently it has been developed that manipulating the catalyst structures can significantly enhance its performance and for solid catalyst particles as in PEM fuel cells, the decrease in particle size helps in significant performance upgrade and increasing the catalyst size can cause a rapid decline in performance [122]. Since Pt is an expensive metal, the control of catalyst design is very eminent for commercial competition of PEM fuel cells with other available energy production devices.

Lee and Cho [123] determined, through chemical quantum calculations, that the arrangement of individual Pt particle can lead to the optimization of catalyst utility and performance. Configurations of 611 Pt atoms with size of 3.1 nm have been found to be the most suitable. However, in PEM fuel cells, not only the size and configuration are important but transport of ions, electrons and reactants to the catalytic sites is also very essential. In PEM fuel cells, coating of larger carbon particles with nano-sized Pt particles submerged in electrolyte material has been termed as one of the most effective catalytic distribution patterns for high utilization [39, 124]. The parameter used to describe the performance of the catalyst in PEM fuel cells is the effective surface area in PEM fuel cells [125]. Using finer particle size leads to an increased effective surface area per unit volume of the catalyst particle and increasing of the catalyst loading (mass per

unit surface area) also results in increased reaction rates [125].

Recently, Siddique and Liu [126] have digitally constructed a 3D model of the catalyst layer at nano-scale using controlled quasi-random algorithms numerically duplicating the experimental fabrication process aiming to quantify porous nanostructure and investigate the mechanism of nano-scale electro-chemical reactions and percolation networks. It was concluded that a threshold percolation exists for species transport through the catalyst structure and also altering the optimum value of the agglomerate number reduces the electro-chemical reactions. Similarly, Lange et al. [127] also performed 3D nano-scale simulations by reconstructing the catalyst layer using a stochastic approach. The focus in this work was to compute effective transport parameters over selected sets of operating conditions for variety of microstructures. Additionally, the effects of water vapor and temperature profiles have been studied in depth. For the validation of the computed results, a detailed comparison has also been performed by experimental results by the same group [128].

6.2 Agglomerate modeling approach

In open literature many mathematical models for the catalyst layer have been proposed from zero to three dimensional models. Among all, the flooded agglomerate model is the most descriptive and predicting model [129]. In this model, the carbon supported Pt particles in form of agglomerate are immersed in a thin film of electrolyte. The catalyst layer consists of a network of interconnected micro- and macro-sized pores through which the gaseous species reach the surface of the agglomerates. There upon, the reactant species diffuse through a thin layer of the electrolyte to reach the reaction site [130]. The agglomerate model has been able to give deeper insight into the physio-electro-chemical phenomena in simulations and modeling of the catalyst layer. However, the consideration of the catalyst layer to be composed of carbon supported Pt with flooded electrolyte film as a continuum medium has made it difficult to analyze the discrete distribution of the catalyst phase in the agglomerate [131].

Yan and Wu [130], Antonio et al. [132] and Bultel et al. [133] have developed various micro-models for the catalyst layers in which mass and ion transfer have been addressed separately by treating the agglomerate and the electrolyte material (Nafion) as discrete and segregated components. The proposed micro-models have been able to provide deeper insight into the detailed mass and ion transfer mechanisms at pore levels, and particle size relation and dependence in the overall performance for the electro-chemical reactions.

The relation between the generation of the current per unit volume as a function of electric and ionic potentials, reactant concentrations and the material properties of the catalyst layer is represented by a modified Butler-Volmer kinetics as [134–136];

$$\nabla \cdot \mathbf{i} = 4FC_{O_2}^{\text{bulk}} \left(\frac{\delta_{\text{film}}}{A_{\text{agg}} D_{O_2, \text{nafion}}} + \frac{1}{kE} \right)^{-1} \quad (16)$$

where δ , A_{agg} , $D_{\text{O}_2, \text{nafion}}$, k and E represent the thickness of Nafion covering the agglomerate, agglomerate area, diffusivity of oxygen through electrolyte, reaction rate and the effectiveness factor. Considering the first order reaction kinetics, the analytical expression for the effectiveness factor yielded by applying the mass conservation equation for spherical agglomerate is given as [136];

$$E = \frac{1}{3\phi^2} [3\phi \coth(3\phi) - 1] \quad (17)$$

where ϕ is the Theiles modulus for the system and is expresses by [8];

$$\phi = \zeta \sqrt{\frac{k}{D_{\text{O}_2, \text{nafion}}}} \quad (18)$$

in which, ζ is the characteristic length of the agglomerate in terms of volume per unit surface area, usually given as $R_{\text{agg}}/3$ for spherical structures as used in preparation of catalyst for PEM fuel cells [136].

7 Model verification

Since all numerical studies have been done theoretically by solving a combination of equations backed by empirical or experimental data with a set of assumptions to make it feasible with respect to both time and computational power at hand, it is very important to validate the results obtained. Most of the fuel cells models have been validated against the measured data using the polarization curve or V-I curve. But mere comparison with V-I curve does not ensure complete robustness and accuracy of the predicted results [16]. According to Mench [16], it is not surprising that a good agreement between the model and a simple polarization curve can be achieved but does not necessarily validate the internal distribution of parameters like heat, water, and charge, since underprediction of one parameter may be balanced by over-prediction of other and vice versa. Additionally, fuel cell system performance fluctuates with different electrode assemblies, however, the numerical simulations are not flexible enough to accommodate all details to represent the fluctuations in the performance [16]. Similarly, Pharoah et al. [43] has also reported anomalies in model comparison methods using the V-I curve for different cases while reviewing the material anisotropic effects on the fuel cell performance. It was noted that the V-I curve for both anisotropic and isotropic electronic conductivity were almost identical, however, the internal current distributions varied significantly for different load conditions. For the same load, the maximum current density occurred under the rib area of the fuel cell for the isotropic conditions but since the anisotropy of electrical conductivity makes the conduction much higher in in-plane direction, it was noticed that the maximum shifted to the channel center line in the latter case.

Since fuel cell predictions are dependent on a number of parameters, and most of which have not yet been properly characterized. Usually to match the predictions, one or

more parameters are tuned to obtain matched results via single V-I curve. But, proper validation of numerical models can only be achieved by a comparison with detailed and local experimental data and results, but lack of such data prohibits the proper validation. Since fuel cells are relatively infant in age comparatively, there is a tremendous need to develop methods and techniques for real-time data acquisition for validation of numerical models. However, it has been suggested by Pharoah et al. [43], in absence of real-time data, that different V-I curves under various operating conditions should be compared. Although this will not ensure complete validation of the models but operation under different set of conditions will posturize the general trend in the performance response of a fuel cell model.

8 Conclusions

PEM fuel cells represent a promising future for the energy production with low to zero greenhouse gas emissions. Although, many advancements have been made in the recent years in PEM technology both in terms of insight into internal phenomena and development, however, some major issues still need to be addressed before rendering PEM fuel cells for large scale commercialization. Among many, water management is an old time problem that has not been fully understood and characterized. Since PEM fuel cells operate under different load conditions, it is quite difficult to set a fixed parameter for the quantity of water as at higher load conditions removal is deemed necessary to avoid blocking of both reaction sites and pathways for gaseous flow, while in low operation levels less water quantity exhibits a decreased ionic conductivity of the electrolyte. So, it is very eminent that the water management issue has to be resolved in the near future to make PEM fuel cell competent with respect to other fuel cell types and conventional energy sources. With the advances in computational technologies in terms of both speed and efficiency, CFD has become an optimum tool to perform detailed study of PEM fuel cells in all aspects from understanding the internal phenomena to design optimization. A great deal of work has been done since then with a variety of models and results. Initially, most models were limited to 2D and single phase flows. But, with deeper interest in managing the water issue inside PEM, later models developed were extended to two-phase with both 2D and 3D geometries. But still a complete model has not been produced yet basically due to both computational limits and inherent complex phenomena occurring inside PEM fuel cells. The discrepancies in modeling water management issue still needs a deeper insight ranging from development of new formulations to include physical and chemical effects. A test case was also presented to study the effects of water saturation. It was observed that the catalyst layer was the most affected area as maximum water saturation effects were noted there with increasing trends with increase in operating current densities.

Although CFD analysis has provided an overall behavior of PEM fuel cells but complete validation of the results in terms of robustness and capability to predict the transport phenomena still needs to be verified against experimentally established results, as it has been often observed that although the predicted V-I curves have same profiles but internal distribution of parameters like current density, heat and water saturation may

vary significantly. Also, PEM fuel cells involve multi-scale parameters and phenomena, e.g., the electro-chemical reactions and the charge transport which are best evaluated at micro- or meso-scale levels, so, the multi-scale approach will further elaborate the secretive picture of the fuel cell operations. Recent developments in application of Lattice Boltzmann method to flow analysis provides the facility to simulate the flows at meso-scale, although, it is computationally expensive to apply to a complete single cell presently, but use of this method to PEM fuel cell technology is pacing up and some researchers have already proven its worth in evaluating physical properties such as permeability with direction dependent profiles when applied to selective and manageable dimensions. Further development in this field can be explored to reveal more insight to PEM fuel cells and establish robust and reliable results.

Acknowledgements

The financial support from the European Research Council (ERC 226238-MMFCs) is gratefully acknowledged.

Nomenclature

Roman Symbols

A_{agg}	Effective agglomerate surface area ($\text{m}^2 \text{ m}^{-3}$)
$C_{\text{O}_2}^{\text{bulk}}$	Local O_2 concentration (mol m^{-3})
D_b, D_i	Bulk diffusion of species i ($\text{m}^2 \text{ s}^{-1}$)
D_k	Knudsen diffusion ($\text{m}^2 \text{ s}^{-1}$)
F	Faraday's constant
h_v	Interstitial heat transfer coefficient ($\text{W m}^{-3} \text{ K}^{-1}$)
i	Current density (A cm^{-2})
K	Permeability (m^2)
k	Reaction rate constant (s^{-1})
k_{con}	Condensation rate constant (s^{-1})
k_{evp}	Evaporation rate constant (Pa s^{-1})
k_n	Knudsen number
l	Characteristic flow dimension (mm)
M_i	Molecular weight of species (kg mol^{-1})
P_c	Capillary pressure (Pa)
R	Universal gas constant ($\text{J mol}^{-1} \text{ K}^{-1}$)
r	Radius (m)
X	Species mass fraction
z	Number of electrons consumed per mole of reactant

Greek Symbols

δ_{film}	Thickness of electrolyte film covering an agglomerate (m)
ε	Porosity of material
ε_{agg}	Proportion of electrolyte in agglomerate
λ	Mean free path of molecules (m)

ϕ	Theile's modulus
ρ	Density (kg m^{-3})
σ	Surface tension (N m^{-1})

Subscripts & Superscripts

agg	Agglomerate
c	Catalyst layer
eff	Effective
f	Fluid phase
i	Species
Pt	Platinum
s	Solid phase
v	Void phase

References

- [1] Summes, N., 2006. *Fuel cell technology - reaching towards commercialization*. Springer, London.
- [2] Sundén, B., and Faghri, M., 2005. *Transport Phenomena in fuel cells*. Devel. Heat Transfer. WIT Press, Southampton.
- [3] Siegel, C., 2008. "Review of computational heat and mass transfer modeling on polymer-electrolyte-membrane (PEM) fuel cells". *J. Energy*, **33**, pp. 1331–52.
- [4] Cheddie, D., and Munroe, N., 2005. "Review and comparison of approaches to proton exchange membrane fuel cell modeling". *J. Power Sources*, **147**, pp. 72–84.
- [5] Natarajan, D., and van Nguyen, T., 2003. "Three-dimensional effects of liquid water flooding in the cathode of a PEM fuel cell". *J. Power Sources*, **115**(1), pp. 66–80.
- [6] Li, H., Tang, Y., Wang, Z., Shi, Z., Wu, S., Song, D., Zhang, J., Fatih, K., Wang, H., Liu, Z., Abouatallah, R., and Mazza, A., 2008. "A review of water flooding issues in the proton exchange membrane fuel cell". *J. Power Sources*, **178**(1), pp. 103–117.
- [7] Song, C., Tang, Y., Zhang, J. L., Zhang, J., Wang, H., Shen, J., McDermid, S., Li, J., and Kozak, P., 2007. "PEM fuel cell reaction kinetics in the temperature range of 23–120 °C". *Electrochimica Acta*, **52**(7), pp. 2552–2561.
- [8] Khan, M., 2009. *Numerical simulation of multi-scale transport processes and reactions in PEM fuel cells using two-phase models*. Licentiate Thesis, ISRN LUTMDN/TMHP-09/7066-SE, Lund University, Lund.
- [9] Ren, X., and Gottesfeld, S., 2001. "Electro-osmotic drag of water in poly(perfluorosulfonic acid) membranes". *J. Electrochem. Soc.*, **148**(1), pp. A87–A93.

-
- [10] Thomas A. Zawodzinski, J., Derouin, C., Radzinski, S., Sherman, R. J., Smith, V. T., Springer, T. E., and Gottesfeld, S., 1993. "Water uptake by and transport through nafionTM117 membranes". *J. Electrochem. Soc.*, **140**(4), pp. 1041–1047.
- [11] Wilkinson, D. P., Voss, H. H., and Prater, K., 1994. "Water management and stack design for solid polymer fuel cells". *J. Power Sources*, **49**(1-3), pp. 117–127.
- [12] Yi, J. S., Yang, J. D., and King, C., 2004. "Water management along the flow channels of PEM fuel cells". *AIChE Journal*, **50**(10), pp. 2594–2603.
- [13] Biyikoglu, A., 2005. "Review of proton exchange membrane fuel cell models". *Int. J. Hydrogen Energy*, **30**(11), pp. 1181–1212.
- [14] Wang, C. Y., 2004. "Fundamental models for fuel cell engineering". *Chem. Rev.*, **104**, pp. 4679–4726.
- [15] Haraldsson, K., and Wipke, K., 2004. "Evaluating PEM fuel cell system models". *J. Power Sources*, **126**, pp. 88–97.
- [16] Mench, M. M., 2010. *Advanced modeling in fuel cell systems: a review of modeling approaches*. Wiley-VCH Verlag GmbH & Co. KGaA, Weinheim, pp. 89–118.
- [17] Standaert, F., Hemmes, K., and Woudstra, N., 2004. "Analytical fuel cell modeling". *J. Power Sources*, **63**, pp. 1231–1242.
- [18] Wang, Q., Song, D., Navessin, T., Holdcroft, S., and Liu, Z., 2004. "A mathematical model and optimization of the cathode catalyst layer structure in PEM fuel cells". *Electrochimica Acta*, **50**(2-3), pp. 725–730.
- [19] Wishart, J., Dong, Z., and Secanell, M., 2006. "Optimization of a PEM fuel cell system based on empirical data and a generalized electrochemical semiempirical model". *J. Power Sources*, **161**(2), pp. 1041–1055.
- [20] Springer, T., Zawodzinski, T., and Gottesfeld, S., 1991. "Polymer electrolyte fuel cell model". *J. Electrochem Soc.*, **138**, pp. 2334–42.
- [21] He, W., Yi, J. S., and Nguyen, T. V., 2000. "Two-phase flow model of the cathode of PEM fuel cells using interdigitated flow fields". *AIChE Journal*, **46**(10), pp. 2053–64.
- [22] Hu, M., Gu, A., Wang, M., Zhu, X., and Yu, L., 2003. "Three dimensional, two phase flow mathematical model for PEM fuel cell: Part I. Model development". *Energy Conv. & Mang.*, **45**, pp. 1861–1882.
- [23] Hwang, J. J., 2007. "A complete two-phase model of a porous cathode of a PEM fuel cell". *J. Power Sources*, **164**(1), pp. 174–181.
- [24] Djilali, N., and Sui, P. C., 2008. "Transport phenomena in fuel cells: from microscale to macroscale". *Int. J. Computational Fluid Dynamics*, **22**(1), pp. 115–133.

- [25] Cheng, C. H., Malek, K., Sui, P. C., and Djilali, N., 2010. "Effect of pt nano particle size on the microstructure of PEM fuel cell catalyst layers: Insight from molecular dynamics simulation". *Electrochimica Acta*, **5**, pp. 1588–97.
- [26] Goddard, W., Merinov, B., van Duin, A., Jacob, T., Blanco, M., Molinero, V., Jang, S. S., and Jang, Y. H., 2006. "Multi-paradigm multi-scale simulations for fuel cell catalysts and membranes". *Mol. Simul.*, **32**, pp. 251–68.
- [27] Kanako, H., Takashi, T., and Katsuhide, O., 2005. "Molecular dynamics simulation for the behaviour of H_2 on the electrode catalyst of fuel cell". *Int. Symp. Adv. Fluid. Inf.*, **5**, pp. 55–58.
- [28] Malek, K., Eikerling, M., Wang, Q., Navessin, T., and Liu, Z., 2007. "Self-organization in the catalyst layers of polymer electrolyte fuel cells". *J. Phys. Chem. C*, **111**(36), pp. 13627–13634.
- [29] Meiler, M., Schmid, M., and Hofer, E. P., 2008. "Dynamic fuel cell stalk model for real-time simulation based on system identification". *J. Power Sources*, **176**(2), pp. 523–528.
- [30] Pathapati, P. R., Xue, X., and Tang, J., 2005. "A new dynamic model for predicting transient phenomena PEM fuel cell system". *Renewable Energy*, **30**(1), pp. 1–22.
- [31] Brown, T. M., Brouwer, J., Sameulsen, G. S., Holcomb, F. H., and King, J., 2008. "Dynamic first principles model of a complete reversible fuel cell system". *J. Power Sources*, **182**(1), pp. 240–253.
- [32] Hatti, M., and Tioursi, M., 2009. "Dynamic neural network controller model of PEM fuel cell system". *Int. J. Hydrogen Energy*, **34**(11), pp. 5015–5021.
- [33] Rouss, V., and Charon, W., 2008. "Multi-input and multi-output neural model of the mechanical behaviour of a PEM fuel cell system". *J. Power Sources*, **175**(1), pp. 1–17.
- [34] Zhang, Y. J., QOuyang, M. G., Lu, Q. C., Luo, J. X., and Li, X. H., 2004. "A model predicting performance of proton exchange membrane fuel cell stack thermal systems". *Appl. Thermal Eng.*, **24**(4), pp. 501–513.
- [35] Meiler, M., Andre, D., Schmid, M., and Hofer, E. P., 2009. "Nonlinear empirical model of gas humidity-related voltage dynamics of a polymer-electrolyte-membrane fuel cell stack". *J. Power Sources*, **190**(1), pp. 56–63.
- [36] Xue, X., Tang, J., Smirnova, A., England, R., and Sammes, N., 2004. "System level lumped-parameter dynamics modeling of PEM fuel cell". *J. Power Sources*, **133**(2), pp. 188–204.
- [37] Muller, E. A., and Stefanopoulou, A. G., 2006. "Analysis, modeling and validation for the thermal dynamics of a polymer electrolyte membrane fuel cell systems". *J. Fuel cell Sci. Tech.*, **3**(2), pp. 99–110.

-
- [38] Vasu, G., and Tangirala, A. K., 2008. "Control-orientated thermal model for proton exchange membrane fuel cell systems". *J. Power Sources*, **183**(1), pp. 98–108.
- [39] Larminie, J., and Dicks, A., 2003. *Fuel Cell Systems Explained*, 2nd ed. John Wiley & Sons Ltd., West Sussex.
- [40] Meng, H., 2006. "A simplified method for solving anisotropic transport phenomena in PEM fuel cells". *J. Power Sources*, **161**(1), pp. 466–469.
- [41] Pasaogullari, U., Mukherjee, P. P., Wang, C.-Y., and Chen, K. S., 2007. "Anisotropic heat and water transport in a pefc cathode gas diffusion layer". *J. Electrochem. Soc.*, **154**(8), pp. B823–B834.
- [42] Nam, J. H., and Kaviani, M., 2003. "Effective diffusivity and water saturation distribution in single- and two- layer PEMFC diffusion medium". *Int. J. Heat Mass Transfer*, **46**, pp. 4595–4611.
- [43] Pharoah, J. G., Karan, K., and Sun, W., 2006. "On effective transport coefficients in PEM fuel cell electrodes: Anisotropy of the porous transport layers". *J. Power Sources*, **161**(1), pp. 214–224.
- [44] Liu, F., and Wang, C.-Y., 2006. "Optimization of cathode catalyst layer for direct methanol fuel cells: Part ii: Computational modeling and design". *Electrochimica Acta*, **52**(3), pp. 1409–1416.
- [45] Senn, S., and Poulikakos, D., 2005. "Multiphase transport phenomena in the diffusion zone of a PEM fuel cell". *J. Heat Transfer*, **127**, pp. 1245–59.
- [46] Hwang, J., and P.Y., C., 2006. "Heat/mass transfer in porous electrodes of fuel cells". *Intl. J. Heat Mass Transfer*, **49**, pp. 2315–27.
- [47] Chao, C., and Hwang, A. J., 2006. "Predictions of phase temperatures in a porous cathode of polymer electrolyte fuel cells using a two-equation model". *J. Power Sources*, **160**, pp. 1122–30.
- [48] Hwang, A. J., Chao, C., Chang, C., Ho, W., and Wang, D., 2007. "Modeling of two-phase temperature in a two-layer porous cathode of polymer electrolyte fuel cells". *Intl. J. Hydrogen Energy*, **32**, pp. 405–14.
- [49] Ju, H., Meng, H., and Wang, C.-Y., 2005. "A single phase, non-isothermal model for PEM fuel cells". *Intl. J. Heat Mass Transfer*, **48**, pp. 1303–15.
- [50] Johnson, M., and Stewart, W., 1965. "Pore structure and gaseous diffusion in solid catalysts". *J. Catalysis*, **4**, pp. 248–252.
- [51] Malek, K., and Coppens, M.-O., 2003. "Knudsen self- and fickian diffusion in rough nanoporous media". *J. Chemical Physics*, **119**(5), pp. 2801–2811.
- [52] Yuan, J., Lv, X., Sundén, B., and Yue, D., 2007. "Analysis of parameter effects on the transport phenomena in conjunction with chemical reactions in ducts relevant for methane reformers". *Intl. J. Hydrogen Energy*, **32**, pp. 3887–98.

- [53] Mu, D., Liu, Z.-S., Huang, C., and Djilali, N., 2008. "Determination of the effective diffusion coefficient in porous media including knudsen effects". *Microfluidics and Nanofluidics*, **4**(3), pp. 257–260.
- [54] ANSYS[®] Fluent[®] software, <http://www.fluent.com>.
- [55] COMSOL Multiphysics[®], <http://www.comsol.com>.
- [56] STAR-CD[®], <http://www.cd-adapco.com/products/star-cd/index.html>.
- [57] CFD-ACE+[®], <http://www.esi-group.com>.
- [58] Choi, K., Peck, D., Kim, C., Shin, T., and Lee, T., 2000. "Water transport in polymer membranes for PEMFC". *J. Power Sources*, **86**, pp. 197–201.
- [59] Yang, X. G., Zhang, F. Y., Lubawy, A. L., and Wang, C. Y., 2004. "Visualization of liquid water transport in a pefc". *Electrochem. and Solid-State Ltrs.*, **7**(11), pp. A408–A411.
- [60] Zhang, F. Y., Yang, X. G., and Wang, C. Y., 2006. "Liquid water removal from a polymer electrolyte fuel cell". *J. Electrochem. Soc.*, **153**(2), pp. A225–A232.
- [61] Pasaogullari, U., and Wang, C. Y., 2004. "Liquid water transport in gas diffusion layer of polymer electrolyte fuel cells". *J. Electrochem. Soc.*, **151**(3), pp. A399–A406.
- [62] Wang, Z., Wang, C., and Chen, K., 2001. "Two-phase flow and transport in the air cathode of proton exchange membrane fuel cells". *J. Power Sources*, **94**, pp. 40–50.
- [63] Borup, R., Meyers, J., Pivovar, B., Kim, Y. S., Mukundan, R., Garland, N., Myers, D., Wilson, M., Garzon, F., Wood, D., Zelenay, P., More, K., Stroh, K., Zawodzinski, T., Boncella, J., McGrath, J. E., Inaba, M., Miyatake, K., Hori, M., Ota, K., Ogumi, Z., Miyata, S., Nishikata, A., Siroma, Z., Uchimoto, Y., Yasuda, K., Kimijima, K.-i., and Iwashita, N., 2007. "Scientific aspects of polymer electrolyte fuel cell durability and degradation". *Chem. Rev.*, **107**(10), pp. 3904–3951.
- [64] He, G., Yamazaki, Y., and Abudula, A., 2009. "A droplet size dependent multiphase mixture model for two phase flow in PEMFCs". *J. Power Sources*, **194**(1), pp. 190–198.
- [65] Yuan, J., and Sundén, B., 2004. "Two-phase flow analysis in a cathode duct of PEFCs". *Electrochimica Acta*, **50**, pp. 677–83.
- [66] Wang, Y., Basu, S., and Wang, C. Y., 2008. "Modeling two-phase flow in PEM fuel cell channels". *J. Power Sources*, **179**, pp. 603–617.
- [67] Le, A. D., and Zhou, B., 2008. "A general model of proton exchange membrane fuel cell". *J. Power Sources*, **182**(1), pp. 197–222.
- [68] Leverett, M. C., 1941. "Capillary behaviour in porous solids". *Pet. Trans., AIME(Am. Inst. Min. Metall. Eng.)*, **142**, pp. 152–169.

-
- [69] You, L., and Liu, H., 2002. "A two phase flow and transport model for cathode of PEM fuel cells". *Int. J. Heat Mass Transfer*, **45**, pp. 2277–87.
- [70] You, L., and Liu, H., 2006. "A two-phase flow and transport model for PEM fuel cells". *J. Power Sources*, **155**(2), pp. 219–230.
- [71] Wang, C. Y., and Cheng, P., 1996. "A multiphase mixture model for multiphase, multicomponent transport in capillary porous media - I. Model development". *Int. J. Heat Mass Transfer*, **39**(17), pp. 3607–3618.
- [72] Abriola, L. M., and Pinder, G. F., 1985. "A multiphase approach to the modeling of porous media contaminations by organic compounds, i. equation development II. Numerical simulation". *Water Resour. Res.*, **21**, pp. 11–26.
- [73] Siegel, N., Ellis, M., Nelson, D., and Spakovsky, M. v., 2004. "A two-dimensional computational model of a PEMFC with liquid water transport". *J. Power Sources*, **128**, pp. 173–184.
- [74] Yu, L. J., Ren, G. P., Qin, M. J., and Jiang, X. M., 2009. "Transport mechanisms and performance simulations of a PEM fuel cell with interdigitated flow field". *Renewable Energy*, **34**(3), pp. 530–543.
- [75] Coppo, M., Siegel, N., and von Spakovsky, M., 2006. "On the influence of temperature on PEM fuel cell operation". *J. Power Sources*, **159**, pp. 560–569.
- [76] You, L., and Liu, H. T., 2001. "A parametric study of the cathode catalyst layer of PEM fuel cells using pseudo-homogeneous model". *Int. J. Hydrogen Energy*, **25**, pp. 991–999.
- [77] Acosta, M., Merten, C., Eigenberger, G., Class, H., Helmig, R., Thoben, B., and MÄijller-Steinhagen, H., 2006. "Modeling non-isothermal two-phase multicomponent flow in the cathode of PEM fuel cells". *J. Power Sources*, **159**(2), pp. 1123–1141.
- [78] Helmig, R., 1997. *Multiphase flow and transport processes in the subsurface - a contribution to the modeling of hydrosystems*. Springer Verlag.
- [79] Class, H., Helmig, R., and Bastian, P., 2002. "Numerical simulations of non-isothermal multiphase multicomponent processes in porous media. 1. an efficient solution technique". *Adv. Water Resour.*, **25**, pp. 533–550.
- [80] Meng, H., 2009. "Multi-component liquid water transport in the cathode of a PEM fuel cell with consideration of the micro-porous layer (mpl)". *Int. J. Hydrogen Energy*, **34**, pp. 5488–5497.
- [81] Nam, J. H., and Kaviani, M., 2003. "Effective diffusivity and water saturation distribution in single- and two- layer PEMFC diffusion medium". *Int. J. Heat Mass Transfer*, **46**, pp. 4595–4611.
- [82] Hickner, M., Siegel, N., Chen, K., Hussey, D., Jacobson, D., and Arif, M., 2008. "In situ high-resolution neutron radiography of cross-sectional liquid water profiles in proton exchange membrane fuel cells". *J. Electrochem Soc.*, **155**(B427–434).

-
- [83] Zhou, B., Huang, W., Zong, Y., and Sobiesiak, A., 2006. "Water and pressure effects on a single PEM fuel cell". *J. Power Sources*, **155**(2), pp. 190–202.
- [84] Berning, T., Lu, D., and Djilali, N., 2002. "Three-dimensional computational analysis of transport phenomena in PEM fuel cells". *J. Power Sources*, **106**, pp. 284–294.
- [85] Berning, T., and Djilali, N., 2003. "A 3d, multiphase, multicomponent model of the cathode and anode of a PEM fuel cell". *J. Electrochem Soc.*, **150**(12), pp. A1589–98.
- [86] Berning, T., and Djilali, N., 2003. "Three-dimensional computational analysis of transport phenomena in a PEM fuel cell - a parametric study". *J. Power Sources*, **124**, pp. 440–452.
- [87] Hu, M., Zhu, X., Wang, M., Gu, A., and Yu, L., 2004. "Three dimensional, two phase flow mathematical model for PEM fuel cell: Part II. analysis and discussion of the internal transport mechanisms". *Energy Conv. & Mang.*, **45**(11-12), pp. 1883–1916.
- [88] Kandlikar, S., 2008. "Microscale and macroscale aspects of water management challenges in PEM fuel cells". *Heat Transfer Engineering*, **29**, pp. 575–587.
- [89] Yan, Q., Toghiani, H., and Wu, J., 2006. "Investigation of water transport through membranes in a PEM fuel cell by water balance experiments". *J. Power Sources*, **158**, pp. 316–325.
- [90] Ge, S., Li, X., Yi, B., and Hsing, I.-M., 2005. "Absorption, desorption, and transport of water on polymer electrolyte membranes for fuel cells". *J. Electrochem Soc.*, **6**, pp. A1149–A1157.
- [91] Yamada, H., Hatanaka, T., Murata, H., and Morimoto, Y., 2006. "Measurement of flooding in gas diffusion layers of polymer electrolyte fuel cells with conventional flow fields". *J. Electrochem. Soc.*, **159**, pp. A1748–1754.
- [92] Benziger, J., Nehlsen, J., Blackwell, D., Brennan, T., and Itescu, J., 2005. "Water flow in gas diffusion layers of PEM fuel cells". *J. Membrane Science*, **261**, pp. 98–108.
- [93] Lin, G., and Nguyen, T., 2005. "Effect of thickness and hydrophobic polymer content of the gas diffusion layer on electrode flooding level in a PEMFC". *J. Electrochem. Soc.*, **152**, pp. A1942–A1948.
- [94] Litster, S., Sinton, D., and Djilali, N., 2006. "Ex situ visualization of liquid water transport in PEM fuel cell gas diffusion layers". *J. Power Sources*, **154**, pp. 95–105.
- [95] Kumbur, E. C., Sharp, K. V., and Mench, M. M., 2006. "Liquid droplet behavior and instability on a polymer electrolyte fuel cell flow channel". *J. Power Sources*, **161**, pp. 333–345.

- [96] Thomas A. Zawodzinski, J., Derouin, C., Radzinski, S., Sherman, R. J., Smith, V. T., Springer, T. E., and Gottesfeld, S., 1993. "Water uptake by and transport through nafion[®] 117 membranes". *J. Electrochem. Soc.*, **140**(4), pp. 1041–1047.
- [97] Sun, W., Peppley, B. A., and Karan, K., 2005. "An improved two-dimensional agglomerate cathode model to study the influence of catalyst layer structural parameters". *Electrochimica Acta*, **50**(16-17), pp. 3359–3374.
- [98] Turhan, A., Kim, S., Hatzell, M., and Mench, M. M., 2010. "Impact of channel wall hydrophobicity on through-plane water distribution and flooding behavior in a polymer electrolyte fuel cell". *Electrochimica Acta*, **55**(8), pp. 2734–2745.
- [99] Weber, A. Z., and Hickner, M. A., 2008. "Modeling and high-resolution-imaging studies of water-content profiles in a polymer-electrolyte-fuel-cell membrane-electrode assembly". *Electrochimica Acta*, **53**(26), pp. 7668–7674.
- [100] Hartnig, C., Manke, I., Kuhn, R., Kardjilov, N., Banhart, J., and Lehnert, W., 2008. "Cross-sectional insight in the water evolution and transport in polymer electrolyte fuel cells". *Appl. Phys. Letters*, **92**(13), p. 134106.
- [101] <http://jgmaas.com/scores/facts.html>.
- [102] Kumbur, E. C., Sharp, K. V., and Mench, M. M., 2007. "On the effectiveness of leverett approach for describing the water transport in fuel cell diffusion media". *J. Power Sources*, **168**(2), pp. 356–368.
- [103] Kumbur, E. C., Sharp, K. V., and Mench, M. M., 2007. "A validated leverett approach to multi-phase flow in polymer electrolyte fuel cell diffusion media. Part 1. Hydrophobicity effect". *J. Electrochem Soc*, **154**, pp. B1295–B1304.
- [104] Kumbur, E. C., Sharp, K. V., and Mench, M. M., 2007. "A validated leverett approach to multi-phase flow in polymer electrolyte fuel cell diffusion media. Part 2. Compression effect and capillary transport". *J. Electrochem Soc*, **154**, pp. B1305–B1314.
- [105] Kumbur, E. C., Sharp, K. V., and Mench, M. M., 2007. "A validated leverett approach to multi-phase flow in polymer electrolyte fuel cell diffusion media. Part 3. Temperature effect and unified approach". *J. Electrochem Soc*, **154**, pp. B1315–B1324.
- [106] Franco, A. A., Schott, P., Jallut, C., and Maschke, B., 2007. "A multi-scale dynamic mechanistic model for the transient analysis of PEFCs". *Fuel Cells*, **7**(2), pp. 99–117.
- [107] Inaba, M., Uno, M., Maruyama, J., Tasaka, A., Katakura, K., and Ogumi, Z., 1996. "Hydrogen oxidation on partially immersed nafion[®]-coated electrodes". *J. Electroanalytical Chem.*, **417**(1-2), pp. 105–111.

- [108] Andersson, M., Yuan, J., and Sundén, B., 2010. “Review on modeling development for multiscale chemical reactions coupled transport phenomena in solid oxide fuel cells”. *Applied Energy*, **87**(5), pp. 1461–1476.
- [109] Chen, S., and Doolen, G. D., 1998. “Lattice boltzmann method for fluid flows”. *A. R. Fluid Mechanics*, **30**(1), pp. 329–364.
- [110] Kadanoff, L. P., 1986. “Fractals: Where’s the physics?”. *Physics Today*, **39**(2), p. 6.
- [111] Succi, S., 2001. *The Lattice Boltzmann Equation for Fluid Dynamics and Beyond (Numerical Mathematics and Scientific Computation)*. Oxford University Press, USA.
- [112] Sukop, M., and Throne Jr, D., 2007. *Lattice boltzmann modeling: An introduction for geoscientists and engineers*. Springer-Verlag Berlin Heidelberg.
- [113] Park, J., Matsubara, M., and Li, X., 2007. “Application of lattice boltzmann method to a micro-scale flow simulation in the porous electrode of a PEM fuel cell”. *J. Power Sources*, **173**(1), pp. 404–414.
- [114] Spaid, M. A. A., and Phelan Jr, F. R., 1997. “Lattice boltzmann methods for modeling microscale flow in fibrous porous media”. *Physics of Fluids*, **9**(9), p. 2468.
- [115] Van Doormaal, M. A., and Pharoah, J. G., 2009. “Determination of permeability in fibrous porous media using the lattice boltzmann method with application to pem fuel cells”. *Int. J. Numerical Methods in Fluids*, **59**(1), pp. 75–89.
- [116] Higuera, F., and JimÁñez, J., 1982. “Boltzmann approach to lattice gas simulations”. *Europhys. Lett.*, **9**, pp. 663–668.
- [117] Hamilton, D., 2005. “A numerical method to determine effective transport coefficients in porous media with application to PEM fuel cells”. PhD thesis.
- [118] Valdes-Parada, F. J., Ochoa-Tapia, J. A., and Alvarez-Ramirez, J., 2009. “Validity of the permeability Carman-Kozeny equation: A volume averaging approach”. *Physica A: Statistical Mechanics and its Applications*, **388**(6), pp. 789–798.
- [119] Park, J., and Li, X., 2008. “Multi-phase micro-scale flow simulation in the electrodes of a PEM fuel cell by lattice boltzmann method”. *J. Power Sources*, **178**, pp. 248–257.
- [120] Karimi, G., and Li, X., 2005. “Electro-osmotic flow through polymer electrolyte membranes in PEM fuel cells”. *J. Power Sources*, **140**, pp. 1–11.
- [121] Okada, T., Xie, G., Gorseth, O., Kjelstrup, S., Nikamura, N., and Arimura, T., 1998. “Ion and water transport of nafion membranes as electrolytes”. *Electrochem Acta*, **43**, pp. 3741–4747.
- [122] Liu, W., 2005. “Catalyst technology development from macro-, micro- down to nano-scale”. *China Particuology*, **3**(6), pp. 383–394.

-
- [123] Lee, B., and Cho, K. Hierarchical multiscale study of metal nanoparticles, 2003., Oct 12-15.
- [124] Basu, S., 2007. *Recent trends in fuel cell science and technology*. Asamaya Publishers, New Delhi.
- [125] Gasteiger, H. A., Panels, J. E., and Yan, S. G., 2004. "Dependence of PEM fuel cell performance on catalyst loading". *J. Power Sources*, **127**(1-2), pp. 162–171.
- [126] Siddique, N. A., and Liu, F., 2010. "Process based reconstruction and simulation of a three-dimensional fuel cell catalyst layer". *Electrochimica Acta*, **55**(19), pp. 5357–5366.
- [127] Lange, K. J., Sui, P.-C., and Djilali, N., 2011. "Pore scale modeling of a proton exchange membrane fuel cell catalyst layer: Effects of water vapor and temperature". *Journal of Power Sources*, **196**(6), pp. 3195–3203.
- [128] Lange, K. J., Sui, P.-C., and Djilali, N., 2010. "Pore scale simulation of transport and electrochemical reactions in reconstructed PEMFC catalyst layers". *J. Electrochem. Soc.*, **157**(10), pp. B1434–B1442.
- [129] Harvey, D., Pharoah, J. G., and Karan, K., 2008. "A comparison of different approaches to modelling the PEMFC catalyst layer". *J. Power Sources*, **179**(1), pp. 209–219.
- [130] Yan, Q., and Wu, J., 2008. "Modeling of single catalyst particle in cathode of PEM fuel cells". *Energy Conv. & Mang*, **49**(8), pp. 2425–2433.
- [131] Um, S., and Wang, C. Y., 2004. "Three-dimensional analysis of transport and electrochemical reactions in polymer electrolyte fuel cells". *J. Power Sources*, **125**(1), pp. 40–51.
- [132] Antonio, O., Bultel, Y., Durand, R., and Ozil, P., 1998. "Catalyst gradient for cathode active layer of proton exchange membrane fuel cell". *Electrochim Acta*, **43**(24), p. 3681.
- [133] Bultel, Y., Ozil, P., and Durand, R., 1998. "Modelling of mass transfer within the PEM fuel cell active layer: Limitations at the particle level". *J. Appl. Electrochem*, **28**, p. 269.
- [134] Bernardi, D., and Verbrugge, M., 1990. "Water-balance calculations for solid-polymer-electrolyte fuel cells". *J. Electrochem Soc*, **137**(11), pp. 3344–3350.
- [135] Bernardi, D. M., and Verbrugge, M. W., 1991. "Mathematical model of a gas diffusion electrode bonded to a polymer electrolyte". *AIChE Journal*, **37**(8), pp. 1151–1163.
- [136] Spiegel, C., 2008. *PEM Fuel Cell Modeling and Simulation Using Matlab*. Academic Press.

Paper B

Khan, M.A., Sundén, B., and Yuan, J., 2011. “Water saturation modeling in polymer electrolyte membrane (PEM) fuel cells using a validated approach”, In *International Green Energy Conference*, 2-9 June, Eskişehir, Turkey (*Invited and recommended to International Journal of Energy Research*).

© 2011 IGEC-VI.
The layout has been revised

Water Saturation Modeling in Polymer Electrolyte Membrane (PEM) Fuel Cells using a Validated Approach

Munir Ahmed Khan, Bengt Sundén, Jinliang Yuan

Abstract

In this work, a 3D model of a PEM fuel cell has been developed for water saturation and its effects using a validated approach considering the internal movement of water across the membrane. For different operating levels, it was found that at lower current densities, the maximum saturation occurs faraway region from the air inlet because of the decrease in ability of air to evaporate the liquid water, while at higher current densities, a shift in the maximum value is noticed towards the inlet region due to increase in electro-chemical reaction rate and the electro-osmotic drag. Apart from water saturation shift at different load conditions, it is also observed that the liquid water tends to accumulate at the interface of the inlet channel and the porous media. Considering the movement of water across the membrane, a linear profile for back diffusion was observed with increasing current density because of higher water content at the cathode. For the electro-osmotic drag, the increase is observed to follow the rate of increase of the electro-chemical reactions and becomes approximately constant at higher current density due to the concentration losses where the electro-chemical reaction rate is limited due to the physical characteristics of the agglomerates. Although the rise trend of the back diffusion and electro-osmotic drag followed a dissimilar pattern, the net transport was calculated to be towards the anode side suggesting that the water content at the cathode side increases with increasing current density, hence causing more problems for the PEM fuel cells in terms of water management.

Key words: *PEM, water saturation, validated approach, back diffusion, electro-osmotic drag.*

1 Introduction

Polymer electrolyte membrane (PEM) fuel cells have become increasingly studied and diagnosed as a prospective low-emission power source. One of the potential domains of PEM fuel cells application is the mobile usage due to its suitable operating conditions, cost effectiveness, high current density and compactness [1–3]. However, considering technological advancement in the field of internal-combustion (IC) engines and batteries, PEM fuel cells still have to overcome a number of technical hurdles to level out the scores with its competitors [4].

Among many, water management is one of the key limiter in fuel cell efficiency and stability [5]. The term ‘water management’ evolves from the reason that both the production of water resulting from oxygen reduction (OR) reaction at the cathode, as given in Eq. (1), and the internal movement of water have to be properly maintained at an appropriate

quantity for two reasons. Firstly, to achieve proper hydration level and secondly, to remove the excess water. Adding to the complexity of the PEM fuel cells, both the above stated processes are against each other and are very important to control to provide optimum conditions for PEM fuel cell operation [6, 7].



Apart from generation of water due to electro-chemical reactions, the intra movement of water in PEM fuel cells between the two electrodes also reduces the margin of error for correct maintenance of the hydration level. This internal movement can be attributed to two processes, i.e.,

- Concentration diffusion or back diffusion (BD), and,
- Electro-osmotic drag (EOD)

Because the thickness of the electrolyte incorporated in PEM fuel cells is quite small, water generated on the cathode side diffuses towards the anode side due to the difference in concentration of the water content. Also, during the PEM operation, water from the anode is dragged to the cathode side for transfer of H^+ ions [8, 9]. Thus, a balance is required to maintain the water movement such that both sides remain well hydrated all the times. Excess water at the cathode side, on the other hand, causes the decline in performance and elevates the degrading mechanism such as ionomer loss, hydrophobicity loss and poisoning of the ionomer [10, 11]. Many authors are of the opinion that the main dictating factor affecting the water saturation levels is the transport mechanism of liquid water which thus controls the PEM fuel cell performance [6, 7]. In short, improper water management results in performance loss, instability, inefficiency and material degradation of the PEM fuel cell [12].

In order to render PEM fuel cells viable for full scale commercialization, the water management issue has to be addressed and a proper remedy is yet to be prescribed for this problem [4]. The minimum hydration level maintenance is comparatively easy to achieve and can be accomplished by the external humidification of air and fuel supply to the PEM fuel cells and many authors have shown that external humidification of the inlet species improves the cell performance [13, 14]. However, the transport mechanism of the liquid water in the diffusion media is still under rigorous work, and knowing the fact that it is the major set back for PEM fuel cells, this field has not been fully overcome in terms of understanding the process and the effect of materials on the transport mechanism of liquid water [15].

With the advances in the computing technology, computational fluid dynamics (CFD) modeling has become one of the most effective tools to study the internal anatomy of PEM fuel cells [1]. To date, a number of models with varying complexity have been formulated and implemented by various researchers for the water management issue in PEM fuel cells with main focus on water saturation and the transport mechanism in the diffusion media especially at the cathode side [16–18]. However, recent analytical techniques used

to capture the liquid water distribution inside the diffusion media have revealed that many of the theories and assumptions used for liquid water transport mechanism are inappropriate under normal operating conditions [19, 20]. One of the reasons for this experimental and modeling deviation is that most of the models utilize the traditional Leverett J-function [7, 21–23] for the liquid water saturation and its transport in the porous media. However, material used for manufacturing of the catalyst and porous transport layer are heterogeneous in nature with mixed wettability characteristics [15] and the Leverett J-function is not sufficient to model the transport mechanism in the porous media of PEM fuel cells. Furthermore, the effects of material hydrophobicity, compression and the temperature are also not encapsulated by the traditional relation [15, 24, 25].

The main force responsible for the transport of liquid water inside a porous media is the capillary pressure which arises due to difference in pressure across the interface between the mating fluids. For conventional Leverett J-function, the capillary pressure for the porous media is presented in the following non-dimensional form;

$$P_c = \gamma \sqrt{\frac{\varepsilon}{k}} J(s) \quad (2)$$

$$J(s) = \begin{cases} 1.417s_w - 2.120s_w^2 + 1.263s_w^3 & \text{if } \theta < 90^\circ \\ 1.417s_{nw} - 2.120s_{nw}^2 + 1.263s_{nw}^3 & \text{if } \theta > 90^\circ \end{cases} \quad (3)$$

where P_c , γ , ε , k and s represent the capillary pressure, surface tension, porosity of the media, permeability and the liquid saturation, respectively. The contact angle is the contact angle represents the degree of wettability of the porous media in such a way that the media is considered hydrophilic if or otherwise it is labelled as hydrophobic in nature. However, in this work, a validated Leverett-type empirical function is used to simulate the capillary pressure of the liquid water inside the diffusion media. This function is capable of accurately predicting the experimentally calculated capillary pressure for selected types of diffusion media. One of the key advantages of using the validated Leverett approach is that it accurately represents the relation between the liquid saturation and the material properties and also it utilizes the actual PTFE (poly-tetrafluoroethylene) content of the diffusion media thus eliminating the need to evaluate the contact angle θ [15].

2 Model Development

2.1 Modeling Domain and Assumptions

The considered domain for this work consists of a section of a single PEM fuel cell with interdigitated flow field design as shown in Fig. 1. The flow configuration is set to counter flow which means that the fuel and air flow in opposite directions with coinciding inlets of fuel and air with the outlets of air and fuel, respectively. For convenience, the air and

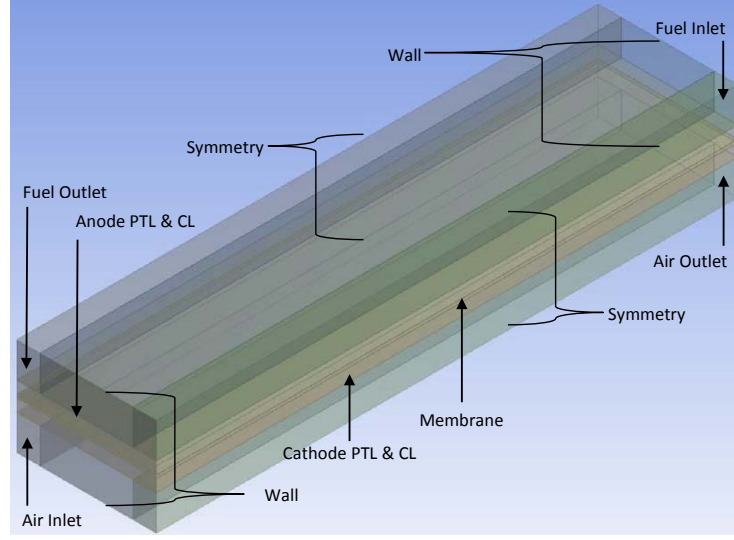


Fig. 1: *The modeling domain of a PEM fuel cell section.*

fuel inlet channels are termed as the high pressure channels and the other one is called the low pressure channel which is maintained at the atmospheric conditions. Since, in interdigitated flow field design, the high pressure and low pressure channels on either sides are separated by a solid region called the anode or cathode current collectors, the reactant species are diverted through the porous media i.e., porous transport layer (PTL) and the catalyst layer (CL). Additionally, the electric poles of the fuel cell are electrically insulated using the polymer electrolyte membrane, which on the other hand, conducts ions in order to complete the electro-chemical reactions.

The present model simulates the steady state conditions and the gaseous species behavior is assumed to be ideal and laminar. The model used for the electro-chemical reactions has been adopted from the improved agglomerate model [26] for spherical agglomerates with few necessary alterations to fit the 3D case [27]. Since, the PEM fuel cells operate between the ranges of 70 to 80 °C, the water produced as result of the OR reactions is assumed to be in the liquid state. Inside the porous media, the flow of liquid water is governed by the capillary action independent of the gaseous flow while inside the gas channel it flow with the same velocity as the gases and is assumed to be in the form of fine mist. Furthermore, the electrical connectivity of different zones at the interfaces is also assumed to be perfect, i.e., there are no leakage currents and interface losses.

2.2 Governing Equations

In this section, the governing equations for liquid water transport, membrane phase potential, back diffusion and the electro-osmotic drag are presented because of their water content dependence. The complete set of equations to simulate a single PEM fuel cell can be found in other references, e.g., He et al. [28], Hwang [29] and Khan [17].

Membrane Phase Potential

The primary driving mechanism in PEM fuel cells is the electro-chemical reactions where hydrogen is split into electrons and protons at the anodic pole. These combine together exothermically in the presence of oxygen at the cathode to produce water. The electrons generated at the anode follow an external circuit through the load while protons are directly transferred via the electrolyte (membrane) towards the cathode. The motivating force for the proton immigration is the protonic phase potential (also called membrane phase potential) given by;

$$\nabla \cdot (\sigma_{\text{mem}} \nabla \phi_{\text{mem}}) + R = 0 \quad (4)$$

where ϕ_{mem} is the membrane phase potential, and σ_{mem} is the membrane phase conductivity calculated as [30];

$$\sigma_{\text{mem}} = \varepsilon (0.514\lambda - 0.326) \exp\left(1268 \left(\frac{1}{303} - \frac{1}{T}\right)\right) \quad (5)$$

In Eq. (4), R is the transfer current or the electro-chemical source term, given as;

$$R = \pm 4F \frac{P_X}{H} \left(\frac{1}{E_r k(1 - \varepsilon)} + \frac{(r_{\text{agg}} + \delta)\delta}{a_{\text{agg}} r_{\text{agg}} D_{X-\text{naf}}} \right)^{-1} \quad (6)$$

Since, the protons are generated and consumed at the anode and cathode, respectively, the source term is used for each catalyst layer with appropriate sign convention to model the reaction and is the partial pressure of the reactant species, i.e., hydrogen at the anode and oxygen at the cathode. For detailed discussion regarding Eqs (4) to (6), the reader is referred to the work presented by Sun et al. [26, 31].

Osmotic Drag Coefficient and Back Diffusion

The effect of water drag due to the proton migration from the anode to the cathode via the PEM fuel cell electrolyte is incorporated using the osmotic drag coefficient, given as [28];

$$n_d = 2.5 \frac{\lambda}{22} \quad (7)$$

where λ is the water content and depends on the water activity based on liquid saturation and the ratio of water vapor partial pressure and the saturation pressure. The transport of water from the cathode to the anode due to the difference in concentration on the respective sides is evaluated as [28];

$$j_w = -\frac{\rho_{\text{mem}}}{M_{\text{mem}}} M_{\text{H}_2\text{O}} D_1 \nabla \lambda \quad (8)$$

where ρ_{mem} and M_{mem} are the density and the equivalent weight of the dry membrane, respectively, and D_1 is the diffusivity of water inside the electrolyte.

Liquid Water Formation and Transport

Because the PEM fuel cell operates at low temperature and pressure conditions, condensation of water vapor into liquid phase is a regular process inside the cell. Although liquid water is eminent for keeping the membrane at hydrated levels, it can also block the gaseous passage and thus reduce the effective diffusion rate and the reactive surface area. In this work the conservation equation to model the liquid water formation and its transport is given as;

$$\nabla \cdot (\rho_l \vec{V}_1 s) = r_w \quad (9)$$

where s is the volume fraction of the liquid water, and r_w is the rate of condensation or evaporation depending on the total temperature and the partial pressure of water vapor in air.

$$r_w = \begin{cases} k_{\text{con}} \varepsilon (1-s) x_{\text{H}_2\text{O}} \frac{P_{\text{wv}} - P_{\text{sat}}}{RT} & \text{if } P_{\text{wv}} > P_{\text{sat}} \\ k_{\text{evp}} \varepsilon s \frac{\rho_w}{M_{\text{H}_2\text{O}}} (P_{\text{wv}} - P_{\text{sat}}) & \text{if } P_{\text{wv}} < P_{\text{sat}} \end{cases} \quad (10)$$

k_{con} and k_{evp} are the condensation and evaporation rate constant, respectively. $x_{\text{H}_2\text{O}}$ is the molar fraction of water vapor. Inside the channels, the liquid velocity, \vec{V}_1 , is assumed to be the same as the gas phase velocity while inside the porous media it is replaced by the capillary diffusion term. The validated approach to model the capillary pressure inside a porous media of PEM fuel cells has been presented by Kumbur et al. [15, 24, 25] and is given here (the effect of compressional loading has been ignored in this work);

$$P_c = \left(\frac{293}{T} \right)^6 (0.1247 - 1.78 \times 10^{-4} T) \sqrt{\frac{\varepsilon}{k}} K(s_{\text{nw}}) \quad (11)$$

$K(s_{\text{nw}})$ is the modified and experimentally evaluated J-type function. The original function was evaluated for both macro and micro porous media, but in this work it has been normalized only for macro porous media over the whole range of saturation because there is no micro porous layer (MPL) in the calculation domain.

$$K(s_{\text{nw}}) = \text{wt}\% (0.0469 - 0.00125 \text{wt}\% - 0.0406 s_{\text{nw}}^2 + 0.143 s_{\text{nw}}^3) + 0.0561 (\ln s_{\text{nw}}) \quad (12)$$

where wt% is the weight percentage of the PTFE content (hydrophobic additive loading) and s_{nw} is the non-wetting phase saturation.

Boundary Conditions, Mesh and Numerical Technique

In order to simulate the real conditions, a repeated section of a single PEM fuel cell has been simulated for all the basic processes such as species, heat and charge (ionic and electronic) transport apart from other supporting equations and the equations explicitly described earlier. The domain is discretized into 0.49 million hexahedral cells with varying mesh density for each zone based on series of mesh independence tests. Because of high pressure-velocity coupling, the SIMPLEC algorithm was utilized while other variables were discretized using the QUICK scheme. Because the simulated domain is a section of a single PEM fuel cell, the sides of the solution domain have been marked as symmetric faces by assuming similar operating conditions on adjacent sections. The front and back ends of the domain are considered as impermeable walls for all variables except for the inlet and outlet surfaces. Both fuel and air enter the solution domain at their respective inlet with an A/F (air to fuel) ratio of 8 where the mass flow rate of air at the inlet is fixed at 3×10^{-6} kg/s and it exits through the domain via pressure outlets maintained at atmospheric conditions. In order to control the temperature, the top wall of the anode and the bottom wall of the cathode have been idealized at 343 K. In the present work, fixed voltage has been used as an input boundary condition to calculate the current density profile at the cathode current collector surface while the anode current collector is set to 0. Also the water saturation in the cathode and anode inlets is fixed to zero, assuming a large water sink. The convergence criterion was set to a difference of less than 1×10^{-5} for each consecutive iteration for all variables, and the current conservation equation was also employed to ensure the continuity of cathodic and anodic electrical currents because of imbalance in reaction rates at the anode and cathode. Appropriate under-relaxation factors have also been used for momentum, pressure, water saturation, species and potential equations. This work has been carried out on commercial CFD software FluentTM by applying modified and self-developed sub models through user defined functions (UDFs).

3 Results and Discussion

The curve for the volume-averaged water saturation simulated by the validated approach in combined PTL and CL domains is presented in Fig. 3 for the PEM fuel cell against the operating voltage. The operating conditions for the present case are listed in Table 1. It can be observed in the figure that at lower voltage levels, the volume-averaged water saturation value is at maximum. The higher saturation at this level can be explained by considering the enhanced rate of electro-chemical reactions taking place, because lower operating levels correspond to higher current densities Fig. 2. Furthermore, initially there is no considerable increase in the liquid water saturation when the operating voltage is decreased or the current density is increased and this trend continues until the operating voltage is approximately 0.6 volts. Beyond the operating level of 0.6 volts, a high rate

Table 1: *Electrode parameters and physical properties.*

Parameter/variable	Value	Units
Fuel cell length	50	mm
GDL thickness	0.2	mm
CL thickness	0.01	mm
Membrane thickness	0.015	mm
Operating pressure	1.5	atm
Operating temperature	343	K
Inlet O ₂ mass fraction	0.21	
Inlet H ₂ O mass fraction (cathode)	0.13	
Inlet H ₂ mass fraction	0.5	
Inlet H ₂ O mass fraction (anode)	0.5	
Evaporation rate constant	100	1/s
Condensation rate constant	100	1/atm s
Faraday constant	96487	C/mol
Universal gas constant	8.3142	J/mol K
GDL porosity	0.4	
CL porosity	0.2	
Absolute permeability	2.55e-13	
Density of liquid water	998	kg/m ³
Weight percentage of PTFE content	10%	
Thickness of Nafion covering agglomerate	10	nm

of increase in the liquid water saturation is observed. The reason for such a drastic increase can be explained by considering the facts that the water generation due to electro-chemical reactions has increases to such an extent that the air flowing through the domain does not have the ability to carry away more water due to the saturation of water vapor in the air. By considering the water saturation, a safe-play zone for the PEM fuel cell can be marked for the present simulation conditions. Additionally, at very low voltage levels, i.e., the operating levels below 0.3 volts (regime corresponding to higher current densities) the saturation profile levels out showing not much increase in the liquid water quantity. The reason for such behavior is because of the limited increase in the current density due to concentration losses at such operating levels.

Figs 4 and 5 Fig. show the water saturation profile at two different operating voltages of 0.3 (higher current density) and 0.7 volts (lower current density) for the cathode side of the catalyst and the porous transport layer at different sections along the air flow direction . Although the maximum water saturation levels differ for both the operating conditions due to different rate of electro-chemical reactions, electro-osmotic drag, back diffusion and phase change, both the profiles suggest that most of the reactions occur in the catalyst layer region which is directly above the high pressure channel due to the higher reactant (oxygen) concentration because maximum saturation effects are observed in this location along the width of the each cross-section. At higher current density, the

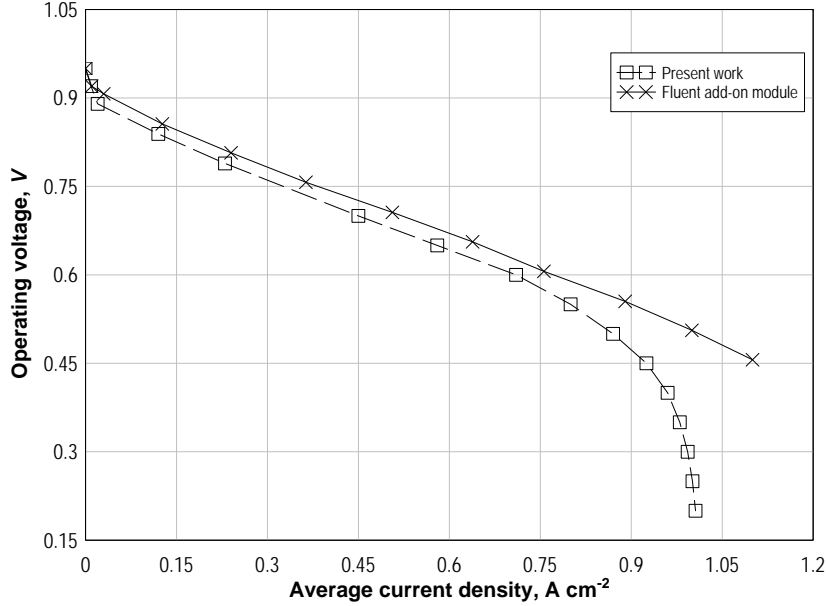


Fig. 2: The V - I comparison of present model and *Fluent*TM add-on module.

maximum water saturation is located close to inlet and since the reaction rate is quite high, much of the oxygen is consumed near the entrance region. Since the reactions are proportional to the oxygen concentration and with decrease in its concentration, the far region to the inlet or the region near the air outlet depicts less water saturation effects because of decreased rate of electro-chemically generated water and the electro-osmotic drag. On the contrary, at lower current density, the maximum relative saturation occurs at the far region which is because of the air flowing through the domain that becomes more and more saturated as it passes through or in other words, the decreasing ability of air to evaporate the liquid water due to the increase in humidity enhances the condensation water vapors to liquid state. In short, a shift occurs in the maximum saturation levels with increase in current density from region near outlet to region near inlet and this shift that can be attributed to the increasing level of relative humidity of air and the rate of electro-chemical reactions. Since in this work, the simulated domain is only 50 mm long, the saturation profiles indicate that fuel cells with longer channels may be affect severely with water saturation effects due to the condensation of the water vapors in the porous media of the fuel cell even for higher operating voltages (lower current densities).

Along the height of the porous media, two regions are worth noticing in each cross-sectional plane. One of them is the region at the interface of the inlet channel and the porous media. As it can be noted that at both operating conditions, the maximum water saturation occurs near the interface of the flow channel (high pressure channel) and the porous transport layer. Since the flow configuration used for this work consists

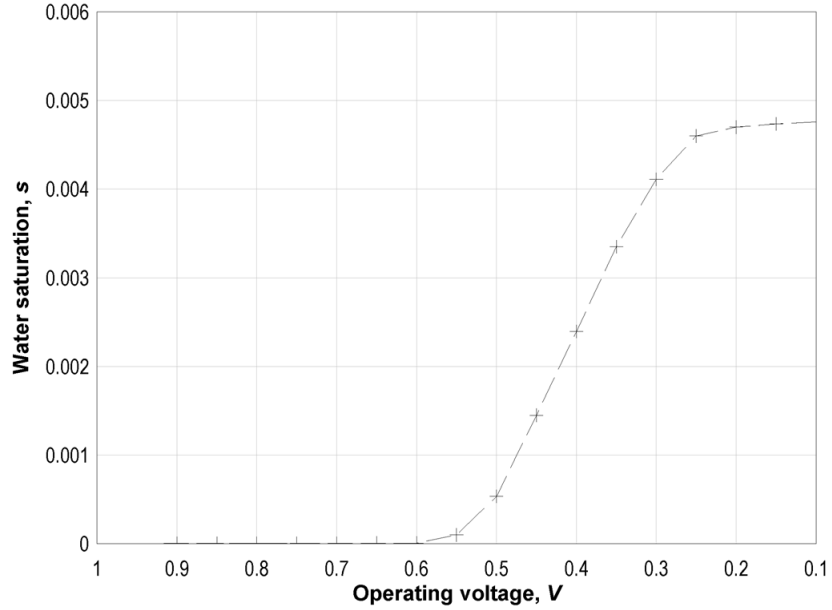


Fig. 3: Variation in volume-averaged water saturation in cathode CL and GDL with operating voltage.

of interdigitated flow field, the high pressure of air helps in limiting the covering of whole interface area by diverting the gaseous flow into the porous media. With conventional straight channels or serpentine flow field designs, such accumulation of liquid water at the interface may pose serious performance setbacks by covering the interface completely and potentially hindering the air from entering the porous media. The other effect of water saturation can be seen at the interface of catalyst layer and the membrane. For each operating load, as can be seen, the catalyst layer has less saturation levels despite of being an active source of water production via electro-chemical reactions and the electro-osmotic drag. The reason for less saturation effects in the catalyst layer are credited to the tendency of liquid water to transport itself to higher porous zone (GDL, $= 0.4$) and the increase in back diffusion rate because of higher water content at the cathode side.

Fig. 6a represents the saturation levels for a 2D case simulated using the conventional Leverett approach (Eq. (2)). The simulated domain in this case is restricted to cathode side only because of its vulnerability for the saturation effects due to the electro-chemical water generation and the electro-osmotic drag. The pre-humidified air at 340 K enters the domain through the pressure inlet and flows out via the outlet maintained at the atmospheric conditions. As it can be observed that the maximum liquid saturation is found near the catalyst layer/membrane interface and minimum is located near both the inlet and the outlet. The boundary conditions assumed for liquid water simulations dictate zero saturation levels at the inlet and outlet boundaries. Such an assumption in applying the boundary condition helps removing the water from the domain by declaring the

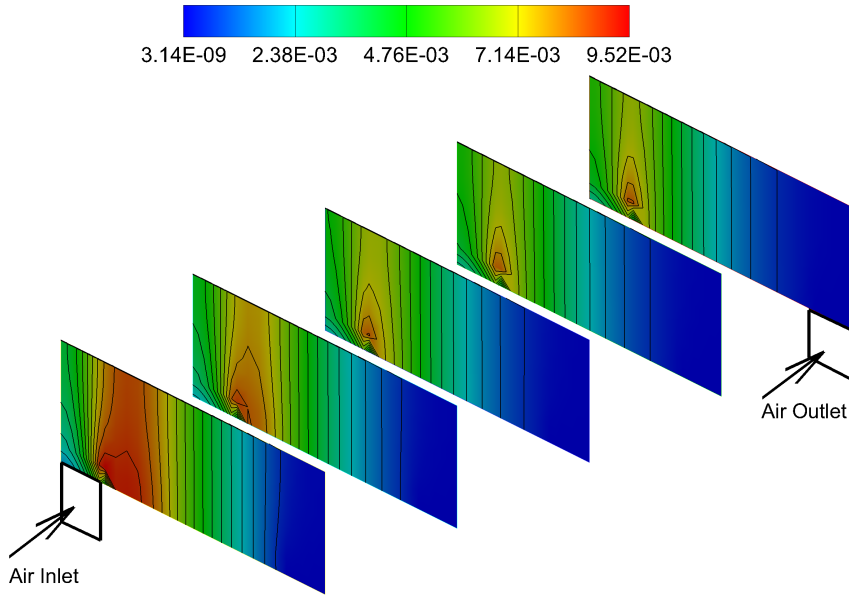


Fig. 4: Water saturation profile along the length of the PEM fuel cell cathode for PTL and Cl at 0.3 V.

boundaries as an infinite sink ($s = 0$) for the liquid water. Whereas, Fig. 6b is the saturation profile as calculated by the validated approach at a cross-section in the middle of the cell ($z = 25$ mm) so as to minimize the effects due to inlet and outlet boundaries located at each end. As it can be observed by comparing the two scenarios, that the saturation profile differs a lot for both the cases. The difference in two scenarios can be explained by considering the fact that in complete cell model the effects due to the anode side of the fuel cell and the gas flow channels are also incorporated that are usually neglected in cathode only simulations and the validated approach, as used in this work, is more stringent in capturing the local effects such as porosity because in Fig. 6b it can be seen that the liquid accumulation is more in the porous transport layer as compared to the catalyst layer.

The pattern of the increase in the back diffusion with decreasing voltage is presented in Fig. 7. As noted, the back diffusion is maximum at lower operating voltages (higher current densities). Since the back diffusion rate depends on the difference in concentration of water between the two sides, i.e., the anode and the cathode, so an increasing rate is observed for the operating levels between 0.9 to approximately 0.4 volts after which there is no considerable addition to the rate of back diffusion. The initial increase in rate is due to the generation of water at the cathode side due to electro-chemical reactions and also the electro-osmotic drag pulls water from anode to cathode leaving the two sides at mismatched concentration levels. Also, as expected, the rate in increase levels to almost a uniform rate at very low operating voltages, which is also due to the limitations in the electro-chemical reactions due to the concentration losses at such levels. Similarly, the

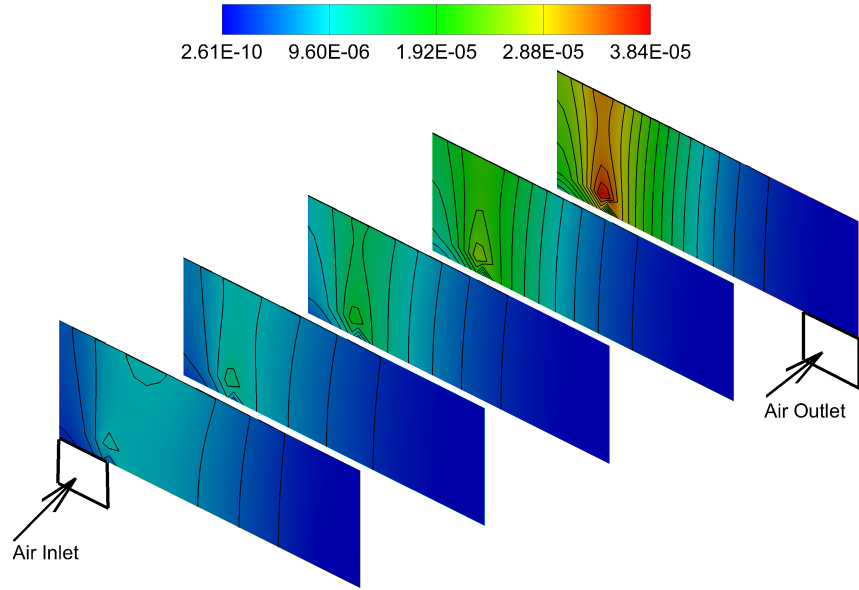


Fig. 5: The $V-I$ comparison of present model and *Fluent™* add-on module.

profile for the electro-osmotic drag is presented in Fig. 8. It can be observed that the electro-osmotic drag is minimum at higher voltages due to low rate of electro-chemical reactions and almost linear increase is observed by decreasing the operating voltages, while, at very low voltages, the increase in the electro-osmotic drag levels out because, as explained earlier, the operating range at such levels falls in the mass limitation zone.

4 Conclusions

In this work a three dimensional repeated section of a PEM fuel cell has been numerically simulated to study the effects of water saturation. Although many attempts have been made with the similar intent previously but few of the researchers have always argued the effectiveness and the applicability of certain modeling equations borrowed from other technologies into PEM fuel cells application. The most common approach found in numerically quantifying the water saturation and its transport in the porous media is the use of Leverett approach originally developed for soil sciences and later modified for PEM applications called the Leverett J-function. However, in this work a validated approach has been used which is function of both the PTFE loading and the saturation level. The flow field configuration used in the present modeling is the interdigitated flow field where electro-chemical reactions are simulated using the agglomerate model. As far as the rate of electro-chemical reactions is concerned, it was found that most of the reactions occur in the region of catalyst layer that is directly above the inlet channel and the same region of the PEM fuel cell has been found to be most affected by the liquid saturation. But, a shift in location of maximum saturation level is observed while increasing the current density. At lower current densities, the maximum occurred in the

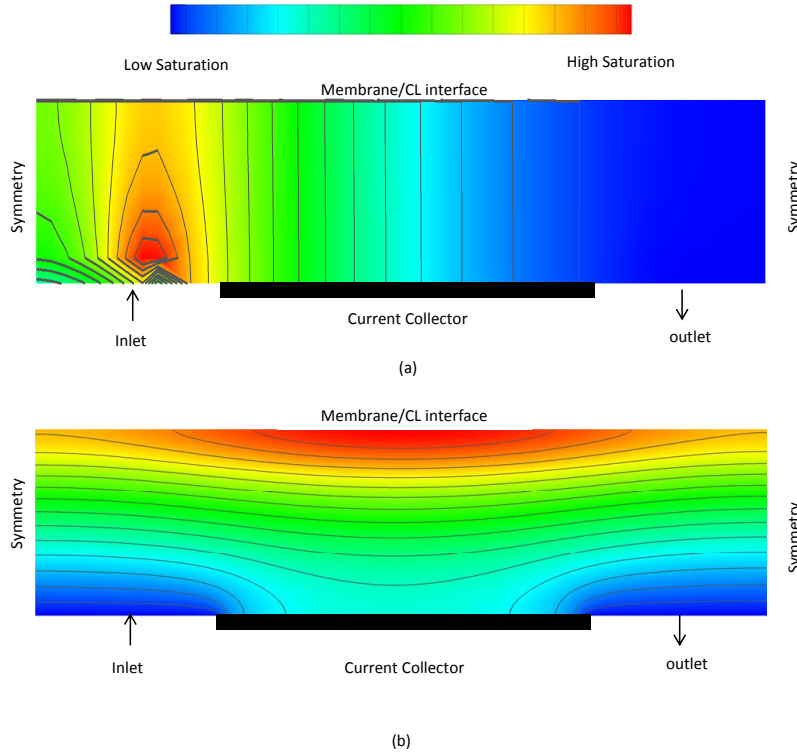


Fig. 6: Comparison between conventional Leverett and the validated approaches for water saturation modeling.

far region of the cell suggesting the increase in inability of air to accommodate more water vapors. While at higher current densities, the maximum moved towards the inlet region. Although the change in operating levels caused variation in the location of most affected region along the length of the fuel cell, but in all cases, the liquid water tends to accumulate at the interface of the inlet channel and the diffusion media.

In concluding the effects of water saturation and the internal movement of water across the membrane, operating the fuel cell at higher current densities makes it more prone to problems associated with the liquid water saturation. Although, at low current densities, the water saturation is quite small but an increasing fuel cell length may make it vulnerable to higher water saturation levels because of the increase in the humidity of air as it passes along the cell. Also, the accumulation of liquid water at the interface of inlet channel and the diffusion media suggest that the conventional flow configurations may face the problem to penetrate through the porous media to reach the reaction sites.

Furthermore, it can be also concluded by comparing the simulation results of 3D full cell model and a 2D cathode only model that, although, cathode only models are a good starting point in studying the effects of all the water management related parameters,

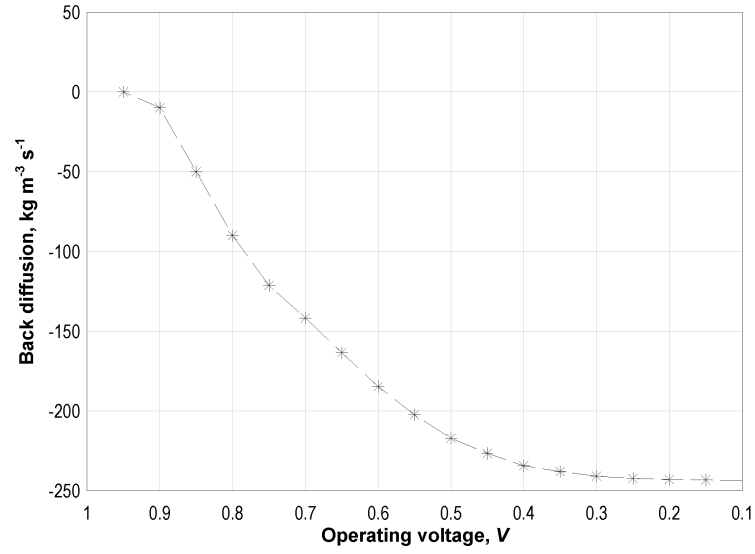


Fig. 7: *PEM fuel cell operating voltages and the back diffusion of water (minus sign indicates the water movement out of the domain).*

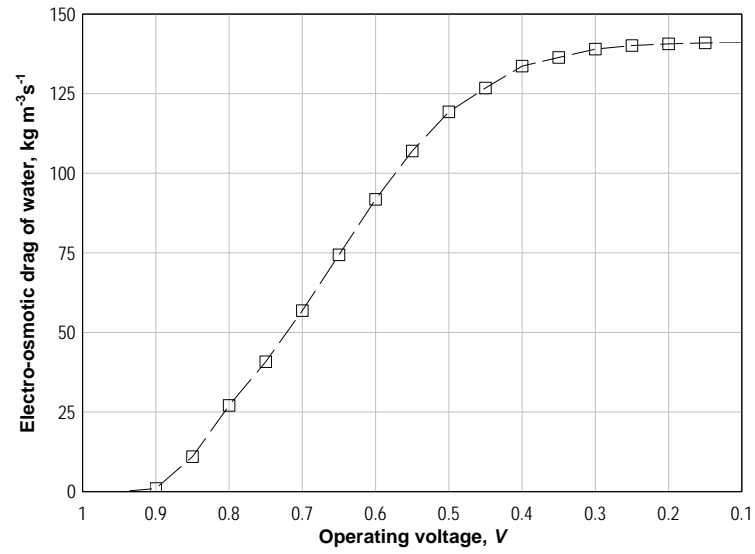


Fig. 8: *Electro-osmotic drag variation with operating voltages into the cathode of PEM fuel cell.*

they have built in limitations in sense that all the effects, i.e., the channel and anode side, cannot be incorporated into the model which have signification impression on the overall performance of the cell. On the other hand, models that are simulated for a complete cell containing all the basic components reveal much better picture and all the effects can be studied and quantized.

Acknowledgements

The European Research Council (ERC 226238-MMFCs) supports the current research.

Nomenclature

Roman Symbols

a	area, m^2
D	diffusion coefficient, m^2/s
E_r	agglomerate effectiveness
F	Faraday constant, C/mol
H	Henry constant, $\text{Pa m}^3/\text{mol}$
J	Leverett function
J_w	water flux, $\text{kg}/\text{m}^2 \text{ s}$
K	validated saturation function
k	permeability, m^2 or reaction rate, $1/\text{s}$
M	molecular weight, kg/mol
n_d	electro-osmotic drag coefficient
P	pressure, Pa
P_c	capillary pressure, Pa
R	electro-chemical reaction rate, A/cm^3
r	radius, m
r_w	evaporation or condensation rate, $\text{kg}/\text{m}^3 \text{ s}$
s	saturation
T	temperature, K
\vec{V}	velocity vector, m/s
wt%	PTFE content loading

Greek Symbols

δ	membrane or ionomer thickness, m
ε	porosity
γ	surface tension, N/m
λ	water content
ϕ	membrane potential, V
ρ	density, kg/m^3
σ	protonic conductivity, S/m
θ	contact angle

Subscripts & Superscripts

agg	agglomerate
-----	-------------

con	condensation
evp	evaporation
l	liquid/water
mem	membrane
naf	Nafion
nw	non wetting
sat	saturation
wv	water vapor
w	water
X	reacting species

References

- [1] Siegel, C., 2008. "Review of computational heat and mass transfer modeling on polymer-electrolyte-membrane (pem) fuel cells". *J. Energy*, **33**, pp. 1331–52.
- [2] Siegel, C., 2008. "Review of computational heat and mass transfer modeling on polymer-electrolyte-membrane (pem) fuel cells". *J. Energy*, **33**, pp. 1331–52.
- [3] Sundén, B., and Faghri, M., 2005. *Transport Phenomena in fuel cells*. Devel. Heat Transfer. WIT Press, Southampton.
- [4] Natarajan, D., and Van Nguyen, T., 2003. "Three-dimensional effects of liquid water flooding in the cathode of a pem fuel cell". *J. Power Sources*, **115**(1), pp. 66–80.
- [5] Li, H., Tang, Y., Wang, Z., Shi, Z., Wu, S., Song, D., Zhang, J., Fatih, K., Wang, H., Liu, Z., Abouatallah, R., and Mazza, A., 2008. "A review of water flooding issues in the proton exchange membrane fuel cell". *J. Power Sources*, **178**(1), pp. 103–117.
- [6] Kowal, J. J., Turhan, A., Heller, K., Brenizer, J., and Mench, M. M., 2006. "Liquid water storage, distribution, and removal from diffusion media in pefcs". *J. Electrochem. Soc.*, **153**(10), pp. A1971–A1978.
- [7] Pasaogullari, U., and Wang, C. Y., 2004. "Liquid water transport in gas diffusion layer of polymer electrolyte fuel cells". *J. Electrochem. Soc.*, **151**(3), pp. A399–A406.
- [8] Ren, X., and Gottesfeld, S., 2001. "Electro-osmotic drag of water in poly(perfluorosulfonic acid) membranes". *J. Electrochem. Soc.*, **148**(1), pp. A87–A93.
- [9] Thomas A. Zawodzinski, J., Derouin, C., Radzinski, S., Sherman, R. J., Smith, V. T., Springer, T. E., and Gottesfeld, S., 1993. "Water uptake by and transport through nafionTM117 membranes". *J. Electrochem. Soc.*, **140**(4), pp. 1041–1047.
- [10] Borup, R., Meyers, J., Pivovar, B., Kim, Y. S., Mukundan, R., Garland, N., Myers, D., Wilson, M., Garzon, F., Wood, D., Zelenay, P., More, K., Stroh, K., Zawodzinski, T., Boncella, J., McGrath, J. E., Inaba, M., Miyatake, K., Hori, M., Ota, K., Ogumi,

- Z., Miyata, S., Nishikata, A., Siroma, Z., Uchimoto, Y., Yasuda, K., Kimijima, K.-i., and Iwashita, N., 2007. "Scientific aspects of polymer electrolyte fuel cell durability and degradation". *Chem. Rev.*, **107**(10), pp. 3904–3951.
- [11] Mench, M. M., 2010. *Advanced modeling in fuel cell systems: a review of modeling approaches*. Wiley-VCH Verlag GmbH & Co. KGaA, Weinheim, pp. 89–118.
- [12] Mench, M. M., 2008. *Fuel cell engines*. John Wiley & Sons, Hoboken, New Jersey.
- [13] Larminie, J., and Dicks, A., 2003. *Fuel Cell Systems Explained*, 2nd ed. John Wiley & Sons Ltd., West Sussex.
- [14] Wang, L., Husar, A., Zhou, T., and Liu, H., 2003. "A parametric study of pem fuel cell performances". *Int. J. Hydrogen Energy*, **28**(11), pp. 1263–1272.
- [15] Kumbur, E. C., Sharp, K. V., and Mench, M. M., 2007a. "A validated leverett approach to multi-phase flow in polymer electrolyte fuel cell diffusion media. part 1. hydrophobicity effect". *J. Electrochem Soc.*, **154**, pp. B1295–B1304.
- [16] Berning, T., and Djilali, N., 2003. "A 3d, multiphase, multicomponent model of the cathode and anode of a pem fuel cell". *J. Electrochem Soc.*, **150**(12), pp. A1589–98.
- [17] Khan, M., 2009. *Numerical simulation of multi-scale transport processes and reactions in PEM fuel cells using two-phase models*. Licentiate Thesis, ISRN LUTMDN/TMHP-09/7066-SE, Lund University, Lund.
- [18] Yuan, J., Sundén, B., Hou, M., and Huamin, Z., 2004. *Three-dimensional analysis of two-phase flow and its effects on the cell performance of PEMFC*, Vol. 46. pp. 669–94.
- [19] Hartnig, C., Manke, I., Kuhn, R., Kardjilov, N., Banhart, J., and Lehnert, W., 2008. "Cross-sectional insight in the water evolution and transport in polymer electrolyte fuel cells". *Appl. Phys. Letters*, **92**(13), p. 134106.
- [20] Turhan, A., Kim, S., Hatzell, M., and Mench, M. M., 2010. "Impact of channel wall hydrophobicity on through-plane water distribution and flooding behavior in a polymer electrolyte fuel cell". *Electrochimica Acta*, **55**(8), pp. 2734–2745.
- [21] Leverett, M. C., 1941. "Capillary behaviour in porous solids". *Pet. Trans., AIME(Am. Inst. Min. Metall. Eng.)*, **142**, pp. 152–169.
- [22] Nam, J. H., and Kaviany, M., 2003. "Effective diffusivity and water-saturation distribution in single- and two-layer pemfc diffusion medium". *Int. J. Heat Mass Transfer*, **46**, pp. 4595–4611.
- [23] Udell, K. S., 1985. "Heat transfer in porous media considering phase change and capillarity—the heat pipe effect". *Int. J. Heat Mass Transfer*, **28**(2), pp. 485–495.
- [24] Kumbur, E., Sharp, K., and Mench, M., 2007. "A validated leverette approach to multiphase flow in polymer electrolyte fuel cell diffusion media. part ii. compression effect and capillary". *J. Electrochem. Soc.*, **154**(12), pp. B1305–B1314.

-
- [25] Kumbur, E., Sharp, K., and Mench, M. M., 2007. “A validated leverette approach to multiphase flow in polymer electrolyte fuel cell diffusion media. part iii. temperature effect and unified approach”. *J. Electrochem. Soc.*, **154**(12), pp. B1315–B1324.
 - [26] Sun, W., Peppley, B. A., and Karan, K., 2005. “An improved two-dimensional agglomerate cathode model to study the influence of catalyst layer structural parameters”. *Electrochimica Acta*, **50**(16-17), pp. 3359–3374.
 - [27] Harvey, D., Pharoah, J. G., and Karan, K., 2008. “A comparison of different approaches to modelling the pemfc catalyst layer”. *J. Power Sources*, **179**(1), pp. 209–219.
 - [28] He, G., Yamazaki, Y., and Abudula, A., 2009. “A droplet size dependent multiphase mixture model for two phase flow in pemfcs”. *J. Power Sources*, **194**(1), pp. 190–198.
 - [29] Hwang, J. J., 2007. “A complete two-phase model of a porous cathode of a pem fuel cell”. *J. Power Sources*, **164**(1), pp. 174–181.
 - [30] Springer, T., Zawodzinski, T., and Gottesfeld, S., 1991. “Polymer electrolyte fuel cell model”. *J. Electrochem Soc.*, **138**, pp. 2334–42.
 - [31] Sun, W., Peppley, B., and Karan, K., 2005b. “Modeling the influence of gdl and flow-field plate parameters on the reaction distribution in the pemfc cathode catalyst layer”. *J. Power Sources*, **144**, pp. 42–53.

Paper C

Khan, M.A., Xiao, Y., Sundén, B., Yuan, J., 2011. “Analysis of multiphase transport phenomena in PEMFCs by incorporating microscopic model for catalyst layer structures”, In *ASME 2011 International Mechanical Engineering Congress*, (IMECE2011-65142), 11-17 November, Colorado, USA.

© 2011 ASME.
The layout has been revised

Analysis of Multiphase Transport Phenomena in PEMFCs by incorporating Microscopic Model for Catalyst Layer Structures

Munir Ahmed Khan, Yexiang Xiao
Bengt Sundén, Jinliang Yuan

Abstract

The catalyst layer (CL) in polymer electrolyte membrane (PEM) fuel cells is one of the key components regulating the overall performance of the cell. In PEM fuel cells, there are two CLs having identical composition for hydrogen oxidation (HO) and oxygen reduction (OR) reactions. There are four phases inside the CL, namely: carbon, Pt particles, ionomer and voids. In this work, a micro-model of the cathode CL has been developed mathematically using finite volume (FV) technique to reconstruct the local structure and further investigate the transport phenomena of reactants and product species, ions and electrons by incorporating the above stated phases at the cathode side only, due to the fact that the OR reactions are the rate limiting as compared to HO reaction. The 3D CL has been reconstructed based on a regularly distributed sphere's method with dimensions $4.1 \times 4.1 \times 4.1 \mu\text{m}^3$. Platinum particles combined with carbon spheres (C/Pt) are regularly placed in the domain, an ionomer layer of a given thickness is extruded from the sphere surfaces. The C/Pt, ionomer and void distribution, as well as the triple phase boundary (TPB) are analysed and discussed. A microscopic model has been developed for water generation and species transport including Knudsen diffusion through the voids and the proton transport in the ionomer has been included here to aim for the rigorousness of the work. In addition, the electro-chemical reactions have been simulated on the surface of Pt particles fulfilling the TBP conditions.

Key words: PEMFC, catalyst layer, micro model, catalyst layer reconstruction.

1 Introduction

Catalyst layers (CLs) are at the heart of PEM fuel cells, the incorporation of nanosized catalysts has been proven highly successful in increasing active areas and catalyst activity, thus leading to significant improvements in the performance and catalyst utilization. There are various phases inside the catalyst layer, namely: carbon, Pt particles, ionomer and voids. Platinum is used as the catalyst to carry out the oxidation and reduction reactions of hydrogen and oxygen at respective catalyst layers while the carbon particles serve as support to Pt and electron conduction. The ionomer establishes the essential skeleton to distribute the so-formed carbon/platinum (C/Pt) and conducts the ions while the voids help in transport of the reactants and the products. They provide pathways for the transport of reactants, protons, electrons and products while facilitate oxygen reduction at the cathode and hydrogen oxidation at the anode [1]. In addition to multiphase transport processes, water generation/transfer processes occurring in nano-structured

CLs are critical and very complicated, particularly when water-phase change is involved at nano/micro-pore levels, if the pore sizes approach extreme values. The CLs play a crucial role in the PEMFC water management aimed at maintaining a delicate balance between reactant transport from the gas channels and water removal from the electrochemically active sites. There are several multi-physics and electrochemical phenomena, taking place in CLs during fuel cell operation. The reactions and the transport phenomena occurring in fuel cell CLs are considered localized rather than uniform. For example, the TPB between catalysts/ionomers/gas pores determines the important parameters, such as electrochemically active area (ECA) and exchange current density. It is also true that the percolation within the CLs provides transport pathways for reactants, as well as water and heat [2].

Detailed description of a porous microstructure is an essential prerequisite to pore-scale modelling. The 3-D volume data of a porous sample can be obtained either by experimental imaging or by computer simulation method. Several experimental techniques can be deployed to image the pore structure even in three dimensions. Non-invasive techniques such as X-ray micro-tomography, magnetic resonance imaging and confocal microscopy are the preferred choices [3–6]. The computer reconstruction of CL can be either stochastic [7–9], semi-deterministic [2, 10] or regular [11]. There have been increasing efforts to reconstruct CL and simulate reactions at the micro scale level. In the following sections, the evaluation of the PEMFC CL microstructures is outlined and highlighted.

The first published work on CL reconstruction was done in two dimensions [12]. This model was later extended to three dimensions and applied to a regular microstructure and a random one. In their research work, the catalyst layer was first represented by idealized regular microstructures [11], followed by computer-generated random microstructures [13] and further by stochastically reconstructed microstructures based on statistical information from 2D TEM images [7]. The latter method was further extended for the generation of bi-layer CL structures with varied pore and electrolyte volume fractions [14]. Their reconstruction involves only two phases, i.e., void and solid, and the electrolyte and Pt/C are treated as a single phase during the reconstruction. A different approach was presented by Kim and Pitsch to computationally reconstruct a PEMFC CL [15]. They represented the CL as consisting of carbon spheres surrounded by an ionomer film. The reconstructed 3D CL includes a thin layer of ionomer phase evenly distributed around the C/Pt spherical agglomerates. It involves three phases (ionomer, C/Pt, void). Knudsen diffusion was accounted for by computing an average pore radius which was used to compute a Knudsen diffusion coefficient for all pores in the solution domain. In another effort, Lange and the co-workers used a stochastic approach to reconstruct a section of a PEMFC CL and modeled transport and electrochemical reactions for a wide range of random microstructures [1, 8, 16]. Hundreds of different microstructures were used, resulting in a large number of effective transport parameters at different pore, ionomer and carbon volume fractions. In those work, the reconstruction also involves three phases: carbon/Pt, ionomer, and pores. In addition, most of the previous CL modeling efforts have used one mean pore radius to compute the Knudsen diffusion coefficient that was further applied to all sized pores in the computational domain. Recently, Siddique and

Liu reconstructed and modeled a small section of PEMFC CL with a high resolution [2]. A random reconstruction algorithm, reflecting the experimental fabrication process, attempts to account for agglomeration in the model. Their reconstruction involved four phases, i.e., the Pt, carbon, ionomer and pore space, and the isolated area for each phase was distinguished in detail. In addition, the electrochemically active area determined by the interface between transport Pt and ionomer regions has been quantified, as a good indicator of phase connection and interaction.

Recent efforts also include 3D experimental imaging of the PEMFC CL microstructure using X-Ray computed tomography. The first published work on PEMFC CL 3D reconstruction was presented by Ziegler and co-workers [17]. They reconstructed 3D morphology of a CL based directly on highly sensitive focused ion beam/scanning electron microscope (FIB/SEM) analysis. The carbon and pore distribution was shown and quantitatively analysed. Based on the reconstruction the pore size distribution is evaluated. By the experimental methods, the reconstruction involves only solid and pore phases. By numerical methods, the reconstruction can only involve three phases and the TPB for the electrochemical reaction and water generation have not been identified, neither. In this study, we use a regular numerical method to reconstruct 4 phase microstructure and TPB by using three-dimensional commercial software directly, for the objective to develop a microscopic model for water generation and species transport via Knudsen diffusion through the voids, i.e., smaller pores in the domain will have lower Knudsen diffusivities than larger pores. The proton transport in the ionomer has been included here to aim for the rigorousness of the work. In addition, local electro-chemical reactions have been simulated at the interfaces satisfying the TBP conditions.

2 Microstructure Reconstruction

2.1 Regularly Distributed Sphere Method

The CL structure is complex, generally composed of four phases: carbon (C), which allows for conduction of electrons (e^-) and support of the platinum nano particles; ionomer, the ionic phase which is typically NafionTM and provides a path for proton (H^+) conduction; platinum (Pt) particles, which provide sites for electrochemical reactions; and pores, which allow reactants and product gases to diffuse through the CLs. In addition to multiphase transport processes, water generation/transfer processes occurring in nano-structured CLs are critical and very complicated, the electrochemical reactions happen on the location of the TPBs. In order to simulate the coupled electrochemical reactions, water-phase change and transport phenomena in PEMFC CL at micro pore scale, a regular sphere-based method was adopted to reconstruct the CL with the four phases and TPBs by directly using three-dimensional commercial software.

2.2 Catalyst Layer Microstructure

The overall morphology of agglomerate structures in the thin film CLs can be characterized by the spatial distribution of C/Pt particles [8, 18]. Because the pore-scale phenomena on the order of 100 nm \sim 1 μ m are of primary interest, e.g., the reactions

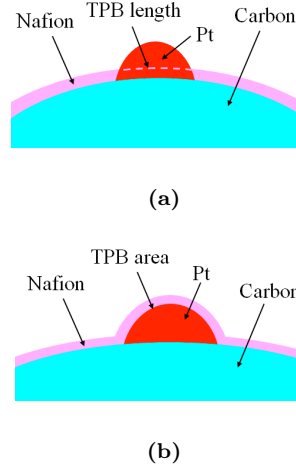


Fig. 1: A schematic drawing of the TPB

happen on the location of the TPBs, the detailed structure of carbon and platinum particles can not be neglected. Carbon supports agglomerates and platinum particles are very close to spherical shapes.

The CL is assumed to consist of connected C/Pt spheres which are covered by a uniform thin ionomer layer. The assumptions of methodology are listed below:

- Each big carbon sphere is combined with a pre-specified number of small Pt spheres, and half of individual Pt particles stick out, which represents the primary carbon/platinum (C/Pt) particle interaction.
- There are two types of TPBs, namely: TPB length and TPB area, in this reconstruction method:
 - all C/Pt are covered by an ionomer layer of specified thickness, except at Pt faces and where carbon spheres overlap. Each Pt particle sticks out from the thin ionomer films, hence, the place of TPBs, where the electronic, ions and void phases meet, can be identified, as illustrated in Fig. 1a. The TPB length is defined by the circle length between a Pt particle and ionomer film, as shown by the dashed line in Fig. 1a.
 - all C/Pt are covered by an ionomer layer of specified thickness, except at where carbon spheres overlap. Each Pt particle is covered by the same thickness of thin ionomer films. In this case, the area of TPBs is the surface of sticking out Pt, as illustrated in Fig. 1b

The reconstruction is performed by arranging the C/Pt spheres regularly in three directions, in such a way that the spatial distribution of the spheres follows that of C/Pt volume fraction in the CL. The ionomer layers are periodic in the same way. According to above assumptions, the proposed reconstruction procedure is performed by using a

Table 1: *Porosity and specific surface area changed with the radii*

	Unit	$l = L/2r = 0.9$				
r	μm	0.2	0.4	0.6	0.8	1
$\frac{V_p}{V_t}$	%	31.16	30.38	31.65	29.90	29.03
$\frac{A_s}{V_t}$	10^6m^{-1}	7.64	3.77	2.51	1.84	1.47

Table 2: *Porosity and specific surface area changed with distance ratio*

	Unit	$r = 1 \mu\text{m}$				
l^a	–	0.8	0.85	0.9	0.95	0.98
$\frac{V_p}{V_t}$	%	15.90	23.98	29.03	36.45	42.61
$\frac{A_s}{V_t}$	10^6m^{-1}	1.29	1.44	1.47	1.51	1.55

^a $l = \frac{L}{2r}$

three-dimensional commercial software directly.

Firstly, only the solid and pore phases is considered to investigate the basical parameters, like porosity and specific surface area (SSA) in micro scales. The porosity is the ratio of the void volume to the total volume; the specific surface area is the ratio of the solid surface area to the total volume. The simulation can supply the void volume and solid surface area directly. It is assumed that all solid spheres radii r , the distance L between each spheres are keep constant, and the arrangement of sphere at x , y and z direction are the same. The ratio between distance and diameter l ($l = L/2r$) is constant (0.9), while the sphere radii varied from 0.2 to 1 μm , the predicted porosity and specific surface area are listed in Table 1. It shows that the porosity is around 30%, while the specific surface area decreased with the radii increasing. To keep the radii constant (1 μm) and change the distance ratio from 0.8 to 0.98, the porosity and specific surface area values are evaluated in Table 2. It shows that the porosity increases from 15.9% to 42.6% with increasing of distance ratio, and the specific surface area increased slightly.

Normally, for the PEM CL, the porosity is about 20% ~ 60%, the specific surface area is around $1 \sim 3 \times 10^6 \text{ m}^{-1}$, the thickness of ionomer is about 10 ~ 80 nm, and the Pt loading is about 0.4 (mg cm^{-2}), the C/Pt agglomerates spherical is about 1 μm . According to the experimental result of pore size distribution, the pore space radius is around 20 nm to 200 nm [17]. Secondly, the 3D CL with 4 phases and TPB is reconstructed using the above given parametric values. If the particles are arranged regularly in x , y and z direction, the size of pore space radius will be very large. In order to decrease the pore

Table 3: *The micro structure parameters of PEM fuel cell CL predicted by four phase reconstruction method*

Parameter	Symbol	Value	Unit
cell size		4.1	μm
carbon radius	r_c	0.99	μm
ionomer thickness	δ	0.01	μm
Pt radius	r_{Pt}	0.1	μm
porosity	$\frac{V_p}{V_t}$	29.95	%
SSA ^a	$\frac{A_s}{V_t}$	1.57	10^6 m^{-1}
TPB LD ^b	$\frac{L_{\text{TPB}}}{V_t}$	0.67	μm^{-2}
Pt loading	m_{Pt}	0.10	mg cm^{-2}

^a SSA = Specific surface area

^b LD = length density

radius, the particles can be offset by a certain distance m , as shown in Fig. 2.

According to the first step above, the distance ratio of 0.9 and the ionomer thickness of 10 nm are used along with the carbon sphere radii of 990 nm and the Pt sphere radii of 100 nm. Each big carbon sphere is combined with 6 Pt spheres, and half of each Pt particles stick out inside the thin ionomer film. The combined C/Pt and ionomer spheres are regularly arranged in the computational domain. Figure 3 shows the reconstructed CL for a domain size $4.1\mu\text{m} \times 4.1\mu\text{m} \times 4.1\mu\text{m}$ and some of the parameters of reconstructed CL are given in Table 3.

The mean porosity of CL cell is calculated using a value counting method [13]. Fig. 4 shows the relationship between the calculated porosity and the size of the domain at the distance ratio of 0.9. Below a certain sample size the porosity of the sample fluctuates due to the local structure effects and is not representative of the entire PEM fuel cell CL. The porosity is required to be independent of the domain size, for the objective to have a structure that is representative of the bulk CL. In order to determine this parameter, a study is performed by increasing the sample size and it is found that the porosity keeps almost constant when the domain size is 6 times of carbon radius, resulting in a domain representing of the entire CL structure.

3 Model Development for transport and Reactions

This work has been carried out by simulating the governing equations for air, energy, protonic current and the electronic current. The inlet humidity of the air has been so selected that the condensation of water vapours into liquid state is avoided i.e., 50%. Additionally, the convective force for species transport has also been neglected i.e., only the diffusive flux governs the species movement inside the domain. The electro-chemical reactions occur at the surface of the Pt particles and quantified by using the Tafel ap-

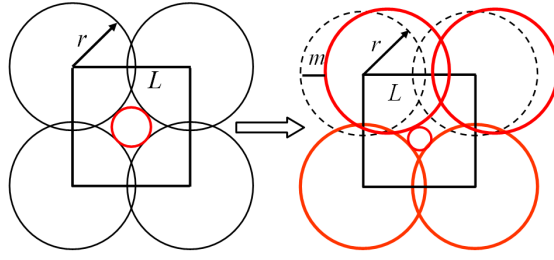


Fig. 2: *Offset arrangement of particles*

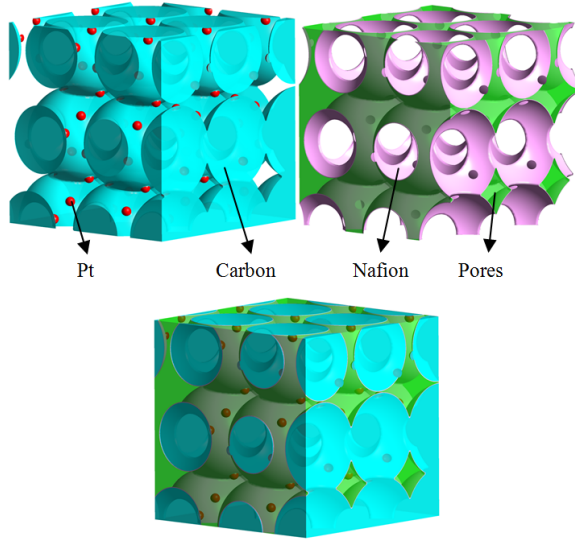


Fig. 3: *Four phase reconstruction ($4.1\mu\text{m} \times 4.1\mu\text{m} \times 4.1\mu\text{m}$). Carbon spheres are in sky blue, Pt particles red, ionomer is pink and pores are green or transparent.*

proximation [19]. The continuity equations for the oxygen transport is given as;

$$0 = \nabla \cdot \left[D_{\text{O}_2} \nabla Y_{\text{O}_2} - \frac{1}{4F} i_o \frac{Y_{\text{O}_2}}{Y_{\text{O}_2, \text{ref}}} \exp \left(\frac{\alpha_c F}{RT} \eta \right) \right] \quad (1)$$

where Y_{O_2} represents the local concentration of oxygen in the air. The Eq. (1) consists of two parts on the right hand side: the first part represents the diffusion of species through the domain while the second part gives the electro-chemical reaction related O_2 consumption. Since in this work there are total of two media through which the O_2 species has to diffuse, i.e., the void and the Nafion, so each species has different diffusion coefficients for the two media while the Pt particles are immune to any sort of diffusion. For diffusion of species in voids, the diffusion coefficient is based on both the bulk diffusion and the Knudsen diffusion because of the small pore diameter,

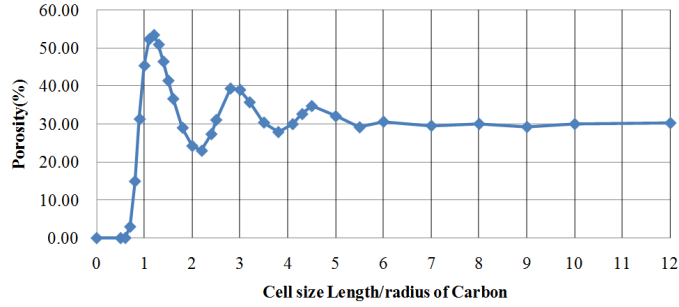


Fig. 4: *Fluctuations in the porosity of the representative volume calculated by increasing the size of the volume.*

$$D_{O_2, kn} = 0.485 d_p \sqrt{\frac{T}{32}} \quad (2)$$

where d_p is the local pore diameter and is based on the average of maximum and minimum values. The bulk diffusivity is based according to the binary diffusion of oxygen into nitrogen [20].

$$D_{O_2, b} = 2.2 \times 10^{-5} \left(\frac{T}{T_o} \right)^{1.5} \left(\frac{p_o}{p} \right) \quad (3)$$

The total oxygen diffusivity is calculated in the void region as [21];

$$\frac{1}{D_{O_2}} = \frac{1}{D_{O_2, kn}} + \frac{1}{D_{O_2, b}} \quad (4)$$

To reach the reaction site i.e., the Pt surface, the oxygen has to diffuse through the nafion (membrane). The diffusivity of oxygen in the ionomer (membrane) is related to local temperature, as [22];

$$D_{O_2} = 10^{-10} \times (0.1543 (T - T_o) - 1.65) \quad (5)$$

Similarly, the governing equation for water vapour diffusion and production takes the following form [19];

$$0 = \nabla \cdot \left[D_{H_2O} \nabla Y_{H_2O} + \frac{n_d \sigma_m}{F} \nabla \phi_m \right] + \nabla \cdot \left[\frac{1}{2F} i_o \frac{Y_{H_2O}}{Y_{H_2O, ref}} \exp \left(\frac{\alpha_c F}{RT} \eta \right) \right] \quad (6)$$

Table 4: *Curve-fitted Parameters for protonic conductivity of membrane (adopted from Lange et al. [19])*

Coefficient	Value
c_1	2.8133×10^{-2}
c_2	1.328355
c_3	-1.1642×10^{-2}
c_4	3.442175×10^{-5}
c_5	-3.33815×10^{-8}
c_6	-7.2939×10^{-2}

The Eq. (6) contains an extra source term for the addition of water in the domain due to the electro-osmotic drag. The bulk diffusion and the Knudsen diffusion coefficient for water vapours in the void region is calculated as [19, 20];

$$D_{\text{H}_2\text{O},b} = 2.93 \times 10^{-5} \left(\frac{T}{T_o} \right)^{1.5} \left(\frac{p_o}{p} \right) \quad (7)$$

and,

$$D_{\text{H}_2\text{O},kn} = 0.485 d_p \sqrt{\frac{T}{18}} \quad (8)$$

For the ionomer region, the diffusion of water vapours have been assumed to have a constant value of $6 \times 10^{-10} \text{ m}^2\text{s}^{-1}$. The term α_c in Eqs (1) and (6) is the cathodic transfer coefficient and is given as [23]

$$\alpha_o = (2.25 \times 10^{-3}) T - 0.178 \quad (9)$$

Also, i_o , the exchange current density, is based on the local temperature as [23];

$$i_o = 0.029825 \times 10^{-1521.93/T} \quad (10)$$

Since there are two types of current flowing in the domain i.e, protonic current and the electronic current, two conservation equations have been employed for simulating the current flow, given as;

$$\nabla \cdot (\sigma_m \nabla \phi_m - S) = 0 \quad (11)$$

where σ_m accounts for the protonic conductivity of the membrane and is given as [19];

$$\sigma_m = (c_1 \exp[(c_2 T - c_3 T^2 + c_4 T^3 - c_5 T^4) \omega] + c_6) \quad (12)$$

where ω is the relative humidity and constants c_1 to c_6 are the curve fitted values [19], as given in Table 4.

Similarly, the conservation equation for the electronic current is given as;

$$\nabla \cdot (\sigma_s \nabla \phi_s - S) = 0 \quad (13)$$

The source term S in both Eqs (11) and (13) models the consumption of protons and electrons at the Pt surface, respectively, and is evaluated as;

$$S = i_o \frac{Y_{O_2}}{Y_{O_2, \text{ref}}} \exp\left(\frac{\alpha_c F}{RT} \eta\right) \quad (14)$$

The activation overpotential, η , used in Eqs (1), (6) and (14) is estimated as [24, 25];

$$\eta = \phi_{m,l} - \phi_{s,l} - \phi_{\text{ref}} \quad (15)$$

where $\phi_{m,l}$ and $\phi_{s,l}$ are the local membrane phase (protonic) and solid phase (electronic) potentials, respectively, and ϕ_{ref} is the reference potential that depends on the type of electrode. Since in this work, only the cathode catalyst layer has been focused, so the reference potential is set to 0 [26].

In order to simulate the temperature distribution inside the calculation domain, the energy conservation equation has been applied and consists of heat conduction through various media of the domain, ohmic heating due to flow of protons and electrons and the reaction heating [19].

$$0 = \nabla \cdot (\lambda \nabla T) + \frac{(\nabla \phi_s)^2}{\sigma_s} + \frac{(\nabla \phi_m)^2}{\sigma_m} + \nabla \cdot \left[i_o \frac{Y_{O_2}}{Y_{O_2, \text{ref}}} \exp\left(\frac{\alpha_c F}{RT} \eta\right) \right] (\eta + \Pi) \quad (16)$$

where Π is the Peltier coefficient for the oxygen reduction reaction approximated as [19, 27];

$$\Pi_h \approx T \frac{\Delta S_h}{4F} \quad (17)$$

ΔS_h is the entropy change for the half cell reaction and has been assumed a constant in this work.

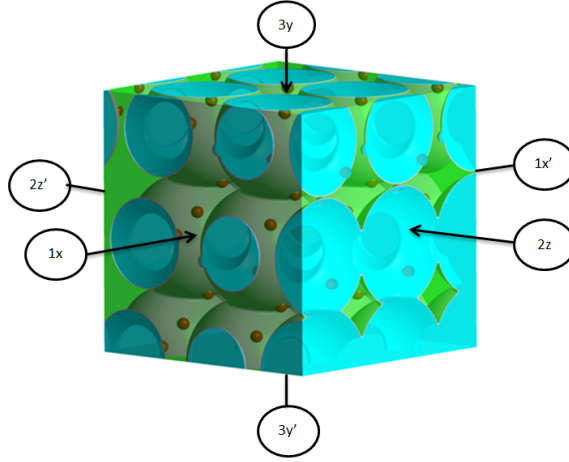


Fig. 5: Boundary faces for the computational domain.

3.1 Boundary Conditions and Numerical Solution Method

Since the sample of cathode catalyst layer represents the arbitrarily chosen portion, the boundary conditions applied are also symmetry/periodic except at the inlet and the outlet. For species transport, the inlet boundary conditions is applied at face 1x as given in Fig. 5 of the void region. For portions of ionomer and carbon spheres intersected by face 1x are set to be symmetry and wall, respectively. Similarly, the portion of void intersected by face 1x' is set to be outflow while the conditions for ionomer and the carbon particle remain same as the inlet. All other sides of the domain (2z, 2z', 3y and 3y') are selected as symmetric for the species, i.e., assuming similar operating conditions on all sides. The boundary condition for membrane phase potential is specified at the face 3y of the domain with continuity of ionic current on all sides except the left (face 1x) and right sides (face 1x') (sides coinciding with species inlet and outlet) where symmetric conditions are applied. For the present work the inlet concentration of species is specified as 0.21 and 0.1 for O_2 and H_2O , respectively, while the potential at the top side for membrane is a constant value of 1 volt.

All the calculations in this work have been performed using ANSYSTM FluentTM. Since only diffusive flow has been assumed in this work, all the governing equations have been solved using the User-Defined-Scalar (UDS) equations with appropriate under relaxation factors for each scalar quantity, given as;

$$-\frac{\partial}{\partial x_i} \left(\Gamma_k \frac{\partial \phi_k}{\partial x_i} \right) = S_{\phi_k} \quad k = 1, \dots, N \quad (18)$$

where Γ_k and S_{ϕ_k} are the diffusion and source term for each scalar variable being solved. In present case the variables being solved are species mass fraction, temperature, solid phase and membrane phase potential. The diffusion and source terms for the variables

are calculated and linked through the UDFs (User Defined Functions). The calculation domain is discretized into 0.49 million hybrid cells with varying mesh density for each material region. In order to verify the grid independency of the calculated results, all the calculations have been performed for various mesh densities ranging from 0.2 to 0.51 million cells. It was observed that by further increasing the mesh density above 0.49 million cells, there was no change in the calculated values of the scalar quantities. For spatial discretization of conservation equations, a 2nd order scheme has been utilized with convergence criteria limited to a difference of 1×10^{-6} between consecutive iterations. All the calculations were performed on i7 core with 8 GB of memory consuming approximately 20 hrs for the converged results.

Assumptions

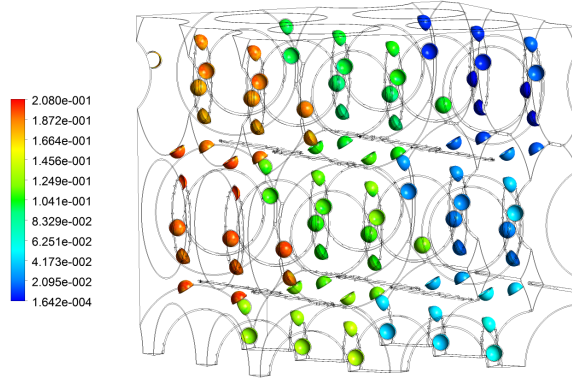
The following assumptions have been applied for this numerical work.

- there is no convective flow.
- to reduce the computing time, both carbon and Pt particles are omitted from the domain and are only represented by a wall boundary condition.
- electrons follow the same path as protons i.e., through ionomer (since, electrical conductivity is usually much higher than protonic conductivity). Also, the ohmic losses due to electron transfer are neglected.
- there are no dead regions in the domain, i.e., all Pt surfaces fulfil the TPB requirements.
- it has been assumed that water inflow due to osmotic drag is balanced by the back diffusion so the only source of water generation in the calculation domain is the electro-chemical reaction.

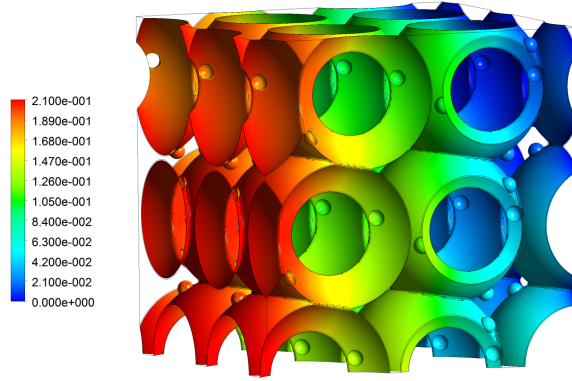
4 Results & Discussion

In this work, 3D micro-scale simulations have been performed for a arbitrary chosen segment of PEM FC cathode side catalyst layer. The electro-chemical reactions are assumed to occur at the interface of Pt particles and the ionomer, i.e., the TPB exists at the surface of the Pt particles satisfying the contact conditions to carryout the electro-chemical reactions. The TPB acts as a sink for the oxygen concentration due to reactions by converting to water. Moving away from the inlet boundary (face 1x) shows a decrease in the oxygen concentration. Since, as already stated, the outlet boundary (face 1x' for the species is treated as continuity, and there is no convective flow, an overall decrease in the concentration is also observed with reducing reaction rates at the TPBs in low concentration zones. Such a boundary condition, i.e., without specifying any outlet mass fraction, has been selected so that parametric effects can be observed for different concentrations of oxygen.

The diffusion coefficient of oxygen for this work is observed to be in the range of $1 \times 10^{-7} \text{ m}^2 \text{ s}^{-1}$ in void area, while the values typically used in macro models are in the range



(a) Triple phase boundary



(b) Ionomer outer surface

Fig. 6: Oxygen mass fraction distribution profile.

of 1×10^{-5} to $1 \times 10^{-6} \text{ m}^2 \text{ s}^{-1}$ [24, 25] showing a considerable mismatch. Additionally, it is also observed that at this scale, approximately 70% of the total diffusion effect is contributed by the knudsen effect where pore dimensions are based on the average of maximum and minimum size through-out the domain. As far as the diffusivity of oxygen in ionomer is concerned, the volume averaged value is calculated to be $6.2 \times 10^{-11} \text{ m}^2 \text{ s}^{-1}$. The oxygen has to diffuse through ionomer to reach the reaction surfaces, hence, the diffusivity of oxygen in ionomer can be considered as the limiting factor for the reaction rates. Although, the agglomerate catalyst model for macro-scale simulations accounts for the thickness of ionomer covering the agglomerate but practically neglects the local effects. The oxygen distribution for the present work is shown in Figs 6a and 6b, at TPB and ionomer interface, respectively.

Apart from oxygen concentration, the protonic conductivity also plays a major role in

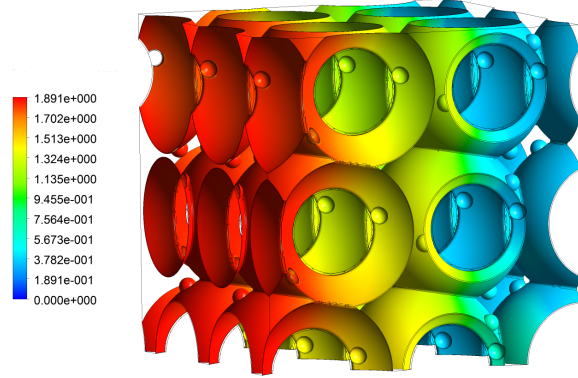


Fig. 7: *Protonic conductivity of ionomer as calculated in this work, S/m.*

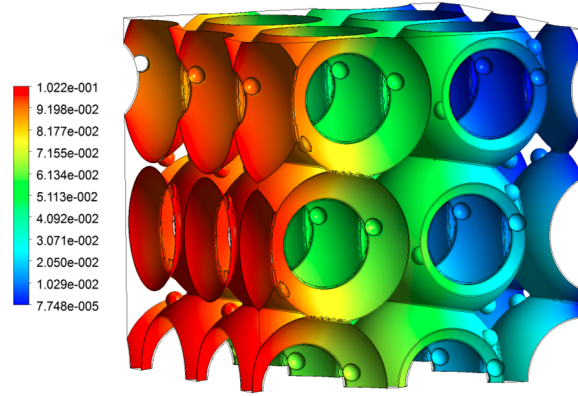


Fig. 8: *Water distribution profile in the ionomer portion of the CL.*

calibrating the reaction rate, which in turn is highly dependant on the water content of the ionomer. Since the reaction rate is higher near the inlet region, which means a higher water production, as seen in Figs 7 and 8 where both the profiles for water mass fraction and protonic conductivity almost overlap in terms of respective magnitude. Similarly, at the exit region, since the water content is quite low, both because of lower reaction rates and water diffusivity, the conductivity is reduced to almost 10~15% of the maximum . This represents another difference in micro- and macro-scale predictions, and in the later case the protonic conductivity has a maximum value of approximately 2.1 S/m and higher [28], depending on the local conditions. So, keeping in view the current analysis and given thickness of the ionomer surrounding the carbon particles, a much lower proton conductivity has been predicted which may significantly alter the macro-scale results depending on the local concentration of oxygen and the water saturation effects.

In the catalyst layer, most the parameters are also highly temperature dependant and

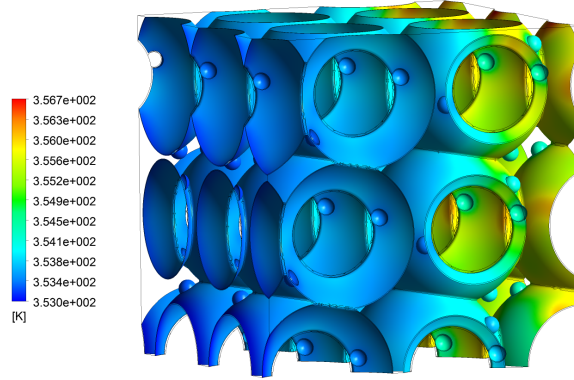


Fig. 9: *Temperature distribution profile in the CL, K.*

in order to perform in-depth analysis, prediction of temperature distribution has to be incorporated with thermal conductivity values adopted from Lange et al. [19]. In this work, the sources for temperature rise are heat released during electro-chemical reactions and the ohmic losses due to proton immigration. For the specific case implemented in this work, it has been observed that the heat released due to electro-chemical reactions only makes up 5~10% of the temperature rise while the major portion is contributed via ohmic losses especially in low conductivity region, as can be seen in Fig. 9. Near the inlet region the temperature rise is quite small (about 0.2 ~ 0.5 K) due to the reaction heat. But, the change in temperature becomes significant near the outlet region of the calculating domain (~3 K).

5 Conclusions

By using 3D commercial software, this study presents a reconstruction of the micro structure of PEMFC CL with 4 phases and TPB distribution. Pre-specified number of Pt particles combined with big carbon spheres are regularly placed in the domain, an ionomer layer of a given thickness is extruded from the sphere surfaces. The C/Pt, ionomer and void distribution, as well as the TPB are analyzed and discussed.

For simulating the species, charge transfer and temperature, a set of governing equations have been applied to study the effects at micro levels by assuming the diffusion mechanism only. The governing equations for species and temperature have been applied in both ionomer and void phase, while the charge transport equations are only applicable in the ionomer phase with appropriate boundary conditions. For species transport in the void phase, it is observed that the knudsen diffusion plays a major role as compared to bulk diffusion. Additionally, the reactions in the CL occur at the surface of Pt particles. The O_2 species has to diffuse through ionomer to reach the reaction site but at very low diffusion rates as limited by the material, representing one of the limitations in increasing the reaction rates. Also, it is observed that the protonic conductivity varies considerably depending on the local conditions i.e., water content. The region of the domain having

higher water content is coupled with higher conductivity but severe losses are exhibited at the water deprived region of the domain. The adverse effect noted due to lower conductivity is presented in form of higher temperature rise in that region.

It is also concluded that by performing the calculations at micro-levels, a more clear picture of the internal transport and reaction phenomena can be obtained with noticeable variations that are usually ignored in the macro-level due to averaging of properties. But, simulations at this scale require much more man-hour work and also need higher computing resources. Also, meshing at such levels requires both skills and extreme care to reduce errors in mating phases and to ensure continuity.

Acknowledgment

The European Research Council (ERC, 226238-MMFCS), the National Natural Science Foundation of China (No. 51009077) and for Dr. Y. Xiao the Erasmus Mundus External Cooperation Window Programme (EMECW) support the current research work.

Nomenclature

Roman Symbols

A	Area, m^2
D	diffusion coefficient, m^2s^{-1}
d	diameter, m
F	faraday's constant, $96485.34 \text{ C mol}^{-1}$
i	current density, A cm^{-2}
L	length, m
n_d	osmotic drag coefficient
p	pressure, Pa
R	universal gas constant, $8.3142 \text{ J mol}^{-1}\text{K}^{-1}$
r	radius, m
ΔS_h	change in entropy, $\text{J mol}^{-1}\text{K}^{-1}$
T	temperature, K
TPB	triple phase boundary
V	volume, m^3
Y	species mass fraction

Greek Symbols

α	cathodic transfer coefficient
δ	thickness, m
η	overpotential, V
Γ	diffusion coefficient for scalar quantity
λ	thermal conductivity, $\text{W m}^{-1}\text{K}^{-1}$
ω	relative humidity
ϕ	potential, V
Π	Peltier coefficient, J C^{-1}

σ charge conductivity, S m^{-1}

Subscripts & Superscripts

b	bulk
C	carbon
c	cathode
k	knudsen
l	local
m	membrane phase
o, ref	reference
p	pore
Pt	platinum
s	solid phase
t	total

References

- [1] Lange, K. J., Chinmay, M., Sui, P. C., and Djilal, N., 2011. "A numerical study on preconditioning and partitioning schemes for reactive transport in a PEMFC catalyst layer". *Comput. Methods Appl. Mech. Eng.*, **200**, pp. 905–916.
- [2] Siddique, N., and Liu, F., 2010. "Process based reconstruction and simulation of a three-dimensional fuel cell catalyst layer". *Electrochimica Acta*, **55**, pp. 5357–5366.
- [3] Moore, K. L., and Reeves, K. S., 2005. In DOE Hydrogen Program Annual Merit Review, 23-26 May, Arlington, USA.
- [4] Xie, Z., Navessin, T., Shi, K., Chow, R., Wang, Q., Song, D., Andreaus, B., Eikerling, M., Liu, Z., and Holdcroft, S., 2010. "Process based reconstruction and simulation of a three-dimensional fuel cell catalyst layer". *Electrochimica Acta*, **55**, pp. 5357–5366.
- [5] Liu, F., and Wang, C., 2006. "Optimization of cathode catalyst layer for direct methanol fuel cells. Part I. experimental investigation". *Electrochimica Acta*, **52**, pp. 1417–1425.
- [6] Lei, C., Bessarabov, D., Ye, S., Xie, Z., Holdcroft, S., and Navessin, T., 2011. "Low equivalent weight short-side-chain perfluorosulfonic acid ionomers in fuel cell cathode catalyst layers". *J. Power Sources*, **142**, p. 82.
- [7] Mukherjee, P., and Wang, C., 2006. "Stochastic microstructure reconstruction and direct numerical simulation of the PEMFC catalyst layer". *J. Electrochem. Soc.*, **153**, pp. A840–A849.
- [8] Lange, K., Sui, P., and Djilali, N., 2010. "Pore scale simulation of transport and electrochemical reactions in reconstructed PEMFC catalyst layers". *J. Electrochem. Soc.*, **157**, pp. B1434–B1442.

-
- [9] Barbosa, R., Andaverde, J., Escobar, B., and Cano, U., 2011. "Stochastic reconstruction and a scaling method to determine effective transport coefficients of a proton exchange membrane fuel cell catalyst layer". *J. Power Sources*, **196**, pp. 1248–1257.
- [10] Hu, J., Sui, P., and Djilali, N., 2008. "Numerical investigation on the transport in a PEMFC using a microstructure reconstruction technique". In Proceedings of the proton exchange membrane fuel cells, 12-17 Oct. Honolulu, USA.
- [11] Wang, G., Mukherjee, P., and Wang, C., 2006. "Direct numerical simulation (DNS) modeling of PEFC electrodes, Part I. regular microstructure". *Electrochimica Acta*, **51**, pp. 3139–3150.
- [12] Wang, G., 2003. Tech. rep., Ph.D. thesis, the Pennsylvania State University, USA.
- [13] Wang, G., Mukherjee, P., and Wang, C., 2006. "Direct numerical simulation (DNS) modeling of PEFC electrodes, Part II. random microstructure". *Electrochimica Acta*, **51**, pp. 3150–3160.
- [14] Mukherjee, P., and Wang, C., 2007. "Direct numerical simulation modeling of bilayer cathode catalyst layers in polymer electrolyte fuel cells". *J. Electrochem. Soc.*, **154**, pp. B1121–B1130.
- [15] Kim, S. H., and Pitsch, H., 2009. "Reconstruction and effective transport properties of the catalyst layer in PEM fuel cells". *J. Electrochem. Soc.*, **156**, pp. B673–B681.
- [16] Lange, K., Sui, P., and Djilali, N., 2011. "Pore scale modeling of a proton exchange membrane fuel cell catalyst layer: Effects of water vapor and temperature". *J. Power Sources*, **196**, pp. 3195–3203.
- [17] Ziegler, C., Thiele, S., and Zengerle, R., 2011. "Direct three-dimensional reconstruction of a nanoporous catalyst layer for a polymer electrolyte fuel cell". *J. Power Sources*, **196**, pp. 2094–2097.
- [18] Wilson, M., and Gottesfeld, S., 1992. "High performance catalyzed membranes of ultra-low Pt loadings for polymer electrolyte fuel cells". *J. Electrochem. Soc.*, **139**, pp. L28–L30.
- [19] Lange, K., Sui, P.-C., and Djilali, N., 2002. "A two phase flow and transport model for cathode of PEM fuel cells". *Int. J. Heat Mass Transfer*, **45**, pp. 2277–87.
- [20] Cussler, E., 2001. *Mass transfer in fluid systems*. Cambridge university press.
- [21] Pollard, W. G., and Present, R. D., 1948. "On gaseous self-diffusion in long capillary tubes". *Phys. Rev.*, **73**(7), pp. 762–774.
- [22] Lee, K., Ishihara, A., Mitsushima, S., Kamiya, N., and ichiro Ota, K., 2004. "Effect of recast temperature on diffusion and dissolution of oxygen and morphological properties in recast nafion". *J. Electrochem. Soc.*, **151**(4), pp. A639–A645.

-
- [23] Parthasarathy, A., Srinivasan, S., Appleby, A. J., and Martin, C. R., 1992. “Temperature dependence of the electrode kinetics of oxygen reduction at the platinum/naTM interface - a microelectrode investigation”. *J. Electrochem. Soc.*, **139**(9), pp. 2530–2537.
- [24] Sun, W., Peppley, B. A., and Karan, K., 2005. “An improved two-dimensional agglomerate cathode model to study the influence of catalyst layer structural parameters”. *Electrochimica Acta*, **50**(16-17), pp. 3359–3374.
- [25] Sun, W., Peppley, B., and Karan, K., 2005. “Modeling the influence of GDL and flow-field plate parameters on the reaction distribution in the PEMFC cathode catalyst layer”. *J. Power Sources*, **144**, pp. 42–53.
- [26] Harvey, D., Pharoah, J. G., and Karan, K., 2008. “A comparison of different approaches to modelling the PEMFC catalyst layer”. *J. Power Sources*, **179**(1), pp. 209–219.
- [27] Weber, A. Z., and Newman, J., 2006. “Coupled thermal and water management in polymer electrolyte fuel cells”. *J. Electrochem. Soc.*, **153**(12), pp. A2205–A2214.
- [28] Khan, M. A., 2009. Numerical simulation of multi-scale transport processes and reactions in pem fuel cells using two-phase models, ISRN LUTMDN/TMHP-09/7066-SE. Tech. rep., Lund University.

Paper D

Khan, M.A., Sundén, B., Yuan, J., 2011. “Numerical quantification of water saturation, back diffusion, electro-osmotic drag and water generation in polymer electrolyte membrane fuel cells”, (*submitted to Journal of Power Sources*)

Numerical quantification of water saturation, back diffusion, electro-osmotic drag and water generation in polymer electrolyte membrane fuel cells

Munir Ahmed Khan, Bengt Sundén, Jinliang Yuan

Abstract

A 3D unit cell has been simulated numerically using a commercial software in order to evaluate and quantify various water related phenomena, i.e., electro-osmotic drag, back diffusion, electro-chemical water generation and the saturation effects in the porous media. The water saturation effects were noticed to be more pronounced in the GDL of the cathode as compared to the catalyst layer due to greater pore dimensions. Also, a comparison of the water saturation effects were studied at different operating voltages of 0.7, 0.5 and 0.3 V. In case of 0.7 and 0.5 V, it was seen that the saturation effects were found to be located in the far region of the inlet because of the decreasing ability of air to accommodate more water. But, at the lower voltage of 0.3, the saturation effects started to appear in the inlet region too due to strong electro-osmotic drag and water generation due to electro-chemical reactions. The transfer of water from the cathode via back diffusion also increased accordingly by lowering the operating voltage. Additionally, the transfer rate of water due to the back diffusion was observed to be larger than the water addition due to both the electro-osmotic drag and the electro-chemical generation.

Key words: *Electro-osmotic drag, back diffusion, water saturation, electro-chemical water generation, fuel cells, PEM modelling, phase change.*

1 Introduction

Polymer electrolyte membrane (PEM) fuel cells offer bright perspective for future energy demands in various sectors especially mobile applications due to their compactness, efficiency and cost effectiveness [1]. Also, regular increase in energy demand and an urge to lessen the dependence on fossil fuels have also propagated the interest in fuel cells around the globe. Through recent technological advancements in fuel cells, many prototypes have been brought in use but the lack of confidence still persists in assuming PEM to be a true alternative to its predecessors especially in mobile units mainly because of two reasons. First, the conventional power sources, e.g., internal combustion engines and batteries are at the zenith of their technological maturity and their history of performance is excellent enough to make them forerunners in the competition and secondly, there are still various issues pending with PEMs that need to be resolved before placing them in line with its competitors. One of the all time problems faced by PEM fuel cell technologists is the complete understanding of the water management issue, which needs

greater attention.

For completion of the electrical circuit, the protons, generated at the anode of the fuel cell, have to travel through the membrane towards the cathode side with minimal resistance. Present PEM technology relies on NafionTM, a propriety of Du-PontTM, as a membrane material for low temperature operations (<100°C). The protonic conductivity of NafionTM is highly water dependent and it is very important that well hydrated conditions exist to reduce proton ohmic losses (for extended details the reader is referred to Larminie and Dicks [2]). Furthermore, the product of overall electro-chemistry in PEM fuel cells result in production of water at the cathode side, given as;



The production of water at the cathode side as given in Eq. (1) would ideally insure keeping the hydration level to the required conditions, while hot air blowing through would help in removing the excess water, but, in reality there are few complications associated with this phenomenon. There is always a water transfer across the membrane in both directions, i.e., from cathode to anode and vice versa. The *back diffusion* occurs from the cathode to the anode due to difference in water concentration on the respective sides because the thickness of the membrane used in PEM fuel cells is quite small [2]. Additionally, during the operation of the PEM fuel cell H⁺ ions migration from anode to cathode drag the water molecules with them, so-called the *electro osmotic drag*, and typically about 1 to 2.5 molecules of water are dragged for the transfer of each hydrogen ion [3]. So, it is essential to establish a balance in the water transfer from either sides so that optimum conditions can be achieved for the efficient operation of the cells.

Apart from keeping a balance between the water movement across the membrane, the water quantity in the membrane itself is very crucial for proper working of the PEM fuel cell. So, it is very important not only to keep the hydration to a required level but also to ensure thorough presence of water in the membrane [2] so that the local dryness or flooding can be avoided but unfortunately the two processes cannot be easily handled at the same time. The inlet gases are pre-humidified to a certain defined level so that they can wet the inlet region to achieve proper functioning. As the air passes through the cell the relative humidity in the cathode increases and may become saturated through the length of the cell, and liquid water might appear because of the decreased ability of air to carry more water.

The water saturation and phase change in the porous catalyst and gas diffusion layer have been termed as a real time performance and efficiency loss [4]. Additionally, the liquid water accumulation in the porous media also results in impurity of material characteristics, e.g., ionomer and hydrophobicity loss [5]. Therefore, the transport of liquid water in the porous media has been termed as the dominating factor that needs to be controlled very effectively and efficiently to achieve graded cell performance [6].

Analytical or experimental approaches to understand the water management issue will

be quite elaborative but the compact nature of the PEM fuel cell limits the ability to explore them experimentally. Comparatively, with latest technological advancements in computational fluid dynamics (CFD) analysis, more and more insight has been gained over the last decades by many researchers and the numerical modelling approach has outpaced the experimental data acquisition for the internal transport processes and other coupling phenomena. With the transport of liquid water being the key controlling factor, much effort has been spared to model and quantify the phenomena [7–9]. One of the common approaches to numerically model the liquid water transport in the porous media is the use of the conventional Leverett J -function [10, 11]. However, some researchers have recently reported a considerable deviation between the CFD results obtained via conventional approaches and the high-resolution neutron [12, 13] and X-ray imaging [14] because of the inability of the conventional function to handle the mixed wettability and heterogeneity characteristics of the porous media [15].

In this work, the water management issue has been given a thorough look in order to quantify and analyse the water transfer and the generation rates in the cathode of a PEM fuel cell. A validated capillary pressure approach has been used to evaluate the saturation levels in the porous media. Furthermore, quantification of the water addition due to electro-osmotic drag and electro-chemical reaction has been compared to the water removal rate due to the back diffusion. To match the as close to real scenario, complete model simulations have been performed by incorporating all the basic phenomena, e.g., species, heat and charge transport keeping in mind the electrical anisotropic properties of the porous media. Additionally detailed descriptions of each phenomena are provided at preselected operating voltages of 0.7, 0.5 and 0.3 volts.

2 Model Development and Solution Method

This section describes the working domain, the governing equations, applied boundary conditions and the solution methodology used for the present work and simulations.

2.1 Working Domain

The working domain of this work consists of a 3D section of a single fuel cell with interdigitated flow field. The electric poles of the cell are electrically insulated with a membrane. The electrodes on the either side consist of the catalyst layer (CL) where the electro-chemical reactions take place and the porous transport layer (PTL), also called gas diffusion layer. The current collectors are connected to PTL, also serving as external coolants for the system. The fuel (H_2) enters the domain at the anode side of the cell and after diffusing through the anodic PTL, it reacts at the anode CL splitting into hydrogen ions (H^+) and electrons (e^-). The hydrogen ions travel to the cathode side due to the potential difference via the membrane while electrons are forced through an external path. The membrane material used in PEM fuel cells is such selected that it poses higher resistance to the electrons whereas minimal resistance for hydrogen ions. At the cathode side, oxygen present in the inlet air reacts electro-chemically in presence of the catalyst (Pt) with hydrogen ions (via the electrolyte) and electrons (via the external

circuit) to produce water (H_2O) in the cathode CL.

Following simplifications are incorporated in the present work to limit the complexity and the time consumption for the simulated work.

- all processes are time independent (steady state).
- the gas behaves as an ideal gas.
- the gaseous flow is assumed to be laminar.
- liquid water is in the form of fine mist in the channels and moves with same velocity as the gases, while inside the porous media, both gas and solid phases can coexist.
- inside the porous media, the flow of liquid water is independent of the gas flow.
- there is no current loss at the interfaces, i.e., perfect connections are assumed between each component.
- to simulate the electro-chemical reactions the catalyst agglomerate model is used, and the local overpotential within an agglomerate is assumed to be constant.

2.2 Transport Phenomena and Governing Equations

For simulation of the flow field inside the gas channels, PTL and the CL, the continuity and the momentum equations are used, i.e.,

$$\frac{\partial}{\partial t}(\varepsilon\rho) + \nabla \cdot (\varepsilon\rho\vec{v}) = S \quad (2)$$

and

$$\frac{\partial}{\partial t}(\varepsilon\rho) + \nabla \cdot (\varepsilon\rho\vec{v}\vec{v}) = -\varepsilon\nabla p + \nabla \cdot (\varepsilon\mu\nabla\vec{v}) + \vec{F} - \frac{\varepsilon^2\mu\vec{v}}{\kappa} \quad (3)$$

where ε , ρ and μ are the porosity, density and the viscosity of the gases. The last term in Eq. (3) is the Darcy's pressure drop due to the resistance in the porous media. However, in gas channels the porosity is equal to unity and the permeability is infinite, so, there is no pressure drop due to porous media resistivity. \vec{F} incorporates the change in momentum due to generation or consumption of species in the catalyst layers of the cell.

In order to predict the local mass fraction X_i of the chemical species in the analysis domain, the conservation equation is used in the following general form;

$$\frac{\partial}{\partial t}(\varepsilon\rho X_i) + \nabla \cdot (\varepsilon\rho\vec{v}X_i) = -\nabla \cdot \vec{J}_i + R_i \quad (4)$$

when solving the species equation for O_2 and H_2 , the term R_i represents the consumption rate due to electro-chemical reactions. For water vapours, the source term consists of two processes, i.e., electro-chemical production and the addition or removal of water vapours due to phase change. \vec{J}_i in Eq. (4) is the diffusion flux of species i due to the concentration gradient, i.e.,

$$\vec{J}_i = -\rho \varepsilon^\tau D_{i,m} \nabla X_i \quad (5)$$

here $D_{i,m}$ is the mass diffusion coefficient for species i in the mixture based on multi-component diffusion with Knudsen effect because of small pore dimensions. It should be remembered that $\varepsilon = 1$ for the channels, and Eq. (5) reduces to the ordinary form without any correction for the porous media. For details regarding incorporating the Knudsen effects in the multi-component diffusion of species, the reader is referred to [10, 11, 16]. The energy conservation equation used in present simulation work is given as;

$$\frac{\partial}{\partial t}(\rho c_p T) + \nabla \cdot (\rho \vec{v} c_p T) = \nabla \cdot q'' + S_h \quad (6)$$

where q'' is the heat flux accounting for the contribution from heat conduction and the species diffusion.

$$q'' = \lambda_{\text{eff}} \nabla T + \sum J_i h_i \quad (7)$$

where J_i and h_i are the species diffusion flux and the enthalpy of gas phase species, respectively. The effective thermal conductivity in the porous media, λ_{eff} , is calculated as [17];

$$\lambda_{\text{eff}} = -2\lambda_s + \frac{1}{\frac{\varepsilon}{2\lambda_s + \lambda_f} + \frac{1-\varepsilon}{3\lambda_s}} \quad (8)$$

where λ_s and λ_f are the thermal conductivities of the solid-matrix and the fluid phase. Furthermore, in present formulation, it is assumed that all the phases (gas, liquid and solid) are in thermal equilibrium, while for the channels, λ_{eff} is evaluated for the gas mixtures only based on the mixing law.

Since not all chemical energy of the reacting species is converted to electrical work, rather some is wasted in form of heat that are incorporated as a source term S_h in Eq. (6) (in form of enthalpy change due to reactions, evaporation and condensation, and ohmic losses, etc.)

Since PEM fuel cells work at temperature conditions of 70 to 80°C, condensation of water vapours into liquid is a regular phenomena, especially at higher current densities when the reaction rate is high. In this work, the liquid water formation and transport

are evaluated in terms of volume fraction of liquid water, s , by applying the following conservation equation;

$$\frac{\partial}{\partial t}(\varepsilon \rho_l s) + \nabla \cdot (\rho_l \vec{v}_l s) = \dot{\omega} \quad (9)$$

where ρ_l and $\dot{\omega}$ are the liquid phase density and the rate of evaporation or condensation based on the partial pressure of water in the gas phase, respectively, and, \vec{v}_l represents the velocity of liquid water. In the gas channels, the liquid is assumed to occur in fine mist form and moves with the same velocity as the gas phase, while in the porous media, since the governing transport mechanism is the capillary action through the pores, so, the convective term is replaced with the capillary diffusion term, given as;

$$\frac{\partial}{\partial t}(\varepsilon \rho_l s) + \nabla \cdot \left[\rho_l \frac{K s^3}{\mu_l} \frac{dp_c}{ds} \nabla s \right] = \dot{\omega} \quad (10)$$

where K and μ_l are the absolute permeability of the porous material and the liquid water viscosity, respectively. $\dot{\omega}$ is rate of mass transfer between the gas and liquid phases and p_c is the capillary pressure and in this work it is calculated based on the validated approach presented by Kumbur et al. [15, 18, 19], as;

$$P_c = \left(\frac{293}{T} \right)^6 \gamma(T) 2^{0.4C} \sqrt{\frac{\varepsilon_c}{k}} K(s) \quad (11)$$

where $K(s)$ is the validated saturation function based on the PTFE loading and the saturation. The clogging of the porous media and the flooding of the reaction surface are modelled by multiplying the porosity and the active surface area by $(1 - s)$, respectively. The electro-osmotic water source due to proton migration from anode to cathode is treated as;

$$\nabla \cdot S_{\text{EOD}} = \pm \frac{n_d \sigma_m}{F} \nabla \phi_m \quad (12)$$

where $\nabla \cdot S_{\text{EOD}}$ is the source term used to account the effect of water addition at the cathode catalyst layer due to the drag of water molecules with protonic migration and n_d is the electro-osmotic drag coefficient and depends on the local water content and the sign convention refers to the source in cathode catalyst layer or the sink in the anode catalyst layer when solving Eq. (4) for water as an extra source term. The back diffusion flux of water due to the concentration difference between the cathode and the anode catalyst layer at the interface of membrane and the catalyst layers on both sides is given as;

$$J_w^{\text{diff}} = - \frac{\rho_m}{M_m} M_{\text{H}_2\text{O}} D_1 \nabla \lambda \quad (13)$$

where ρ_m and M_m are the density and the equivalent weight of the dry membrane, respectively. λ is the local water content and can be obtained using the correlation by Springer et al. [20] and D_1 is the membrane water diffusivity and is a function of both temperature and the total (gas and liquid) water content [8].

In PEM fuel cells, there are two types of charges, i.e., H^+ and e^- , under electro-neutral conditions, and the continuity in flow of both the charges is simulated as;

$$\nabla \cdot \mathbf{i} = 0 \quad (14)$$

Since the charge flow in PEM fuel cells follows different paths, i.e., the electrons flow through external path while hydrogen ions transverse via the membrane (polymer), two equations are employed for the potentials causing the charge flow, as;

$$\nabla \cdot (\sigma_s \nabla \phi_s) + S_s = 0 \quad (15)$$

and

$$\nabla \cdot (\sigma_m \nabla \phi_m) + S_m = 0 \quad (16)$$

where σ_m is the protonic conductivity of the ionomer given by Springer et al. [20] and modified by Das et al. [21] to accommodate the porous media effects while σ_s is the tensor of electronic conductivity of the solid-matrix with different in-plane and through-plane values [22], and ϕ_m and ϕ_s are the respective charge potentials. The source terms S_s and S_m in Eqs (15) and (16) represent the transfer currents due to anodic and cathodic electro-chemical reactions. The total electrical current produced in the cathode and the anode catalyst layers is the same, so, the current conservation has been achieved by balancing both the anodic and cathodic reaction rates, given as:

$$\int_c R_c dV = \int_a R_a dV \quad (17)$$

In PEM fuel cells, the electro-chemical reactions occur in the catalyst layers at anode and cathode. Since the electro-chemical reactions are the heart of PEM fuel cells, many models have been proposed to date with varying complexity. Among all, the agglomerate model is the most descriptive in nature as it accounts for more physical processes including the actual morphology of the catalyst layer, as compared to others [23]. The current density divergence, based on the agglomerate model, is used in this work [24, 25].

$$\nabla \cdot \mathbf{i}_{X_i} = zF \frac{P_{X_i}}{H_i} \left(\frac{1}{E_r k_{a,c} (1 - \varepsilon_{a,c})} + \frac{(r_{agg} + \delta) \delta}{a_{agg} r_{agg} D_{i-naf}} \right)^{-1} \quad (18)$$

The detailed discussion regarding Eq. (18) and its implementation in CFD analysis can be found in [10, 23, 24]. The source terms based on Eq. (18) (agglomerate model) for the species, energy and charge transport are listed in Table 2.

2.3 Numerical solution

A unit PEM fuel cell has been simulated numerically in this work as shown in Fig. 1. Dynamic mesh adoption has been used to obtain mesh independency with different mesh density for each component. Keeping in view the pressure-velocity coupling SIMPLEC scheme has been utilized and all other variables have been discretized using the QUICK scheme. The inlet boundary conditions for the species have been set to mass flow rate while the outlet is fixed as the out flow at atmospheric conditions. The sides of the unit cell have been assumed symmetric while the ends are impermeable wall for all variables as shown in Fig. 1. Pre-humidified air enters into the cathode side at fixed rate of 3×10^{-6} kg/s at 343 K with air/fuel (A/F) ratio of 8. The unit is also assumed to be cooled ideally at both the anode and cathode current collector boundaries at 343 K and the same boundary is used to define the operating voltage to simulate the charge conservation equations.

3 Results and Discussion

3.1 Liquid Water Saturation

The materials used in manufacturing of PEM fuel cell porous electrodes is highly heterogeneous in nature representing mixed wettability properties and the standard formulation for modelling the water saturation is considered ineffective for such calculations due to such material property [15]. Also, the effects of hydrophobic (PTFE) loading, assembly compression and the operating temperature on the capillary transport mechanism are not incorporated in the standard approach. The validated approach for modelling the water saturation is compared to the extended (conventional) leverett approach in Fig. 2. As it can be seen that the capillary pressure calculated with PTFE content of 5% is almost comparable with the extended leverett model. But by increasing the hydrophobicity of the material i.e., more PTFE loading, the difference is significant to be neglected. Additionally, between 10% and 20% PTFE loading, both profiles follow a similar pattern until the saturation level is approximately 0.25, but after this, the increase in the capillary pressure for higher PTFE loading (20%) is higher than that for the 10% loading. For this work, the PTFE content of 10% has been used as the standard loading. The advantage associated with such approach is that the validated formulation eliminates the need for selecting a representative contact angel. Furthermore, it correlates the water saturation to material properties thus accounting for the structural heterogeneity.

Excluding the back diffusion that transports the water out of the cathode of PEM fuel cell (gas diffusion and catalyst layer), all other processes such as inlet humidification, electro-osmotic drag, condensation and electro-chemical generation of water make the

cathode more vulnerable to liquid saturation effects. Fig. 3 shows the different water saturation patterns at the cathode side of PEM fuel cell for various operating voltages (0.7, 0.5 and 0.3 volts). As it can be seen that at 0.7 V operating level, Fig. 3a, the water saturation level is minimum near the inlet region. But as the air flows through the domain, the relative humidity becomes higher because of water production due to electro-chemical reactions and the capacity to hold the water decreases as it transverses through the domain. At the far region of inlet, the water saturation increases because, as explained, the capacity of air to hold water reduces. At 0.5 V, Fig. 3b, the water saturation profile follows the same pattern as at 0.7 V but the maximum level of water saturation has increased owing to the fact that the rate of electro-chemical reactions has also increased due to increased current density. The water saturation profile at 0.3 V, Fig. 3c, shows increased levels near the air inlet region as compared to other cases due to the fact that the rate of electro-chemical reactions is quite high at such voltages and the capacity of air to collect more water vapours has reduced considerably.

Other water saturation trend noteworthy in Figs 3a to 3c is the location of maximum effect along the same cross-section being on the left side corresponding to the region near and above the inlet channel. These higher saturation levels suggest that most of the water accumulation in the PEM fuel cell domain occurs near the inlet region. Since the flow field used in present work has interdigitated design where inlet channel and outlet channel are not directly connected as in the case of conventional flow fields, so the pressure field formed due to such configuration helps preventing the formation of liquid film at the interface of the GDL and the channel.

Comparing the liquid water saturation in the same cross-sections also reveals that GDL shows more storage capacity than the catalyst layer. As can be seen in Fig. 3, most of the liquid water accumulation occur in the GDL zone. This accumulation can be attributed to the fact that GDL has higher pore radius than the catalyst layer and the capillary pressure being inversely proportional to the pore radius, thus the water accumulation in GDL is more as compared to the catalyst layer.

3.2 Electro-Osmotic Drag

Electro-osmotic drag of the water molecules occurs when the protons migrate from the anode to the cathode via the electrolyte for the completion of electric circuit. These protons combine in the cathode catalyst layer in presence of a catalyst (Pt) with oxygen and the electrons from the external circuit to produce water. The drag of water makes up another reason for addition of water to the cathode alongside the electro-chemical reactions. The pattern distribution for the electro-osmotic drag for the present work is shown in Fig. 4 for 0.7, 0.5 and 0.3 V at the interface of the cathode and the membrane of the PEM fuel cell. Fig. 4a shows the electro-osmotic drag coefficient for the operating voltage of 0.7 V. The maximum value occurs near the inlet of the cathode. It can be also noted that high values of the electro-osmotic drag occur above the inlet channel as compared to outlet channel or the region above the current collector. Since at higher voltage levels the current density is low which indicates less migration of protons from anode to cathode thus limiting the maximum value of electro-osmotic drag coefficient

to 1.16 as compared to other operating levels (1.38 and 1.55, respectively). Similarly, at operating voltage of 0.5 V, Fig. 4b, the pattern follows the same distribution as for the one given in Fig. 4a, but the range of the coefficient is between 0.70 to 1.38 that also indirectly means increase in the current density. Comparing Fig. 4c to Figs 4a and 4b indicates that the range of electro-osmotic drag has increased to higher values between 0.89 to 1.5 but the distribution pattern follows the similar trend. Additionally, by studying the electro-osmotic drag pattern, it can be seen that highest coefficients occur above the inlet channel for all operating voltages, i.e., most of the electro-chemical reactions occur in the region of the catalyst layer nearest to the inlet channel.

Along the length of the the inlet channel, there is also a decreasing trend in the electro-osmotic drag coefficient. The peak value is located near the inlet region (50 mm in Fig. 5) and the minimum is observed at the opposite end. Comparing the electro-osmotic drag coefficients for the different operating voltages in Fig. 5, it can be found that, for all operating levels, there is a higher rate of decrease at the near and far ends corresponding to the inlet and blocked end of the inlet channel, while a linear trend is represented within the body of the cell. The initial decrease in the coefficient of the electro-osmotic drag can be explained by considering the higher rate of the electrochemical reactions because of the fresh air inlet. At the blocked end of the channel, the decrease in the coefficient can be coupled with the boundary conditions used in the present work. Since both the front and the back end of the working domain have been labelled as wall boundary condition, except for the inlets and the outlets (Fig. 1), the stagnation zones occur in the corner of the inlet pressure channel at the blocked end, so the rate of reaction is lower as compared to rest of the length.

3.3 Back Diffusion

The generation of water via the electro-chemical reactions in the cathode and the water drag from anode to cathode during proton migration add up the amount of water in the cathode side. In ideal situations, the water generation or accumulation due to the reasons stated before should suffice to keep the well hydrated state inside the PEM fuel cell. But it has been observed that the increase in the concentration of water at the cathode side generates a concentration difference across the thin membrane between the anode and the cathode. Due to this difference of the concentration, there is always a water back diffusion from the cathode to anode via the membrane to balance the difference. The back diffusion, being concentration dependant, varies for different operating voltages. As can be seen in Fig. 6, comparatively, the back diffusion source (mathematically, the back diffusion is a sink term represented by a minus sign for the cathode side of the PEM fuel cell, but here it has been multiplied by -1 for the sake of comparison) is minimum for the operating voltage of 0.7 but as the voltage increases the back diffusion also increases due to both increase in the electro-chemical reaction rate and the electro-osmotic drag which cause a considerable increase in the water quantity at the cathode side. Also, comparing the water removal and addition in the cathode due to the back diffusion and the electro-osmotic drag, respectively, it can be seen that water removal rate is much higher even at the higher voltage levels, when the both the electro-osmotic drag coefficient and the water generation due to the electro-chemical reactions are quite

low (i.e., low current density). Additionally, the water removal rate due to back diffusion at all operating voltages is always more than the combined effect on water addition due to the electro-osmotic drag and the electro-chemical generation. It can also be observed that at lower higher operating voltages, the difference is quite large. But as the operating voltage is decreased, the difference in water generation and removal from the cathode is also reduced which also indicates the increase in electro-chemical reaction rate and the osmotic drag.

In Fig. 6 the water generation rate due to the electro-chemical reactions has been compared to those by the back diffusion and electro-osmotic drag sources. There are two significant unique trends in terms of the electro-chemical water generation rate. Firstly, by comparison it can be observed that the water generation rate in the cathode of the PEM fuel cell is less than the water addition due to the electro-osmotic drag and difference becomes exaggerated at lower voltages as compared to the high voltage level. This difference in the generation of water due to osmotic drag and electro-chemical reaction is due to the fact that the volume averaged value of the electro-osmotic drag coefficient is higher than unity in all cases. Secondly, by observing Fig. 6, it can be seen that the water production rate increases by reducing the operating voltage, as expected, because of the enhanced rate of electro-chemical reactions, but, from reducing the voltage level from 0.7 to 0.5 V, the increase in the water generation due to the electro-chemical reactions is approximately 60%. Whereas, by decreasing the voltage from 0.5 to 0.3 V, the increase in the average electro-chemical water generation is only ~11%. Thus, the small increase in the water generation rate at low operating voltage (0.3 V) due to electro-chemical reactions indicate the concentration losses have increased considerably and fuel cell is operating in the mass limitation range.

3.4 Validation

The CFD analysis involve a solution of set of mathematical equations and parameters simultaneously. In order to keep the solution in manageable limits both in terms of time and computations, there are always some simplifications applied to the governing equations. Furthermore, usually the parameters used in modelling of PEM fuel cells simulations are borrowed from open literature and not all of them have been validated due to the practical limitations in the experimental work and the large diversity of the precesses occurring inside the fuel cell [5]. Furthermore, the characteristics presented by each component of the fuel cell are quite different and and same physical process may vary in different components. So, the validation of the results for CFD modelling have prime importance as they determine the applicability of certain set of assumptions, simplifications and the parametric values.

Usually, for CFD modeling of PEM fuel cells, the V-I curve has become a standard to compare the results of modelling and experimental work. However, the applicability of such comparison is questionable because the V-I curve only presents the overall effect. As stated by Mench [5], there can be a good agreement between the models based on a simple V-I curve but internal parameters can be quite different, e.g., the under-prediction of one parameter may be balanced by the over prediction of the other. Furthermore, the

comparison of different models to each other based on the V-I curve can also be ambiguous because the operating conditions set in one model may not be applicable to others or not all operating conditions are stated in the literature.

Despite of urgent need to address the validation limitations stated above, this work has been compared to the add-on PEM fuel cell module by FluentTM, with similar operating conditions. As can be seen in Fig. 7, there is an overall difference in the magnitude of the current density profile for a specific cell voltage arising due to the fact that the add-on module utilizes Butler-Volmer kinetics for simulating the electro-chemical reactions while in this work an improved agglomerate model presented by Sun et al. [24] has been employed which is more conservative by considering the structural limitations of the catalyst layer. The other difference between the two cases is the sudden dip of the V-I curve at higher current densities in present model due to the fact that Butler-Volmer kinetics cannot account for the concentration losses at higher current densities and always over-predicts by large amount.

4 Conclusions

In this work a section of a PEM fuel cell with an interdigitated flow field has been numerically simulated to study the water management issue over water saturation effects, covering the back diffusion, the electro-osmotic drag and the electro-chemical generation of water. In order to study the above stated phenomena, all the basic processes have also been included e.g., species transport, heat generation and transport, and the charge transfer, etc. For simulating the electro-chemical reactions, the advanced agglomerate model has also been included. Additionally, keeping in view the anisotropy of electrical conductivity of the porous media, the electrical conductivity has been assumed to vary between in-plane and through-plane directions to match the real conditions as close as possible. Furthermore, for modelling the liquid water transport in the cell, a experimentally validated approach has been applied.

Studying the water saturation behaviour for various operating voltages revealed that the maximum saturation appears in the cathode region adjacent to the inlet channel. The water saturation also increases by operating the cell at lower voltages due to increase in the electro-chemical generation and the osmotic drag of water from the anode side. Also, the ability of flowing air to extract water from the domain also reduces due to increase in the partial pressure of water vapours as it passes through the porous media (which results in condensation of water vapour to liquid state). For operating voltages from high to medium range, it was noted that the maximum saturation levels occur at the outlet region of the porous medium. But lower the voltage to small values indicated a shift in maximum water saturation levels to inlet region due to enhanced electro-chemical reaction rates and the electro-osmotic drag. Similarly, the material used for constructing the GDL exhibit larger pore radius as compared to the catalyst layer, the water saturation effects were more prominent in the GDL of the cathode.

The predictions of electro-osmotic drag in the present work reveals that for all operating

voltages, the maximum drag from the anode to the cathode occurs at the interface of the cathode catalyst layer and the membrane, directly above the inlet channel. It can be concluded that most of the electro-chemical reactions take place at the same region, so, the utilization of the catalyst material in the most of the domain is not performing at the optimum or at their capacity. Additionally, it was also observed that for operating voltages of 0.7 to 0.3 V, the volume averaged electro-osmotic drag coefficient varied between 1.01 to 1.31, respectively.

The back diffusion, caused due to water concentration gradients between the anode and the cathode, was found to be always higher than water addition due to both electro-osmotic drag and the electro-chemical generation. So, the extra amount needed to balance the water removal due to back diffusion and the carrying away by the hot air passing through the porous media by pre-humidification. Furthermore, the difference in the back diffusion and water addition was found to be maximum at the higher voltages but by reducing the operating voltage it was noticed that the difference was also reduced.

The decrease in operating voltage causes an increase in the water generation rate due to the enhanced electro-chemical generation of water, but, the increase in the generation rate is limited at very low voltages due to the concentration losses occurring at such levels. Since, the electro-osmotic drag coefficient, as calculated in present work, is always larger than unity, so the water addition rate due to osmotic drag was more than the water addition due to the electro-chemical reactions.

Acknowledgements

The European Research Council (ERC, 226238-MMFCs) supports the current research.

Nomenclature

Roman Symbols

a	specific area, m^2
C	compression pressure, Pa
c_p	constant-pressure heat capacity, $\text{J kg}^{-1}\text{K}^{-1}$
D	diffusion coefficient, m^2s^{-1}
E_r	effectiveness of spherical agglomerates
F	faraday constant, C mol^{-1}
H	Henry's constant, Pa m mol^{-1}
\mathbf{i}	current density vector, A m^{-2}
\vec{J}	diffusion flux, $\text{kg m}^{-1}\text{s}^{-1}$
k	reaction rate, s^{-1}
$K(s)$	water saturation function
M_M	equivalent weight of the dry membrane
n_d	electro-osmotic drag coefficient
p	pressure, Pa
q''	heat flux, W m^{-2}

R	transfer current, A m ⁻³
r	radius of agglomerate
S	transfer current or electro-chemical source, A m ⁻³
T	temperature, K
\vec{V}	liquid velocity, m s ⁻¹
\vec{v}	velocity vector, m s ⁻¹
X	mass fraction of species
z	number of electrons

Greek Symbols

δ	thickness of ionomer covering agglomerate, m
ε	porosity
γ	surface tension, N m ⁻¹
κ	permeability, m ²
λ	thermal conductivity, W m ⁻¹ K ⁻¹
λ	water content (Eq. (13))
μ	viscosity, kg m ⁻¹ s ⁻¹
ϕ	charge potential, V
ρ	density, kg m ⁻³
σ	charge conductivity, S m ⁻¹
τ	tortuosity

Subscripts & Superscripts

$\dot{\omega}$	condensation rate, kg m ⁻³ s ⁻¹
a	anode
agg	agglomerate
C	compression
c	cathode
eff	effective
EOD	electro-osmotic drag
f	fluid phase
i	species identity
M	membrane
m	membrane phase
naf	nafion
s	solid phase

References

- [1] Sundén, B., and Faghri, M., 2005. *Transport Phenomena in Fuel Cells*. Devel. Heat Transfer. WIT Press, Southampton.
- [2] Larminie, J., and Dicks, A., 2003. *Fuel Cell Systems Explained*, 2nd ed. John Wiley & Sons Ltd., West Sussex.
- [3] Zawodzinski, J. T. A., Derouin, C., Radzinski, S., Sherman, R. J., Smith, V. T.,

- Springer, T. E., and Gottesfeld, S., 1993. "Water uptake by and transport through NafionTM 117 membranes". *J. Electrochem. Soc.*, **140**(4), pp. 1041–1047.
- [4] Mench, M. M., 2008. *Fuel cell engines*. John Wiley & Sons, Hoboken, New Jersey.
- [5] Mench, M. M., 2010. *Advanced modeling in fuel cell systems: a review of modeling approaches*. Wiley-VCH Verlag GmbH & Co. KGaA, Weinheim, pp. 89–118.
- [6] Borup, R., Meyers, J., Pivovar, B., Kim, Y. S., Mukundan, R., Garland, N., Myers, D., Wilson, M., Garzon, F., Wood, D., Zelenay, P., More, K., Stroh, K., Zawodzinski, T., Boncella, J., McGrath, J. E., Inaba, M., Miyatake, K., Hori, M., Ota, K., Ogumi, Z., Miyata, S., Nishikata, A., Siroma, Z., Uchimoto, Y., Yasuda, K., Kimijima, K.-i., and Iwashita, N., 2007. "Scientific aspects of polymer electrolyte fuel cell durability and degradation". *Chem. Rev.*, **107**(10), pp. 3904–3951.
- [7] Hwang, J. J., 2007. "A complete two-phase model of a porous cathode of a PEM fuel cell". *J. Power Sources*, **164**(1), pp. 174–181.
- [8] He, G., Yamazaki, Y., and Abudula, A., 2009. "A droplet size dependent multiphase mixture model for two phase flow in PEMFCs". *J. Power Sources*, **194**(1), pp. 190–198.
- [9] Senn, S., and Poulikakos, D., 2005. "Multiphase transport phenomena in the diffusion zone of a PEM fuel cell". *J. Heat Transfer*, **127**, pp. 1245–59.
- [10] Khan, M. A., Sundén, B., and Yuan, J., 2009. *Numerical simulation of multi-scale transport processes and reactions in PEM fuel cells using two-phase models*. Licentiate Thesis, ISRN LUTMDN/TMHP-09/7066-SE, Lund University, Lund.
- [11] Khan, M. A., Sundén, B., and Yuan, J., 2011. "Analysis of multi-phase transport phenomena with catalyst reactions in polymer electrolyte membrane fuel cells - A review". *J. Power Sources*, **196**(19), pp. 7899–7916.
- [12] Turhan, A., Kim, S., Hatzell, M., and Mench, M. M., 2010. "Impact of channel wall hydrophobicity on through-plane water distribution and flooding behavior in a polymer electrolyte fuel cell". *Electrochimica Acta*, **55**(8), pp. 2734–2745.
- [13] Weber, A. Z., and Hickner, M. A., 2008. "Modeling and high-resolution-imaging studies of water-content profiles in a polymer-electrolyte-fuel-cell membrane-electrode assembly". *Electrochimica Acta*, **53**(26), pp. 7668–7674.
- [14] Hartnig, C., Manke, I., Kuhn, R., Kardjilov, N., Banhart, J., and Lehnert, W., 2008. "Cross-sectional insight in the water evolution and transport in polymer electrolyte fuel cells". *Appl. Phys. Letters*, **92**(13), p. 134106.
- [15] Kumbur, E. C., Sharp, K. V., and Mench, M. M., 2007. "A validated leverett approach to multi-phase flow in polymer electrolyte fuel cell diffusion media. Part I. Hydrophobicity effect". *J. Electrochem Soc*, **154**, pp. B1295–B1304.
- [16] Yuan, J., Lv, X., Sundén, B., and Yue, D., 2007. "Analysis of parameter effects on the transport phenomena in conjunction with chemical reactions in ducts relevant for methane reformers". *Intl. J. Hydrogen Energy*, **32**, pp. 3887–98.

-
- [17] Frano, B., 2005. *PEM Fuel Cells*. Theory and Practice. Academic Press, Burlington.
- [18] Kumbur, E. C., Sharp, K. V., and Mench, M. M., 2007. "A validated leverett approach to multi-phase flow in polymer electrolyte fuel cell diffusion media. Part II. Compression effect and capillary transport". *J. Electrochem Soc.*, **154**, pp. B1305–B1314.
- [19] Kumbur, E. C., Sharp, K. V., and Mench, M. M., 2007. "A validated leverett approach to multi-phase flow in polymer electrolyte fuel cell diffusion media. Part III. Temperature effect and unified approach". *J. Electrochem Soc.*, **154**, pp. B1315–B1324.
- [20] Springer, T., Zawodzinski, T., and Gottesfeld, S., 1991. "Polymer electrolyte fuel cell model". *J. Electrochem Soc.*, **138**, pp. 2334–42.
- [21] Das, P., Li, X., and Liu, Z.-S., 2010. "Effective transport coefficient in PEM fuel cell catalyst and gas diffusion layers: Beyond Bruggeman approximation". *Appl. Energy*, **87**, pp. 2785–2796.
- [22] Pharoah, J. G., Karan, K., and Sun, W., 2006. "On effective transport coefficients in PEM fuel cell electrodes: Anisotropy of the porous transport layers". *J. Power Sources*, **161**(1), pp. 214–224.
- [23] Harvey, D., Pharoah, J. G., and Karan, K., 2008. "A comparison of different approaches to modelling the PEMFC catalyst layer". *J. Power Sources*, **179**(1), pp. 209–219.
- [24] Sun, W., Peppley, B. A., and Karan, K., 2005. "An improved two-dimensional agglomerate cathode model to study the influence of catalyst layer structural parameters". *Electrochimica Acta*, **50**(16-17), pp. 3359–3374.
- [25] Sun, W., Peppley, B., and Karan, K., 2005. "Modeling the influence of GDL and flow-field plate parameters on the reaction distribution in the PEMFC cathode catalyst layer". *J. Power Sources*, **144**, pp. 42–53.
- [26] Dawes, J. E., Hanspal, N. S., Family, O. A., and Turan, A., 2009. "Three-dimensional CFD modelling of PEM fuel cells: An investigation into the effects of water flooding". *Chem. Eng. Sci.*, **64**(12), pp. 2781–2794.
- [27] Grujicic, M., and Chittajallu, K., 2004. "Design and optimization of polymer electrolyte membrane (PEM) fuel cells". *Appl. Surface Chem.*, **227**, pp. 56–72.

Table 1: *Values of parameters [8, 10, 23–27].*

Physical properties	Value	Units
Faraday's constant, F	96487	C mol ⁻¹
Permeability of the electrodes, κ	8×10^{-10}	m ²
Thickness of the cell, t_{cell}	1.662	mm
Width of the cell, w_{cell}	2.4	mm
Length of the cell, l_{cell}	50	mm
Thickness of the catalyst layer, t_{cat}	0.012	mm
Thickness of membrane, t_{mem}	0.018	mm
Thickness of gas diffusion layer, t_{gdl}	0.21	mm
Porosity of gas diffusion layer, ε_{gdl}	0.4	
Porosity of catalyst layer, ε_{cl}	0.112	
Compression pressure, C	0.6	MPa
Cell operating pressure, P	1.5	atm
Inlet O ₂ mass fraction, $X_{\text{O}_2}^{\text{inlet}}$	0.2	
Inlet H ₂ O mass fraction, $X_{\text{H}_2\text{O}}^{\text{inlet,c}}$	0.13	
Inlet H ₂ mass fraction, $X_{\text{H}_2}^{\text{inlet}}$	0.51	
Inlet H ₂ O mass fraction, $X_{\text{H}_2\text{O}}^{\text{inlet,a}}$	0.49	
Operating temperature, T	343	K
Evaporation rate constant, k_{evp}	100	s ⁻¹
Condensation rate constant, k_{con}	100	atm ⁻¹ s ⁻¹
Universal gas constant, R	8.314	J mol ⁻¹ K ⁻¹
Density of liquid water, ρ_l	998	kg m ⁻³
Weight percentage of PTFE loading, wt%	10%	
Thickness of ionomer covering, δ	10	nm
Agglomerate surface area, a_{agg}	3.6×10^5	m ² m ⁻³
Agglomerate radius, r_{agg}	1	μm
Operating pressure, p	1.5	atm
Mass of dry membrane, M_{m}	2000	kg m ⁻³
Density of dry membrane, ρ_{m}	1.1	kg mol ⁻¹
Henry's constant, O ₂	3.2×10^4	Pa m ³ mol ⁻¹
Henry's constant, H ₂	3.9×10^4	Pa m ³ mol ⁻¹

Table 2: Source terms for species, charge and energy transport based on Eq. (18).

Equations	Source term	Zones	
		Cathode CL	Anode CL
Species	$R_{i=O_2}$	$-\frac{M_{O_2}}{4F} (\nabla \cdot i)_{X_i=O_2}$	-
	$R_{i=H_2O}$	$\frac{M_{H_2O}}{2F} (\nabla \cdot i)_{X_i=O_2}$	-
	$R_{i=H_2}$	-	$-\frac{M_{H_2}}{4F} (\nabla \cdot i)_{X_i=H_2}$
Charge	S_m	$-(\nabla \cdot i)_{X_i=O_2}$	$(\nabla \cdot i)_{X_i=H_2}$
	S_s	$(\nabla \cdot i)_{X_i=O_2}$	$-(\nabla \cdot i)_{X_i=H_2}$
Temperature	S_h	$\eta_c^{a,b} (\nabla \cdot i)_{X_i=O_2}$	$\eta_a^{a,c} (\nabla \cdot i)_{X_i=H_2}$

^a η is the activation over-potential

^b $\eta_c = (\phi_s - \phi_m - V_{OC})$

^c $\eta_c = (\phi_s - \phi_m)$

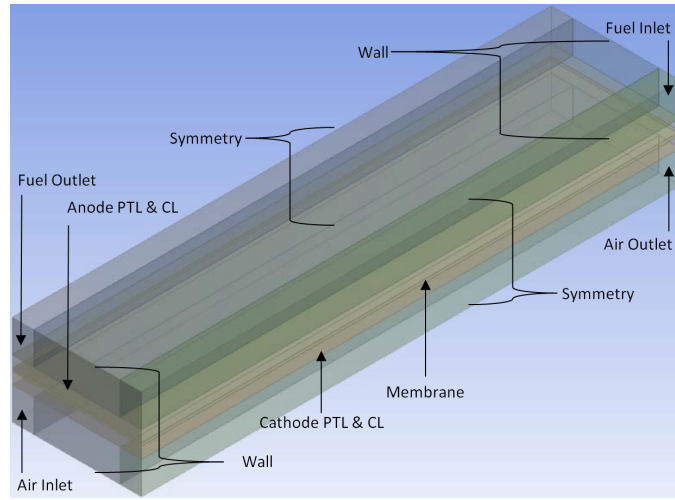


Fig. 1: Working domain of the PEM fuel cell with interdigitated flow field design

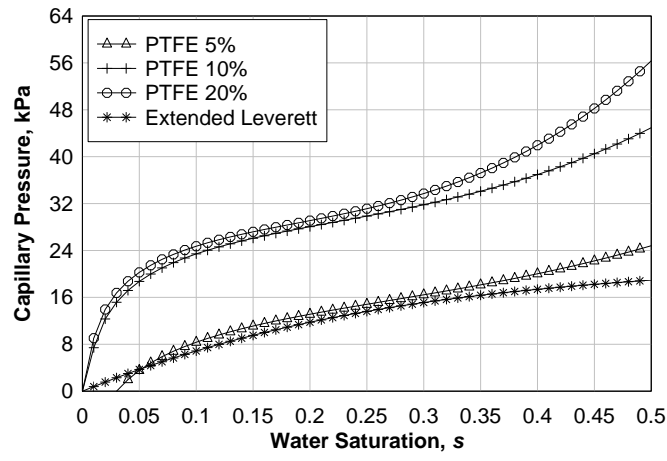
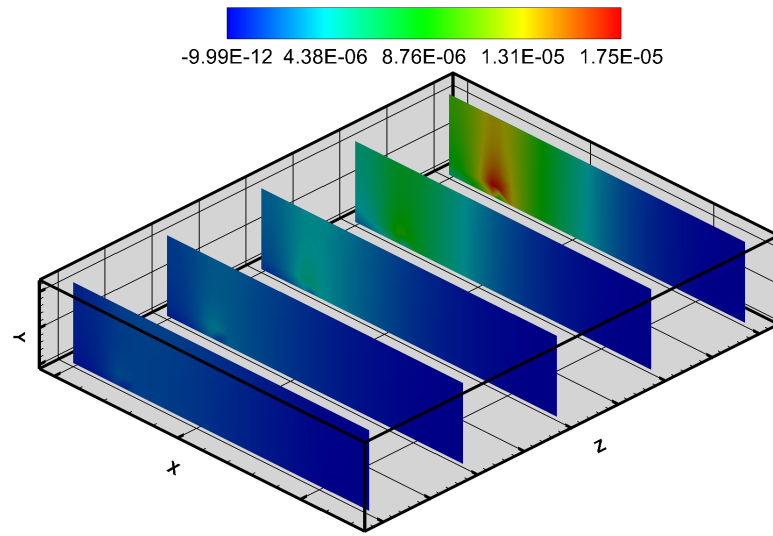
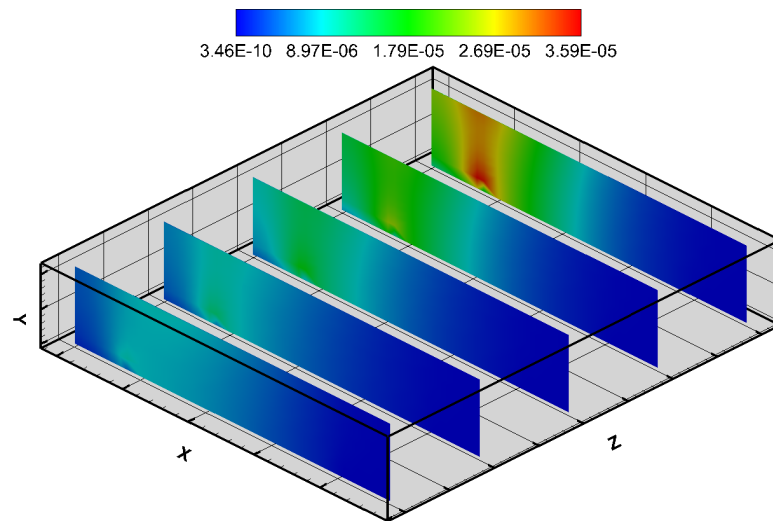


Fig. 2: Comparison of capillary pressures based on extended leverett and validated leverett approach.

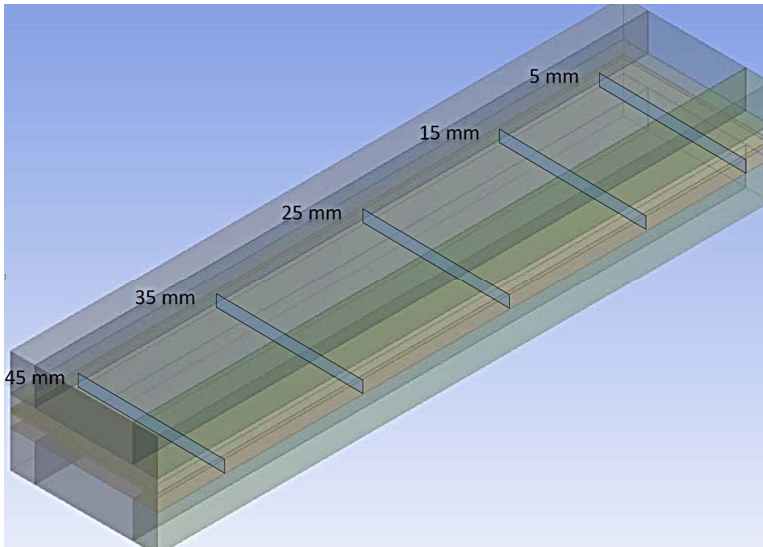
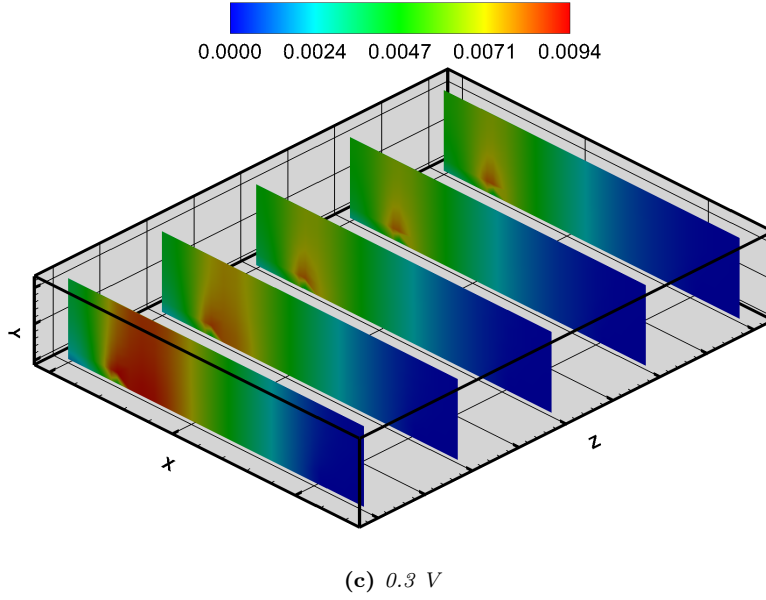


(a) 0.7 V



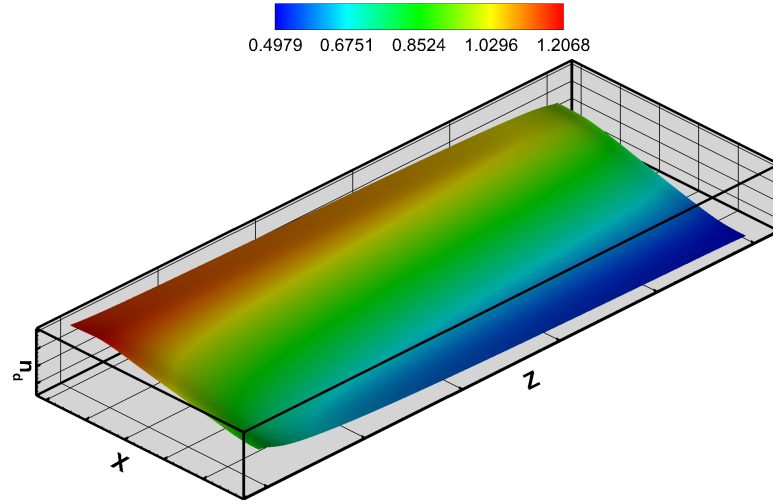
(b) 0.5 V

Fig. 3: *Liquid water distribution for different cross-sections at various operating voltages.*

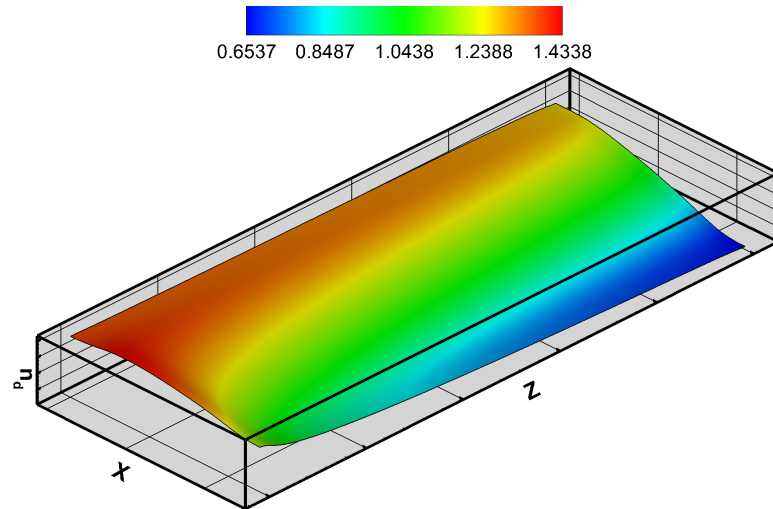


(d) location of cross-sections along the length of the fuel cell

Fig. 3: Electro-osmotic drag coefficient distribution at the interface of the membrane and the cathode catalyst layer for different operating voltages.

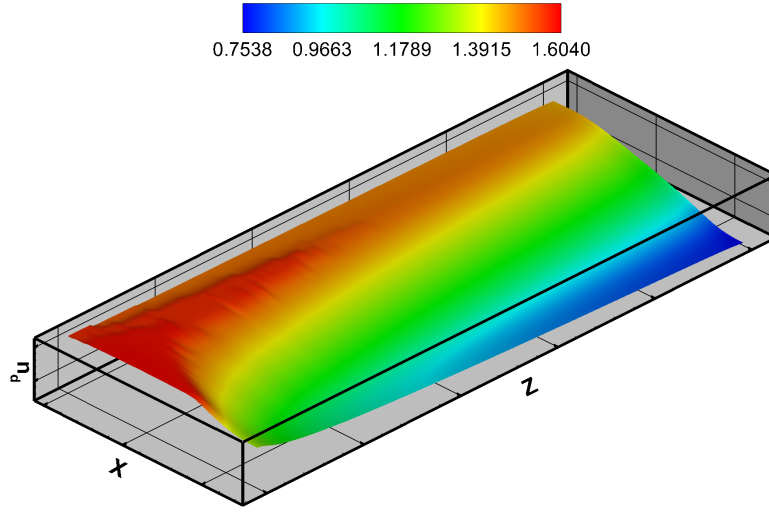


(a) 0.7 V

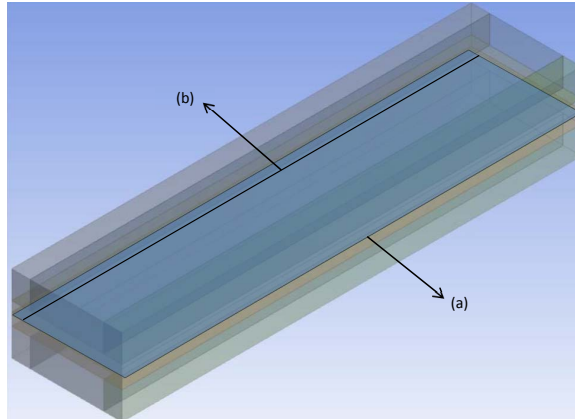


(b) 0.5 V

Fig. 4: *Electro-osmotic drag coefficient distribution at the interface of the membrane and the cathode catalyst layer for different operating voltages.*



(c) 0.3 V



(d) location of the cross-section (interface of the catalyst layer and the membrane). (a) location of the plane (b) reference location for Fig. 5.

Fig. 4: Electro-osmotic drag coefficient distribution at the interface of the membrane and the cathode catalyst layer for different operating voltages.

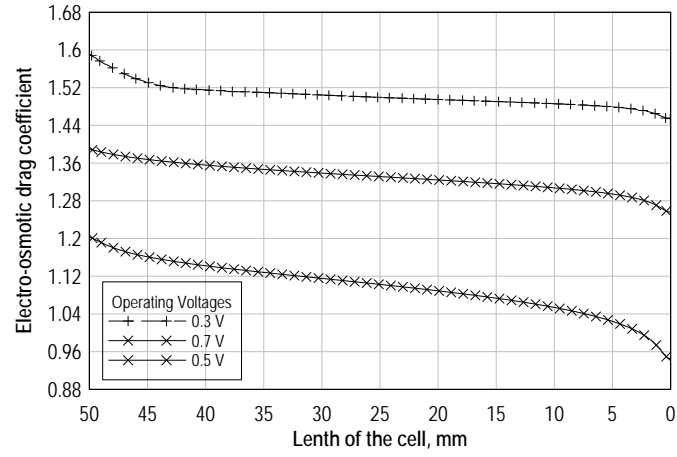


Fig. 5: Variation of electro-osmotic drag coefficient along the length of the inlet channel at the interface of the catalyst layer and the membrane.

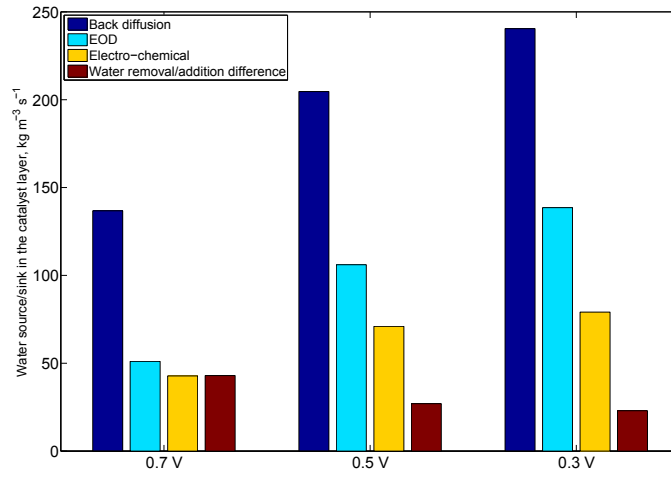


Fig. 6: Back diffusion, electro-osmotic drag and the electro-chemical generation of water for different operating voltages at the cathode side of PEM fuel cell (averaged over the cathode catalyst layer volume).

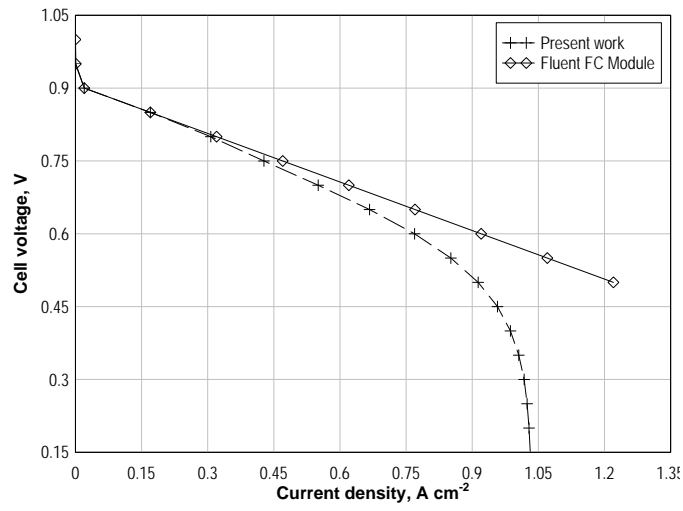


Fig. 7: Comparison between the V - I curves for the present model and the *Fluent*TM add-on module.

Paper E

Khan, M.A., Johansson, E., Sundén, B., Yuan, J., 2011. “Analysis of anisotropic transport in the polymer electrolyte membrane fuel cells and its effect on performance”, (*submitted to Journal of Power Sources*)

Anisotropic transport in the Polymer Electrolyte Membrane Fuel Cells and its Effect on Performance

Munir Ahmed Khan, Erik Johansson
Bengt Sundén, Jinliang Yuan

Abstract

This work presents a multi-phase 3D model of a PEM fuel cell with interdigitated flow field configuration developed to investigate the effects of various transport parameters keeping in mind the material behaviour for each transport mechanism. The heat transport in the solid has been considered isotropic in most of the PEM fuel cell modelling and only a slight increase in temperature was noted. However, using the anisotropy of the gas diffusion media, an increase of almost 1 K was observed compared to the inlet temperature, whereas, in the isotropic transport, the rise is only 0.5 K which is an under-estimation of the temperature rise even though the predicted current density is much higher. Furthermore, the so called Bruggeman correlation has been adopted to correct the protonic conduction in the ionomer phase of the catalyst layer in previous models but in this work, a more suitable correlation has been applied keeping in mind the volume fraction of each material phase in the catalyst layer.

A major challenge simulations of PEM fuel cells is the modelling of liquid water transport coupled with the heat management. Although, the conventional Leverett function has provided good predictions previously, but, it has not been verified for the porous media of PEM fuel cells yet. In the present work, a validated approach has been utilized while keeping in mind the effect of anisotropic permeability of the gas diffusion media. It was observed that the permeability of the material has a profound effect on the water saturation such that higher through-plane permeability resulted in more water accumulation in the GDL while with higher in-plane permeability, the catalyst layer is equally affected by water saturation.

Key words: *anisotropy, thermal conductivity, effective ionomer conduction, liquid water, permeability, CFD modelling, PEM fuel cells.*

1 Introduction

Over the past decades, the polymer electrolyte membrane (PEM) fuel cells have gained considerable attention for their portable, mobile and stationary co-generation applications. The credit for such worth of PEM fuel cells is mainly because of its low operating temperature, high power density, high responsiveness and cold start-up [1, 2]. To-date many experimental analysis have been carried out to study the fundamental phenomena and optimize the performance and efficiency of the PEM fuel cells [3–7]. However, during the same time, computational fluid dynamics (CFD) has gained much respect in the research community due to its ability to explore the system in full-depth because the compact nature of PEM fuel cells limits the experimental investigations [8].

A quantified 3D multi-physics model is a reasonable choice, but unfortunately, the CFD modelling is also limited in description of physics of a fuel cell system. One of the main limitations for obtaining well descriptive models is inclusion of complete and validated parameters for transport processes, i.e., charge, heat and mass, inside the PEM fuel cells [8]. Thus, for non-empirical models, there is certainly a need to develop accurate descriptive transport parameters in order to predict the performance of the fuel cell. Additionally, the characteristics presented by each component in PEM fuel cells are quite distinctive, yet it is difficult to distinguish the same physical processes in a component to that occurring in the other components [9].

In recent years, there has been an exponential growth in CFD modelling of PEM fuel cells with varying complexity [9, 10]. However, in most of the models, the transport models are treated with simplicity and the true effects of the fuel cell multifunctional materials structural morphology are usually ignored [11]. For the porous media, as encountered in the catalyst and the gas diffusion layers of PEM fuel cells, the Effective Medium Theory (EMT) has been widely adopted as a tool to estimate the effective properties. Among many, Bruggeman approximation is one of the EMT tools with wide range of applicability [1]. However, recent studies performed on the micro-structure of the porous media of PEM fuel cells, i.e., the gas diffusion layer, revealed that the structure consists of randomly laid out cylindrical fibres, whereas, most of the models for effective properties are based on granular porous media [11–13]. Thus, the morphology of the structure suggests that the anisotropy of properties exist in PEM fuel cells that needs to be fully incorporated in modelling so that more precise behaviour can be predicted.

For effective transport of the gas species in the diffusion medium, the Bruggeman correlation has been a popular tool to evaluate the effect in terms of porosity and tortuosity, but it neglects the directional dependence of the flow. By comparing the results of the Bruggeman correlation and the model presented by Tomadakis and Sotirchos [14], it was revealed that there is a difference of 65% in effective diffusion coefficient at a porosity of 0.4 in the in-plane direction [11]. Such an over-estimation in the effective diffusion of species will always predict higher power density and efficiency of the PEM fuel cell [11].

Similarly, for the diffusion of protons in the ionomer of the catalyst layer, most of the models ignored different material phases and the volume fraction occupied by each phase. It has been observed by Das et al. [15] in their work that the Bruggeman correlation over estimates the protonic conduction in the catalyst layer in the porosity range of $0.2 < \epsilon < 0.6$. The catalyst layer is comprised of four different material phases, i.e., the carbon/Pt assemblage, the ionomer (for proton conduction) and the void space (for fluid transport) and among all, only the ionomer phase is responsible for the conduction of protons to the reaction sites. In order to accurately predict the effective protonic conductivity of the ionomer in the catalyst layer, it is essential to use a true representative model that can distinguish each phase and incorporate its effects accordingly.

Apart from the direction dependent effective transport properties, water and heat management are also significant factors affecting the PEM fuel cell performance [4]. Water management has been on the priority list of all CFD analysts and many models have

been adopted to study the science of two phase flows in the porous media of PEM fuel cells [10]. Among all the processes related to the water management issue, e.g., back diffusion, electro-osmotic drag and the liquid water saturation and its transport, the transport of liquid water in the pores of the diffusion media has been a long time hurdle for the model developers. Most of the present day models for the liquid water transport utilize the conventional Leverett function proposed by Leverett [16] and Udell [17] that has not been experimentally verified [18]. For accurate predictions, it is imperative to have fully defined and validated approaches for the liquid water transport in the porous media of the PEM fuel cells. Additionally, the heat management is also coupled with the water management in such a sense that the mass transfer rate between the liquid and vapour phases of water is highly dependent on the temperature [4].

The heat management of the PEM fuel cells is crucial due to large amount of heat produced in the cathode catalyst layer that must travel through the gas diffusion layer in order to reach the cooling plate (the current collector). The thermal conductivity of the gas diffusion layer materials is anisotropic, due to the alignment of their fibres. Thermal conductivity in the gas diffusion layer is often treated as isotropic. However, the thermal conductivity is stated as ~ 12 times higher for the in-plane as compared to the through-plane direction by the manufacturers [18], which can lead to large anisotropic effects in the heat conduction. Bapat and Thynell [19] investigated the effects of anisotropic conductance explicitly and found that an in-plane conductivity that is higher than the through-plane conductivity leads to a more uniform heat distribution, while a lower in-plane conductivity can lead to undesirable local hot spots, and that the in-plane conductivity is of the highest importance in order to keep the thermal gradient to a minimum. Similarly, Pasaogullari et al. [18] compared the case when the heat conduction is taken to be isotropic and reached similar conclusions that the anisotropic case displayed a more uniform temperature distribution.

The permeability of gas diffusion layer materials is important to consider for a serpentine or an interdigitated fuel cell design where convective flow is of importance. Pharoah [20] showed that the onset of convective flow in the diffusion layer occurs at permeabilities of 10^{-13} m^2 , and because virtually all the experimental measurements are larger than this value, convective flow can safely be assumed to occur. Pharoah [20] also explored the gas diffusion layer as orthotropic media, and found that the in-plane parameter is the most significant one. There is also a pressure drop in the diffusion media in the in-plane direction due to a pressure difference from channel to channel making convective flow between channels possible and in the through-plane direction due to the consumption of reactants in the fuel cells [21]. Gostick et al. [22] investigated the difference between the in-plane and the through-plane permeabilities of several common diffusion layer materials, and found that the permeability can vary by a factor of two between the different directions, and thus the anisotropic permeability is an important parameter to take into consideration when modelling fuel and air flow through the gas diffusion layers. It is common to evaluate the permeability of the GDL as orthotropic, as seen in models by Pasaogullari et al. [18] and Yang et al. [23]. Both of the aforementioned models use an in-plane permeability of $3.00 \times 10^{-12} \text{ m}^2$ [24] and a through-plane permeability of $8.69 \times 10^{-12} \text{ m}^2$ [25]. It is interesting to note that other sources cited the in-plane permeability

to be higher than the through-plane permeability by almost a factor of 4 [26]. It was also revealed both experimentally and numerically that the permeability is dependent on the porosity of the material [26], and the same conclusion was reached as well by van Doormaal and Pharoah [21].

In this study, a multi-phase, three dimensional simulation is performed for a PEM fuel cell with interdigitated flow field configuration considering the anisotropic transport of the species, electrons and heat. Additionally, the protonic phase conduction of the ionomer in the catalyst layer of both the anode and cathode are corrected for accurate phase fraction. Furthermore, keeping in mind the strong impact of liquid water transport in the porous media of the fuel cell, a validated approach by Kumbur et al. [27–29] has been utilized instead of the conventional Leverett function. Additionally, in-order to simulate the anisotropic effect of the permeability of the gas diffusion layer on liquid water transport, two different approaches have been utilized, namely those presented by Pasaogullari et al. [18] and Becker et al. [26].

2 Mathematical Model

The 2D schematic and 3D domain for the present study are given in Figs 1 and 2, respectively. The pre-humidified air enters its inlet channel and is directed into the gas diffusion layer due to the flow field configuration and flows out of the domain via the outlet channel. Similarly the fuel, i.e., hydrogen enters the domain at the anode side (for present study, the upper half is assumed as the anode) which is also pre-humidified. Both the air and fuel have the inlet temperature of 343 K. Additionally, the unit is also cooled ideally by assuming a constant temperature of 343 K at the surfaces of both the anode and the cathode current collectors. The simulated domain is considered as a section of a fuel cell unit, so, the sides of the domain act as symmetric faces, while the front and back ends coinciding with the inlet and outlet faces are assumed as a wall for all the transport processes.

2.1 Governing Equations

This section highlights the set of governing equations and the transport parameters necessary to simulate a single PEM fuel cell.

2.1.1 Continuity and Momentum Transport

The general form of the continuity and momentum equations used in the present work except for the solid current collectors are given as;

$$\nabla \cdot (\rho \vec{v}) = \sum S_i \quad (1)$$

$$\nabla \cdot (\rho \vec{v} \vec{v}) = -\nabla P + \nabla \cdot (\bar{\tau}) + \rho \vec{g} + \vec{F} \quad (2)$$

where $\sum S_i$ is the rate of production or consumption of gaseous species in the PEM fuel cell, p is the static pressure and \vec{F} represents the external body forces. In modeling a PEM fuel cell, two types of external forces are taken into account;

- the rate of change of momentum due to consumption or production of reacting species, and,
- porous media

$$\vec{F} = \sum S_i \vec{v} - \xi \mu \vec{v} \quad (3)$$

where the first term in Eq. (3) accounts for the momentum change due to production or consumption of species i . The second term represents the viscous loss term also called the Darcy pressure drop, where ξ is the reciprocal of the permeability of the porous media in consideration.

2.1.2 Charge Transport and Electro-Chemistry

PEM fuel cells are labeled as clean energy production devices compared to conventional power generators where combustion of a fuel is the main source of energy. The primary driving mechanism in PEM fuel cells is the electro-chemical reactions where hydrogen is split into electrons and protons at the anode side and combine exothermically with oxygen at the cathode to produce water. The electrons generated at the anode follow an external circuit through the load while protons are directly transferred via electrolyte (*membrane*) towards the cathode. Therefore, for complete electro-chemical reaction description, two equations have been used in the present model. One of the equations deals with the electron (e^-) transport, while the other quantifies the protonic (H^+) conduction through the electrolyte.

$$\nabla \cdot (\sigma_{\text{sol}} \nabla \phi_{\text{sol}}) + R_{\text{sol}} = 0 \quad (4)$$

$$\nabla \cdot (\sigma_{\text{mem}} \nabla \phi_{\text{mem}}) + R_{\text{mem}} = 0 \quad (5)$$

where R in Eqs (4) and (5) is the transfer current or the electro-chemical source term at the anode and the cathode catalyst layer with conventions as given in Table 1. Because the electro-chemical reactions are occurring both at the anode and cathode catalyst layers with different reacting species i , the rate equations for anodic and cathodic reactions are given as;

$$\nabla \cdot i_{\text{cat}} = zF \frac{p_{\text{O}_2}}{H} \left(\frac{1}{E_r k_c (1 - \varepsilon_{\text{cat}})} + \frac{(r_{\text{agg}} + \delta) \delta}{a_{\text{agg}} r_{\text{agg}} D_{\text{O}_2 - \text{naf}}} \right)^{-1} \quad (6)$$

$$\nabla \cdot i_{\text{an}} = zF \frac{p_{\text{H}_2}}{H} \left(\frac{1}{E_r k_a (1 - \varepsilon_{\text{an}})} + \frac{(r_{\text{agg}} + \delta) \delta}{a_{\text{agg}} r_{\text{agg}} D_{\text{H}_2 - \text{naf}}} \right)^{-1} \quad (7)$$

where k_c and k_a are the reaction rates for the cathodic and the anodic electro-chemical reactions, respectively, and are calculated as;

$$k_c = \frac{a_{\text{Pt}}^{\text{eff}}}{4F(1 - \varepsilon_{\text{cat}})} \left(\frac{i_{\text{O}}^{\text{ref}}}{C_{\text{O}_2}^{\text{ref}}} \right) \left[-\exp\left(\frac{\alpha_{\text{an}} F}{RT} \eta_{\text{cat}}\right) + \exp\left(\frac{-\alpha_{\text{cat}} F}{RT} \eta_{\text{cat}}\right) \right] \quad (8)$$

$$k_a = \frac{a_{\text{Pt}}^{\text{eff}}}{4F(1 - \varepsilon_{\text{an}})} \left(\frac{i_{\text{O}}^{\text{eff}}}{C_{\text{H}_2}^{\text{eff}}} \right) \left[\exp\left(\frac{\alpha_{\text{an}} F}{RT} \eta_{\text{an}}\right) - \exp\left(\frac{-\alpha_{\text{cat}} F}{RT} \eta_{\text{an}}\right) \right] \quad (9)$$

The energy required or consumed to carry out the electro-chemical reactions is represented as η_{cat} and η_{an} in Eqs (8) and (9), respectively, referred to as *the activation loss*.

$$\eta_{\text{an}} = \Delta\phi \quad (10)$$

$$\eta_{\text{cat}} = \Delta\phi - V_{\text{OC}} \quad (11)$$

where $\Delta\phi$ and V_{OC} represent the local potential difference between the solid and membrane phases, and the open circuit voltage, respectively. To ensure the continuity of the anodic and cathodic electrical currents due to reaction rate imbalance, a current conservation equation is also employed. This is given as;

$$\int_{\text{an}} R_{\text{an}} dV = \int_{\text{cat}} R_{\text{cat}} dV \quad (12)$$

For detailed discussion regarding Eqs (6) to (12), the reader is referred to the work presented by Sun et al. [30, 31] and Khan [32]

2.1.3 Species Transport

A species equation is applied to both the anode and the cathode sides in the following form;

$$\nabla \cdot (\rho \vec{v} X_i) = -\nabla \cdot \vec{J}_i + S_i \quad (13)$$

where S_i is the source term for the electrochemical reactions and calculated based on the transfer current as;

$$S_{\text{H}_2} = -\frac{M_{w,\text{H}_2}}{2F} \nabla \cdot i_{\text{an}} \quad (14)$$

$$S_{\text{O}_2} = -\frac{M_{w,\text{O}_2}}{4F} \nabla \cdot i_{\text{cat}} \quad (15)$$

$$S_{\text{H}_2\text{O}} = \frac{M_{w,\text{H}_2\text{O}}}{2F} \nabla \cdot i_{\text{cat}} \quad (16)$$

In Eq. (13), \vec{J}_i is the diffusion flux of species i which is a function of both concentration gradient and the temperature variation in the fuel cell. It is calculated as;

$$\vec{J}_i = -\rho D_{i,m} \nabla X_i \quad (17)$$

where $D_{i,m}$ is the diffusion coefficient of species i in mixture m . The movement of the gas molecules within the porous GDL is restricted by the pore walls, which lowers the diffusion flux. The effective diffusion coefficient can be calculated based on the porosity and tortuosity, as;

$$D^{\text{eff}} = D_{i,m} \frac{\varepsilon}{\tau} \quad (18)$$

A common modelling assumption is the Bruggeman correlation, which assumes that the material is homogeneous and the tortuosity is approximated as;

$$\tau = \varepsilon^{-0.5} \quad (19)$$

So, the effective diffusion coefficient using the Bruggeman approximation is given as [33];

$$D^{\text{eff}} = D_{i,m} \varepsilon^{1.5} \quad (20)$$

The Bruggeman correlation has been a popular tool in CFD modelling of fuel cells due to its simplicity. However, it assumes that the GDL is isotropic, which is not always a fair assumption. Flückinger et al. [34] did a comparative study of common GDL materials, measuring the anisotropy, and found that in general, the in-plane (ip) diffusivity is on average about twice as large as the through-plane (tp) diffusivity. They also found that the amount of Teflon used in the GDL has a strong effect on diffusivity of species, where

a smaller amount of Teflon will have the increasing effect. To account for this anisotropy in modelling, there have been several attempts made by different research groups. The models can be said to be correlated to structural parameters as well as liquid water saturation according to the following general formulation [35]:

$$D^{\text{eff}} = D_{i,m} f(\varepsilon) g(s) \quad (21)$$

where $f(\varepsilon)$ is a function of the structural parameters only, corresponding to the transport of gaseous species in a dry GDL, and the function $g(s)$ takes into account the impact of liquid water saturation. Tomadakis and Sotirchos [14] suggested a percolation type correlation which was later expanded by Nam and Kaviani [36]. Das et al. [1] developed an expression for the relative diffusivity using an effective bulk modulus formulation originally developed to investigate the effective conductivity of a coated sphere assemblage. Wu et al. [35] developed an expression using a pore network modelling approach, also accounting for the impact of different degrees of Teflon layer coating, and Wu et al. [37] developed a fractal model for determining the effective diffusivity, stressing the impact of Knudsen diffusion. Table 2 summarizes some of the models presented for anisotropic diffusion. In the Tomadakis and Sotirchos-model, ε_p is a percolation threshold and α is an empirical constant; in the model by Wu et al., C_p is the teflon content, and λ_{max} , λ_{min} , L_0 , d_t , and d_f are maximum and minimum capillary diameter, GDL thickness, tortuosity fractal dimension and area fractal dimension as used by Wu et al [37], respectively. $g(s)$ is most often given in the form:

$$g(s) = (1 - s)^m \quad (22)$$

where s is the liquid water saturation, and m is an empirical constant that varies a lot depending on which model is used. Nam and Kaviani [36] suggested a value of 2.0, and Wu et al. [35] suggested that m should vary between 2.6 and 3.6 with a change of the GDL structure. For the Bruggeman case presented in Eq. (20) the value of m is usually taken to be 1.5. In this work, the expression developed by Nam and Kaviani [36] is used, and with the numerical values inserted for percolation threshold and the empirical constant m , it reads:

$$D_{i,m} f(\varepsilon) g(s) = D_{i,m} \varepsilon \left(\frac{\varepsilon - \varepsilon_p}{1 - \varepsilon_p} \right)^\alpha (1 - s)^{2.0} \quad (23)$$

$$\alpha = \begin{cases} 0.521 & \text{in-plane} \\ 0.785 & \text{through-plane} \end{cases}$$

where the percolation critical value, ε_p is taken as 0.11 [11].

2.1.4 Thermal Distribution

Because the electro-chemical reactions occurring at the catalyst layers of PEM fuel cells are exothermic in nature, a temperature variation exists through the length of the cell causing a change in physical properties. The equation utilized in this work to calculate the thermal distribution is given as;

$$\nabla \cdot (\rho c_p \vec{v} T) = \nabla \cdot (\mathbf{J}_{\text{cond}}) + S_h \quad (24)$$

where \mathbf{J}_{cond} is the conduction heat flux, given as;

$$\mathbf{J}_{\text{cond}}^{\text{solid+fluid}} = -k_{\text{eff}}^{\text{solid+fluid}} \cdot \nabla T \quad (25)$$

k_{eff} is the effective thermal conductivity of the medium (solid and fluid). The most common approach used in CFD modelling is to calculate the effective thermal conductivity based on the mixing law assuming that the thermal conductivities of the fluid and solid-matrix are comparable and do not differ by large magnitudes [38].

The thermal conductivity of the GDL, not like the case as usually modelled in PEM fuel cell, exhibits anisotropic behaviour and needs to be accounted for. It has been found that a difference of 14× exists between in-plane and through-plane directions [18]. Therefore, the conductivity of the solid-matrix is accounted for in the present model through effective conductivity tensor for the solid matrix as;

$$k_{\text{eff}}^{\text{solid}} = \begin{bmatrix} k_{\text{in-plane}}^{\text{solid}} & 0 & 0 \\ 0 & k_{\text{through-plane}}^{\text{solid}} & 0 \\ 0 & 0 & k_{\text{in-plane}}^{\text{solid}} \end{bmatrix} \quad (26)$$

so, the conduction heat flux for the porous media of the gas diffusion layer is given as [18];

$$\begin{aligned} \mathbf{J}_{\text{cond}} &= j_{\text{in-plane}} \mathbf{i} + j_{\text{through-plane}} \mathbf{j} + j_{\text{in-plane}} \mathbf{k} \\ j_{\text{in-plane}} &= - \left[(1 - \varepsilon) k_{\text{in-plane}}^{\text{solid}} + \varepsilon k^{\text{fluid}} \right] \frac{\partial T}{\partial x} \\ j_{\text{through-plane}} &= - \left[(1 - \varepsilon) k_{\text{through-plane}}^{\text{solid}} + \varepsilon k^{\text{fluid}} \right] \frac{\partial T}{\partial y} \\ j_{\text{in-plane}} &= - \left[(1 - \varepsilon) k_{\text{in-plane}}^{\text{solid}} + \varepsilon k^{\text{fluid}} \right] \frac{\partial T}{\partial z} \end{aligned} \quad (27)$$

Because the conversion efficiency is not 100%, the term S_h is incorporated in Eq. (24) to include all the irreversible effects occurring inside the cells as;

$$S_h = \Delta h_{\text{reaction}} - [R_{\text{an}} \eta_{\text{an}} \text{ or } R_{\text{cat}} \eta_{\text{cat}}] + I^2 R_{\text{ohm}} + \Delta h_L \quad (28)$$

where $\Delta h_{\text{reaction}}$ is the net enthalpy change due to electro-chemical reactions, $R_{\text{an}}\eta_{\text{an}}$ and $R_{\text{cat}}\eta_{\text{cat}}$ are due to the overpotential losses at the anode and cathode to drive the reactions, respectively. Δh_L is the enthalpy change due to evaporation or condensation of water while the term $I^2 R$ represents the ohmic losses due to the charge transfer resistance of the conducting media.

2.1.5 Liquid Water Transport Equation

Since the operating temperature of PEM fuel cell is relatively low ($< 100^\circ\text{C}$), condensation of water vapour to liquid phase is a regular process. The transport of liquid water inside porous media is governed by the pressure difference at the interface of liquid water and gases called the capillary pressure. Assuming the pores to be of cylindrical shape, the capillary pressure is given as [27, 39].

$$P_c = P_{\text{nw}} - P_{\text{w}} = \frac{2\gamma \cos \theta}{r} \quad (29)$$

where γ , θ and r are the surface tension, contact angle and pore radius, respectively. A common approach currently used in modelling studies for predicting the fluid distribution profiles in porous media is the direct implementation of an empirical correlation describing the capillary pressure as a function of liquid saturation. Several empirical and semi-empirical expressions are available that attempt to describe the behaviour of capillary pressure in terms of porous media and fluid properties. The traditional Leverett approach proposed by Leverett [16] and later modified by Udell [40] has been widely adopted by the PEM fuel cell community. Although the modified Leverett approach represents a useful starting point towards achieving an accurate two-phase transport model in fuel cell studies, the origin of this approach does not precisely represent the complex heterogeneous structure of the fuel cell diffusion media.

Gostick et al. [41] performed porosimetry for different GDLs to generate the relation between capillary pressure and the saturation and found that the acquired data can only be approximated with either van Genuchten [42] or the Leverett approach. Kumbur et al. [27–29], later on, presented three distinct levels of water saturation capturing the heterogeneous and mixed wettability characteristics of the GDLs using an extended form of the Leverett function. It was noted that in this approach, the calculated capillary function provided a superior fit to the experimental data obtained via porosimetric studies of the selected GDLs.

In this work, an experimentally validated approach [27–29] has been used to study the behaviour of water saturation in fuel cell porous media. The key feature of this correlation is that the connection between the liquid saturation and the mixed wettability characteristics of the diffusion media is precisely linked to the capillary pressure and further incorporating the temperature and compressional effects of the media are incorporated.

$$P_c = \left(\frac{293}{T} \right)^6 \gamma(T) 2^{0.4C} \left(\frac{\varepsilon}{K} \right)^{1/2} K(s_{nw}) \quad (30)$$

where T is the local temperature, $\gamma(T)$ is the temperature corrected surface tension, and $K(s_{nw})$ represents the latest developed water saturation function, evaluated as;

$$K(s_{nw}) = \begin{cases} \text{wt}\%[0.0469 - 0.00152(\text{wt}\%) - 0.0406s_{nw}^2] + 0.143s_{nw}^3 + 0.0561 \ln s_{nw} & 0 < s_{nw} < 0.50 \\ \text{wt}\%[1.534 - 0.00152(\text{wt}\%) - 12.68s_{nw}^2] + 18.824s_{nw}^3 + 3.416 \ln s_{nw} & 0.50 < s_{nw} < 0.65 \\ \text{wt}\%[1.7 - 0.0324(\text{wt}\%) - 14.1s_{nw}^2] - 14.1s_{nw}^3 + 3.79 \ln s_{nw} & 0.65 < s_{nw} < 1.00 \end{cases} \quad (31)$$

where wt% and s_{nw} represent the weight percentage of PTFE content in the diffusion media and nonwetting phase saturation, respectively. The detailed experimental details and information about derivation of Eqs (30) and (31) can be found in [27–29]. In the present study, a conservation equation for the volume fraction of liquid water is employed based on the moisture diffusion model, given as [5];

$$\nabla \cdot \left[\rho_l \frac{\kappa s^3}{\mu_l} \frac{dP_c}{ds} \nabla s \right] = \dot{\omega} \quad (32)$$

where $\dot{\omega}$ is the rate of phase change based on the saturation pressure of water vapour in air [43].

$$\dot{\omega} = \begin{cases} k_{\text{con}} (1-s) X_{\text{H}_2\text{O}} \frac{P_{\text{wv}} - P_{\text{sat}}}{RT_f} & P_{\text{wv}} - P_{\text{sat}} \geq 0 \\ k_{\text{evp}} (s) \frac{\rho_l}{M_{\text{H}_2\text{O}}} (P_{\text{wv}} - P_{\text{sat}}) & P_{\text{wv}} - P_{\text{sat}} < 0 \end{cases} \quad (33)$$

Because the permeability of the gas diffusion layer is also anisotropic in nature and to account for the effects of such material behaviour, the permeability κ in Eq. (32) is also a tensor, given as;

$$\kappa = \begin{bmatrix} \kappa_{\text{in-plane}} & 0 & 0 \\ 0 & \kappa_{\text{through-plane}} & 0 \\ 0 & 0 & \kappa_{\text{in-plane}} \end{bmatrix} \quad (34)$$

where κ_{xx}, κ_{yy} and κ_{zz} represent the different permeabilities in x, y and z axis of the domain. Eq. (32) models various physical processes such as condensation, vaporization, capillary diffusion, and surface tension. The clogging of the porous media and the flooding of the reaction surface are modeled by multiplying the porosity and the active surface area by $(1-s)$, respectively.

2.1.6 Electrolyte Phase Conductivity

For PEM fuel cells, the electrolyte phase conductivity is modeled as [44];

$$\sigma_m = (0.514\lambda - 0.326) e^{1268(\frac{1}{303} - \frac{1}{T})} \quad (35)$$

where λ is the water content. The electro-osmotic drag phenomena associated with transport of protons that causes water molecules to migrate from the anode to the cathode is modelled using a coefficient called osmotic drag coefficient and is calculated as;

$$n_d = 2.5 \frac{\lambda}{22} \quad (36)$$

The transport of water from cathode to anode due to the difference in concentration on the interface of the catalyst layer and the electrolyte is evaluated as;

$$J_w^{\text{diff}} = -\frac{\rho_m}{M_m} M_{\text{H}_2\text{O}} D_1 \nabla \lambda \quad (37)$$

where ρ_m and M_m are the density and the equivalent weight of the dry membrane, respectively. The diffusivity of water D_1 inside the membrane is given as [4];

$$D_1 = 10^{-10} \exp \left[2416 \left(\frac{1}{303} - \frac{1}{T} \right) \right] \times f(\lambda) \quad (38)$$

where,

$$f(\lambda) = \begin{cases} 2.563 - 0.33\lambda + 0.0264\lambda^2 - 0.000671\lambda^3 & (4 < \lambda) \\ -1.25\lambda + 6.65 & (3 < \lambda \leq 4) \\ 2.05\lambda - 3.25 & (2 < \lambda \leq 3) \\ 1 & (2 \geq \lambda) \end{cases} \quad (39)$$

The water content λ in Eqs (35) to (38) is calculated based on a relation provided by Springer et al. [44];

$$\lambda = \begin{cases} 0.043 + 17.18a - 39.85a^2 + 36a^3 & (a < 1) \\ 14 + 1.4(a - 1) & (a > 1) \end{cases} \quad (40)$$

where a is the water activity defined as;

$$a = \frac{P_{\text{wv}}}{P_{\text{sat}}} + 2s; \quad (41)$$

P_{vv} and P_{sat} are the vapour and saturation pressure at local temperature conditions, respectively. In the catalyst layer of a PEM fuel cell, there are three material phases, namely: carbon/Pt assemblage, ionomer and the void phase. Because the void space and carbon/Pt assemblage are not able to conduct protons because none contain free acid group to act as an electrolyte, it is assumed that only the ionomer takes part in the process. The total volume discretized over the material phases in the catalyst layer is given as;

$$f_s + f_v + f_m = 1 \quad (42)$$

where f is the volume fraction of each phase and subscripts s, v and m represent the solid phase (carbon/Pt), void and the membrane phase, respectively. Correcting the proton conductivity to the volume fraction of the ionomer yields,

$$\sigma_{\text{m,eff}} = \Phi(\sigma_{\text{m}}, f_{\text{m}}) \quad (43)$$

Among various techniques available to evaluate the effective properties of the composite system [1, 45, 46], the Bruggeman approximation has been used widely especially by CFD analysts because of its broad range and application diversity. The Bruggeman correlation adopted for protonic conductivity of ionomer in PEM fuel cells is given as;

$$\sigma_{\text{m,eff}} = \sigma_{\text{m}} (f_{\text{m}} (1 - f_{\text{v}})) \quad (44)$$

However, Das et al. [1], recently compared the Bruggeman model to Hashin-Shtrikman model [47] and calculated the applicable conditions and found that the applicability of the correlations depends on the porosity or the volume fraction of the void, i.e., Bruggeman approximation shows a better agreement for $0 < \varepsilon < 0.2$. However, for the porosity range of $0.2 < \varepsilon < 0.6$, the Hashin-shtrikman model has better agreement for the effective protonic conductivity.

$$\sigma_{\text{m,eff}} = \sigma_{\text{m}} - \frac{3\lambda_{\text{m}}(1 - f_{\text{m}})\sigma_{\text{m}}}{3 - f_{\text{m}}} - \frac{3\lambda_{\text{m}}f_{\text{v}}\left(\sigma_{\text{m}} - \frac{3(1 - f_{\text{m}})}{3 - f_{\text{m}}}\right)}{2 + f_{\text{v}}} \quad (45)$$

where λ_{m} is the multiplying factor depending on the geometrical structure of the membrane phase in the catalyst layer. In this work λ_{m} has been assumed as unity and the fraction of the membrane phase has been borrowed from Das et al. [1, 15] and Song et al. [48]. For the conductivity of electrons through the porous media in the gas diffusion layer and the catalyst layer, the Bruggeman approximation has been used because the electric conductivity is much higher than the protonic conductivity and it is reasonable to assume the simple correction [1].

2.2 Computational Mesh and Solution Technique

The simulation domain for the present study is shown in Fig. 2. The air enters the cathode side via the inlet at a mass flow rate of 1.5×10^{-6} kg/s. The fuel, i.e., hydrogen is fed into the inlet channel at a rate of 3.0×10^{-7} kg/s at the anode side. Both the air and fuel are pre-humidified to a certain degree as given in Table 1. The mesh for the model is divided into a total of 0.6 million hexahedral cells with varying mesh density in different zones. 75% of the total number of the cells are located in the membrane, the catalyst layers and the gas diffusion layers of the anode and the cathode, while the remaining components, i.e., the gas channels and the current collectors on both side, comprise of only 25% of the cells. Additionally, the inlet temperatures of fuel and air, and the current collector surface are maintained at 343 K because Eq. (30) has been validated only upto 353 K. It was intended to keep the temperatures within the limits. For pressure-velocity coupling, the SIMPLEC scheme has been applied due to strong coupling between the components and the QUICK scheme has been used for spatial discretization. FluentTM has been used for carrying out the simulations. For species, saturation and charge conservation, the user defined scalar (UDS) equations have been used in the following general form [49];

$$\frac{\partial}{\partial x_i} \left(\rho u_i \phi_k - \Gamma \frac{\partial \phi_k}{\partial x_i} \right) = S_{\phi_k} \quad k = 1, \dots, N \quad (46)$$

where Γ_k and S_{ϕ_k} are the diffusion coefficient and source term for each of the scalar parameters, while, Γ is the tensor in the case of anisotropic diffusivity. The diffusion term incorporated in the equations is $\Gamma \frac{\partial \phi_k}{\partial x_i}$. Additionally, for providing custom diffusion coefficients and source terms, user defined functions (UDFs) have been used. The boundary conditions for simulating the charge transfer are presented in Fig. 1, while for water saturation, the inlet of the cathode has been assumed at $s = 0$. Furthermore, the electrolyte is assumed non-permeable for all gaseous species so that both sides are perfectly insulated for all the species.

3 Results and Discussion

In order to investigate the effects of various effective transport parameters, simulations of a PEM fuel cell with interdigitated flow field configuration have been performed and a comparative study is carried out at various operating voltages, i.e., 0.6, 0.5 and 0.4 volts. Furthermore, considering the high performance dependence, water saturation and heat distribution are also undertaken so that a combined effect can be studied and analysed.

The in-plane conductivity of the gas diffusion layer is higher than the through-plane conductivity because of the configuration of the material that are typically used, i.e., the fibre orientation in the medium. The reason for such a weak thermal conductivity in through-plane direction is due to the void space present between the layers of carbon fibre bundles, while in in-plane direction, the heat is transferred through the length of each fibre thus depicting more thermal conductivity. Fig. 3a, shows the thermal distribution for the cathode side only at a cross-section in the middle of the cell (25

mm, 0.5 V). It can be observed that the maximum temperature exists at the left upper corner of the plane corresponding to the region of the catalyst layer right above the inlet channel for the air. Because the thermal conductivity of the gas diffusion layer is 21 W/m K in the in-plane direction and only 1.7 W/m K in through-plane direction, the high temperature zone is restricted to the upper side of the cathode opposite to the air channels, but, in the horizontal direction, the maximum temperature region stretches almost to the middle of the plane or section. The region near to the current collector is noted to be at a minimum because it is being cooled by the current collector that also serves as the heat sink, maintained at 343 K. Also, the air in the channel also helps in reducing the temperature. On the contrary, Fig. 3b, shows the temperature profile while simulating the cell using isotropic heat conduction of the diffusion media at operating voltage of 0.5 volts. The maximum temperature region, for this scenario, is also located in the region directly above the inlet channel. Comparing Figs 3a and 3b, a considerable difference is observed. In the case with isotropic thermal conductivity, the maximum temperature region is confined to the upper left corner and equally extends into the gas diffusion layer while in anisotropic case it is limited to the region near to the upper boundary but extends in the horizontal direction. This can be explained by the equal conduction of heat in all directions in the isotropic case while in anisotropic case it is restricted in the through-plane direction. The other difference is the maximum value of the temperature in the domain. As observed, the maximum temperature for isotropic conductivity increases by just a fraction of the inlet temperature, i.e., 343.508 K, but, for anisotropic conductivity, there is a difference of almost 1 K. The difference becomes even more noticeable when considering the current densities for the two cases. Although both the simulations present the result for 0.5 V operating level but the current densities are quite different, i.e., approximately 0.62 A/cm² for the anisotropic and 0.78 A/cm² for the isotropic case, as can be seen in Fig. 9. Since higher current densities have higher electro-chemical reactions and thus higher reaction heat, but, as seen in the figures, the anisotropic case is not capable of showing the accurate temperature profile inside the cell.

Fig. 4 compares the temperature distribution in the PEM fuel cell for the operating voltages of 0.6 and 0.4 volts. A major difference in the temperature distributions for these two operating levels is the range of maximum temperature. Since, as expected, the electro-chemical reaction rate is higher at lower voltage levels, so, the temperature profile also depicts higher temperature. For both the operating levels, it can be observed, that the high temperature zone thins down along the length of the cell, while the rate of shrinkage is high for 0.6 V operating voltage. The reduction in the maximum temperature zone along the length of the fuel cell can be explained by considering the electro-chemical reactions rate that reduces as the oxygen is being consumed along the length. One of the most important facts to note in Figs 4a and 4b is that the maximum temperature zone exists in the cathode side of the fuel cell. The catalyst and the gas diffusion layers on the anode side do not achieve the same temperature levels due to the fact that the heat generated at the anode catalyst layer due to electro-chemical reactions is lower as compared to the heat generated at the cathode side. The second reason for the lower temperature profile on the anode side is that the membrane which is separating the two electrodes has a very low thermal conductivity, i.e., 0.21 W/m K. The transfer of the major part of the heat - generated in the cathode catalyst layer - is directed

through the GDL to the current collector at the cathode side. Furthermore, because the membrane is also considered impermeable to all species (diffusion and convection), there is no convective heat removal in the membrane.

Figs 5a and 5b compare the heat generation due to electro-chemical reactions and the ohmic heat generation in the middle of the cell length at the catalyst layer and the membrane interface. Concerning the heat generation due to the electro-chemical reactions, it has been already established that most of the reactions take place above the inlet channel because of the fresh supply of oxygen. The trend shown in Fig. 5a also suggests that the area above the current collector and the outlet channel does not fully participate in the electro-chemical reactions. The ohmic heat generation due to the flow of charges, on the other hand, shows an increasing trend while moving from the area above the inlet channel to the current collector and is maximum at the position directly above the channel and the current collector boundary. Afterwards, the losses start to decrease and reach a minimum in the area above the outlet channel. The minimum ohmic heat generation above the outlet channel can be explained by considering the fact that most of the electro-chemical reactions are occurring on the other side of the cell, that dictate more consumption of charge in that location, hence, the charge flow shifts towards the area above the inlet channel. However, in order to explain the sudden increase and decrease after reaching the maximum in the area above the inlet channel can be explained by considering Figs 6 and 7. As can be seen in Fig. 6, near the left corner of the current collector at the interface of the gas diffusion layer, there is a concentration of the current flux. Due to this grouping of the current flux at this location, an increase in the current is observed in the area above the boundary of the current collector and the inlet gas channel. Additionally, Fig. 7 also shows an increased value of protonic conductivity at the same location, so, it can be concluded that a higher proton transfer from the anode takes place at the same location.

The protonic conductivity of the ionomer in the catalyst layer is a function of the water content and the volume fraction of the conducting phase. One of the most common techniques to calculate the effective protonic conductivity of the ionomer in the catalyst layer is to utilize the Bruggeman correlation that corrects the effectiveness considering the porosity and tortuosity of the porous medium. However, it has been noticed that the Bruggeman correlation is only accurate for certain conditions, i.e., when the porosity is less than 20%. Otherwise, the conduction values are always over-estimated by the Bruggeman correlation. In this study a different approach has been utilized to calculate the effective conductivity considering not only the water content and the porosity but also it was corrected for the exact amount of the conductive material present because both voids (pores) and the solid particles present in the catalyst layer do not take part in the conduction of the ions. Furthermore, keeping in mind the porosity of the catalyst layer, it has been already established that the new correlation works quite well for the porosity range selected in present modelling. Figs 7a and 7b represent the protonic conductivity at different operating voltages at the interface of the catalyst layer and the membrane in the cathode of the PEM fuel cell at locations near the inlet (45 mm) and outlet (5 mm) of the air. As can be found in Fig. 7a that the protonic conductivity is maximum at the location at 45 mm, i.e., near the air inlet boundary and reduces along the length

of the cell. Additionally, there is also a reduction in the protonic conductivity along the width of the cell. Since, the protonic conductivity of the ionomer is heavily water dependent and because the electro-chemical generation of water is mostly taking part in the region above the air inlet channel, so, the same region shows highest conductivity. Similarly, for Fig. 7b, the pattern for the protonic conductivity remains the same but the maximum value range has increased in the magnitude. The increase in the protonic conductivity at lower voltages is due to the increase in water content both due to the electro-chemical generation and the electro-osmotic drag of water from the anode side. Thus, the build up of water at lower voltages helps in providing better hydration states for the ionomer phase. Additionally, in Figs 7a and 7b, it can be observed that, initially there is an increase in the protonic conductivity upto approximately $x = 0.4$ mm, for both the voltage levels. This hump or the increase in the values is due to the water saturation effects as shown in Fig. 8.

The permeability of the gas diffusion layer has been known to have significant effects on the water saturation in the PEM fuel cells. The quantity and distribution of the liquid phase is dependent on the temperature, oxygen and charge distributions that in turn determine the current density. In the present study, two cases have been simulated for the same operating levels, i.e., 0.4 V, with different permeabilities as given in the literature. Pasaogullari and co-workers [18] previously published results based on permeabilities being higher in the through-plane direction as compared to the in-plane direction. However, the opposite has been proposed in the literature by different sources [26]. Therefore, both cases have been simulated and the results are shown in Fig. 8.

Fig. 8a presents the case for the higher through-plane permeability as given in [18], while, Fig. 8b shows the results for higher in-plane permeability as given in [26]. As can be observed in the two figures, both the cases present unique results. The general trend in both the figures is that the saturation level increases along the length of the cell which is due to the decrease in the ability of air to accommodate water as the partial pressure of water vapour increases and approaches the saturation pressure. Another common trend in both the cases is that the liquid water tends to accommodate in the gas diffusion layer near the interface of the current collector due to higher porosity of the gas diffusion layer. However, it can also be noted by comparing the two cases that when the in-plane permeability is higher than the through-plane permeability (Fig. 8b), the catalyst layer is equally affected with the saturation effects which leads to decrease in the current densities by blocking the pathways for species transport and insulating the active sites for the electrochemical reactions. Another notable difference in the two cases is the total saturation level where the case with higher through-plane permeability has higher saturation levels (Fig. 8a) than the case with higher in-plane permeability (Fig. 8b). This difference in the total saturation levels can be explained by considering the fact that the electrochemical reaction rate is higher when only the gas diffusion layer is the most affected part, i.e., less blockage of pathways and the reaction sites in the catalyst layer which leads to higher reaction rates.

The overall performance of the present model is shown in Fig. 9, where a typical V-I curve for PEM fuel cell performance is shown. As can be observed that there is an initial

sharp decline in the voltage with only a minor increase in the current density. Such losses are caused by the slowness of the electro-chemical reactions because a part of the energy is wasted in driving the reactions and because energy production at such high voltages is quite low, therefore, most of it is consumed within the cell. The linear portion of the graph represents a linear increase in the average ohmic loss which is linearly proportional to the amount of current flowing through the material. At low voltage levels, mass transport or the concentration losses make the curve to bend sharply which is a result from the change in the concentration of reactants, i.e., oxygen and hydrogen, as the fuel is consumed. However, considering the performance of the present model to the one simulated without accounting for the effective transport mechanism as highlighted in this manuscript shows better performance in terms of the current density is found. But, in actual scenarios, as there are limitations in transport of species, charge and heat due to porosity, tortuosity, volume fraction of ionomer in the catalyst layer and the anisotropy of the gas diffusion layer, the present study reveals more realistic results.

4 Conclusion

In this study, a 3D model of PEM fuel cells has been used for the simulation for better understanding of the limitations for species, charge and heat transport so that a more realistic picture can be obtained. Furthermore, because the liquid water transport is one of the most important phenomena in PEM fuel cells due to their low operating temperatures ($<100^{\circ}\text{C}$), transport of liquid water has been modelled using a validated approach.

Considering the anisotropy of the heat conduction through the gas diffusion layer, it was observed that heat was trapped in the catalyst layer because of the low thermal conductivity in the through-plane direction. Additionally, because of the lower heat conduction of the membrane between the two electrodes, the highest temperature within the cell was noted in the cathode catalyst layer. Previously it has been shown that the catalyst layer of the PEM fuel cell is more problematic than the anode side because of two reasons. The first reason is that the oxidation reduction reactions are much slower than the hydrogen oxidation reactions, and, secondly, due to the water generation at the cathode side makes it more prone to flooding effects. However, considering the anisotropic heat conduction of the gas diffusion layer, the third problem can be listed as high temperature rise at the cathode side of the PEM fuel cell. All these three scenarios make the cathode of PEM fuel cell the centre hub of inefficiencies of the cell.

The present study also utilizes a more conservative approach to calculate the protonic conductivity of the membrane phase in the catalyst layer. It was previously established that the Bruggeman approximation over-predicts the effective material properties for the porous media when the porosity is higher than 0.2. It was further shown that the protonic conductivity varied in the cell for the cathode catalyst layer both in width and the length of the cell. However, a unique trend was observed where an increase was noted in the protonic conduction when the water saturation effects were maximum. Additionally, while studying the heat generation due to flow of charges (electrons and protons), it was observed that a similar trend to the protonic conduction was observed, i.e., a peak at the

same location where high protonic conductivity was observed. Since both the electronic and protonic currents contribute to the ohmic losses, it was seen that the same region showed clustering of the current density flux, hence, generating more heat as a result.

The anisotropic permeability of the gas diffusion layer also affects the water saturation in the PEM fuel cell. In the present work a comparative study was also carried out at different in-plane and through-plane permeabilities. It was noted that with higher permeability in through-plane direction, the maximum saturation was located near the current collector and the inlet gas channel. However, in other case when the through-plane permeability was lower as compared to the in-plane permeability, the location of maximum saturation shifted to the opposite side, i.e, in the catalyst layer. Furthermore, considering all the transport limitations, as incorporated in this work, were compared to the one having isotropic heat and species transport and isotropic permeability of the gas diffusion layer, it was observed that the present model under-performed at the same operating levels and mass limitation effects or the concentration losses were seen to come into effect at quite low current densities, i.e., approximately less than 0.6 A/cm^2 for the present case.

Acknowledgements

The European Research Counsel (ERC 226238-MMFCs) supports the current research.

Nomenclature

Roman Symbols

c_p	constant-pressure heat capacity, J/kg K
C	compression pressure, Pa
D	diffusion coefficient, m^2/s
E_r	agglomerate effectiveness
F	faraday constant, C/mol
\vec{F}	body force, N
H	henry constant, Pa m/mol
\vec{J}	species diffusion flux, $\text{kg}/\text{m}^2 \text{ s}$
$k_{a,c}$	reaction rate, 1/s
M_M	equivalent weight of the dry membrane
n_d	electro-osmotic drag coefficient
p	pressure, Pa
Pt	platinum
R	gas constant, J/mol K
R	transfer current, A/m^3
r	radius, m
s	saturation
T	temperature, K
\vec{v}	velocity, m/s
X	species mass fraction, kg/kg

z number of electrons

Greek Symbols

α percolation critical value
 δ thickness, m
 ε porosity
 η activation over-potential, V
 γ surface tension, N/m
 λ capillary diameter, m
 μ viscosity, kg/m s
 $\dot{\omega}$ condensation rate, kg/m³ s
 ϕ charge potential, V
 ρ density, kg/m³
 σ charge conductivity, 1/ Ω m
 τ tortuosity
 ξ reciprocal of permeability, 1/m²

Subscripts & Superscripts

agg agglomerate
an anode
cat cathode
C compression
eff effective
i species identification
l liquid phase
m mixture
mem membrane
naf nafion
OC open circuit
ref reference value
sol solid

References

- [1] Das, P., Li, X., and Liu, Z.-S., 2010. “Effective transport coefficients in pem fuel cell catalyst and gas diffusion layers: Beyond bruggeman approximation”. *Applied Energy*, **87**(9), pp. 2785 – 2796.
- [2] Sundén, B., and Faghri, M., 2005. *Transport Phenomena in Fuel Cells*. Devel. Heat Transfer. WIT Press, Southampton.
- [3] Masuda, H., Ito, K., Oshima, T., and Sasaki, K., 2008. “Comparison between numerical simulation and visualization experiment on water behavior in single straight flow channel polymer electrolyte fuel cells”. *J. Power Sources*, **177**(2), pp. 303–313.
- [4] He, G., Yamazaki, Y., and Abudula, A., 2010. “A three-dimensional analysis of the effect of anisotropic gas diffusion layer(GDL) thermal conductivity on the heat

- transfer and two-phase behavior in a proton exchange membrane fuel cell(PEMFC)". *J. Power Sources*, **195**(6), pp. 1551–1560.
- [5] He, G., Zhao, Z., Ming, P., Abuliti, A., and Yin, C., 2007. "A fractal model for predicting permeability and liquid water relative permeability in the gas diffusion layer (GDL) of PEMFCs". *J. Power Sources*, **163**(2), pp. 846–852.
- [6] Turhan, A., Kim, S., Hatzell, M., and Mench, M. M., 2010. "Impact of channel wall hydrophobicity on through-plane water distribution and flooding behavior in a polymer electrolyte fuel cell". *Electrochimica Acta*, **55**(8), pp. 2734–2745.
- [7] Weber, A. Z., and Hickner, M. A., 2008. "Modeling and high-resolution-imaging studies of water-content profiles in a polymer-electrolyte-fuel-cell membrane-electrode assembly". *Electrochimica Acta*, **53**(26), pp. 7668–7674.
- [8] Mench, M. M., 2010. *Advanced modeling in fuel cell systems: a review of modeling approaches*. Wiley-VCH Verlag GmbH & Co. KGaA, Weinheim, pp. 89–118.
- [9] Shah, A., Luo, K., Ralph, T., and Walsh, F., 2011. "Recent trends and developments in polymer electrolyte membrane fuel cell modelling". *Electrochimica Acta*, **56**, pp. 3731–3757.
- [10] Khan, M. A., Sundén, B., and Yuan, J., 2011. "Analysis of multi-phase transport phenomena with catalyst reactions in polymer electrolyte membrane fuel cells – A review". *J. Power Sources*, **196**(19), pp. 7899–7916.
- [11] Pharoah, J. G., Karan, K., and Sun, W., 2006. "On effective transport coefficients in PEM fuel cell electrodes: Anisotropy of the porous transport layers". *J. Power Sources*, **161**(1), pp. 214–224.
- [12] Park, J., Matsubara, M., and Li, X., 2007. "Application of Lattice Boltzmann Method to a micro-scale flow simulation in the porous electrode of a PEM fuel cell". *J. Power Sources*, **173**(1), pp. 404–414.
- [13] Park, J., and Li, X., 2008. "Multi-phase micro-scale flow simulation in the electrodes of a PEM fuel cell by Lattice Boltzmann Method". *J. Power Sources*, **178**, pp. 248–257.
- [14] Tomadakis, M. M., and Sotirchos, S. V., 1993. "Ordinary and transition regime diffusion in random fiber structures". *AIChE Journal*, **39**(3), pp. 397–412.
- [15] Das, P. K., Li, X., and Liu, Z.-S., 2007. "Analytical approach to polymer electrolyte membrane fuel cell performance and optimization". *J. Electroanal. Chem.*, **604**(2), pp. 72–90.
- [16] Leverett, M. C., 1941. "Capillary behaviour in porous solids". *Pet. Trans., AIME(Am. Inst. Min. Metall. Eng.)*, **142**, pp. 152–169.
- [17] Udell, K. S., 1985. "Heat transfer in porous media considering phase change and capillarity—the heat pipe effect". *Int. J. Heat Mass Transfer*, **28**(2), pp. 485–495.

-
- [18] Pasaogullari, U., Mukherjee, P. P., Wang, C. Y., and Chen, K., 2007. "Anisotropic heat and water transport in pefc cathode gas diffusion layer". *J. Electrochem. Soc.*, **154**(8), pp. B823–B834.
- [19] Bapat, C., and Thynell, S., 2007. "Anisotropic heat conduction effects in proton-exchange membrane fuel cells". *J. Heat Transfer*, **129**(9), pp. 1109–1118.
- [20] Pharoah, J. G., 2005. "On the permeability of the gas diffusion media used in PEM fuel cells". *J. Power Sources*, **144**(1), pp. 77–82.
- [21] Van Doormaal, M. A., and Pharoah, J. G., 2009. "Determination of permeability in fibrous porous media using the lattice boltzmann method with application to pem fuel cells". *Int. J. Numerical Methods in Fluids*, **59**(1), pp. 75–89.
- [22] Gostick, J. T., Fowler, M. W., Pritzker, M. D., Ioannidis, M. A., and Behra, L., 2006. "In-plane and through-plane gas permeability of carbon fiber electrode backing layer". *J. Power Sources*, **162**(1), pp. 228–238.
- [23] Yang, W., Zhao, T., and He, Y., 2008. "Modelling of coupled electron and mass transport in anisotropic proton-exchange membrane fuel cell electrodes". *J. Power Sources*, **185**(2), pp. 765–775.
- [24] M. Bluemle, V. Gurau, J. M. T. Z. E. D. C., and Tsou, Y., 2004. "Characterization of transport properties in gas diffusion layers for pemfcs". In 206th Meeting of The Electrochemical Society, Inc.
- [25] Williams, M. V., Begg, E., Bonville, L., Kunz, H. R., and Fenton, J. M., 2004. "Characterization of gas diffusion layers for PEMFC". *Journal of The Electrochemical Society*, **151**(8), pp. A1173–A1180.
- [26] Becker, J., Fluckiger, R., Reum, M., Buchi, F. N., Marone, F., and Stampanoni, M., 2009. "Determination of material properties of gas diffusion layers: Experiments and simulations using phase contrast tomographic microscopy". *Journal of The Electrochemical Society*, **156**(10), pp. B1175–B1181.
- [27] Kumbur, E. C., Sharp, K. V., and Mench, M. M., 2007. "A validated leverette approach to multiphase flow in polymer electrolyte fuel cell diffusion media. part i. hydrophobicity effect". *J. Electrochem. Soc.*, **154**(12), pp. B1295–B1304.
- [28] Kumbur, E. C., Sharp, K. V., and Mench, M. M., 2007. "A validated leverette approach to multiphase flow in polymer electrolyte fuel cell diffusion media. part ii. compression effect and capillary". *J. Electrochem. Soc.*, **154**(12), pp. B1305–B1314.
- [29] Kumbur, E. C., Sharp, K. V., and Mench, M. M., 2007. "A validated leverette approach to multiphase flow in polymer electrolyte fuel cell diffusion media. part iii. temperature effect and unified approach". *J. Electrochem. Soc.*, **154**(12), pp. B1315–B1324.
- [30] Sun, W., Peppley, B. A., and Karan, K., 2005. "An improved two-dimensional agglomerate cathode model to study the influence of catalyst layer structural parameters". *Electrochem. Acta*, **50**, pp. 3359–3374.

-
- [31] Sun, W., Peppley, B., and Karan, K., 2005. "Modeling the influence of gdl and flow-field plate parameters on the reaction distribution in the pemfc cathode catalyst layer". *J. Power Sources*, **144**, pp. 42–53.
- [32] Khan, M., 2009. *Numerical simulation of multi-scale transport processes and reactions in PEM fuel cells using two-phase models*. Licentiate Thesis, ISRN LUTMDN/TMHP-09/7066-SE, Lund University, Lund.
- [33] Jiao, K., and Li, X., 2011. "Water transport in polymer electrolyte membrane fuel cells". *Prog. Ener. Comb. Sci.*, **37**, pp. 221–291.
- [34] Flückiger, R., Freunberger, S. A., Kramer, D., Wokaun, A., Scherer, G. G., and Büchi, F. N., 2008. "Anisotropic, effective diffusivity of porous gas diffusion layer materials for pefc". *Electrochimica Acta*, **54**(2), pp. 551 – 559.
- [35] Wu, R., Zhu, X., Liao, Q., Wang, H., dong Ding, Y., Li, J., and ding Ye, D., 2010. "Determination of oxygen effective diffusivity in porous gas diffusion layer using a three-dimensional pore network model". *Electrochimica Acta*, **55**(24), pp. 7394 – 7403.
- [36] Nam, J. H., and Kaviani, M., 2003. "Effective diffusivity and water-saturation distribution in single- and two-layer pemfc diffusion medium". *International Journal of Heat and Mass Transfer*, **46**(24), pp. 4595 – 4611.
- [37] Wu, R., Liao, Q., Zhu, X., and Wang, H., 2011. "A fractal model for determining oxygen effective diffusivity of gas diffusion layer under the dry and wet conditions". *International Journal of Heat and Mass Transfer*, **54**(19-20), pp. 4341 – 4348.
- [38] Faghri, A., and Zhang, Y., 2006. *Transport Phenomena in Multiphase Systems*. Elsevier Academic Press.
- [39] Corey, T. A., 1994. *Mechanics of Immiscible Fluids in Porous Media*, 1st ed. Water Resources Publications, Highlands Ranch USA.
- [40] Udell, K. S., 1985. "Heat transfer in porous media considering phase change and capillarity—the heat pipe effect". *Int.l J. Heat Mass Trans.*, **28**(2), pp. 485–495.
- [41] Gostick, J. T., Fowler, M. W., Ioannidis, M. A., Pritzker, M. D., Volfkovich, Y. M., and Sakars, A., 2006. "Capillary pressure and hydrophilic porosity in gas diffusion layers for polymer electrolyte fuel cells". *J. Power Sources*, **156**(2), pp. 375–387.
- [42] van Genuchten, M., 1980. "A closed-form equation for predicting the hydraulic conductivity of unsaturated soils". *Soil Sci. Soc. America J.*, **44**(5), pp. 892–898.
- [43] Hwang, J. J., 2007. "A complete two-phase model of a porous cathode of a PEM fuel cell". *J. Power Sources*, **164**(1), pp. 174–181.
- [44] Springer, T. E., Zawodzinski, T. A., and Gottesfeld, S., 1991. "Polymer electrolyte fuel cell model". *J. Electrochem. Soc.*, **138**, pp. 2334–2342.
- [45] Uvarov, N., 2000. "Estimation of composites conductivity using a general mixing rule". *Solid State Ionics*, **136**, pp. 1267–1272.

-
- [46] Belova, I., and Murch, G., 2005. "Calculation of the effective conductivity and diffusivity in composite solid electrolytes". *J. Phys. Chem. Solids*, **66**, pp. 772–778.
 - [47] Hashin, Z., and Shtrikman, S., 1962. "A variational approach to the theory of the effective magnetic permeability of multiphase materials". *J. Applied Physics*, **33**(10), pp. 3125–3131.
 - [48] Song, D., Wang, Q., Liu, Z., Eikerling, M., Xie, Z., Navessin, T., and Holdcroft, S., 2005. "A method for optimizing distributions of nafion and pt in cathode catalyst layers of pem fuel cells". *Electrochimica Acta*, **50**(16-17), pp. 3347–3358.
 - [49] "ANSYS FLUENT 12.0, Theory guide, www.fluent.com, 2009".
 - [50] Spiegel, C., 2008. *PEM Fuel Cell Modeling and Simulation Using Matlab*. Academic Press.

Table 1: *Physical parameters and properties [4, 5, 18, 22, 30, 31, 50].*

Parameters	Value	Units
Faraday constant, F	96487.0	C/mol
Gas Constant, R	8.3142	J/mol K
Thickness of GDL	0.21	mm
Porosity of GDL	0.7	-
Thickness of CL	0.012	mm
Porosity of CL	0.2	-
Compression pressure, C	0.6	MPa
Pt loading, m_{Pt}	0.4	mg/cm ²
Pt particle diameter, r_{Pt}	2.5	nm
Agglomerate Radius, r_{agg}	1	μm
Effective agglomerate surface area, a_{agg}	3.6×10^5	m ² /m ³
Cathodic transfer coefficient, a_{cat}	1	-
	Low slope ($\geq 0.8V$)	-
	High slope ($< 0.8V$)	-
Anodic transfer coefficient, a_{an}	1	-
Reference exchange current density, i_{ref}	3.85×10^{-8}	A/cm ²
	Low slope ($\geq 0.8V$)	A/cm ²
	High slope ($< 0.8V$)	Pa m ³ /mol
Henry's constant for hydrogen, H_{H_2}	1.5×10^{-6}	Pa m ³ /mol
Henry's constant for oxygen, H_{O_2}	3.9×10^4	mol/m ³
Reference hydrogen concentration, $C_{H_2}^{eff}$	3.2×10^4	mol/m ³
Reference oxygen concentration, $C_{O_2}^{eff}$	$Y_{H_2, in} \times p_o / H_{H_2}$	mol/m ³
Inlet O ₂ mass fraction	$Y_{O_2, in} \times p_o / H_{O_2}$	mol/m ³
Inlet H ₂ mass fractions	0.2	-
Inlet H ₂ O mass fraction	0.5	-
Inlet H ₂ O mass fraction	0.13	-
Agglomerate covering thickness, δ	0.5	-
Electrolyte fraction in agglomerate, ϵ_{agg}	8.0×10^{-9}	m
Effective Pt surface ratio, ϵ_{eff}	0.3	-
PTFE wight percentage, wt%	0.75	-
	10	-

Continued on next page

Table 1 – continued ...

Parameters	Value	Units
Fuel and air inlet temperature, T	343	K
Thermal conductivity of electrolyte, k_{mem}	0.21	W/m K
Thermal conductivity of CL, k_{CL}	0.29	W/m K
Thermal conductivity of GDL, k_{GDL}	21	W/m K
	1.7	W/m K
Permeability of GDL, κ	3×10^{-12}	m^2
	8.69×10^{-12}	m^2
Permeability of GDL, κ	0.6×10^{-11}	m^2
	0.2×10^{-11}	m^2
Electrical conductivity of GDL, σ_{sol}	17857	S/m
	1250	S/m
Specific heat capacity, GDL	1000	J/kg K
Specific heat capacity, CL	1000	J/kg K
Specific heat capacity, mem	800	J/kg K
Specific heat capacity, CC	800	J/kg K
Electro-Chemical Transfer Current Convention	Anode	Cathode
R_{sol}	$-\nabla \cdot i_{\text{an}}$	$+\nabla \cdot i_{\text{cat}}$
R_{mem}	$+\nabla \cdot i_{\text{an}}$	$-\nabla \cdot i_{\text{cat}}$

Table 2: *Different models for capturing anisotropic effects on diffusion in the GDL material.*

Contributor	$f(\varepsilon)$
Tomadakis and Soitchos [14]	$\varepsilon \left(\frac{\varepsilon - \varepsilon_p}{1 - \varepsilon_p} \right)^\alpha$
Das et. al [1]	$1 - \left(\frac{3(1-\varepsilon)}{3-\varepsilon} \right)$
Wu et. al [35]	$\exp \left(\varepsilon - \frac{1}{0.222} - 0.161 C_p \right)$
Wu et al. [37]	$\frac{\varepsilon(2-d_f)(\lambda_{\max}^{1+d_t-d_f} - \lambda_{\min}^{1+d_t-d_f})}{L_0^{d_t-1}(1+d_t-d_f)(\lambda_{\max}^{2-d_f} - \lambda_{\min}^{2-d_f})}$

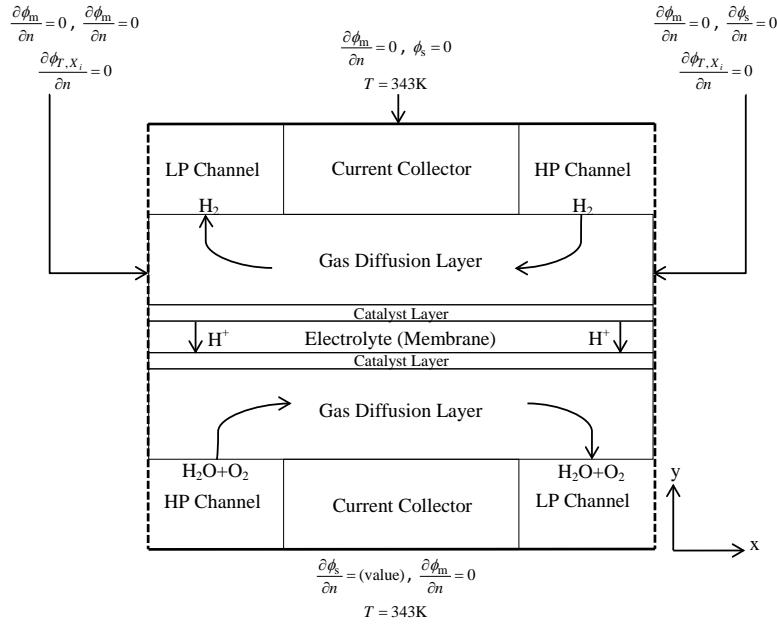


Fig. 1: *The schematics of the simulated domain presented in 2D (not to scale).*

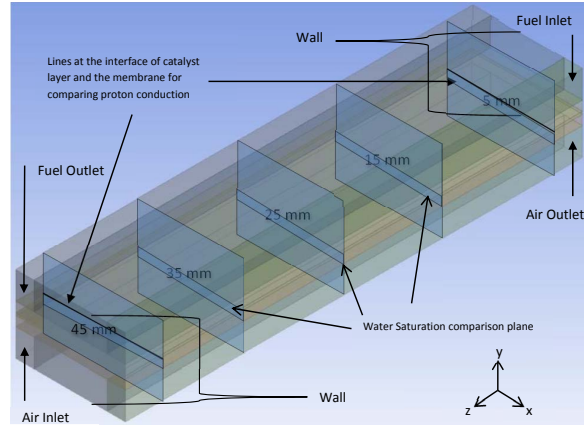
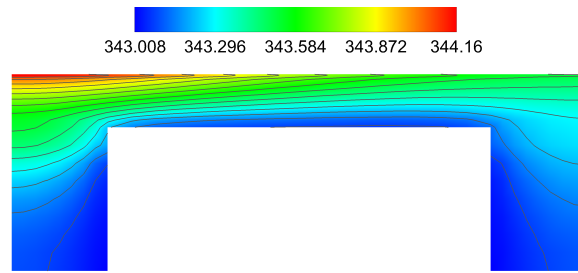
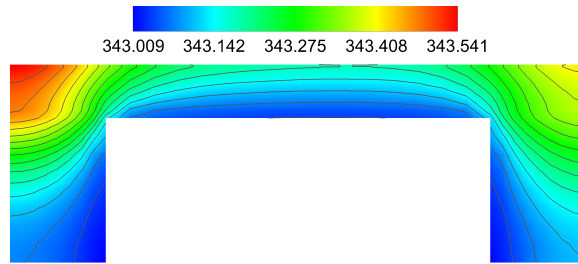


Fig. 2: The simulation domain for the present study in 3D.

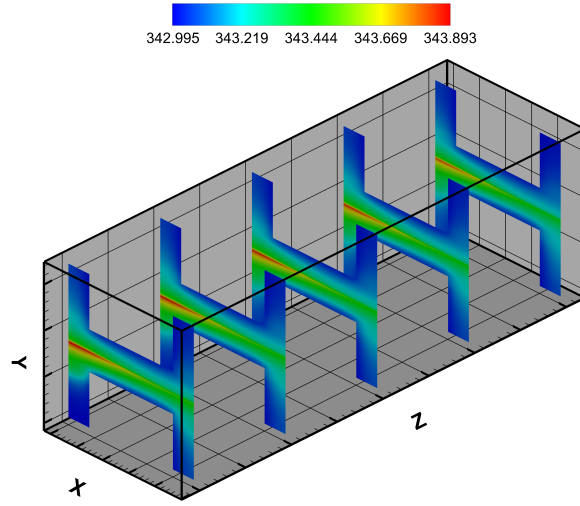


(a) Anisotropic thermal conductivity

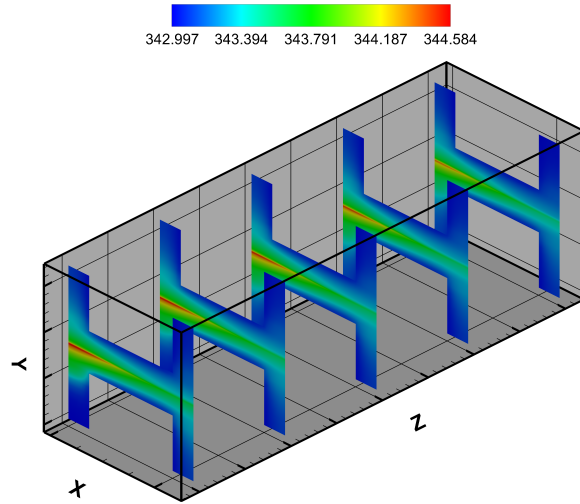


(b) Isotropic thermal conductivity

Fig. 3: Comparison of temperature profile with isotropic and anisotropic thermal conductivities at 0.5 volts.

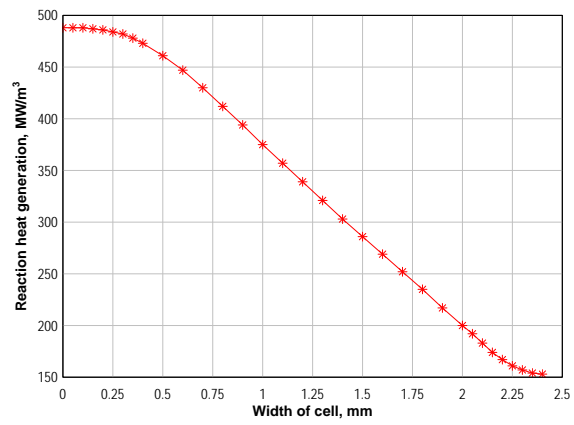
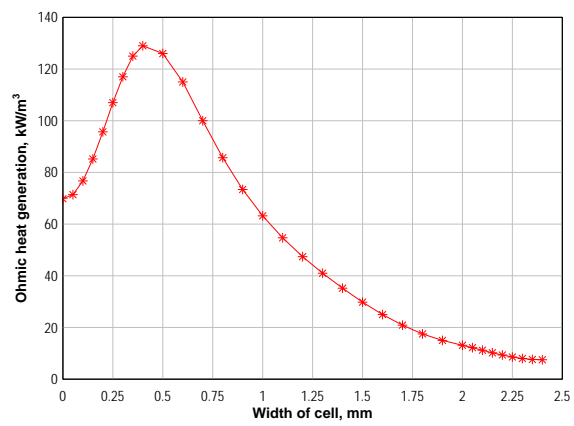


(a) Operating voltage = 0.6 V



(b) Operating voltage = 0.4 V

Fig. 4: Thermal distribution in the PEM fuel cell along the length of the cell.

(a) *Reactions heat*(b) *Ohmic heat***Fig. 5:** Heat generation in the PEM fuel cell.

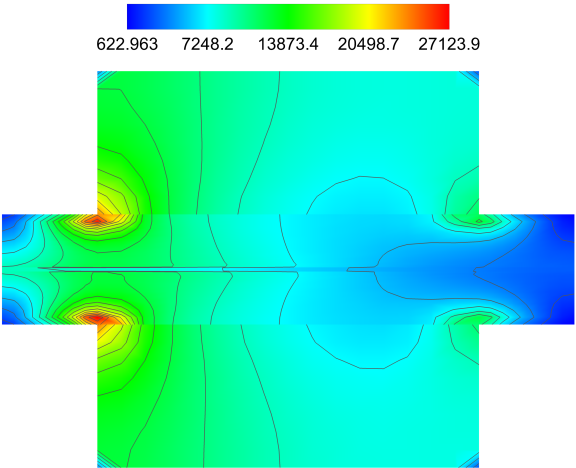
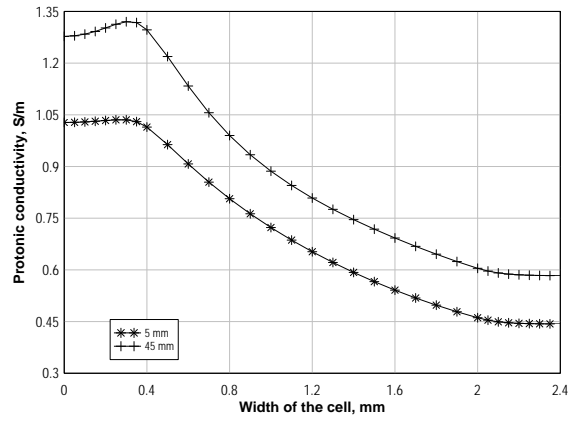
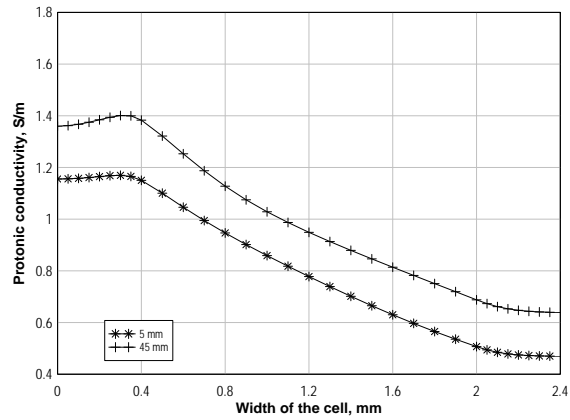


Fig. 6: *Magnitude of current flux density, A/m².*

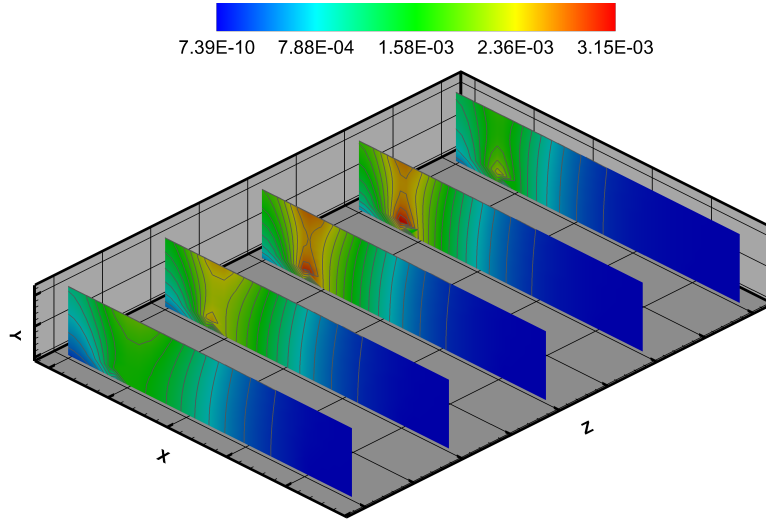


(a) Operating voltage = 0.6 V

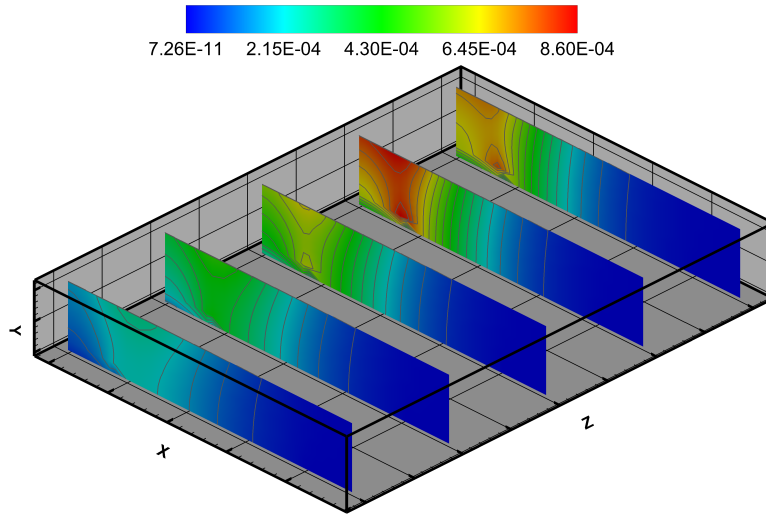


(b) Operating voltage = 0.4 V

Fig. 7: The protonic conductivity of the ionomer in the catalyst layer along the width of fuel cell.



(a) *Higher through-plane permeability [18]*



(b) *Higher in-plane permeability [26]*

Fig. 8: Water saturation profile at 0.5 V for different material behaviours.

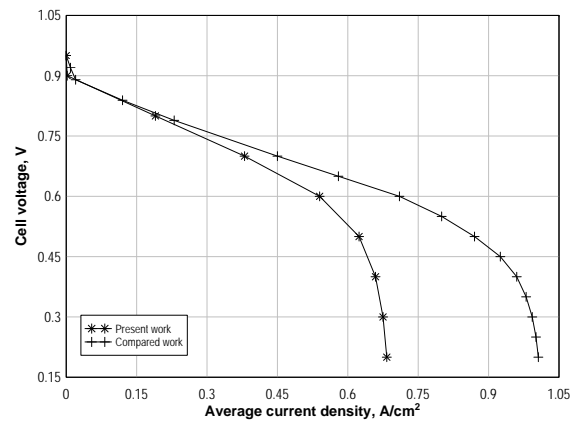


Fig. 9: *Comparison of the modelling approaches.*